Modulation of ion channels by natural products – Identification of hERG channel inhibitors and $GABA_A$ receptor ligands from plant extracts

Inauguraldissertation

zur
Erlangung der Würde eines Doktors der Philosophie
vorgelegt der
Philosophisch-Naturwissenschaftlichen Fakultät
der Universität Basel

von

Anja Schramm
aus Wiedersbach (Thüringen), Deutschland

Basel, 2014

Genehmigt von der Philosophisch-Naturwissenschaftlichen Fakultät

auf Antrag von

Prof. Dr. Matthias Hamburger

Prof. Dr. Judith Maria Rollinger

Basel, den 18.02.2014

Prof. Dr. Jörg Schibler

Dekan

Attribution-NonCommercial-NoDerivatives 3.0 Switzerland
(CC BY-NC-ND 3.0 CH)

You are free: **to Share** — to copy, distribute and transmit the work

Under the following conditions:

Attribution — You must attribute the work in the manner specified by the author or licensor (but not in any way that suggests that they endorse you or your use of the work).

Noncommercial — You may not use this work for commercial purposes.

No Derivative Works — You may not alter, transform, or build upon this work.

With the understanding that:

- **Waiver —** Any of the above conditions can be **waived** if you get permission from the copyright holder.
- **Public Domain —** Where the work or any of its elements is in the **public domain** under applicable law, that status is in no way affected by the license.
- **Other Rights —** In no way are any of the following rights affected by the license:
    - Your fair dealing or **fair use** rights, or other applicable copyright exceptions and limitations;
    - The author's **moral** rights;
    - Rights other persons may have either in the work itself or in how the work is used, such as **publicity** or privacy rights.
- **Notice —** For any reuse or distribution, you must make clear to others the license terms of this work. The best way to do this is with a link to this web page.

Quelle: creativecommons.org/licenses/by-nc-nd/3.0/ch/deed.en Datum: 12.11.2013

Für meine Familie

In den frühen Zeiten unserer Erde waren Pflanzen der Menschen natürliche Nahrung und blieben es seither als lebenserhaltendes Mittel und Medizin zur Wiederherstellung der Gesundheit.

John Gerard, *The Herbal*, 1597

Table of Contents

Summary

Ion channels are expressed in virtually all cell types in the human body and are involved in various physiological processes. Hence, it is not surprising that ion channels play an important role in modern drug discovery. Lead compounds are nowadays routinely tested against a panel of ion channels to evaluate selectivity and potential off-target activities.

The human ether-à-go-go-related gene (hERG) channel, a voltage-gated potassium channel, is the currently most critical antitarget with respect to cardiac safety. Inhibition of the hERG channel can prolong the QT interval on the electrocardiogram (ECG) and, as a consequence, lead to life-threatening arrhythmia. Considering the daily intake of plant-derived foods and herbal products, surprisingly few natural products have been tested for hERG blocking properties. In the course of an interdisciplinary hERG project, a selection of widely used herbal drugs and dietary plants was screened by means of a two-microelectrode voltage-clamp assay with *Xenopus* oocytes. Moderate hERG block was observed for the traditional Chinese herbal drug Coptidis rhizoma and black pepper fruits, and successfully tracked by HPLC-based activity profiling to dihydroberberine and piperine, respectively. The hERG blocking activity of cinnamon, guarana, and nutmeg, in contrast, was attributed to tannins. Our screening data suggest that major European medicinal plants and frequently consumed food plants are associated with a low risk for hERG inhibition. However, the case of Coptidis rhizoma pointed towards a need for a more thorough assessment of herbal drugs of the traditional Chinese medicine (TCM). Subsequent screening of a plant-derived alkaloid library led to the identification of several potent hERG blockers. Further investigations are certainly warranted to assess the cardiac safety profile of these alkaloids.

Dehydroevodiamine (DHE), a major bioactive constituent of the traditional Chinese herbal drug Evodiae fructus, has been previously shown to inhibit several cardiac ion currents *in vitro*.

For further evaluation of its *in vivo* pharmacological and toxicological properties, gram amounts of DHE were needed. Since DHE is not commercially available, we developed an efficient method for its gram-scale isolation from a crude *Evodia* extract. Our approach is based on a combination of cation-exchange chromatography and preparative RP-HPLC. Moreover, the DHE content in commercially available *Evodia* products was assessed by HPLC-PDA analysis. A daily intake of up to mg amounts of DHE was calculated from recommended doses of these products. We also devised a procedure for the production of DHE-depleted *Evodia* products, should DHE indeed turn out to be toxicologically relevant.

The gamma-aminobutyric acid type A ($GABA_A$) receptor, a ligand-gated chloride channel, mediates fast inhibitory neurotransmission in the central nervous system (CNS), and is thus a clinically important drug target. In the search for positive $\alpha_1\beta_2\gamma_{2S}$ $GABA_A$ receptor modulators of plant origin, we investigated an extract of *Curcuma kwangsiensis* rhizomes. HPLC-based activity profiling was used in combination with a two-microelectrode voltage-clamp assay on *Xenopus* oocytes to identify the active constituents. Targeted isolation afforded a series of 11 structurally related labdane diterpenoids, including four new natural products. Structure elucidation was achieved by comprehensive analysis of HR-ESI-TOF-MS and NMR data. The absolute configuration of the compounds was assigned by electronic circular dichroism (ECD). The highest $GABA_A$ receptor modulating activity was observed for zerumin A.

From a more general perspective, this study demonstrates that HPLC-based activity profiling is an effective strategy to characterize bioactive compounds in crude natural extracts.

Zusammenfassung

Ionenkanäle werden in nahezu allen Zelltypen des menschlichen Körpers exprimiert und sind in verschiedene physiologische Prozesse involviert. Daher ist es nicht verwunderlich, dass Ionenkanäle eine wichtige Rolle in der modernen Arzneimittelforschung spielen. Um die Selektivität und mögliche Off-Target-Aktivitäten von Leitsubstanzen zu beurteilen, werden diese heutzutage routinemässig an einer Vielzahl von Ionenkanälen auf ihre Aktivität hin untersucht.

Der hERG Kanal, ein spannungsgesteuerter Kaliumkanal, ist das derzeit bedeutenste Antitarget hinsichtlich der kardialen Sicherheit von Arzneistoffen. Eine Blockade des hERG Kanals kann zu einer Verlängerung des QT-Intervalls im Elektrokardiogramm (EKG) führen und infolgedessen lebensbedrohliche Herzrhythmusstörungen hervorrufen. Trotz der steigenden Popularität von Naturheilmitteln und des täglichen Verzehrs von pflanzlichen Nahrungsmitteln ist die Interaktion von Naturstoffen mit dem hERG Kanal bisher wenig erforscht. Im Rahmen eines interdisziplinären hERG Projektes wurden sowohl bedeutende Medizinalpflanzen als auch gebräuchliche Nahrungspflanzen in einem Zwei-Mikroelektroden-Spannungsklemm-Assay an *Xenopus* Oozyten getestet. Die chinesische Arzneidroge Coptidis Rhizoma und der schwarze Pfeffer riefen beide eine moderate, aber nennenswerte hERG Blockade hervor. Mittels HPLC-basiertem Aktivitätsprofiling konnten die entsprechenden aktiven Inhaltsstoffe als Dihydroberberine und Piperin identifiziert werden. Die hERG-blockierende Wirkung von Zimt, Guarana und Muskatnuss wurde hingegen auf Tannine zurückgeführt. Die Screeningergebnisse zeigen, dass die wichtigsten europäischen Heilpflanzen und pflanzlichen Nahrungsmittel ein geringes Risiko für eine Blockade des hERG Kanals aufweisen. Das Beispiel von Coptidis Rhizoma weist jedoch darauf hin, dass pflanzliche Arzneidrogen der traditionellen chinesischen Medizin (TCM) gründlich überprüft werden müssen. In einem zweiten Screening wurden ausgewählte pflanzliche Alkaloide getestet und einige potente hERG Blocker identifiziert. Um die

kardiale Sicherheit dieser Alkaloide beurteilen zu können, sind weitere Untersuchungen erforderlich.

Dehydroevodiamine (DHE) ist ein pharmakologisch wirksames Hauptalkaloid aus der chinesischen Arzneidroge Evodiae Fructus. In einer früheren Arbeit wurde gezeigt, dass DHE mehrere kardiale Ionenströme hemmen kann. Die Substanz wird derzeit in verschiedenen Tiermodellen auf kardiotoxische Effekte hin untersucht. Für die Durchführung dieser Studien wurden Gramm-Mengen an DHE benötigt. Da DHE als Referenzsubstanz kommerziell nicht verfügbar ist, wurde die Verbindung aus einem *Evodia*-Extrakt isoliert. Unter Verwendung eines selektiven Kationaustauschers und präparativer RP-HPLC konnte DHE einfach und effizient aufgereinigt werden. Des Weiteren wurde mit Hilfe einer HPLC-UV Methode der DHE-Gehalt in kommerziell erhältlichen *Evodia*-Präparaten bestimmt. In den jeweiligen empfohlenen Tagesdosen dieser Produkte wurde DHE im Milligramm-Bereich nachgewiesen. Zusätzlich wurde ein Verfahren für die Abreicherung von DHE aus *Evodia*-Extrakten entwickelt, sollte DHE sich tatsächlich als toxikologisch relevant erweisen.

Der Gamma-Aminobuttersäure Typ A ($GABA_A$) Rezeptor, ein ligandengesteuerter Chloridkanal, ist der wichtigste inhibitorische Rezeptor im zentralen Nervensystem (ZNS). Viele Arzneistoffe, die die neuronale Reizleitung hemmen, binden an $GABA_A$ Rezeptoren und verstärken den GABA-induzierten Chloridstrom. Zudem ist bekannt, dass zahlreiche Naturstoffe die Aktivität des $GABA_A$ Rezeptors beeinflussen können. In einem breit angelegten Screening rief ein Extrakt aus den Rhizomen von *Curcuma kwangsiensis* einen positiv modulierenden Effekt an $GABA_A$ Rezeptoren des $\alpha_1\beta_2\gamma_{2S}$ Subtyps hervor. Als Testsystem diente ein Zwei-Mikroelektroden-Spannungsklemm-Assay an *Xenopus* Oozyten. Die aktiven Extraktkomponenten wurden mittels HPLC-basiertem Aktivitätsprofiling als Labdanditerpene identifiziert. Insgesamt wurden 11 strukturell verwandete Labdanditerpene im semipräparativen Maßstab aufgereinigt.

Anhand von NMR-Messungen und hochaufgelösten massenspektrometrischen Daten konnte deren Struktur eindeutig aufgeklärt werden. Die absolute Konfiguration einzelner Verbindungen wurde mittels Zirculardichroismus bestimmt. Darüber hinaus wurden vier der isolierten Substanzen als neue Naturstoffe identifiziert. Von den getesteten Labdanditerpenen verstärkte Zerumin A den GABA-induzierten Chloridstrom am stärksten.

Bei der Suche nach biologisch aktiven Substanzen in komplexen Pflanzenextrakten erwies sich das HPLC-basierte Aktivitätsprofiling als erfolgreiche Strategie.

1. Aim of the work

Medicinal plants and phytomedicines continue to increase in popularity all over the world. Many herbal remedies that are used as alternatives to conventional pharmacotherapy or as complementary medicines are available as over-the-counter (OTC) products. It is also widely accepted that a plant-based diet with high intakes of fruits and vegetables brings numerous health benefits. Various therapeutic properties and health claims have been attributed to particular plant secondary metabolites. However, one has to consider that any pharmacologically active compound may also possess undesirable properties or even direct toxicity. It has been estimated that the consumption of plant-derived foods and the use of medicinal herbs result in an intake of plant secondary metabolites that may reach up to several grams per day. This clearly warrants a critical assessment of frequently consumed botanicals for potential safety liabilities.

The currently most important antitarget with respect to cardiac safety is the human ether-à-go-go-related gene (hERG) channel. Inhibition of hERG can delay the cardiac action potential repolarization and, as a consequence, lead to severe complications, such as ventricular tachyarrhythmia and sudden cardiac death. In contrast to synthetic drug substances which nowadays are routinely tested for hERG liability during preclinical development, very little is known about the hERG inhibitory potential of plant-derived natural products. Our goal was to evaluate whether widely used herbal medicines and edible plants are associated with a risk for hERG channel inhibition. The first step was to screen a focused plant extract library by means of a two-microelectrode voltage-clamp assay on *Xenopus* oocytes. A test concentration of 100 µg/mL was used, and extracts inhibiting the hERG current (I_{hERG}) by $\geq 30\%$ were considered as active. Next, the active principles had to be identified and characterized in more detail. The aim was to follow up the activity with the aid of an HPLC-based profiling approach, and to study the hERG channel blocking effects of purified compounds *in vitro*.

Cardiovascular safety concerns had been previously raised for the quaternary indoloquinazoline alkaloid dehydroevodiamine (DHE), a major constituent of the traditional Chinese herbal drug Evodiae fructus (*Evodia rutaecarpa* fruits). For example, the compound has been shown to inhibit several cardiac ion currents *in vitro*. In view of further risk assessment studies, gram amounts of highly pure DHE were needed. Since the compound is not commercially available, it had to be isolated from the herbal drug. Hence, a method for the efficient large-scale purification of DHE had to be developed. Quantitative data on the DHE intake are, however, essential to obtain an overall safety profile. An additional aim was, therefore, to determine the DHE content in commercially available *Evodia* products in order to calculate the DHE intake in recommended daily doses for these products. Also, we devised a procedure for the selective removal of DHE from *Evodia* extracts, should DHE indeed be a safety issue.

The third part of this thesis aimed at the discovery of new plant-derived $GABA_A$ (gamma-aminobutyric acid type A) receptor modulators. The $GABA_A$ receptor mediates fast inhibitory neurotransmission in the central nervous system (CNS), and is thus a clinically important drug target. Over the last few years, our research group searched for new scaffolds for this target, and successfully identified numerous structurally diverse plant secondary metabolites with positive $GABA_A$ receptor modulating activity. In the course of this ongoing *in vitro* screening approach, an ethyl acetate extract of *Curcuma kwangsiensis* rhizomes showed moderate but significant activity, and was of sufficient interest for further investigation. The aim was to identify the main active extract constituents, to fully elucidate their structures, and to evaluate their individual $GABA_A$ receptor modulating properties in a functional *Xenopus* oocyte assay.

2. Introduction

2.1. The hERG channel

The *human ether-à-go-go-related gene* (*hERG*, or *KCNH2* in the new nomenclature) encodes the pore-forming α–subunit of a voltage-gated potassium channel which conducts the rapid component of the delayed rectifier potassium current (I_{Kr}). According to the International Union of Pharmacology, the fully assembled ion channel is referred to as hERG or $K_v11.1$ channel [1]. The family name "*ether-à-go-go*" (*eag*) was coined in 1969 by Kaplan and Trout, who investigated the behavior of four neurological mutants of *Drosophila melanogaster*. All mutant flies showed an increased neuronal excitability following etherization and started to shake their legs vigorously [2]. One mutant phenotype was termed "*ether-à-go-go*" because its rapid leg-shaking resembled the action of go-go dancers in the 1960s at the nightclub "Whisky a Go Go" in West Hollywood (California, United States) [3]. Later, in 1994, Warmke and Ganetzky screened a human hippocampal cDNA library and looked as to whether an *eag*-like channel is expressed in human tissue. They found a corresponding human channel gene and named it *human ether-à-go-go-related gene* (*hERG*) [4].

Structure and gating of the hERG channel

Functional hERG channels have a tetrameric structure and are formed by co-assembly of four identical α–subunits, each containing six transmembrane domains (denoted S1–S6). Each subunit comprises a voltage sensor domain (S1–S4) and a pore domain (S5–S6). As the S4 domain contains multiple basic amino acids, it is regarded as the "voltage sensor" which responds to changes in the membrane potential. The pore domain consists of an outer (S5), inner (S6), and an intervening pore loop, the later forming the pore helix and the selectivity filter (Figure 1) [5]. Sanguinetti et al. showed that hERG channels are highly selective for K^+ ions over Na^+ ions by a factor of > 100 [6]. In addition to the membrane-spanning helices, the hERG α–subunit contains

large intracellularly located COOH- and NH_2-terminal domains (Figure 1). The C-terminus is known to have only small influence on the channel conductance, but seems to be important for the post-translational processing of the hERG channel. Deletion studies and point mutations revealed that the N-terminus plays a crucial role in the deactivation process [3,7].

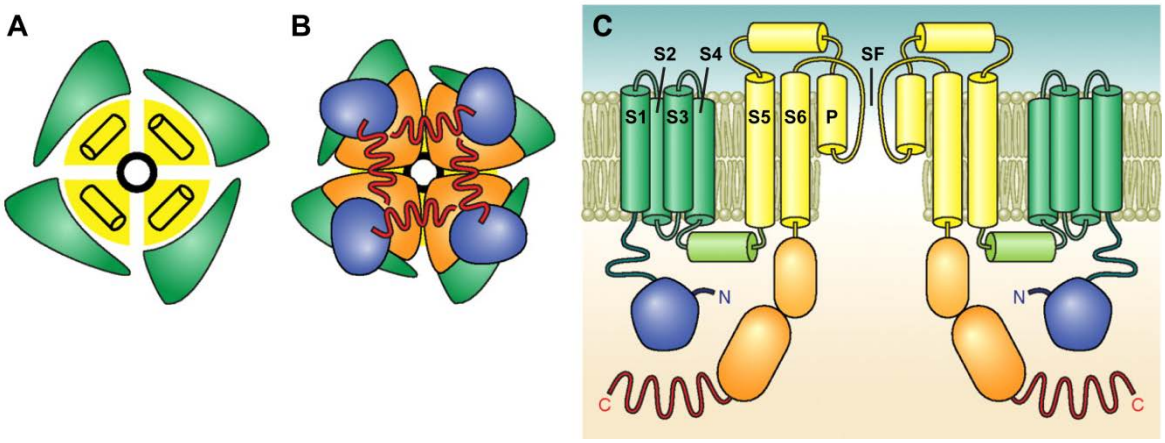

Figure 1. Topology and structure of the hERG channel. Schematic representations of the extracellular view (**A**) and intracellular view (**B**) of the tetrameric hERG channel. Transmembrane topology of two opposing hERG α-subunits (**C**). Color coding of the voltage sensor domain (S1–S4, green) and pore domain (S5–S6, yellow) is the same as in (A) and (B). P indicates the pore helix, and SF represents the selectivity filter. Adapted from Vandenberg et al., 2012 [3].

The conformation of the hERG channel and, thus, the dimension of its central cavity changes voltage-dependently. Depending on the transmembrane potential, the hERG channel is either closed, open or inactivated. Characteristic for hERG channels are their unique gating kinetics, namely a slow transition between open and closed states, and a rapid transition between open and inactivated states (Figure 2). The hERG channel is closed at the resting membrane potential. Upon depolarization, channels slowly open and pass an outward K^+ current (I_{Kr}). However, depolarization to voltages > 0 mV limits I_{Kr} due to rapid channel inactivation. Following repolarization inverts the transitions between these channel states. Rapid recovery from

inactivation elicits a huge tail current, which progressively decreases as the electrochemical gradient for K^+ ions declines and channels slowly return to the closed state (Figure 3) [3,7].

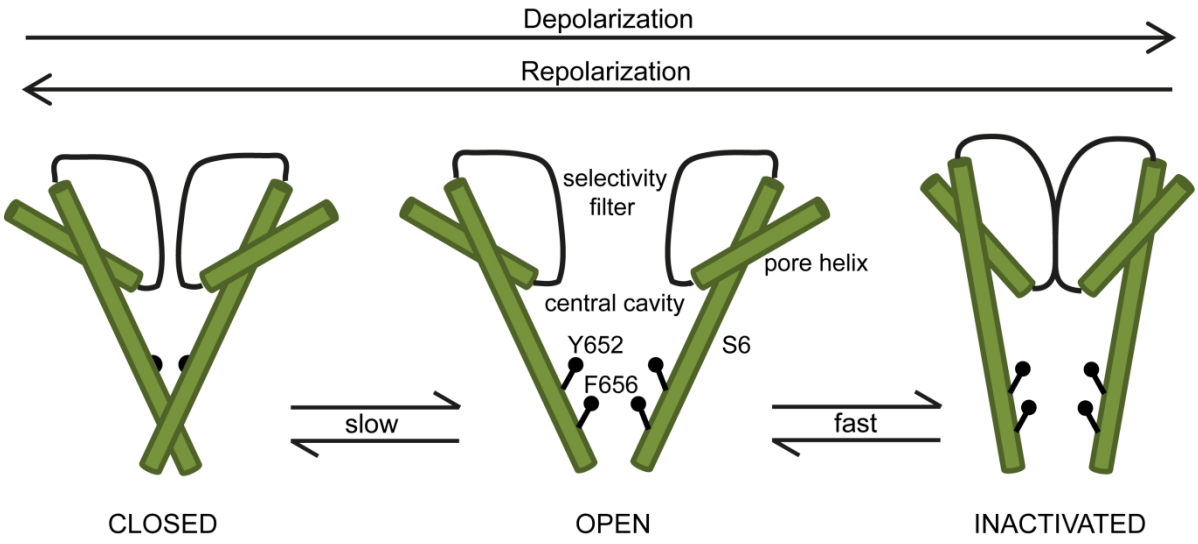

Figure 2. Conduction and kinetics of the hERG channel. The channel conformation and K^+ ion conductance is controlled by the membrane potential. Key high-affinity drug-binding sites are the aromatic residues Y652 and F656 on the S6 helix. Only two of the four channel subunits are shown. Adapted from Raschi et al., 2008 [5].

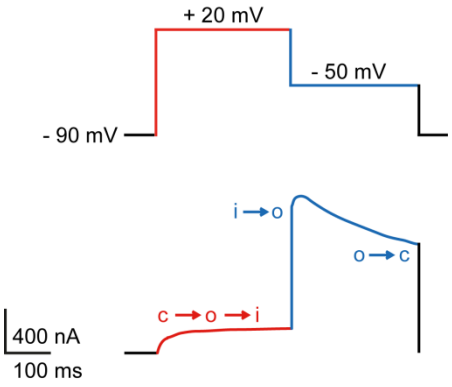

Figure 3. Gating of hERG channels. Exemplary hERG current trace recorded from a transfected *Xenopus* oocyte (bottom) in response to a two-step voltage protocol (top). Transitions between the different states (c: closed, o: open, i: inactivated) are color-coded.

Localization and physiological role of the hERG current I_{Kr}

In humans, hERG channels are expressed throughout the body in a wide range of tissues, but the physiological role is best characterized in the heart. Western blot analysis of human ventricular and atrial membrane proteins revealed that the expression of hERG channels is much higher in ventricles than in atria [8]. The unusual hERG channel gating properties make the underlying current particularly suitable for controlling the terminal repolarization phase of the cardiac action potential. As phase 3 repolarization starts, hERG channels recover from inactivation, hence passing more K^+ ions and contributing to consecutive repolarization. Overall, I_{Kr} turned out as the most important potassium current for repolarization, and any change in hERG channel activity will consequently affect the action potential duration (APD) [3]. The cardiac action potential defines the electrical activity of the heart, which can be measured by means of the surface electrocardiogram (ECG). On the ECG, the ventricular APD is represented by the QT interval (Figure 4). The QT interval exhibits a high degree of intra-individual variability, which makes a definition of "normal" values difficult [9]. As the QT interval has an inverse relationship to heart rate, the measured QT interval is typically corrected for heart rate with the aid of mathematical functions, leading to comparable QTc values [10].

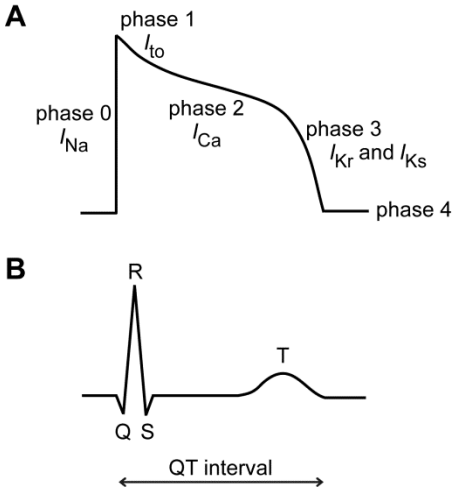

Figure 4. Correlation between ventricular APD and QT interval. (**A**) Action potential of human ventricular myocytes with phases 0−4 and major underlying ion currents. The K^+ current I_{Kr} is part of an ensemble of ion currents that characterizes the morphology and duration of the ventricular action potential. (**B**) The QT interval on the surface ECG is a measure of the elapsed time between ventricular depolarization (QRS complex) and repolarization (T wave). Adapted from Fermini et al., 2003 [10].

Apart from myocytes, hERG channels are also expressed in the central nervous system, gastrointestinal smooth muscles, and endocrine cells. However, the precise physiological role of hERG channels in these tissues is not as well characterized as in ventricular myocytes. Numerous studies suggested that I_{Kr} has an impact on the excitability of these cells by influencing the resting membrane potential. Moreover, hERG channels have been detected in various cancer cell lines, such as leukemia, neuroblastoma, and endometrial adenocarcinoma cells. Interestingly, highest expression levels were found in metastatic cancers, hence hERG channels have been implicated in the control of tumor cell invasion and angiogenesis [3,5,11].

Pharmacology of hERG channels

Whether the hERG channel is regarded as a target or an antitarget depends on the intended therapeutic indication. In arrhythmology, the hERG channel is the molecular target of class III anti-arrhythmic drugs, such as amiodarone, sotalol, and dofetilide. These drugs inhibit I_{Kr} and reduce the net outflow of K^+ ions. Delayed repolarization increases the effective refractory period and is thought to reduce the risk of re-entry arrhythmias. However, the therapeutic potential of class III anti-arrhythmic agents is limited due to the simultaneous propensity to be arrhythmogenic. Excessive QT prolongation (long QT syndrome [LQTS]) can induce a polymorphic ventricular tachycardia called torsades de pointes (TdP). TdP arrhythmia can result in palpitations, syncope or seizures, and is often self-limiting. Occasionally, it can also degenerate into life-threatening ventricular fibrillation and lead to sudden cardiac death [12].

In clinical practice, an overwhelming number of non-cardiac drugs, belonging to different therapeutic classes and with distinct structural features, have been shown to prolong the QT interval (Figure 5) [13]. In this context it is important to note that inhibition of I_{Kr} accounts for the vast majority of drug-induced QT prolongation [14]. Drug-induced LQTS represents a major

safety issue for both the pharmaceutical industry and drug-regulatory agencies. Several non-cardiac drugs have been restricted in their use, or even withdrawn as a consequence of their arrhythmogenic liability, plus the availability of safer drug alternatives [5].

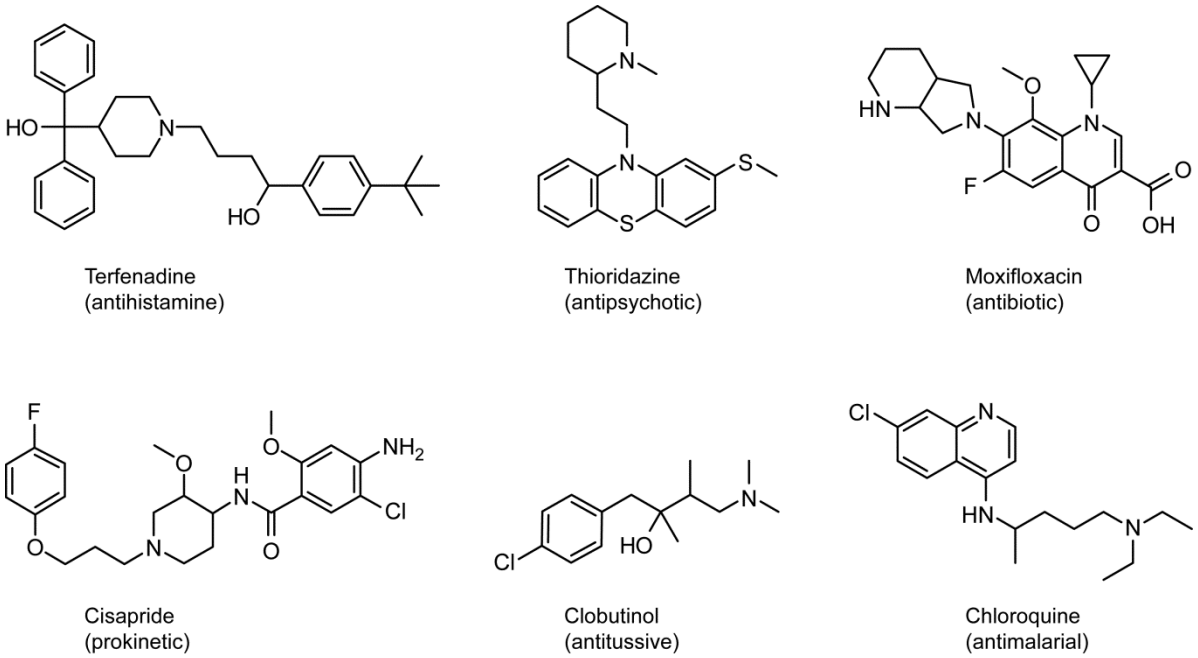

Figure 5. Structures of hERG channel blocking drugs. Risk assessment studies provided substantial evidence that these drugs can induce TdP arrhythmia through QT prolongation. This potentially fatal side effect has led to several drug withdrawals (e.g., terfenadine, cisapride, and clobutinol), restrictions of use (e.g., thioridazine and moxifloxacin), or specific labelings (e.g., chloroquine).

However, not every hERG channel blocker necessarily leads to QT prolongation. As numerous overlapping ion currents contribute to the morphology and duration of the ventricular action potential (Figure 4), effects on multiple ion channels may counteract the reduced hERG current flow. An excellent example is the hERG channel blocker verapamil. This drug also blocks L-type Ca^{2+} channels and is thus devoid of pro-arrhythmic properties [3,7]. Moreover, QT prolongation alone is not sufficient to trigger TdP arrhythmia in patients. Additional risk factors linked to an increased incidence of TdP arrhythmia include inherited LQTS, female

gender, electrolyte disorders (e.g., hypokalemia, hypomagnesemia), and pre-existing cardiac diseases (e.g., bradycardia, cardiomyopathy). Any concurrent medication, be it a prescription or over-the-counter medicine, is critical in the view of pharmacodynamic and pharmacokinetic drug-drug interactions. The risk assessment is further complicated in the presence of hepatic diseases and renal insufficiency as the extent of metabolism and excretion remarkably affects the plasma concentration of a drug. Hence, the severity of QT prolongation and the susceptibility to TdP arrhythmia vary from drug to drug, and from patient to patient [15].

Drug-binding site

Homology models suggest that, unlike other voltage-gated K^+ channels, the hERG channel has a comparatively large inner cavity. Most of the drugs that reduce I_{Kr} directly bind within the central cavity, thereby blocking the outward flow of K^+ ions. Typically, the drugs gain access to the channel pore from the intracellular side of the membrane, when the channel is in the open or inactivated state (Figure 2). Both site-directed mutagenesis studies and docking studies have identified several pore-lining residues which are crucial for the high-affinity binding of various hERG channel blockers. The aromatic residues Y652 and F656 located on the S6 domain are the most important drug-binding sites, whereas the contribution of polar pore helix residues (e.g., T623, S624, and V625) to drug binding appears compound-specific. Based on comprehensive docking simulations, it has been proposed that the aromatic side chain at position Y652 forms either cation-π or π-stacking interactions with the hERG channel blocker, whereas F656 is essential due to its hydrophobic properties [3,16]. Replacement of either Y652 or F656 with alanine drastically attenuates the potency of numerous hERG channel blocking drugs (e.g., terfenadine and cisapride) [17]. Similar findings have been observed among hERG channel blockers of plant origin (see Chapter 2.3). The potency of ajmaline is completely abolished in

Y652A and F656A mutant channels, indicating that ajmaline presumably interacts with those residues [18]. In contrast, the inhibitory effects of hesperetin and naringenin remain unaltered in Y652A mutant channels, but are significantly reduced in F656A mutant channels [19,20]. Interestingly, unique blocking characteristics have been identified for the pungent irritant capsaicin. The Y652A mutation increases the potency of capsaicin by approximately fourfold, whereas the F656A mutation does not significantly alter its affinity [21].

References

1 *Gutman GA, Chandy KG, Grissmer S, Lazdunski M, McKinnon D, Pardo LA, Robertson GA, Rudy B, Sanguinetti MC, Stühmer W, Wang XL*. International Union of Pharmacology. LIII. Nomenclature and molecular relationships of voltage-gated potassium channels. Pharmacol Rev 2005; 57: 473-508

2 *Kaplan WD, Trout WE*. The behavior of four neurological mutants of *Drosophila*. Genetics 1969; 61: 399-409

3 *Vandenberg JI, Perry MD, Perrin MJ, Mann SA, Ke Y, Hill AP*. HERG K^+ channels: Structure, function, and clinical significance. Physiol Rev 2012; 92: 1393-1478

4 *Warmke JW, Ganetzky B*. A family of potassium channel genes related to *eag* in *Drosophila* and mammals. P Natl Acad Sci USA 1994; 91: 3438-3442

5 *Raschi E, Vasina V, Poluzzi E, De Ponti F*. The hERG K^+ channel: Target and antitarget strategies in drug development. Pharmacol Res 2008; 57: 181-195

6 *Sanguinetti MC, Jiang CG, Curran ME, Keating MT*. A mechanistic link between an inherited and an acquired cardiac arrhythmia: HERG encodes the I_{Kr} potassium channel. Cell 1995; 81: 299-307

7 *Witchel HJ*. The hERG potassium channel as a therapeutic target. Expert Opin Ther Tar 2007; 11: 321-336

8 *Pond AL, Scheve BK, Benedict AT, Petrecca K, Van Wagoner DR, Shrier A, Nerbonne JM*. Expression of distinct ERG proteins in rat, mouse, and human heart: Relation to functional I_{Kr} channels. J Biol Chem 2000; 275: 5997-6006

9 *European Medicines Agency*. Points to consider: The assessment of the potential for QT interval prolongation by non-cardiovascular medicinal products (CPMP/986/96); 1997

10 *Fermini B, Fossa AA*. The impact of drug-induced QT interval prolongation on drug discovery and development. Nat Rev Drug Discov 2003; 2: 439-447

11 *Arcangeli A*. Expression and role of hERG channels in cancer cells. In: Chadwick DJ, Goode J, editors. Novartis Foundation Symposium 266 - The hERG cardiac potassium channel: Structure, function, and long QT syndrome. Chichester: John Wiley & Sons, Ltd; 2005: 225-234

12 *Brendorp B, Pedersen OD, Torp-Pedersen C, Sahebzadah N, Køber L*. A benefit-risk assessment of class III antiarrhythmic agents. Drug Safety 2002; 25: 847-865

13 *AZCERT*. Composite list of drugs that prolong QT and/or cause torsades de pointes (TdP). Available at: http://www.crediblemeds.org. Accessed September 2, 2013.

14 *European Medicines Agency*. Guideline ICH S7B: The non-clinical evaluation of the potential for delayed ventricular repolarization (QT interval prolongation) by human pharmaceuticals (CHMP/ICH/423/02); 2005

15 *De Ponti F, Poluzzi E, Cavalli A, Recanatini M, Montanaro N*. Safety of non-antiarrhythmic drugs that prolong the QT interval or induce torsade de pointes: An overview. Drug Safety 2002; 25: 263-286

16 *Stansfeld PJ, Sutcliffe MJ, Mitcheson JS*. Molecular mechanisms for drug interactions with hERG that cause long QT syndrome. Expert Opin Drug Met 2006; 2: 81-94

17 *Kamiya K, Niwa R, Morishima M, Honjo H, Sanguinetti MC*. Molecular determinants of hERG channel block by terfenadine and cisapride. J Pharmacol Sci 2008; 108: 301-307
18 *Kiesecker C, Zitron E, Lück S, Bloehs R, Scholz EP, Kathöfer S, Thomas D, Kreye VAW, Katus HA, Schoels W, Karle CA, Kiehn J*. Class Ia anti-arrhythmic drug ajmaline blocks hERG potassium channels: Mode of action. N-S Arch Pharmacol 2004; 370: 423-435
19 *Scholz EP, Zitron E, Kiesecker C, Thomas D, Kathöfer S, Kreuzer J, Bauer A, Katus HA, Remppis A, Karle CA, Greten J*. Orange flavonoid hesperetin modulates cardiac hERG potassium channel via binding to amino acid F656. Nutr Metab Cardiovas 2007; 17: 666-675
20 *Scholz EP, Zitron E, Kiesecker C, Lück S, Thomas D, Kathöfer S, Kreye VAW, Katus HA, Kiehn J, Schoels W, Karle CA*. Inhibition of cardiac hERG channels by grapefruit flavonoid naringenin: Implications for the influence of dietary compounds on cardiac repolarisation. N-S Arch Pharmacol 2005; 371: 516-525
21 *Xing JL, Ma JH, Zhang PH, Fan XR*. Block effect of capsaicin on hERG potassium currents is enhanced by S6 mutation at Y652. Eur J Pharmacol 2010; 630: 1-9

2.2. Preclinical strategies for assessing the cardiac safety profile

Since inhibition of I_{Kr} is the most common mechanism that underlies acquired LQTS and TdP arrhythmia, the hERG channel is considered as a "promiscuous" target in basic research and safety pharmacology. Assessing the hERG liability of a test compound can be achieved using several different *in vitro* approaches. Non-electrophysiological screening techniques include, for example, binding competition (detecting radioligand displacement), rubidium efflux (measuring extracellular Rb^+ ion concentration, based on the ability of Rb^+ ions to permeate through hERG channels), and fluorescence-based assays (monitoring changes in fluorescence, based on voltage-sensitive dyes). These testing strategies are favorable for high-throughput experimentation, although it is important to note their inherent limitations [1-3]. A major drawback of these techniques is that the cell membrane potential cannot be controlled (e.g., clamped at a preset value). At present, only electrophysiological measurements allow a direct voltage control and, hence, are considered as "gold standard" to study the hERG channel function on a millisecond timescale. The mediated charge transfer across the cell membrane (K^+ ion efflux) can thus be measured directly and quantitatively [4]. Electrophysiological recordings on native cardiomyocytes face some technical difficulties, like the existence of overlapping ion currents that need to be selectively excluded. Heterologous expression systems are, therefore, increasingly favored for primary electrophysiological screens. In this case, the hERG channel protein is either transiently or stably expressed in non-cardiac cell lines. The most common expression systems include human embryonic kidney cells (HEK293), Chinese hamster ovary cells (CHO), and *Xenopus laevis* oocytes [2,3].

Such electrophysiological measurements provide valuable information about a compound's potential to reduce the hERG channel activity *in vitro*. However, these approaches alone are not sufficient to evaluate its cardiac safety profile [5]. To estimate the risk for delayed

ventricular repolarization and QT prolongation, the following data are needed: (i) effects on other cardiac ion currents, (ii) action potential parameters in isolated cardiac preparations, (iii) ECG parameters in conscious or anesthetized animals, and clinically most relevant, (iv) the arrhythmogenic potential in isolated cardiac preparations or animals. General considerations regarding appropriate test systems, and specific recommendations for an integrated risk assessment are described in the ICH (International Conference on Harmonization) safety guideline S7B [6]. *In vitro* effects on cardiac electrophysiology can be further studied with multicellular preparations, the most commonly used tissues being Purkinje fibers, papillary muscles, and intact hearts. Cardiac preparations from guinea pig, rabbit, and dog are generally considered as the most suitable ones, as the ionic mechanism of repolarization in these animal species is similar to that of humans [1,6]. However, only *in vivo* ECG recordings can ultimately detect pro-arrhythmic effects under physiological conditions and, thus, are a reliable measure of hERG-related safety liabilities. One important advantage of such *in vivo* studies is that numerous safety parameters (e.g., QTc interval, heart rate, and blood pressure) can be assessed simultaneously. Furthermore, blood samples can be collected for determination of plasma concentrations of the administered compound and its metabolites [1,6,7]. Advantages and disadvantages of the most widely used preclinical models have been reviewed in detail elsewhere [7,8]. Within the past decade, zebrafish (*Danio rerio*) have emerged as an attractive and promising *in vivo* model to study various aspects of cardiotoxicity [9]. Several studies showed that drugs known to induce QT prolongation in humans induced bradycardia or arrhythmia in three-day-old zebrafish embryos, and that similar effects were observed after knocking down the *Zerg* protein (the zebrafish ortholog of human *KCNH2*) [9-12].

The key challenge in extrapolating *in vitro*/*in vivo* electrophysiological results to clinical settings is interpreting those data with regard to the pharmacokinetic profile of a compound.

Besides the peak free plasma concentration (c_{max}), properties like the apparent volume of distribution, protein binding, lipophilicity, and metabolic pathways should be considered. Especially if the compound has a large volume of distribution, myocardial binding and, hence, the effective cardiac tissue concentration becomes increasingly important [8,13]. In this context, the often-cited study from Redfern and colleagues appears quite noteworthy. They performed a comprehensive literature survey to evaluate the relationships between preclinical cardiac electrophysiology data, clinical QT prolongation and TdP arrhythmia for a broad range of drugs. Their dataset suggested that a 30-fold margin between the hERG *in vitro* IC_{50} value and c_{max} "would be adequate to ensure an acceptable degree of safety from arrhythmogenesis, with a low risk of obtaining false positives" [14]. This study clearly implicates that a thorough risk assessment should primarily focus on safety margins rather than absolute hERG channel blocking potencies.

Comparatively little is known about the pharmacokinetics of plant secondary metabolites, especially with respect to their oral bioavailability. Numerous natural products mentioned in the next chapter displayed hERG *in vitro* IC_{50} values in the range of 5-100 µM. While these values do not point towards a high-affinity block, possible *in vivo* effects on ventricular repolarization cannot be ruled out. Even relatively weak hERG *in vitro* inhibitors can produce clinically relevant QT prolongation if plasma levels are sufficiently high [15]. This phenomenon, for example, has been observed with the fluoroquinolone sparfloxacin. Its average plasma levels (~1.8 µM) after therapeutic doses clearly approximate concentrations that diminish the hERG channel activity *in vitro* (studies in mammalian cells revealed IC_{50} values between 13.5 and 44.0 µM) [2,16].

References

1 *Priest BT, Bell IM, Garcia ML*. Role of hERG potassium channel assays in drug development. Channels 2008; 2: 87-93

2 *Polak S, Wiśniowska B, Brandys J*. Collation, assessment and analysis of literature *in vitro* data on hERG receptor blocking potency for subsequent modeling of drugs' cardiotoxic properties. J Appl Toxicol 2009; 29: 183-206
3 *Hancox JC, McPate MJ, El Harchi A, Zhang YH*. The hERG potassium channel and hERG screening for drug-induced torsades de pointes. Pharmacol Therapeut 2008; 119: 118-132
4 *Kvist T, Hansen KB, Bräuner-Osborne H*. The use of *Xenopus* oocytes in drug screening. Expert Opin Drug Dis 2011; 6: 141-153
5 *Fermini B, Fossa AA*. The impact of drug-induced QT interval prolongation on drug discovery and development. Nat Rev Drug Discov 2003; 2: 439-447
6 *European Medicines Agency*. Guideline ICH S7B: The non-clinical evaluation of the potential for delayed ventricular repolarization (QT interval prolongation) by human pharmaceuticals (CHMP/ICH/423/02); 2005
7 *Thomsen MB, Matz J, Volders PGA, Vos MA*. Assessing the proarrhythmic potential of drugs: Current status of models and surrogate parameters of torsades de pointes arrhythmias. Pharmacol Therapeut 2006; 112: 150-170
8 *Raschi E, Ceccarini L, De Ponti F, Recanatini M*. HERG-related drug toxicity and models for predicting hERG liability and QT prolongation. Expert Opin Drug Met 2009; 5: 1005-1021
9 *Crawford AD, Esguerra CV, de Witte PAM*. Fishing for drugs from nature: Zebrafish as a technology platform for natural product discovery. Planta Med 2008; 74: 624-632
10 *Langheinrich U, Vacun G, Wagner T*. Zebrafish embryos express an orthologue of hERG and are sensitive toward a range of QT-prolonging drugs inducing severe arrhythmia. Toxicol Appl Pharm 2003; 193: 370-382
11 *Milan DJ, Peterson TA, Ruskin JN, Peterson RT, MacRae CA*. Drugs that induce repolarization abnormalities cause bradycardia in zebrafish. Circulation 2003; 107: 1355-1358
12 *Mittelstadt SW, Hemenway CL, Craig MP, Hove JR*. Evaluation of zebrafish embryos as a model for assessing inhibition of hERG. J Pharmacol Toxicol Methods 2008; 57: 100-105
13 *European Medicines Agency*. Points to consider: The assessment of the potential for QT interval prolongation by non-cardiovascular medicinal products (CPMP/986/96); 1997
14 *Redfern WS, Carlsson L, Davis AS, Lynch WG, MacKenzie I, Palethorpe S, Siegl PKS, Strang I, Sullivan AT, Wallis R, Camm AJ, Hammond TG*. Relationships between preclinical cardiac electrophysiology, clinical QT interval prolongation and torsade de pointes for a broad range of drugs: Evidence for a provisional safety margin in drug development. Cardiovasc Res 2003; 58: 32-45
15 *Rampe D, Brown AM*. A history of the role of the hERG channel in cardiac risk assessment. J Pharmacol Toxicol Methods 2013; 68: 13-22
16 *Kang JS, Wang L, Chen XL, Triggle DJ, Rampe D*. Interactions of a series of fluoroquinolone antibacterial drugs with the human cardiac K^+ channel hERG. Mol Pharmacol 2001; 59: 122-126

2.3. Plant-derived natural products as hERG channel inhibitors

Considering hERG channel inhibition as a major liability in safety pharmacology, data on plant-derived natural products and possible hERG-related effects are still scarce. This chapter provides an overview on plant secondary metabolites for which hERG *in vitro* electrophysiological data are available in accessible scientific literature. Depending on the study design, the underlying hERG current is termed I_{Kr} when referring to studies in native cardiomyocytes, or I_{hERG} when referring to studies in heterologous expression systems. Most of the plant-derived compounds mentioned here showed hERG channel blocking effects, but one will also find reports on inactive natural products and hERG channel activators (Tables 1–3). It is important to emphasize that all of those findings are highly valuable for an integrated risk assessment. Although representing relevant information, studies that have focused only on crude plant extracts or corresponding fractions were not considered. Additional data regarding *in vitro* and/or *in vivo* electrocardiographic effects (action potential parameters in isolated cardiac preparations and ECG parameters in animals) were also not included and are beyond the scope of this compilation.

It is important to note that for some natural products the reported hERG channel blocking potencies vary remarkably. Most *in vitro* electrophysiological studies have been carried out in heterologous expression systems, primarily with *Xenopus* oocytes and mammalian cells (HEK293 and CHO cells). In general, IC_{50} values obtained in *Xenopus* oocytes are considerably higher than those from mammalian cell lines. For instance, a nearly 100-fold difference in the sensitivity to papaverine could be found in the literature [1,2]. Such a decreased compound potency in *Xenopus* oocytes has been mainly attributed to the large amounts of lipophilic yolk. The yolk particles can adsorb molecules, and thus lower the effective intracellular free compound concentration [3]. However, even if the same expression system is used, IC_{50} values obtained in different

laboratories may still vary by more than one magnitude [4]. Papaverine, for example, blocks hERG currents in HEK293 cells with IC_{50} values ranging from 7.3 µM to 0.58 µM [1,5]. The degree of hERG channel inhibition could be further influenced by a variety of parameters, such as electrolyte concentrations, pulse protocol, and temperature. Based on comparative studies, the impact of these experimental parameters appears compound-specific [4,6]. Increasing the extracellular K^+ concentration $[K^+]_o$ has been shown to attenuate the hERG channel inhibitory potency of cisapride. Concentration-response experiments in the presence of 0, 5, and 135 mM $[K^+]_o$ yielded IC_{50} values of 7.5, 24.1, and 108.8 nM, respectively [7]. In contrast, the hERG channel block of cocaine was independent of changes in $[K^+]_o$ [8]. The applied pulse protocol, especially the duration and amplitude of the voltage steps, allows a direct control for how long the hERG channel stays in the open, inactivated, and closed state. Thus, the potency of particular hERG channel blockers may vary depending on their state-dependent binding. Moreover, the pulsing rate (stimulation frequency) can have an impact on the estimation of IC_{50} values [9]. Electrophysiological measurements on mammalian cells can be performed at both room (20–24°C) and near-physiological temperature (35–37°C). It has been demonstrated that hERG channel gating kinetics are markedly affected by changes in temperature, and that the rates of activation, inactivation, recovery from inactivation, and deactivation all show different temperature sensitivities [10,11]. In principle, it is also possible that an increased temperature affect the binding kinetics (association and dissociation rate constants) of hERG channel ligands, and, thus, the onset and degree of inhibition. In this context, it is worth mentioning that oxymatrine showed opposing *in vitro* effects on hERG channel gating when tested at different temperatures. In HEK293 cells, oxymatrine (100 µM) potentiated I_{hERG} at 20°C (potentiation of I_{hERG} by 50.1 ± 0.9%), but exhibited hERG channel blocking properties at 30°C (inhibition of I_{hERG} by 31.6 ± 0.5%) [12].

Alkaloids tested for hERG channel inhibition

Recently, the stereoselective inhibition of hERG channels has been reviewed for selected chiral drugs, such as bupivacaine, verapamil, and methadone [13]. Although numerous reports of chiral natural products inhibiting the hERG current could be found in the literature, virtually nothing is known about potential enantioselective effects. An historical and probably the most prominent example among hERG channel blockers of plant origin are the *Cinchona* alkaloids quinidine and quinine. Both alkaloids have opposite absolute configurations at two centers (Figure 6) and, thus, are diastereomers. Quinidine served as a class I anti-arrhythmic drug, whereas quinine is used for treating multidrug-resistant malaria. Interestingly, both alkaloids can block the cardiac Na^+ current I_{Na}, and even though quinidine has a greater potency against some malarial strains, quinine is the preferred antimalarial drug. Moreover, severe *in vivo* cardiotoxicity (QT prolongation) has only been reported for quinidine [13-15]. Just 10 years ago, the two diastereomers were tested for their hERG liability by means of two-microelectrode voltage-clamp recordings in *Xenopus* oocytes. The *in vitro* results revealed that quinidine and quinine inhibited I_{hERG} with IC_{50} values of 4.6 ± 1.2 µM and 57.0 ± 3.3 µM, respectively [16]. The distinct hERG channel inhibitory properties may explain why quinidine has a pronounced *in vivo* effect on ventricular repolarization. In this case, the stereoselective pharmacodynamic effects determined both the clinical indication and the cardiac safety profile of the two stereoisomers [13].

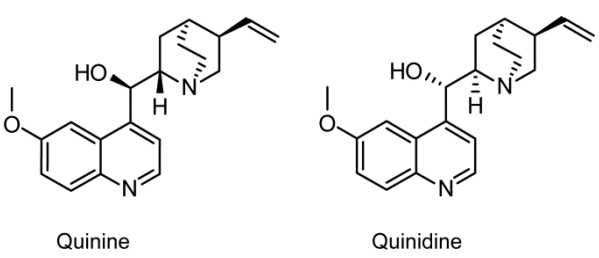

Quinine Quinidine

Figure 6. Structures of the stereoisomers quinine and quinidine.

Table 1. Alkaloids tested for hERG channel inhibition.

Substance	Source	Bioassay	Observed Effect	Reference
Aconitine	*Aconitum anthora* (Ranunculaceae)	Whole-cell patch-clamp assay using CHO cells 1) Conc.: 10 µM 2) Screening of 23 structurally related diterpene alkaloids Conc.: 10 µM	1) Inhibition of I_{hERG} by 44.9 ± 7.4% 2) Inhibition of I_{hERG} ranged from 6.5% to 39.6%	[17]
		Whole-cell patch-clamp assay using HEK293 cells Screening of five structurally related diterpene alkaloids Conc.: 1, 10 µM	No significant effect on I_{hERG}	[18]
		Patch-clamp assay	IC_{50}: 13.5 µM	[19]
		Two-microelectrode voltage-clamp assay using *Xenopus* oocytes	IC_{50}: 1.801 ± 0.332 µM	[20]
Ajmaline	*Rauvolfia serpentina* (Apocynaceae)	Whole-cell patch-clamp assay using HEK293 cells	IC_{50}: 1.0 ± 0.1 µM	[21]
		Two-microelectrode voltage-clamp assay using *Xenopus* oocytes 1) Concentration-response experiment 2) Conc.: 300 µM 3) Mutation study (hERG F656A, conc.: 300 µM) 4) Mutation study (hERG Y652A, conc.: 300 µM)	1) IC_{50}: 42.3 ± 11.9 µM 2) Reduction of I_{hERG} to 10.7 ± 3.0% 3) No significant effect on I_{hERG} 4) No significant effect on I_{hERG}	[21]
		HERG-Lite® assay Conc.: 10 µM	Classified as hERG blocker	[5]
Allocryptopine	*Corydalis cava* (Fumariaceae)	Whole-cell patch-clamp assay using HEK293 cells	IC_{50}: 49.65 µM	[22]
Arecoline	*Areca catechu* (Arecaceae)	Whole-cell patch-clamp assay using HEK293 cells	IC_{50}: 9.55 µM	[23]
Benzoylecgonine	*Erythroxylum coca* (Erythroxylaceae)	Whole-cell patch-clamp assay using HEK293 cells Conc.: 20, 1000 µM	Inhibition of I_{hERG} by 6 ± 2% (20 µM), 15 ± 8% (1000 µM)	[24]

Substance	Source	Bioassay	Observed Effect	Reference
Berberine	*Coptis chinesis* (Ranunculaceae)	Whole-cell patch-clamp assay using HEK293 cells	IC_{50}: 3.1 ± 0.5 µM	[25]
		Two-microelectrode voltage-clamp assay using *Xenopus* oocytes	IC_{50}: 75 ± 12 µM	[26]
		Two-microelectrode voltage-clamp assay using *Xenopus* oocytes 1) Concentration-response experiment 2) Mutation study (hERG F656T, conc.: 300 µM) 3) Mutation study (hERG Y652A, conc.: 300 µM)	1) IC_{50}: 80 ± 5 µM 2) No significant effect on I_{hERG} 3) No significant effect on I_{hERG}	[25]
		Guinea pig ventricular myocytes – I_{Kr} Conc.: 30 µM	No effect on I_{Kr}	[27]
Caffeine	*Coffea arabica* (Rubiaceae)	Whole-cell patch-clamp assay using HEK293 cells Conc.: 5, 20 mM	Reduction of I_{hERG} to 61.1 ± 2.2% (5 mM), 12.7 ± 1.1% (20 mM)	[28]
		Two-microelectrode voltage-clamp assay using *Xenopus* oocytes 1) Conc.: 5 mM 2) Mutation study (hERG F656A, conc.: 5 mM) 3) Mutation study (hERG Y652A, conc.: 5 mM)	1) Reduction of I_{hERG} to 77.8 ± 2.4% 2) Reduction of I_{hERG} to 93.6 ± 1.4% 3) Reduction of I_{hERG} to 92.6 ± 1.4%	[28]
Capsaicin	*Capsicum frutescens* (Solanaceae)	Two-microelectrode voltage-clamp assay using *Xenopus* oocytes 1) Concentration-response experiment 2) Conc.: 5, 10 µM 3) Mutation study (hERG F656A) 4) Mutation study (hERG Y652A, conc.: 5, 10 µM)	1) IC_{50}: 17.45 ± 2.63 µM 2) Inhibition of I_{hERG} by 18.9 ± 3.5% (5 µM), 34.7 ± 4.8% (10 µM) 3) No significant difference to hERG WT, compound potency was not altered 4) Inhibition of I_{hERG} by 53.9 ± 6.0% (5 µM), 73.4 ± 6.1% (10 µM); IC_{50}: 4.11 ± 0.96 µM	[29]
Changrolin	*Dichroa febrifuga* (Hydrangeaceae)	Whole-cell patch-clamp assay using HEK293 cells	IC_{50}: 18.23 µM	[30]

Substance	Source	Bioassay	Observed Effect	Reference
Chelerythrine	*Chelidonium majus* (Papaveraceae)	Whole-cell patch-clamp assay using HEK293 cells	IC_{50}: 0.11 ± 0.01 μM	[31]
		Canine ventricular myocytes – I_{Kr} Conc.: 1, 10 μM	Inhibition of I_{Kr} by 87.2% (1 μM), 100% (10 μM)	[31]
Cocaine	*Erythroxylum coca* (Erythroxylaceae)	Whole-cell patch-clamp assay using HEK293 cells	IC_{50}: 7.2 μM	[32]
		Whole-cell patch-clamp assay using HEK293 cells	IC_{50}: 4.4 ± 1.1 μM	[24]
		Whole-cell patch-clamp assay using HEK293 cells 1) Concentration-response experiment 2) Mutation study (hERG F656W, hERG F656Y, hERG F656V, hERG F656T) 3) Mutation study (hERG Y652A)	1) IC_{50}: 8.7 ± 1.6 μM 2) IC_{50}: 8.4 ± 0.8 μM (hERG F656W), 12.2 ± 1.6 μM (hERG F656Y), 88.9 ± 11.8 μM (hERG F656V), 161.8 ± 24.2 μM (hERG F656T) 3) IC_{50}: 309.6 ± 49.0 μM	[8]
		Whole-cell patch-clamp assay using tsA201 cells‡	IC_{50}: 5.6 ± 0.4 μM	[33]
		Guinea pig ventricular myocytes – I_{Kr} 1) Concentration-response experiment 2) Conc.: 3, 10, 30 μM	1) IC_{50}: 4 μM 2) Inhibition of I_{Kr} by 39.7 ± 11.3% (3 μM), 66.7 ± 7.2% (10 μM), 81.4 ± 4.6% (30 μM)	[34]
Codeine	*Papaver somniferum* (Papaveraceae)	Whole-cell patch-clamp assay using CHO cells	IC_{50}: 97 ± 5 μM	[35]
		Whole-cell patch-clamp assay using HEK293 cells	IC_{50}: > 300 μM	[36]
Cyclovirobuxine D	*Buxus microphylla* (Buxaceae)	Whole-cell patch-clamp assay using HEK293 cells 1) Concentration-response experiment 2) Conc.: 1, 10, 30, 100 μM	1) IC_{50}: 19.7 μM 2) Inhibition of I_{hERG} by 12.3 ± 4.7% (1 μM), 21.7 ± 16.1% (10 μM), 57.7 ± 7.5% (30 μM), 71.2 ± 5.1% (100 μM)	[37]
Dauricine	*Menispermum dauricum* (Menispermaceae)	Whole-cell patch-clamp assay using HEK293 cells	IC_{50}: 3.5 μM	[38]
		Guinea pig ventricular myocytes – I_{Kr}	IC_{50}: 16 μM	[39]

Substance	Source	Bioassay	Observed Effect	Reference
Daurisoline	*Menispermum dauricum* (Menispermaceae)	Whole-cell patch-clamp assay using HEK293 cells 1) Concentration-response experiment 2) Conc.: 1, 3, 10, 30 μM	1) IC_{50}: 9.6 μM 2) Inhibition of I_{hERG} by 16.7 ± 5.8% (1 μM), 31.1 ± 4.5% (3 μM), 55.1 ± 7.2% (10 μM), 81.2 ± 7.0% (30 μM)	[40]
Ephedrine / **Pseudoephedrine**	*Ephedra sinica* (Ephedraceae)	Whole-cell patch-clamp assay using HEK293 cells Conc.: 10 μM	No effect on I_{hERG}	[5]
		HERG-Lite® assay Conc.: 100 μM	Classified as non-hERG blockers	[5]
Galanthamine	*Galanthus nivalis* (Amaryllidaceae)	Whole-cell patch-clamp assay using HEK293 cells	IC_{50}: 760.2 μM	[41]
Guanfu base A	*Aconitum coreanum* (Ranunculaceae)	Whole-cell patch-clamp assay using HEK293 cells	IC_{50}: 1.64 mM	[42]
		Whole-cell patch-clamp assay using HEK293 cells 1) Conc.: 0.025, 0.1, 0.4, 1.0, 2.5 mM 2) Mutation study (hERG F656C, conc.: 0.4, 1 mM)	1) Inhibition of I_{hERG} by 1.5% (0.025 mM), 13.6% (0.1 mM), -5.9% (0.4 mM), 30.1% (1.0 mM), 38.5% (2.5 mM) 2) Inhibition of I_{hERG} by 12.2% (0.4 mM), 23.4% (1 mM)	[43]
Guanfu base G	*Aconitum coreanum* (Ranunculaceae)	Whole-cell patch-clamp assay using HEK293 cells	IC_{50}: 17.9 μM	[42]
Liensinine	*Nelumbo nucifera* (Nelumbonaceae)	Whole-cell patch-clamp assay using HEK293 cells 1) Conc.: 1, 3, 10, 30, 100, 300 μM 2) Mutation study (hERG F656V, conc.: 100, 300 μM) 3) Mutation study (hERG Y652A, conc.: 100, 300 μM)	1) Concentration-dependent inhibition of I_{hERG} 2) Inhibition of I_{hERG} is attenuated 3) Inhibition of I_{hERG} is attenuated	[44]
Lobeline	*Lobelia inflata* (Campanulaceae)	Whole-cell patch-clamp assay using HEK293 cells	IC_{50}: 0.34 μM	[45]
Matrine	*Sophora flavescens* (Fabaceae)	Whole-cell patch-clamp assay using CHO cells	IC_{50}: 411 ± 23 μM	[46]

Substance	Source	Bioassay	Observed Effect	Reference
Matrine (continued)		Whole-cell patch-clamp assay using HEK293 cells Conc.: 1, 10, 100 µM	Potentiation of I_{hERG} at 1 and 10 µM, inhibition of I_{hERG} at 100 µM	[47]
Methylecgonine	*Erythroxylum coca* (Erythroxylaceae)	Whole-cell patch-clamp assay using HEK293 cells Conc.: 20, 1000 µM	Inhibition of I_{hERG} by 12 ± 3% (20 µM), 21 ± 4% (1000 µM)	[24]
Morphine	*Papaver somniferum* (Papaveraceae)	Whole-cell patch-clamp assay using HEK293 cells	IC_{50}: > 1 mM	[36]
Neferine	*Nelumbo nucifera* (Nelumbonaceae)	Whole-cell patch-clamp assay using HEK293 cells 1) Concentration-response experiment 2) Conc.: 1, 3, 10, 30 µM	1) IC_{50}: 7.419 ± 1.162 µM 2) Inhibition of I_{hERG} by 21.8 ± 6.1% (1 µM), 39.8 ± 5.1% (3 µM), 56.6 ± 2.7% (10 µM), 65.8 ± 2.6% (30 µM)	[48]
		Whole-cell patch-clamp assay using HEK293 cells 1) Conc.: 1, 3, 10, 30, 100, 300 µM 2) Mutation study (hERG F656V, conc.: 100, 300 µM) 3) Mutation study (hERG Y652A, conc.: 100, 300 µM)	1) Concentration-dependent inhibition of I_{hERG} 2) Inhibition of I_{hERG} is attenuated 3) Inhibition of I_{hERG} is attenuated	[44]
Nicotine	*Nicotiana tabacum* (Solanaceae)	Two-microelectrode voltage-clamp assay using *Xenopus* oocytes	IC_{50}: 16.8 ± 2.2 µM [#]	[49]
		Canine ventricular myocytes – I_{Kr}	IC_{50}: 1.3 ± 0.5 µM [#]	[50]
		Guinea pig ventricular myocytes – I_{Kr} Conc.: 10, 30, 100 µM	Inhibition of I_{Kr} by 36.7 ± 1.3% (10 µM), 75.1 ± 3.6% (30 µM), 87.8 ± 2.9% (100 µM)	[51]
Oxymatrine	*Sophora flavescens* (Fabaceae)	Whole-cell patch-clamp assay using HEK293 cells Impact of temperature on compound potency was studied 1) Concentration-response experiment, temp.: 30°C 2) Conc.: 1, 10, 100, 300 µM; temp.: 30°C 3) Conc.: 1, 10, 100, 300 µM; temp.: 20°C	1) IC_{50}: 665.0 ± 1.3 µM 2) Inhibition of I_{hERG} by 6.9 ± 0.2% (1 µM), 19.0 ± 0.2% (10 µM), 31.6 ± 0.5% (100 µM), 43.2 ± 0.3% (300 µM) 3) Potentiation of I_{hERG} by 29.5 ± 1.8% (1 µM), 40.0 ± 0.6% (10 µM), 50.1 ± 0.9% (100 µM); inhibition of I_{hERG} by 36.5 ± 0.4% (300 µM)	[12]

Substance	Source	Bioassay	Observed Effect	Reference
Papaverine	*Papaver somniferum* (Papaveraceae)	Whole-cell patch-clamp assay using HEK293 cells	IC_{50}: 7.3 µM	[5]
		Whole-cell patch-clamp assay using HEK293 cells	IC_{50}: 0.58 µM	[1]
		Two-microelectrode voltage-clamp assay using *Xenopus* oocytes 1) Concentration-response experiment 2) Mutation study (hERG F656A, conc.: 50 µM) 3) Mutation study (hERG Y652A, conc.: 50 µM)	1) IC_{50}: 30.0 ± 1.8 µM 2) No significant effect on I_{hERG} 3) Inhibition of I_{hERG} is attenuated	[1]
		Two-microelectrode voltage-clamp assay using *Xenopus* oocytes	IC_{50}: 71.03 ± 4.75 µM	[2]
		HERG-Lite® assay Conc.: 10 µM	Classified as hERG blocker	[5]
Quinidine§	*Cinchona officinalis* (Rubiaceae)	Whole-cell patch-clamp assay using HEK293 cells	IC_{50}: 0.41 ± 0.04 µM	[52]
		Whole-cell patch-clamp assay using CHO cells	IC_{50}: 3.2 ± 0.3 µM	[53]
		Two-microelectrode voltage-clamp assay using *Xenopus* oocytes 1) Concentration-response experiment 2) Mutation study (hERG F656A) 3) Mutation study (hERG Y652A)	1) IC_{50}: 4.6 ± 1.2 µM 2) 125-fold reduction of compound potency 3) IC_{50}: 16.0 ± 1.7 µM	[16]
		Two-microelectrode voltage-clamp assay using *Xenopus* oocytes 1) Conc.: 10 µM 2) Mutation study (hERG Y652F, conc.: 10 µM)	1) Inhibition of I_{hERG} by 59.7 ± 2.7% 2) No significant difference to hERG WT, compound potency was not altered	[54]
Quinine	*Cinchona officinalis* (Rubiaceae)	Two-microelectrode voltage-clamp assay using *Xenopus* oocytes	IC_{50}: 57.0 ± 3.3 µM	[16]
Rhynchophylline	*Uncaria rhynchophylla* (Rubiaceae)	Two-microelectrode voltage-clamp assay using *Xenopus* oocytes 1) Concentration-response experiment 2) Conc.: 10, 100, 1000 µM	1) IC_{50}: 773.4 ± 42.5 µM 2) Inhibition of I_{hERG} by 9.5 ± 7.5% (10 µM), 16.2 ± 5.9% (100 µM), 72.6 ± 2.3% (1000 µM)	[55]

Substance	Source	Bioassay	Observed Effect	Reference
Reserpine	*Rauvolfia serpentina* (Apocynaceae)	FluxOR thallium influx assay using U-2 OS cells[Δ]	IC_{50}: 4.9 ± 1.7 µM	[56]
		Whole-cell patch-clamp assay using CHO-K1 cells[₸]	IC_{50}: 1.9 µM	[56]
Sophocarpine	*Sophora flavescens* (Fabaceae)	Whole-cell patch-clamp assay using HEK293 cells Conc.: 10, 30, 100, 300 µM	Inhibition of I_{hERG} by 1.1 ± 3.0% (10 µM), 17.1 ± 3.3% (30 µM), 32.7 ± 1.9% (100 µM), 56.0 ± 2.4% (300 µM)	[57]
		Whole-cell patch-clamp assay using HEK293 cells Conc: 10, 30, 100, 300 µM	Inhibition of I_{hERG} by 0.5 ± 3.0% (10 µM), 16.5 ± 1.9% (30 µM), 37.0 ± 1.7% (100 µM), 60.9 ± 1.4% (300 µM)	[58]
Sophoridine	*Sophora flavescens* (Fabaceae)	Whole-cell patch-clamp assay using HEK293 cells Conc: 10, 30, 100, 300 µM	Inhibition of I_{hERG} by 5.4 ± 2.3% (10 µM), 16.3 ± 2.6% (30 µM), 29.3 ± 2.1% (100 µM), 41.9 ± 2.0% (300 µM)	[58]
Theobromine	*Theobroma cacao* (Sterculiaceae)	Whole-cell patch-clamp assay using CHO cells Conc.: 100 µM	No significant effect on I_{hERG}	[35]
Theophylline	*Camellia sinensis* (Theaceae)	Two-microelectrode voltage-clamp assay using *Xenopus* oocytes Conc.: 500 µM	No effect on I_{hERG}	[2]

[‡] tsA201 cells: cells derived from HEK293 cells by stable transfection with SV40 temperature-sensitive T antigen.

[#] Decreases in step current amplitudes were taken as a measure of hERG channel inhibition.

[§] Representative *in vitro* data are listed. The available reports in the literature are by far higher.

[Δ] U-2 OS cells: human osteosarcoma cells.

[₸] CHO-K1 cells: subclone from the parental CHO cell line.

Flavonoids tested for hERG channel inhibition

The effects of flavonoids on heterologously expressed hERG channels have been first studied by Zitron et al., who screened a focused library of flavonoids and coumarin derivatives (Figure 7). The flavanone naringenin showed the highest activity among the compounds tested, and its hERG channel blocking properties were later on studied in more detail, both *in vitro* and *in vivo* [59-62].

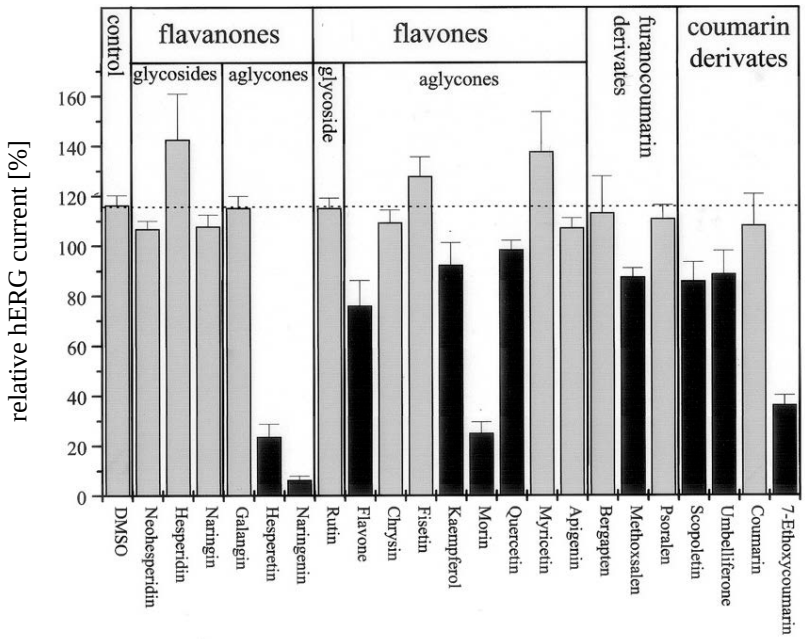

Figure 7. Blockade of hERG channels by selected flavonoids and coumarin derivatives. Compounds were tested at a concentration of 1 mM by means of a two-microelectrode voltage-clamp assay on *Xenopus laevis* oocytes. Relative hERG currents are given as mean ± SEM. Significant difference from control (DMSO, left column) is indicated by a darker color. Figure by Zitron et al., 2005 [59].

Naringenin is the main flavonoid in grapefruits and naturally occurs in glycosylated forms, with naringin being the most prominent glycoside. Quantitative data revealed that fresh grapefruits contain high amounts of naringin in the albedo tissue, where concentrations of up to 3.15 mg/g have been detected. Significantly lower concentrations were found in the flavedo layer and in the pulp, whereas the seeds showed the lowest naringin content [63]. It is well known that the naringin content in both commercially available and freshly prepared grapefruit juices can vary considerably. Regarding its concentration in commercial juices, ranges of 174-1492 µM,

82-2062 µM, and 309-1182 µM have been reported in literature [63-65]. Marked variations have been observed among different brands, and even among various batches of the same brand product. If the juice is prepared from fresh grapefruits, the squeezing procedure will have a major impact on the naringin level. Hand-squeezed juices typically show lower amounts of naringin compared to juices prepared with a squeezer or blender. Juices prepared by blending the whole fruits (with peel) will undoubtedly exhibit the highest naringin content. A notable finding from these studies was that the aglycone naringenin was either not detectable or only present in very low concentrations [63-65].

It has been shown that the consumption of 1 L of freshly squeezed pink grapefruit juice leads to a mild prolongation of the QTc interval in both young healthy volunteers and cardiomyopathy patients [59,62]. The observed effect is presumably attributable to naringenin, but synergistic effects with other grapefruit constituents cannot be ruled out. As mentioned in the previous chapter, an integrated risk assessment should always include information about the pharmacokinetic profile of the particular hERG channel blocker. Naringenin is comparatively well characterized in terms of human plasma concentrations after a single intake of grapefruit juice. The aglycone is formed in the distal parts of the small intestine and/or in the colon by hydrolysis of its native glycosides. There are, however, quite high interindividual variations with respect to its bioavailability [62,66]. For example, a mean peak plasma concentration of 6.0 ± 5.4 µM was found in healthy volunteers after consumption of a defined volume of grapefruit juice (8 mL/kg body weight, 349 mg/L naringenin[1]) [66].

[1] The concentration of naringenin in the grapefruit juice was determined after enzymatic hydrolysis of its naturally occurring glycosides.

Table 2. Flavonoids tested for hERG channel inhibition.

Substance	Source	Bioassay	Observed Effect	Reference
Acacetin	*Saussurea tridactyla* (Asteraceae)	Whole-cell patch-clamp assay using HEK293 cells	IC_{50}: 32.4 µM	[67]
Epigallocatechin-3-gallate (EGCG)	*Camellia sinensis* (Theaceae)	Whole-cell patch-clamp assay using CHO cells Conc.: 30, 100 µM	Inhibition of I_{hERG} by 1.3 ± 2.4% (30 µM), 22.7 ± 6.6% (100 µM)	[68]
		Whole-cell patch-clamp assay using HEK293 cells	IC_{50}: 6.0 µM	[69]
		Two-microelectrode voltage-clamp assay using *Xenopus* oocytes 1) Concentration-response experiment Conc.: 20 µM 2) Conc.: 20 µM	1) IC_{50}: 20.5 µM 2) Inhibition of I_{hERG} by 40.7 ± 4.4%	[69]
Hesperetin	*Citrus sinensis* (Rutaceae)	Two-microelectrode voltage-clamp assay using *Xenopus* oocytes	IC_{50}: 288.8 µM	[59]
		Two-microelectrode voltage-clamp assay using *Xenopus* oocytes 4) Concentration-response experiment 5) Conc.: 1 mM 6) Mutation study (hERG F656A, conc.: 1 mM) 7) Mutation study (hERG Y652A, conc.: 1 mM)	1) IC_{50}: 267.4 ± 26.5 µM 2) Reduction of I_{hERG} to 13.7 ± 5.3% 3) Reduction of I_{hERG} to 51.8 ± 5.1% 4) No significant difference to hERG WT, compound potency was not altered	[70]
Morin	*Morus alba* (Moraceae)	Two-microelectrode voltage-clamp assay using *Xenopus* oocytes	IC_{50}: 111.4 µM	[59]
Naringenin	*Citrus paradisi* (Rutaceae)	Whole-cell patch-clamp assay using HEK293 cells 1) Concentration-response experiment 2) Conc.: 1 µM	1) IC_{50}: 36.5 µM 2) Inhibition of I_{hERG} by 13.8 ± 2.4%	[59]
		Two-microelectrode voltage-clamp assay using *Xenopus* oocytes 1) Concentration-response experiment 2) Mutation study (hERG F656A, conc.: 1 mM) 3) Mutation study (hERG Y652A, conc.: 1 mM)	1) IC_{50}: 102.6 µM 2) Inhibition of I_{hERG} is attenuated 3) No significant difference to hERG WT, compound potency was not altered	[60]

Substance	Source	Bioassay	Observed Effect	Reference
Naringenin (continued)		Two-microelectrode voltage-clamp assay using *Xenopus* oocytes	IC_{50}: 102.3 µM	[59]
		Two-microelectrode voltage-clamp assay using *Xenopus* oocytes 1) Concentration-response experiment 2) Conc.: 10, 100, 1000 µM 3) Conc.: 100 µM, co-administration of a hERG channel blocking drug (1 µM: quinidine, azimilide, dofetilide, amiodarone) 4) Conc.: 100 µM, co-administration of a hERG channel blocking drug (10 µM: quinidine, azimilide, dofetilide, amiodarone)	1) IC_{50}: 173.3 ± 3.1 µM 2) Inhibition of I_{hERG} by 15 ± 5% (10 µM), 31 ± 6% (100 µM), 75 ± 5% (1000 µM) 3) Increased inhibition of I_{hERG} during co-application 4) Increased inhibition of I_{hERG} during co-application	[61]
Taxifolin-3-O-*β*-D-glycopyranoside	*Rhododendron mucronulatum* (Ericaceae)	Whole-cell patch-clamp assay using CHO cells Conc.: 5, 10, 30, 50, 100 µM	Inhibition of I_{hERG} by 12.0 ± 2.5% (5 µM), 18.1 ± 4.7% (10 µM), 26.3 ± 4.5% (30 µM), 35.4 ± 5.6% (50 µM), 36.9 ± 3.0% (100 µM)	[71]
5,7,4`-Trimethyl-apigenin	*Citrus sinensis* (Rutaceae)	Whole-cell patch-clamp assay using HEK293 cells	IC_{50}: 18.4 ± 1.2 µM	[72]

Miscellaneous structural classes tested for hERG channel inhibition

The naturally occurring triterpenoid celastrol has been shown to impair the hERG channel function by a dual mode of action. When tested at 10 μM in HEK293 cells, celastrol acutely inhibits I_{hERG} by 63 ± 10%. As revealed by Western blot analysis, celastrol also reduces the cell surface expression of the mature, fully glycosylated hERG channel protein after overnight incubation, with approximately 30% inhibition observed at a concentration of 200 nM [73]. Both mechanisms occur over different time and concentration scales, but the effect can appear additive following long-term exposure. From a clinical perspective, disrupting the hERG channel trafficking has been associated with a delayed onset of LQTS [74]. The cardiac glycoside digitoxin, for example, displays no direct hERG channel block but clearly reduces the cell surface expression of hERG channels at clinically relevant concentrations. However, digitoxin has typically not been associated with QT prolongation and TdP arrhythmia. As discussed by the authors, the observed hERG trafficking inhibition may contribute to the complex electrocardiographic changes seen with digitoxin in the clinic [75].

Table 3. Miscellaneous structural classes tested for hERG channel inhibition.

Substance	Source	Bioassay	Observed Effect	Reference
Celastrol	*Celastrus scandens* (Celastraceae)	Whole-cell patch-clamp assay using HEK293 cells Conc.: 10 µM	Inhibition of I_{hERG} by 63 ± 10%	[73]
Curcumin	*Curcuma zedoaria* (Zingiberaceae)	Whole-cell patch-clamp assay using HEK293 cells	IC_{50}: 5.55 µM	[76]
		Whole-cell patch-clamp assay using HEK293 cells	IC_{50}: 4.9 µM	[77]
		Whole-cell patch-clamp assay using HEK293 cells 1) Conc.: 10 µM 2) Mutation study (hERG F656A, conc.: 10 µM) 3) Mutation study (hERG Y652A, conc.: 10 µM)	1) Reduction of I_{hERG} to 14.9% 2) Reduction of I_{hERG} to 41.5% 3) Reduction of I_{hERG} to 25.3%	[78]
		Whole-cell patch-clamp assay using CHO-K1 cells[T]	IC_{50}: 22 µM	[56]
Digitoxin	*Digitalis purpurea* (Plantaginaceae)	Guinea pig ventricular myocytes – I_{Kr} Conc.: 500 nM	No effect on I_{Kr}	[75]
Digoxin	*Digitalis lanata* (Plantaginaceae)	Whole-cell patch-clamp assay using HEK293 cells Conc.: 500 nM	No significant effect on I_{hERG}	[75]
		Guinea pig ventricular myocytes – I_{Kr} Conc.: 1 µM	No significant effect on I_{Kr}	[79]
Digoxigenin	*Digitalis lanata* (Plantaginaceae)	Whole-cell patch-clamp assay using HEK293 cells Conc.: 1 µM	No significant effect on I_{hERG}	[75]
Dihydroartemisinin	*Artemisia annua* (Asteraceae)	Whole-cell patch-clamp assay using HEK293 cells	IC_{50}: 9.6 ± 1.0 µM (IC_{50}: 7.7 ± 0.9 µM in a second set of experiments)	[80]
Ginsenoside Re	*Panax ginseng* (Araliaceae)	Two-microelectrode voltage-clamp assay using *Xenopus* oocytes Conc.: 1 µM	No significant effect on I_{hERG}	[81]

Substance	Source	Bioassay	Observed Effect	Reference
Ginsenoside Re (continued)		Guinea pig ventricular myocytes – I_{Kr} Conc.: 3 µM	Inhibition of I_{Kr}	[82]
Ginsenoside Rg_3	*Panax ginseng* (Araliaceae)	Two-microelectrode voltage-clamp assay using *Xenopus* oocytes Screening of 7 ginsenosides and 2 ginsenoside aglycons Conc.: 1 µM	Potentiation of I_{hERG} – Rg_3 showed highest activity (potentiation of I_{hERG} by 18.8 ± 4.8%)	[81]
Glycyrrhetinic acid	*Glycyrrhiza glabra* (Fabaceae)	Two-microelectrode voltage-clamp assay using *Xenopus* oocytes 1) 18α- Glycyrrhetic acid, conc.: 100 µM 2) 18β- Glycyrrhetic acid, conc.: 100 µM	1) No significant effect on I_{hERG} 2) No significant effect on I_{hERG}	[83]
Hirsutenone	*Alnus japonica* (Betulaceae)	Whole-cell patch-clamp assay using CHO cells 1) Concentration-response experiment 2) Conc.: 5, 10, 20, 30, 50 µM	3) IC_{50}: 14.9 ± 2.0 µM 4) Inhibition of I_{hERG} by 13.3 ± 3.1% (5 µM), 29.5 ± 2.9% (10 µM), 42.2 ± 10.2% (20 µM), 55.9 ± 8.8% (30 µM), 83.7 ± 10.8% (50 µM)	[84]
Mallotoxin	*Mallotus philippensis* (Euphorbiaceae)	Whole-cell patch-clamp assay using CHO cells Conc.: 0.1, 0.5, 2.5, 10 µM	Concentration-dependent potentiation of I_{hERG}	[85]
Ouabain	*Strophanthus gratus* (Apocynaceae)	Patch-clamp assay Conc.: ≥ 100 µM	No effect on I_{hERG}	[19]
Oxypeucedanin	*Angelica dahurica* (Apiaceae)	Whole-cell patch-clamp assay using HEK293 cells Conc.: 1 µM	No effect on I_{hERG}	[86]
Paeoniflorin	*Paeonia lactiflora* (Paeoniaceae)	Whole-cell patch-clamp assay using HEK293 cells Conc.: 100 µM	No effect on I_{hERG}	[87]
Phorbol-12-myristate-13-acetate	*Croton tiglium* (Euphorbiaceae)	Guinea pig ventricular myocytes – I_{Kr} Conc.: 1, 10, 100 nM	Inhibition of I_{Kr} by 2.7 ± 8.7% (1 nM), 20.0 ± 7.3% (10 nM), 44.0 ± 7.4% (100 nM)	[88]
Resveratrol	Phytoalexin in red wine	Whole-cell patch-clamp assay using HEK293 cells Conc.: 1, 10, 100 µM	Concentration-dependent inhibition of I_{hERG}	[89]

Substance	Source	Bioassay	Observed Effect	Reference
Resveratrol (continued)		Whole-cell patch-clamp assay using HEK293 cells Conc.: 10 µM	No effect on I_{hERG}	[5]
		Guinea pig ventricular myocytes – I_{Kr} Conc.: 100 µM	No significant effect on I_{Kr}	[90]
		HERG-Lite® assay Conc.: 100 µM	Classified as non-hERG blocker	[5]
Tanshinone IIA	*Salvia miltiorrhiza* (Lamiaceae)	Whole-cell patch-clamp assay using HEK293 cells Conc.: 100 µM	No significant effect on I_{hERG}	[91]

[₸] CHO-K1 cells: subclone from the parental CHO cell line.

References

1 *Kim YJ, Hong HK, Lee HS, Moh SH, Park JC, Jo SH, Choe H*. Papaverine, a vasodilator, blocks the pore of the hERG channel at submicromolar concentration. J Cardiovasc Pharm 2008; 52: 485-493

2 *Kim CS, Lee N, Son SJ, Lee KS, Kim HS, Kwak YG, Chae SW, Lee S, Jeon BH, Park JB*. Inhibitory effects of coronary vasodilator papaverine on heterologously expressed hERG currents in *Xenopus* oocytes. Acta Pharmacol Sin 2007; 28: 503-510

3 *Witchel HJ, Milnes JT, Mitcheson JS, Hancox JC*. Troubleshooting problems with *in vitro* screening of drugs for QT interval prolongation using hERG K^+ channels expressed in mammalian cell lines and *Xenopus* oocytes. J Pharmacol Toxicol Methods 2002; 48: 65-80

4 *Kirsch GE, Trepakova ES, Brimecombe JC, Sidach SS, Erickson HD, Kochan MC, Shyjka LM, Lacerda AE, Brown AM*. Variability in the measurement of hERG potassium channel inhibition: Effects of temperature and stimulus pattern. J Pharmacol Toxicol Methods 2004; 50: 93-101

5 *Wible BA, Hawryluk P, Ficker E, Kuryshev YA, Kirsch G, Brown AM*. HERG-Lite®: A novel comprehensive high-throughput screen for drug-induced hERG risk. J Pharmacol Toxicol Methods 2005; 52: 136-145

6 *Yao JA, Du X, Lu D, Baker RL, Daharsh E, Atterson P*. Estimation of potency of hERG channel blockers: Impact of voltage protocol and temperature. J Pharmacol Toxicol Methods 2005; 52: 146-153

7 *Lin JJ, Guo J, Gang HY, Wojciechowski P, Wigle JT, Zhang ST*. Intracellular K^+ is required for the inactivation-induced high-affinity binding of cisapride to hERG channels. Mol Pharmacol 2005; 68: 855-865

8 *Guo J, Gang HY, Zhang ST*. Molecular determinants of cocaine block of human ether-a-go-go-related gene potassium channels. J Pharmacol Exp Ther 2006; 317: 865-874

9 *Stork D, Timin EN, Berjukow S, Huber C, Hohaus A, Auer M, Hering S*. State dependent dissociation of hERG channel inhibitors. Brit J Pharmacol 2007; 151: 1368-1376

10 *Vandenberg JI, Varghese A, Lu Y, Bursill JA, Mahaut-Smith MP, Huang CL*. Temperature dependence of human ether-a-go-go-related gene K^+ currents. Am J Physiol Cell Physiol 2006; 291: C165-C175

11 *Zhou ZF, Gong QM, Ye B, Fan Z, Makielski JC, Robertson GA, January CT*. Properties of hERG channels stably expressed in HEK293 cells studied at physiological temperature. Biophys J 1998; 74: 230-241

12 *Hu MQ, Dong ZX, Zhao WX, Sun J, Zhao X, Gu DF, Zhang Y, Li BX, Yang BF*. The novel mechanism of oxymatrine affecting hERG currents at different temperatures. Cell Physiol Biochem 2010; 26: 513-522

13 *Grilo LS, Carrupt PA, Abriel H*. Stereoselective inhibition of the hERG1 potassium channel. Front Pharmacol 2010; 1: 137

14 *Brocks DR, Mehvar R*. Stereoselectivity in the pharmacodynamics and pharmacokinetics of the chiral antimalarial drugs. Clin Pharmacokinet 2003; 42: 1359-1382

15 *White NJ*. Cardiotoxicity of antimalarial drugs. Lancet Infect Dis 2007; 7: 549-558

16 *Sanchez-Chapula JA, Ferrer T, Navarro-Polanco RA, Sanguinetti MC*. Voltage-dependent profile of human ether-a-go-go-related gene channel block is influenced by a single residue in the S6 transmembrane domain. Mol Pharmacol 2003; 63: 1051-1058

17 *Forgo P, Borcsa B, Csupor D, Fodor L, Berkecz R, Molnár A, Hohmann J*. Diterpene alkaloids from *Aconitum anthora* and assessment of the hERG-inhibiting ability of *Aconitum* alkaloids. Planta Med 2011; 77: 368-373

18 *Kiss T, Orvos P, Bánsághi S, Forgo P, Jedlinszki N, Tálosi L, Hohmann J, Csupor D*. Identification of diterpene alkaloids from *Aconitum napellus* subsp. *firmum* and GIRK channel activities of some *Aconitum* alkaloids. Fitoterapia 2013; 90: 85-93

19 *Guo L, Dong Z, Guthrie H*. Validation of a guinea pig Langendorff heart model for assessing potential cardiovascular liability of drug candidates. J Pharmacol Toxicol Methods 2009; 60: 130-151

20 *Li YF, Tu DN, Xiao H, Du YM, Zou AR, Liao YH, Dong SH*. Aconitine blocks hERG and Kv1.5 potassium channels. J Ethnopharmacol 2010; 131: 187-195

21 *Kiesecker C, Zitron E, Lück S, Bloehs R, Scholz EP, Kathöfer S, Thomas D, Kreye VAW, Katus HA, Schoels W, Karle CA, Kiehn J*. Class Ia anti-arrhythmic drug ajmaline blocks hERG potassium channels: Mode of action. N-S Arch Pharmacol 2004; 370: 423-435

22 *Lin K, Liu YQ, Xu B, Gao JL, Fu YC, Chen Y, Xue Q, Li Y*. Allocryptopine and benzyltetrahydropalmatine block hERG potassium channels expressed in HEK293 cells. Acta Pharmacol Sin 2013; 34: 847-858
23 *Zhao XY, Liu YQ, Fu YC, Xu B, Gao JL, Zheng XQ, Lin M, Chen MY, Li Y*. Frequency- and state-dependent blockade of human ether-a-go-go-related gene K^+ channel by arecoline hydrobromide. Chinese Med J-Peking 2012; 125: 1068-1075
24 *Ferreira S, Crumb WJ, Carlton CG, Clarkson CW*. Effects of cocaine and its major metabolites on the hERG-encoded potassium channel. J Pharmacol Exp Ther 2001; 299: 220-226
25 *Rodriguez-Menchaca A, Ferrer-Villada T, Lara J, Fernandez D, Navarro-Polanco RA, Sanchez-Chapula JA*. Block of hERG channels by berberine: Mechanisms of voltage- and state-dependence probed with site-directed mutant channels. J Cardiovasc Pharm 2006; 47: 21-29
26 *Li BX, Yang BF, Zhou J, Xu CQ, Li YR*. Inhibitory effects of berberine on I_{K1}, I_K, and hERG channels of cardiac myocytes. Acta Pharmacol Sin 2001; 22: 125-131
27 *Wang YX, Zheng YM*. Ionic mechanism responsible for prolongation of cardiac action potential duration by berberine. J Cardiovasc Pharm 1997; 30: 214-222
28 *Cockerill SL, Mitcheson JS*. Direct block of human ether-a-go-go-related gene potassium channels by caffeine. J Pharmacol Exp Ther 2006; 316: 860-868
29 *Xing JL, Ma JH, Zhang PH, Fan XR*. Block effect of capsaicin on hERG potassium currents is enhanced by S6 mutation at Y652. Eur J Pharmacol 2010; 630: 1-9
30 *Chen WH, Wang WY, Zhang J, Yang D, Wang YP*. State-dependent blockade of human ether-a-go-go-related gene (hERG) K^+ channels by changrolin in stably transfected HEK293 cells. Acta Pharmacol Sin 2010; 31: 915-922
31 *Harmati G, Papp F, Szentandrássy N, Bárándi L, Ruzsnavszky F, Horváth B, Bányász T, Magyar J, Panyi G, Krasznai Z, Nánási PP*. Effects of the PKC inhibitors chelerythrine and bisindolylmaleimide I (GF 109203X) on delayed rectifier K^+ currents. N-S Arch Pharmacol 2011; 383: 141-148
32 *Zhang ST, Rajamani S, Chen YM, Gong QM, Rong YJ, Zhou ZF, Ruoho A, January CT*. Cocaine blocks hERG, but not KvLQT1+minK, potassium channels. Mol Pharmacol 2001; 59: 1069-1076
33 *O'Leary ME*. Inhibition of human ether-a-go-go potassium channels by cocaine. Mol Pharmacol 2001; 59: 269-277
34 *Clarkson CW, Xu YQ, Chang CT, Follmer CH*. Analysis of the ionic basis for cocaine's biphasic effect on action potential duration in guinea-pig ventricular myocytes. J Mol Cell Cardiol 1996; 28: 667-678
35 *Deisemann H, Ahrens N, Schlobohm I, Kirchhoff C, Netzer R, Möller C*. Effects of common antitussive drugs on the hERG potassium channel current. J Cardiovasc Pharm 2008; 52: 494-499
36 *Katchman AN, McGroary KA, Kilborn MJ, Kornick CA, Manfredi PL, Woosley RL, Ebert SN*. Influence of opioid agonists on cardiac human ether-a-go-go-related gene K^+ currents. J Pharmacol Exp Ther 2002; 303: 688-694
37 *Zhao J, Wang QX, Xu J, Zhao J, Liu G, Peng SQ*. Cyclovirobuxine D inhibits the currents of hERG potassium channels stably expressed in HEK293 cells. Eur J Pharmacol 2011; 660: 259-267
38 *Zhao J, Lian Y, Lu CF, Jing L, Yuan HT, Peng SQ*. Inhibitory effects of a bisbenzylisoquinline alkaloid dauricine on hERG potassium channels. J Ethnopharmacol 2012; 141: 685-691
39 *Xia JS, Guo DL, Zhang Y, Zhou ZN, Zeng FD, Hu CJ*. Inhibitory effects of dauricine on potassium currents in guinea pig ventricular myocytes. Acta Pharmacol Sin 2000; 21: 60-64
40 *Liu QN, Mao XF, Zeng FD, Jin S, Yang XY*. Effect of daurisoline on hERG channel electrophysiological function and protein expression. J Nat Prod 2012; 75: 1539-1545
41 *Vigneault P, Bourgault S, Kaddar N, Caillier B, Pilote S, Patoine D, Simard C, Drolet B*. Galantamine (Reminyl®) delays cardiac ventricular repolarization and prolongs the QT interval by blocking the hERG current. Eur J Pharmacol 2012; 681: 68-74
42 *Huang XF, Yang YM, Zhu J, Xu DL, Peng J, Liu JH*. Comparative effects of Guanfu base A and Guanfu base G on hERG K^+ channel. J Cardiovasc Pharm 2012; 59: 77-83
43 *Huang XF, Yang YM, Zhu J, Dai Y, Pu JL*. The effects of a novel anti-arrhythmic drug, acehytisine hydrochloride, on the human ether-a-go-go related gene K^+ channel and its trafficking. Basic Clin Pharmacol Toxicol 2009; 104: 145-154
44 *Dong ZX, Zhao X, Gu DF, Shi YQ, Zhang J, Hu XX, Hu MQ, Yang BF, Li BX*. Comparative effects of liensinine and neferine on the human ether-a-go-go-related gene potassium channel and pharmacological activity analysis. Cell Physiol Biochem 2012; 29: 431-442

45 *Jeong I, Choi BH, Hahn SJ*. Effects of lobeline, a nicotinic receptor ligand, on the cloned Kv1.5. Pflug Arch Eur J Phy 2010; 460: 851-862
46 *Wu HJ, Zou AR, Xie F, Du YM, Cao Y, Liu YN, Yang JY, Li XM*. Effect of matrine on human ether a go-go related gene (hERG) channels expressed in Chinese hamster ovary cells. Chin J Integr Med 2010; 16: 430-434
47 *Zhang Y, Dong ZX, Jin LY, Zhang KP, Zhao X, Fu J, Gong Y, Sun MM, Yang BF, Li BX*. Arsenic trioxide-induced hERG K^+ channel deficiency can be rescued by matrine and oxymatrine through up-regulating transcription factor Sp1 expression. Biochem Pharmacol 2013; 85: 59-68
48 *Gu DF, Li XL, Qi ZP, Shi SS, Hu MQ, Liu DM, She CB, Lv YJ, Li BX, Yang BF*. Blockade of hERG K^+ channel by isoquinoline alkaloid neferine in the stable transfected HEK293 cells. N-S Arch Pharmacol 2009; 380: 143-151
49 *Wang HZ, Shi H, Liao SJ, Wang ZG*. Inactivation gating determines nicotine blockade of human hERG channels. Am J Physiol-Heart C 1999; 277: H1081-H1088
50 *Wang HZ, Shi H, Wang ZG*. Nicotine depresses the functions of multiple cardiac potassium channels. Life Sci 1999; 65: PL143-PL149
51 *Satoh H*. Modulation by nicotine of the ionic currents in guinea pig ventricular cardiomyocytes: Relatively higher sensitivity to I_{Kr} and I_{K1}. Vasc Pharmacol 2002; 39: 55-61
52 *Paul AA, Witchel HJ, Hancox JC*. Inhibition of the current of heterologously expressed hERG potassium channels by flecainide and comparison with quinidine, propafenone and lignocaine. Brit J Pharmacol 2002; 136: 717-729
53 *Perrin MJ, Kuchel PW, Campbell TJ, Vandenberg JI*. Drug binding to the inactivated state is necessary but not sufficient for high-affinity binding to human ether-a-go-go-related gene channels. Mol Pharmacol 2008; 74: 1443-1452
54 *Ishii K, Kondo K, Takahashi M, Kimura M, Endoh M*. An amino acid residue whose change by mutation affects drug binding to the hERG channel. Febs Lett 2001; 506: 191-195
55 *Gui L, Li ZW, Du R, Yuan GH, Li W, Ren FX, Li J, Yang JG*. Inhibitory effect of rhynchophylline on human ether-a-go-go related gene channel. Acta Pharmacol Sin 2005; 57: 648-652
56 *Xia MH, Shahane SA, Huang RL, Titus SA, Shum E, Zhao Y, Southall N, Zheng W, Witt KL, Tice RR, Austin CP*. Identification of quaternary ammonium compounds as potent inhibitors of hERG potassium channels. Toxicol Appl Pharm 2011; 252: 250-258
57 *Zhao XL, Qi ZP, Fang C, Chen MH, Lv YJ, Li BX, Yang BF*. HERG K^+ channel blockade by the novel antiviral drug sophocarpine. Biol Pharm Bull 2008; 31: 627-632
58 *Zhao XL, Gu DF, Qi ZP, Chen MH, Wei T, Li BX, Yang BF*. Comparative effects of sophocarpine and sophoridine on hERG K^+ channel. Eur J Pharmacol 2009; 607: 15-22
59 *Zitron E, Scholz E, Owen RW, Lück S, Kiesecker C, Thomas D, Kathöfer S, Niroomand F, Kiehn J, Kreye VAW, Katus HA, Schoels W, Karle CA*. QTc prolongation by grapefruit juice and its potential pharmacological basis: hERG channel blockade by flavonoids. Circulation 2005; 111: 835-838
60 *Scholz EP, Zitron E, Kiesecker C, Lück S, Thomas D, Kathöfer S, Kreye VAW, Katus HA, Kiehn J, Schoels W, Karle CA*. Inhibition of cardiac hERG channels by grapefruit flavonoid naringenin: Implications for the influence of dietary compounds on cardiac repolarisation. N-S Arch Pharmacol 2005; 371: 516-525
61 *Lin CR, Ke XG, Ranade V, Somberg J*. The additive effects of the active component of grapefruit juice (naringenin) and antiarrhythmic drugs on hERG inhibition. Cardiology 2008; 110: 145-152
62 *Piccirillo G, Magri D, Matera S, Magnanti M, Pasquazzi E, Schifano E, Velitti S, Mitra M, Marigliano V, Paroli M, Ghiselli A*. Effects of pink grapefruit juice on QT variability in patients with dilated or hypertensive cardiomyopathy and in healthy subjects. Transl Res 2008; 151: 267-272
63 *De Castro WV, Mertens-Talcott S, Rubner A, Butterweck V, Derendorf H*. Variation of flavonoids and furanocoumarins in grapefruit juices: A potential source of variability in grapefruit juice-drug interaction studies. J Agr Food Chem 2006; 54: 249-255
64 *Ho PC, Saville DJ, Coville PF, Wanwimolruk S*. Content of CYP3A4 inhibitors, naringin, naringenin and bergapten in grapefruit and grapefruit juice products. Pharm Acta Helv 2000; 74: 379-385
65 *Vandermolen KM, Cech NB, Paine MF, Oberlies NH*. Rapid quantitation of furanocoumarins and flavonoids in grapefruit juice using ultra-performance liquid chromatography. Phytochem Analysis 2013; 24: 654-660

66 *Erlund I, Meririnne E, Alfthan G, Aro A*. Plasma kinetics and urinary excretion of the flavanones naringenin and hesperetin in humans after ingestion of orange juice and grapefruit juice. J Nutr 2001; 131: 235-241

67 *Li GR, Wang HB, Qin GW, Jin MW, Tang Q, Sun HY, Du XL, Deng XL, Zhang XH, Chen JB, Chen L, Xu XH, Cheng LC, Chiu SW, Tse HF, Vanhoutte PM, Lau CP*. Acacetin, a natural flavone, selectively inhibits human atrial repolarization potassium currents and prevents atrial fibrillation in dogs. Circulation 2008; 117: 2449-2457

68 *Kang JS, Cheng H, Ji JZ, Incardona J, Rampe D. In vitro* electrocardiographic and cardiac ion channel effects of (-)-epigallocatechin-3-gallate, the main catechin of green tea. J Pharmacol Exp Ther 2010; 334: 619-626

69 *Kelemen K, Kiesecker C, Zitron E, Bauer A, Scholz E, Bloehs R, Thomas D, Greten J, Remppis A, Schoels W, Katus HA, Karle CA*. Green tea flavonoid epigallocatechin-3-gallate (EGCG) inhibits cardiac hERG potassium channels. Biochem Bioph Res Co 2007; 364: 429-435

70 *Scholz EP, Zitron E, Kiesecker C, Thomas D, Kathöfer S, Kreuzer J, Bauer A, Katus HA, Remppis A, Karle CA, Greten J*. Orange flavonoid hesperetin modulates cardiac hERG potassium channel via binding to amino acid F656. Nutr Metab Cardiovas 2007; 17: 666-675

71 *Yun J, Bae H, Choi SE, Kim JH, Choi YW, Lim I, Lee CS, Lee MW, Ko JH, Seo SJ, Bang H*. Taxifolin glycoside blocks human ether-a-go-go related gene K^+ channels. Korean J Physiol Pharmacol 2013; 17: 37-42

72 *Liu Y, Xu XH, Liu Z, Du XL, Chen KH, Xin X, Jin ZD, Shen JZ, Hu Y, Li GR, Jin MW*. Effects of the natural flavone trimethylapigenin on cardiac potassium currents. Biochem Pharmacol 2012; 84: 498-506

73 *Sun HY, Liu XD, Xiong QJ, Shikano S, Li M*. Chronic inhibition of cardiac Kir2.1 and hERG potassium channels by celastrol with dual effects on both ion conductivity and protein trafficking. J Biol Chem 2006; 281: 5877-5884

74 *Yeung KS, Meanwell NA*. Inhibition of hERG channel trafficking: An under-explored mechanism for drug-induced QT prolongation. Chemmedchem 2008; 3: 1501-1502

75 *Wang L, Wible BA, Wan XP, Ficker E*. Cardiac glycosides as novel inhibitors of human ether-a-go-go-related gene channel trafficking. J Pharmacol Exp Ther 2007; 320: 525-534

76 *Hu CW, Sheng Y, Zhang Q, Liu HB, Xie X, Ma WC, Huo R, Dong DL*. Curcumin inhibits hERG potassium channels *in vitro*. Toxicol Lett 2012; 208: 192-196

77 *Helson L, Shopp G, Bouchard A, Majeed M*. Liposome mitigation of curcumin inhibition of cardiac potassium delayed-rectifier current. Journal of Receptor, Ligand and Channel Research 2012; 5: 1-8

78 *Choi SW, Kim KS, Shin DH, Yoo HY, Choe H, Ko TH, Youm JB, Kim WK, Zhang YH, Kim SJ*. Class 3 inhibition of hERG K^+ channel by caffeic acid phenethyl ester (CAPE) and curcumin. Pflug Arch Eur J Phy 2013; 465: 1121-1134

79 *Rocchetti M, Besana A, Mostacciuolo G, Ferrari P, Micheletti R, Zaza A*. Diverse toxicity associated with cardiac Na^+/K^+ pump inhibition: Evaluation of electrophysiological mechanisms. J Pharmacol Exp Ther 2003; 305: 765-771

80 *Borsini F, Crumb W, Pace S, Ubben D, Wible B, Yan GX, Funck-Brentano C. In vitro* cardiovascular effects of dihydroartemisin-piperaquine combination compared with other antimalarials. Antimicrob Agents Ch 2012; 56: 3261-3270

81 *Choi SH, Shin TJ, Hwang SH, Lee BH, Kang J, Kim HJ, Jo SH, Choe H, Nah SY*. Ginsenoside Rg_3 decelerates hERG K^+ channel deactivation through Ser631 residue interaction. Eur J Pharmacol 2011; 663: 59-67

82 *Bai CX, Sunami A, Namiki T, Sawanobori T, Furukawa T*. Electrophysiological effects of ginseng and ginsenoside Re in guinea pig ventricular myocytes. Eur J Pharmacol 2003; 476: 35-44

83 *Du YM, Xia CK, Zhao N, Dong Q, Lei M, Xia JH*. 18β-Glycyrrhetinic acid preferentially blocks late Na current generated by ΔKPQ Nav1.5 channels. Acta Pharmacol Sin 2012; 33: 752-760

84 *Yun J, Bae H, Choi SE, Kim JH, Choi YW, Lim I, Lee CS, Lee MW, Ko JH, Seo SJ, Bang H*. Hirsutenone directly blocks human ether-a-go-go related gene K^+ channels. Biol Pharm Bull 2011; 34: 1815-1822

85 *Zeng HY, Lozinskaya IM, Lin ZJ, Willette RN, Brooks DP, Xu XP*. Mallotoxin is a novel human ether-a-go-go-related gene (hERG) potassium channel activator. J Pharmacol Exp Ther 2006; 319: 957-962

86 *Eun JS, Park JA, Choi BH, Cho SK, Kim DK, Kwak YG*. Effects of oxypeucedanin on hKv1.5 and action potential duration. Biol Pharm Bull 2005; 28: 657-660

87 *Wang RR, Li N, Zhang YH, Ran YQ, Pu JL*. The effects of paeoniflorin monomer of a Chinese herb on cardiac ion channels. Chinese Med J-Peking 2011; 124: 3105-3111

88 *Kiehn J, Karle C, Thomas D, Yao X, Brachmann J, Kübler W*. HERG potassium channel activation is shifted by phorbol esters via protein kinase A-dependent pathways. J Biol Chem 1998; 273: 25285-25291

89 *Zhao WX, Qi ZP, Bai YL, Zhang Y, Zhao XL, Lue YJ, Li BX, Yang BF*. Effect of resveratrol on function of hERG K^+ channels (English abstract). Chinese Pharmacological Bulletin 2007; 23: 865-869

90 *Zhang Y, Liu YY, Wang T, Li BX, Li HW, Wang ZG, Yang BF*. Resveratrol, a natural ingredient of grape skin: Antiarrhythmic efficacy and ionic mechanisms. Biochem Bioph Res Co 2006; 340: 1192-1199

91 *Sun DD, Wang HC, Wang XB, Luo Y, Jin ZX, Li ZC, Li GR, Dong MQ*. Tanshinone IIA: A new activator of human cardiac KCNQ1/KCNE1 (I_{Ks}) potassium channels. Eur J Pharmacol 2008; 590: 317-321

2.4. Identification of ion channel ligands from plant extracts

Ion channels are pore-forming membrane proteins that permit the passive flow of ions down their electrochemical gradients. Key features are the gating properties, and ion channels are typically classified into multiple classes based on how their opening and closure is regulated. Modulation of gating can occur, for example, in response to chemical stimuli (intracellular or extracellular ligands), changes in transmembrane potential, changes in temperature, or mechanical forces. Ion channels are expressed in virtually all cell types in the human body and are involved in various physiological processes, including nerve and muscle excitation, hormone secretion, salt and water balance, learning and memory, fertilization, and sensory transduction. Defects in ion channel function have been associated with a wide range of diseases; hence, it is not surprising that ion channels are attractive targets in current and future drug discovery [1-3]. Moreover, profiling of putative lead compounds against a panel of ion channels is nowadays routinely performed to evaluate selectivity within a family of related ion channels as well as potential safety liabilities (so-called off-target activities) [4].

Natural product-based drug discovery has been a historically successful approach for the discovery of new lead compounds. They can either be used as such or serve as inspiration for synthetic efforts [5]. A recent review on new chemical entities (NCEs) approved as drugs over a 30-year time frame (January 1, 1981 to December 31, 2010) highlighted that approximately 34% of all small molecules directly derived from natural products [6]. We currently pursue an interdisciplinary screening approach aiming at the identification of ion channel ligands in plant extracts. Special emphasis has been placed on a screening for hERG channel inhibition (representing the most critical ion channel for cardiac safety) and the discovery of new scaffolds for positive $GABA_A$ receptor modulators (representing a primary drug target in the central nervous system). One of the principle challenges in studying ion channels and their ligands is to

obtain detailed information regarding the nature of interactions, especially whether a test compound has agonistic or antagonistic effects, or a preference for a particular channel subtype [7]. Electrophysiology has a solid and undisputed position in the analysis of ion channels, although this methodology is in general labor-intensive, time-consuming, and has a low throughput [8,9]. Recent advances have focused on increasing the throughput by automating certain process steps, thus allowing parallel recordings from several cells [7,9]. Automated patch-clamp platforms usually require stably transfected cell lines, which makes the system less flexible when working with multiple ion channels. Two-electrode voltage-clamp (TEVC) recordings from *Xenopus* oocytes are an equally useful means for the functional characterization of heterologously expressed ion channels. Several properties make the *Xenopus* oocyte system particularly suitable for such studies: (i) oocytes are robust cells, easy to handle (up to 1.2 mm in diameter), and can be obtained in large numbers; (ii) they are easily maintained in inorganic buffer solution; (iii) exogenous membrane proteins are expressed at relatively high levels; (iv) the *Xenopus* oocyte expression system is highly flexible with respect to the targets, meaning that different mutant channels (e.g., hERG Y652A and hERG F656A) or certain channel subtypes (e.g., $GABA_A$ receptors composed of $\alpha_1\beta_2\gamma_{2S}$ subunits) can be investigated; (v) only few ion channels are endogenously expressed in *Xenopus* oocytes, allowing the ion channel of interest to be studied in virtual isolation [9,10]. In the search for new plant-derived hERG channel inhibitors and positive $\alpha_1\beta_2\gamma_{2S}$ $GABA_A$ receptor modulators, we employed a medium-throughput two-microelectrode voltage-clamp assay with *Xenopus* oocytes which transiently expressed the desired ion channel. The principle of this approach is shown in Figure 8.

Herbal extracts are highly complex mixtures and usually contain several hundreds of constituents. Among the wealth of plant secondary metabolites, probably only one or just a few are responsible for a particular pharmacological effect. Tracking bioactive compounds in such

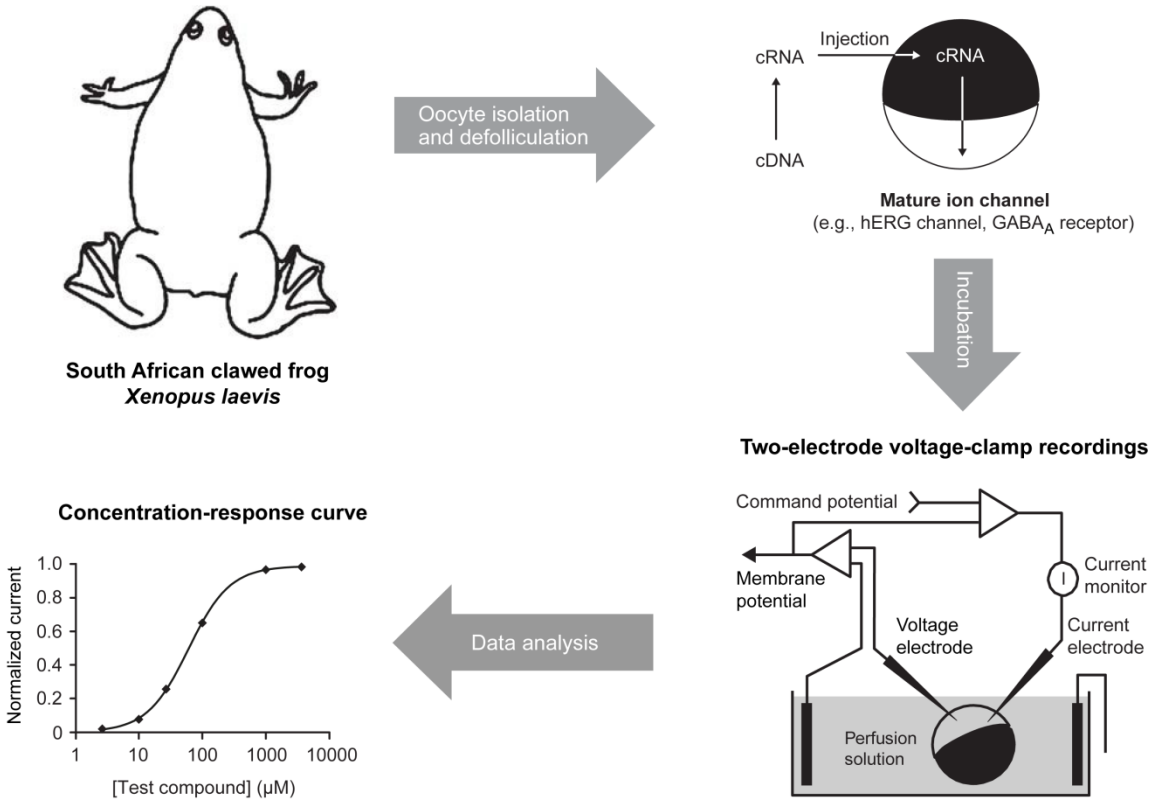

Figure 8. Schematic workflow of TEVC recordings from *Xenopus* oocytes. The oocytes are surgically removed from *Xenopus laevis* and defolliculated by enzymatic treatment. Stage V–VI oocytes are injected with the desired cRNA and incubated to ensure expression of functional ion channels. TEVC recordings allow a direct measurement of ion channel activity by quantifying the ion flux across the oocyte membrane. Standardized solution applications to the oocytes and a medium sample throughput can be achieved by means of an automated fast perfusion system (for details, see [11]). Adapted from Kvist et al., 2011 [9].

matrices is like “searching for the needle in the haystack” and, thus, a highly challenging task. The judicious interfacing of biological data with chemo-analytical information remains a cornerstone to match the timelines and the workflow of modern natural product-based drug discovery. Numerous innovative approaches have emerged over the past two decades and opened new possibilities for the rapid localization and characterization of bioactive compounds in crude extracts. The unbroken trend towards miniaturization, automation, and multi-hyphenated systems has also considerably increased the potential of bioactivity screening [12-14]. High-performance liquid chromatography (HPLC) has undoubtedly become the most versatile technique for the

efficient separation of extract constituents prior to their detection. An overview of the detection methods used in natural product analysis, as well as their potential and limitations can be found in a dedicated review [15].

For the discovery of plant-derived ion channel ligands, we have used an HPLC-based activity profiling approach which combines HPLC microfractionation with on-line and off-line spectroscopy, and bioactivity testing of each fraction (Figure 9) [13,14]. This strategy enables the activity to be assigned to chromatographic peaks, and to be correlated with on-line HPLC-UV-MS data. Measuring the UV-Vis absorbance is particularly useful for the detection of natural products with characteristic chromophores, whereas MS detection provides important information on the structure of the analytes, such as molecular weight, molecular formula, and diagnostic ion

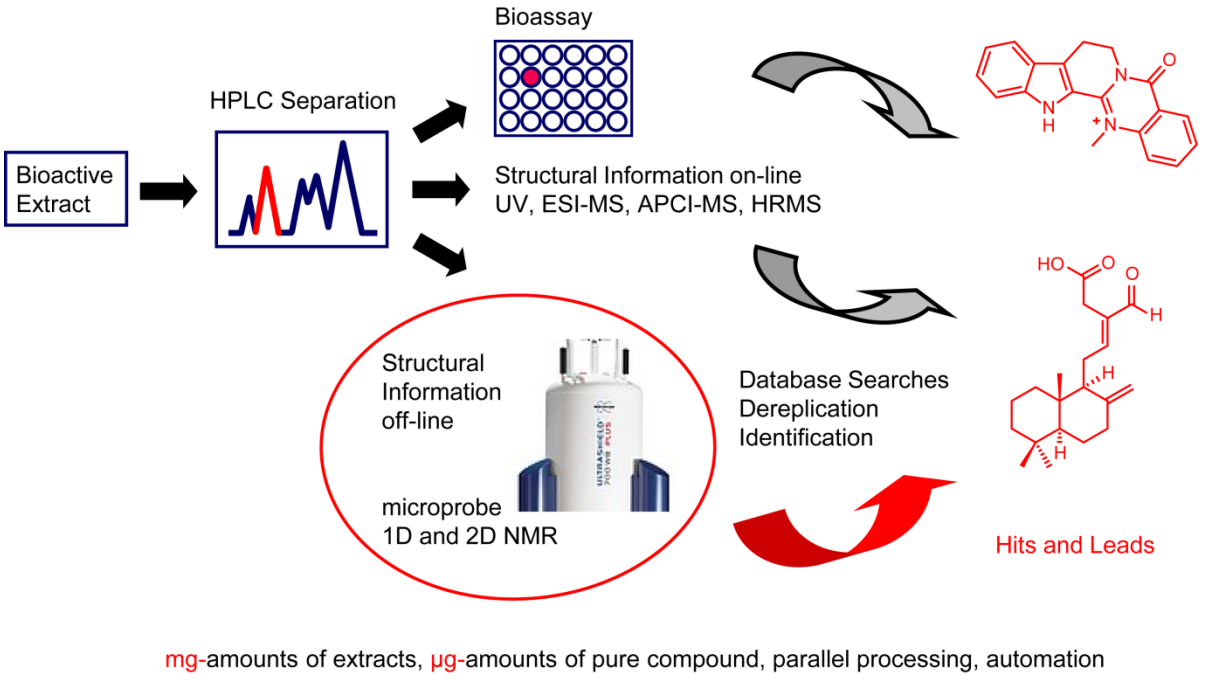

Figure 9. Principle of HPLC-based activity profiling. An extract is separated by gradient HPLC, and collected microfractions are tested in the particular bioassay. Simultaneously, on-line (UV and MS) and off-line (microprobe NMR) spectroscopic data are recorded. Spectral data are evaluated in combination with chemotaxonomic information and physicochemical data provided by natural product databases. Note that the characterization of bioactive compounds in crude extracts is already possible with minute sample amounts. Adapted from Potterat and Hamburger, 2013 [14].

fragments. Compound dereplication and identification, however, often requires additional structural information (e.g., NMR data) to distinguish between already known constituents and new metabolites. Determining the absolute configuration of chiral natural products is also of great importance to understand stereoselective pharmacological effects and to establish reliable structure-activity relationships. A targeted preparative isolation is carried out if the active principles are of sufficient interest for further pharmacological evaluation, or in the case of compounds possessing novel spectroscopic features for complete structure elucidation.

References

1 *Ashcroft FM*. From molecule to malady. Nature 2006; 440: 440-447

2 *Bagal SK, Brown AD, Cox PJ, Omoto K, Owen RM, Pryde DC, Sidders B, Skerratt SE, Stevens EB, Storer RI, Swain NA*. Ion channels as therapeutic targets: A drug discovery perspective. J Med Chem 2013; 56: 593-624

3 *Restrepo-Angulo I, De Vizcaya-Ruiz A, Camacho J*. Ion channels in toxicology. J Appl Toxicol 2010; 30: 497-512

4 *Kaczorowski GJ, Garcia ML, Bode J, Hess SD, Patel UA*. The importance of being profiled: Improving drug candidate safety and efficacy using ion channel profiling. Front Pharmacol 2011; 2: 78

5 *Potterat O, Hamburger M*. Drug discovery and development with plant-derived compounds. In: Petersen F, Amstutz R, editors. Progress in Drug Research, Volume 65: Natural compounds as drugs (I). Basel/Boston/Berlin: Birkhäuser Verlag AG; 2008: 45-118

6 *Newman DJ, Cragg GM*. Natural products as sources of new drugs over the 30 years from 1981 to 2010. J Nat Prod 2012; 75: 311-335

7 *Priest BT, Bell IM, Garcia ML*. Role of hERG potassium channel assays in drug development. Channels 2008; 2: 87-93

8 *Grewer C, Gameiro A, Mager T, Fendler K*. Electrophysiological characterization of membrane transport proteins. Annu Rev Biophys 2013; 42: 95-120

9 *Kvist T, Hansen KB, Bräuner-Osborne H*. The use of *Xenopus* oocytes in drug screening. Expert Opin Drug Dis 2011; 6: 141-153

10 *Kapur A, Derry JMC, Hansen RS*. Expression and study of ligand-gated ion channels in *Xenopus laevis* oocytes. In: Lajtha A, Baker G, Dunn S, Holt A, editors. Handbook of neurochemistry and molecular neurobiology: Practical neurochemistry methods. New York: Springer Science+Business Media, LLC; 2007: 323-340

11 *Baburin I, Beyl S, Hering S*. Automated fast perfusion of *Xenopus* oocytes for drug screening. Pflug Arch Eur J Phy 2006; 453: 117-123

12 *Potterat O*. Targeted approaches in natural product lead discovery. Chimia 2006; 60: 19-22

13 *Potterat O, Hamburger M*. Natural products in drug discovery: Concepts and approaches for tracking bioactivity. Curr Org Chem 2006; 10: 899-920

14 *Potterat O, Hamburger M*. Concepts and technologies for tracking bioactive compounds in natural product extracts: Generation of libraries, and hyphenation of analytical processes with bioassays. Nat Prod Rep 2013; 30: 546-564

15 *Wolfender JL*. HPLC in natural product analysis: The detection issue. Planta Med 2009; 75: 719-734

3. Results and discussion

3.1. Natural products as potential hERG channel inhibitors – Outcomes from a screening of widely used herbal medicines and edible plants

Schramm A, Jähne EA, Baburin I, Hering S, Hamburger M.

Planta Med, accepted for publication

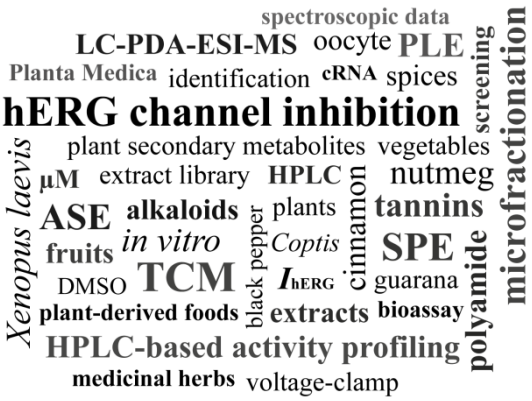

Extracts obtained from widely used herbal drugs and edible plants were screened for *in vitro* hERG channel inhibition by means of a functional *Xenopus* oocyte assay. The hERG channel blocking properties of selected extracts were tracked by HPLC-based activity profiling to tannins and alkaloids. Major European medicinal plants and frequently consumed vegetables, fruits, and spices were found to be associated with a low risk for hERG toxicity.

Extraction of plant material (herbal medicines), recording and interpretation of analytical data for extract analysis (LC-PDA-ESI-MS), polyamide solid phase extraction, HPLC microfractionation, electrophysiological studies on fractions, tannin-depleted extracts and piperine (preparation of Xenopus oocytes, two-microelectrode voltage-clamp measurements, data analysis), writing the draft of the manuscript, and preparation of figures were my contributions to this publication.

Anja Schramm

Natural Products as Potential hERG Channel Inhibitors – Outcomes from a Screening of Widely Used Herbal Medicines and Edible Plants

Anja Schramm[1], Evelyn A. Jähne[1], Igor Baburin[2], Steffen Hering[2], Matthias Hamburger[1]

[1] Division of Pharmaceutical Biology, University of Basel, Klingelbergstrasse 50, 4056 Basel, Switzerland

[2] Institute of Pharmacology and Toxicology, University of Vienna, Althanstrasse 14, 1090 Vienna, Austria

Address for correspondence

Prof. Dr. Matthias Hamburger

Department of Pharmaceutical Sciences

Division of Pharmaceutical Biology

University of Basel

Klingelbergstrasse 50

CH-4056 Basel

Tel. +41 (0)61 267 14 25

Fax +41 (0)61 267 14 74

Email: Matthias.Hamburger@unibas.ch

Abstract

Inhibition of the hERG channel is the single most important risk factor leading to acquired long QT syndrome. Drug-induced QT prolongation can cause severe cardiac complications including arrhythmia, and is thus a liability in drug development. Considering the importance of hERG as an antitarget and the daily intake of plant-derived foods and herbal products, surprisingly few natural products have been tested for hERG channel blocking properties. In an assessment of possible hERG liabilities, a selection of widely used herbal medicines and edible plants (vegetables, fruits, and spices) was screened by means of a functional two-microelectrode voltage-clamp assay with *Xenopus* oocytes. The hERG channel blocking activity of selected extracts was investigated with the aid of an HPLC-based profiling approach, and attributed to tannins and alkaloids. Major European medicinal plants and frequently consumed food plants were found to have a low risk for hERG toxicity.

Keywords: herbal drugs, dietary plants, hERG channel inhibition, *Xenopus* oocyte assay, HPLC-based activity profiling, alkaloids

Abbreviations:

LQTS	long QT syndrome
hERG	human ether-a-go-go-related gene
WHO	World Health Organization
QTc	corrected QT interval
PLE	pressurized liquid extraction
SPE	solid phase extraction
TCM	traditional Chinese medicine

Introduction

A growing number of non-antiarrhythmic drugs have been shown to exhibit side effects associated with QT prolongation [1]. Drug-induced long QT syndrome (LQTS) can cause ventricular tachyarrhythmia (torsades de pointes arrhythmia) and sudden cardiac death. Due to this potentially fatal side effect, drugs such as terfenadine and cisapride had to be withdrawn from the market. The most important determinant of acquired LQTS is inhibition of I_{Kr} (I_{hERG}), the rapidly activating component of the delayed rectifier potassium current that is mediated by the hERG (human ether-a-go-go-related gene) channel. Reduction of I_{hERG} can delay the repolarization phase of the cardiac action potential and, as a consequence, lead to prolongation of the QT interval [2]. Hence, hERG channel blockage is nowadays considered as a major safety liability in preclinical drug development and clinical practice.

Medicinal plants and phytomedicines are used worldwide, either as alternatives to conventional pharmacotherapy, or as complementary medicines. For example, preparations containing ginkgo, garlic, echinacea, saw palmetto, or St. John`s wort belong to the top-selling herbal products in the United States [3]. An increased understanding of the impact of nutrition on human health led to specific dietary recommendations aimed at lowering the incidence of certain diseases. Dietary phytochemicals such as flavonoids and organosulfur compounds are believed to possess preventive effects in chronic diseases, e.g., cancer and cardiovascular diseases [4-6]. The WHO (World Health Organization) dietary guideline recommends a daily intake of at least 400 g of fruits and vegetables [7]. Consumption of plant-derived foods (vegetables, fruits, and spices) and the use of medicinal herbs/phytomedicines result in a remarkable intake of total plant secondary metabolites. It has been estimated that the human dietary intake of phytochemicals may reach up to several grams per day [8,9]. Plant-derived compounds possess a spectrum of beneficial properties, but

they may also show adverse effects and/or interactions with prescription and OTC drugs [10,11].

Considering the importance of hERG as an antitarget, surprisingly few natural products have been tested for hERG channel blocking properties. A number of structurally diverse natural products have been shown to diminish hERG channel activity *in vitro*, e.g., naringenin, trimethyl-apigenin, curcumin, lobeline, chelerythrine, papaverine, and capsaicin [12-18]. It has been shown that the consumption of 1 L of freshly squeezed pink grapefruit juice (containing the hERG channel blocking flavanone naringenin) leads to a mild prolongation of the QTc interval in both young healthy volunteers and patients suffering from cardiomyopathy [12,19]. The fact that not only synthetic drug substances but also widely occurring natural products, such as flavonoids and alkaloids, block I_{hERG} warrants an assessment of widely used medicinal and dietary plants for their potential to inhibit I_{hERG}. Also, the concomitant use of QT-prolonging medications along with hERG channel blocking natural products may lead to clinically relevant drug interactions and may be a concern with respect to consumer safety.

In the present study, we wanted to address the following questions: (i) Do herbal medicines and plant-derived foods contain hERG channel blocking constituents and, if so, (ii) do their *in vitro* activity, daily intake in diet and/or herbal medicines point towards possible risks that would warrant an investigation in animal models for cardiac arrhythmia? For this purpose, we prepared a focused library of plant extracts from herbal drugs widely used in Europe, US, and China, and from frequently consumed spices, vegetables, and fruits. Food plants were selected according to consumption pattern in Central Europe, taxonomic considerations (in order to cover a broad range of chemically diverse secondary metabolites), and seasonal availability. The hERG channel inhibition was assessed by means of a two-microelectrode voltage-clamp assay with transfected *Xenopus laevis* oocytes.

Results and Discussion

A total of 79 plant samples were successively extracted with solvents of increasing polarities to afford a library of 187 extracts. This library was tested in a functional assay with transfected *Xenopus laevis* oocytes expressing hERG channels (Table 1S–3S, Supporting Information). An initial test concentration of 100 µg/mL was used, and extracts inhibiting the hERG current (I_{hERG}) by ≥ 30% were selected for further investigation. Of the extracts tested, six were found to be active, including methanolic extracts from cinnamon (*Cinnamomum zeylanicum* Nees, Lauraceae), guarana (*Paullinia cupana* Kunth, Sapindaceae), nutmeg (*Myristica fragrans* L., Myristicaceae), and Coptidis rhizoma (*Coptis chinensis* Franch., Ranunculaceae), and ethyl acetate and methanolic extracts from fruits of black pepper (*Piper nigrum* L., Piperaceae).

The active extracts were submitted to HPLC-based activity profiling in order to identify and characterize hERG channel blocking constituents [20]. Prior to microfractionation, they were analyzed by LC-PDA-ESI-MS to obtain a qualitative phytochemical fingerprint, and HPLC-based activity profiling was then carried out after optimization of separation. Aliquots of each extract (5 mg) were separated by semi-preparative RP-HPLC, and microfractions of 90 s each were collected and tested in the oocyte assay.

The methanolic extracts of cinnamon (*Cinnamomum zeylanicum*), guarana (*Paullinia cupana*), and nutmeg (*Myristica fragrans*) were among the most active extracts in our screening (inhibition of I_{hERG} by 64.5 ± 5.7%, 45.3 ± 10.2%, and 42.3 ± 1.0%, respectively). However, the chromatograms all showed broad humps in the region of activity (Fig. 1, left column), indicative of a possible presence of tannins in the extract. Therefore, tannins were selectively removed from the extracts by solid phase extraction on polyamide columns [21]. Comparison of HPLC profiles before and after polyamide filtration confirmed the

effectiveness of tannin removal, without significant alterations of the HPLC chromatograms (Fig. 1, right column). The hERG inhibitory activity of tannin-depleted extracts was significantly lower (see insets in Fig. 1), and we concluded that tannins were responsible for the *in vitro* hERG channel blocking properties of these extracts. Given the negligible oral bioavailability of tannins [22,23], one can reasonably assume that no *in vivo* effects are to be expected. Moreover, gallic acid (**1**), ellagic acid (**2**), and (+)-catechin (**3**) (Fig. 3), which can be formed by the intestinal microflora as breakdown products of tannins and are known to be resorbed [22,23], were devoid of hERG inhibitory activity when tested at 100 µM in the oocyte assay. We conclude that the activity of tannins in our *in vitro* assay was likely due to non-specific interactions [20,21]. High levels of tannins are present in nuts, fruits, and some widely used spices (e.g., bay leaves, cinnamon, star anise, nutmeg, allspice, and juniper), whereas most vegetables lack them completely [24-26].

Ethyl acetate and methanolic extracts from fruits of black pepper (*Piper nigrum*) reduced I_{hERG} by 32.4 ± 0.5% and 36.9 ± 9.1%, respectively. For both extracts, the activity profiles showed that the activity peak correlated with the major peak in the HPLC chromatogram (Fig. 2A-B). By analysis of LC-PDA-ESI-MS data and comparison with literature data, this peak was readily identified as piperine (**4**) (Fig. 3) [27]. The hERG inhibitory activity of the alkaloid was determined in the oocyte assay. Piperine (**4**) inhibited I_{hERG} by 15.3 ± 1.1% and 35.7 ± 2.5% when tested at 100 µM and 300 µM concentrations, respectively (Fig. 2C-D). With an IC_{50} value > 300 µM, piperine (**4**) was a weak hERG channel blocker. The pronounced activity peak observed in the EtOAc extract (microfraction ten inhibited I_{hERG} by 64.3 ± 7.3%) was due to the high piperine content in the extract [28]. Piperine (**4**) has been previously identified as a promising scaffold for novel $GABA_A$ receptor modulators with anticonvulsant and anxiolytic activity [27,29].

The methanolic extract of the TCM (traditional Chinese medicine) herbal drug Coptidis rhizoma (*Coptis chinensis*) reduced I_{hERG} by 31.7 ± 2.0%. By means of HPLC-based activity profiling of the crude extract, the hERG channel blocking constituents were tracked to known protoberberine alkaloids. Dihydroberberine was most active, as it reduced I_{hERG} at 100 µM by 30.1 ± 10.1%, while berberine at the same concentration was less active (inhibition of I_{hERG} by 16.3 ± 2.0%) [30]. While these values do not point towards a high-affinity block, possible effects on ventricular repolarization cannot be ruled out. Even relatively weak hERG *in vitro* inhibitors can produce clinically relevant QT prolongation if plasma levels are sufficiently high [31]. Moreover, if the metabolites are more lipophilic than the administered compound, they could accumulate in the systemic compartment more efficiently. This has been recently demonstrated for berberine and its main metabolite berberrubine formed by O-demethylation [32]. Also, biodistribution, metabolism, and accumulation in target organs may differ between single-dose and chronic administration.

To our knowledge, this is the first screening study evaluating the potential of herbal drugs and plant-derived foods for *in vitro* hERG channel inhibition. Our data suggest that widely used European medicinal plants, frequently consumed spices, vegetables, and fruits are associated with a low risk for hERG toxicity. However, the case of Coptidis rhizoma emphasizes the need for a more extensive assessment of herbal remedies from other traditional health systems (e.g., TCM, Ayurveda, Kampo, and Unani) that are increasingly used worldwide for therapeutic purposes and/or as nutritional supplements.

Materials and Methods

General experimental procedures

Analytical and semi-preparative HPLC separations were carried out with SunFire C18 columns (3 × 150 mm i.d., 3.5 µm; 10 × 150 mm i.d., 5 µm). ESI-MS data were recorded on an Esquire 3000 plus ion trap mass spectrometer (Bruker Daltonics) coupled via a T-splitter (split ratio 1:5) to an Agilent 1100 system consisting of an autosampler, degasser, binary pump, column oven, and PDA detector. Semi-preparative HPLC separations were performed on an Agilent 1100 system consisting of an autosampler, quaternary pump with degasser module, column thermostat, and PDA detector. Unless otherwise stated, H_2O (solvent A) and MeCN (solvent B) were used as mobile phase. The flow rate was 0.5 mL/min for LC-PDA-ESI-MS, and 4 mL/min for semi-preparative HPLC. Detection was at 254 nm, while PDA spectra were measured from 210 to 400 nm. Data acquisition and analysis were performed using HyStar 3.2 software.

Solvents and Chemicals

Solvents used for extraction and polyamide filtration were of analytical grade, whereas HPLC-grade solvents were used for HPLC separations. HPLC-grade water was obtained by an EASY-pure II water purification system. Formic acid (98.0–100.0%) and HPLC-grade MeCN were from Scharlau. Ellagic acid dihydrate (≥ 97% by HPLC), (+)-catechin (≥ 98% by HPLC), gallic acid (≥ 98.5% by GC), and piperine (≥ 97% by TLC) were purchased from Sigma-Aldrich.

Plant material

The origin of plant species used in this study is listed in Tables 1S–3S of the Supporting Information. Fresh plant material and freshly squeezed grapefruit juice were shock frozen and lyophilized. Voucher specimens are preserved at the Division of Pharmaceutical Biology, University of Basel, Switzerland.

Extraction

Prior to extraction, the dried plant material was ground in a ZM 1 ultracentrifugal mill (sieve size 2.0 mm; Retsch). Unless otherwise stated, plant extracts were prepared by pressurized liquid extraction (PLE) using an ASE 200 instrument connected to a solvent controller (all Dionex). Ground plant material was packed into steel cartridges (11 mL; Dionex) and consecutively extracted with solvents of increasing polarity (petroleum ether [PE], EtOAc, and MeOH). Extraction temperature was at 70°C, and the pressure was set at 120 bar. Duration of a static extraction cycle was 5 min, and 3 extraction cycles were used for each solvent to obtain exhaustive extraction [33,34]. Plant-derived foods containing high amounts of sugars, proteins, or triglycerides were extracted by percolation at room temperature, using the same solvents as for PLE. The following edible plants were extracted by percolation: *Brassica nigra*, *Citrus paradisi*, *Coffea arabica*, *Euterpe oleracea*, *Ficus carica*, *Glycine max*, *Lycium barbarum*, *Malus domestica*, *Morinda citrifolia*, *Myristica fragrans*, *Opuntia ficus-indica*, *Phaseolus vulgaris*, *Rheum rhabarbarum*, *Sinapis alba*, *Theobroma cacao*, and *Vaccinium macrocarpon*. Extracts were dried under reduced pressure, and stored at 4°C until use.

HPLC-based activity profiling

A validated HPLC-based profiling protocol for the identification of hERG channel inhibitors in herbal extracts was used [30]. Briefly, an aliquot (5 mg) of crude extract (100 µL of 50 mg/mL in DMSO) was separated by semi-preparative RP-HPLC using H_2O (solvent A) and MeCN (solvent B) as mobile phase, unless otherwise stated. The gradient profiles were as follows: MeOH extract of *Paullinia cupana*: 10–70% B in 20 min, hold 70% B for 5 min (Fig. 1B); MeOH extract of *Myristica fragrans*: 20–100% B in 30 min, hold 100% B for 5 min (Fig. 1C); EtOAc extract of *Piper nigrum*: 30–100% B in 30 min, hold 100% B for 10 min (Fig. 2A); MeOH extract of *Piper nigrum*: 20–100% B in 30 min, hold 100% B for 10 min (Fig. 2B). The MeOH extract of *Cinnamomum zeylanicum* was separated with 0.1% aqueous formic acid (solvent C) and MeCN containing 0.1% formic acid (solvent D) using the following gradient: 5–70% D in 30 min, hold 70% D for 5 min (Fig. 1A). Time-based microfractions of 90 s each were manually collected into glass tubes. Evaporation of microfractions was achieved with an EZ-2 Plus vacuum evaporator (Genevac). Prior to testing for hERG channel inhibition, residues were re-dissolved in 30 µL of DMSO and diluted with 2.97 mL of bath solution.

Polyamide solid phase extraction

To remove tannins from methanolic extracts of cinnamon, guarana, and nutmeg, the crude extracts were subjected to solid phase extraction (SPE) on polyamide. Polyamide (0.05–0.16 mm, Carl Roth GmbH) was conditioned in MeOH for 24 h, and packed into glass columns of 1.7 cm diameter to give bed heights of approximately 6 cm. A portion (100 mg) of each extract was dissolved in MeOH (50 mL), applied to the column, and eluted at a flow rate of 1 mL/min. Columns were washed with 300 mL of MeOH. For crude cinnamon extract,

polyamide filtration was also performed using MeOH/H_2O 7:3 (v/v) as eluent. The tannin-depleted effluents were collected, evaporated to dryness, and analyzed along with the untreated extracts.

Electrophysiological bioassay: expression of hERG channels in Xenopus oocytes and voltage-clamp experiments

Oocyte preparation

Oocytes from the South African clawed frog, *Xenopus laevis*, were prepared as follows: After 15 min exposure of female *Xenopus laevis* to the anesthetic (0.2% solution of MS-222; the methane sulfonate salt of 3-aminobenzoic acid ethyl ester; Sigma-Aldrich), parts of the ovary tissue were surgically removed. Defolliculation was achieved by enzymatical treatment with 2 mg/mL collagenase type 1A (Sigma-Aldrich). Stage V–VI oocytes were selected and injected with the hERG-encoding cRNA. Injected oocytes were stored at 18°C in ND96 bath solution containing 1% penicillin-streptomycin solution (Sigma-Aldrich). ND96 bath solution contained 96 mM NaCl, 2 mM KCl, 1 mM $MgCl_2 \times 6H_2O$, 1.8 mM $CaCl_2 \times 2H_2O$, and 5 mM HEPES (pH 7.4).

Automated two-microelectrode voltage-clamp studies

Currents through hERG channels were studied with the two-microelectrode voltage-clamp technique using a TURBO TEC-03X amplifier (npi electronic GmbH). Electrophysiological experiments were performed one to three days after cRNA injection. Voltage-recording and current-injecting microelectrodes (Harvard Apparatus) were filled with 3 M KCl and had resistances between 0.5 and 2 MΩ. Oocytes with maximal current

amplitudes > 3 µA were discarded to avoid voltage-clamp errors. The following voltage protocol was used: From a holding potential of -80 mV, the cell membrane was initially depolarized to +20 mV (300 ms) in order to achieve channel activation and subsequent rapid inactivation. During following repolarization to -50 mV (300 ms) channels recover from inactivation and elicit the hERG current (I_{hERG}). A final step to the holding potential ensured that channels returned to the closed state. The protocol was applied either in 3-s intervals (extract screening) or in 1-s intervals (bioactivity studies on fractions and pure compounds). Measurements were started after the initial current 'run up' (slow increase of hERG current amplitudes during repetitive pulsing) reached a steady baseline. The automated fast perfusion system ScreeningTool (npi electronic GmbH, see [35] for details) was used to apply the test solutions to the oocyte. Sample stock solutions (prepared in DMSO) were freshly diluted every day with ND96 bath solution. Steady-state block of I_{hERG} was evaluated at ambient temperature (20–24°C). Decreases in tail current amplitudes were taken as a measure of block development during repetitive pulsing. The final maximum DMSO concentration (1%) in test solutions did not affect hERG currents (data not shown). Cisapride (Sigma-Aldrich; purity ≥ 98%) was used as positive control. The IC_{50} value for hERG current inhibition at 0.3 Hz pulse frequency was 1.6 ± 0.4 µM (n = 3, Fig. 1S of the Supporting Information, see also [36] for comparison). Data acquisition and processing were performed using pCLAMP 10.0 software and Clampfit 10.2 software, respectively.

Data analysis

Inhibition of the hERG potassium current (I_{hERG}) was defined as $[1 - I_{(hERG,drug)}/I_{(hERG,ctrl)}] * 100$, where $I_{(hERG,drug)}$ is the current amplitude in the presence of the indicated test material (extract, fraction, or pure compound) and $I_{(hERG,ctrl)}$ is the control

current amplitude. Data were analyzed using Origin software 7.0 (OriginLab Corporation). Data points represent the mean ± S.E. from at least two oocytes and two oocyte batches.

Supporting Information

Data on the hERG channel inhibitory activity of 18 European medicinal plants (Table 1S), 5 traditional Chinese herbal drugs (Table 2S), and 56 food plants and spices (Table 3S) are available as Supporting Information.

Acknowledgments

The project was conducted within the International Research Staff Exchange Scheme (IRSES), project "hERG Related Risk Assessment of Botanicals" PIRSES-GA-2011-295174 Marie Curie Actions funded under the 7th Framework Programme of the European Commission. Financial support by the Swiss National Science Foundation (Project 31600-113109) is gratefully acknowledged (M.H.). We thank for research scholarships from the Freiwillige Akademische Gesellschaft Basel (A.S.) and Stud*Ex* (Leonardo da Vinci Programm) (E.A.J.).

Conflict of Interest

The authors declare no conflict of interest.

References

1 *De Ponti F, Poluzzi E, Cavalli A, Recanatini M, Montanaro N*. Safety of non-antiarrhythmic drugs that prolong the QT interval or induce torsade de pointes: An overview. Drug Safety 2002; 25: 263-286

2 *Sanguinetti MC, Tristani-Firouzi M*. hERG potassium channels and cardiac arrhythmia. Nature 2006; 440: 463-469

3 *Blumenthal M, Lindstrom A, Ooyen C, Lynch ME*. Herb supplement sales increase 4.5% in 2011. HerbalGram 2012; 95: 60-64

4 *Biesalski HK*. Nutraceuticals: The link between nutrition and medicine. J Toxicol Cutan Ocul Toxicol 2002; 21: 9-30

5 *Heber D*. Vegetables, fruits and phytoestrogens in the prevention of diseases. J Postgrad Med 2004; 50: 145-149

6 *Kris-Etherton PM, Hecker KD, Bonanome A, Coval SM, Binkoski AE, Hilpert KF, Griel AE, Etherton TD*. Bioactive compounds in foods: Their role in the prevention of cardiovascular disease and cancer. Am J Med 2002; 113: 71S-88S

7 *WHO*. Technical report series 916: Diet, nutrition and the prevention of chronic diseases – Report of a joint WHO/FAO expert consultation (Geneva, Switzerland); 2003

8 *Manach C, Scalbert A, Morand C, Rémésy C, Jiménez L*. Polyphenols: Food sources and bioavailability. Am J Clin Nutr 2004; 79: 727-747

9 *Ames BN*. Dietary carcinogens and anticarcinogens: Oxygen radicals and degenerative diseases. Science 1983; 221: 1256-1264

10 *Ernst E*. The risk-benefit profile of commonly used herbal therapies: Ginkgo, St. John's wort, ginseng, echinacea, saw palmetto, and kava. Ann Intern Med 2002; 136: 42-53

11 *Singh D, Gupta R, Saraf SA*. Herbs – Are they safe enough? An Overview. Crit Rev Food Sci 2012; 52: 876-898

12 *Zitron E, Scholz E, Owen RW, Lück S, Kiesecker C, Thomas D, Kathöfer S, Niroomand F, Kiehn J, Kreye VAW, Katus HA, Schoels W, Karle CA*. QTc prolongation by grapefruit juice and its potential pharmacological basis: hERG channel blockade by flavonoids. Circulation 2005; 111: 835-838

13 *Liu Y, Xu XH, Liu Z, Du XL, Chen KH, Xin X, Jin ZD, Shen JZ, Hu Y, Li GR, Jin MW*. Effects of the natural flavone trimethylapigenin on cardiac potassium currents. Biochem Pharmacol 2012; 84: 498-506

14 *Hu CW, Sheng Y, Zhang Q, Liu HB, Xie X, Ma WC, Huo R, Dong DL*. Curcumin inhibits hERG potassium channels *in vitro*. Toxicol Lett 2012; 208: 192-196

15 *Jeong I, Choi BH, Hahn SJ*. Effects of lobeline, a nicotinic receptor ligand, on the cloned Kv1.5. Pflug Arch Eur J Phy 2010; 460: 851-862

16 *Harmati G, Papp F, Szentandrássy N, Bárándi L, Ruzsnavszky F, Horváth B, Bányász T, Magyar J, Panyi G, Krasznai Z, Nánási PP*. Effects of the PKC inhibitors chelerythrine and bisindolylmaleimide I (GF 109203X) on delayed rectifier K^+ currents. N-S Arch Pharmacol 2011; 383: 141-148

17 *Kim YJ, Hong HK, Lee HS, Moh SH, Park JC, Jo SH, Choe H*. Papaverine, a vasodilator, blocks the pore of the hERG channel at submicromolar concentration. J Cardiovasc Pharm 2008; 52: 485-493

18 *Xing JL, Ma JH, Zhang PH, Fan XR*. Block effect of capsaicin on hERG potassium currents is enhanced by S6 mutation at Y652. Eur J Pharmacol 2010; 630: 1-9

19 *Piccirillo G, Magrì D, Matera S, Magnanti M, Pasquazzi E, Schifano E, Velitti S, Mitra M, Marigliano V, Paroli M, Ghiselli A*. Effects of pink grapefruit juice on QT variability in patients with dilated or hypertensive cardiomyopathy and in healthy subjects. Transl Res 2008; 151: 267-272

20 *Potterat O, Hamburger M*. Concepts and technologies for tracking bioactive compounds in natural product extracts: Generation of libraries, and hyphenation of analytical processes with bioassays. Nat Prod Rep 2013; 30: 546-564

21 *Jones WP, Kinghorn AD*. Extraction of plant secondary metabolites. In: Sarker SD, Latif Z, Gray AI, editors. Natural products isolation (2nd edition). Totowa, New Jersey: Humana Press Inc.; 2005: 323-351

22 *Saura-Calixto F, Pérez-Jiménez J*. Tannins: Bioavailability and mechanisms of action. In: Knasmüller S, DeMarini DM, Johnson I, Gerhäuser C, editors. Chemoprevention of cancer and DNA damage by dietary factors. Weinheim: Wiley-VCH Verlag GmbH & Co. KGaA; 2009: 499-508

23 *Rasmussen SE, Frederiksen H, Struntze Krogholm K, Poulsen L*. Dietary proanthocyanidins: Occurrence, dietary intake, bioavailability, and protection against cardiovascular disease. Mol Nutr Food Res 2005; 49: 159-174

24 *Schulz JM, Herrmann K*. Occurrence of catechins and proanthocyanidins in spices. V. Phenolics of spices. Z Lebensm Unters For 1980; 171: 278-280

25 *Hellström JK, Törrönen AR, Mattila PH*. Proanthocyanidins in common food products of plant origin. J Agr Food Chem 2009; 57: 7899-7906

26 *Gu L, Kelm MA, Hammerstone JF, Beecher G, Holden J, Haytowitz D, Prior RL*. Screening of foods containing proanthocyanidins and their structural characterization using LC-MS/MS and thiolytic degradation. J Agr Food Chem 2003; 51: 7513-7521

27 *Zaugg J, Baburin I, Strommer B, Kim HJ, Hering S, Hamburger M*. HPLC-based activity profiling: Discovery of piperine as a positive $GABA_A$ receptor modulator targeting a benzodiazepine-independent binding site. J Nat Prod 2010; 73: 185-191

28 *Friedman M, Levin CE, Lee SU, Lee JS, Ohnisi-Kameyama M, Kozukue N*. Analysis by HPLC and LC/MS of pungent piperamides in commercial black, white, green, and red whole and ground peppercorns. J Agr Food Chem 2008; 56: 3028-3036

29 *Khom S, Strommer B, Schöffmann A, Hintersteiner J, Baburin I, Erker T, Schwarz T, Schwarzer C, Zaugg J, Hamburger M, Hering S*. $GABA_A$ receptor modulation by piperine and a non-TRPV1 activating derivative. Biochem Pharmacol 2013; 85: 1827-1836

30 *Schramm A, Baburin I, Hering S, Hamburger M*. hERG channel inhibitors in extracts of Coptidis rhizoma. Planta Med 2011; 77: 692-697

31 *Rampe D, Brown AM*. A history of the role of the hERG channel in cardiac risk assessment. J Pharmacol Toxicol Methods 2013; 68: 13-22

32 *Spinozzi S, Colliva C, Camborata C, Roberti M, Ianni C, Neri F, Calvarese C, Lisotti A, Mazzella G, Roda A*. Berberine and its metabolites: Relationship between

physicochemical properties and plasma levels after administration to human subjects. J Nat Prod 2014; doi: 10.1021/np400607k

33 *Basalo C, Mohn T, Hamburger M*. Are extraction methods in quantitative assays of pharmacopoeia monographs exhaustive? A comparison with pressurized liquid extraction. Planta Med 2006; 72: 1157-1162

34 *Benthin B, Danz H, Hamburger M*. Pressurized liquid extraction of medicinal plants. J Chromatogr A 1999; 837: 211-219

35 *Baburin I, Beyl S, Hering S*. Automated fast perfusion of *Xenopus* oocytes for drug screening. Pflug Arch Eur J Phy 2006; 453: 117-123

36 *Stork D, Timin EN, Berjukow S, Huber C, Hohaus A, Auer M, Hering S*. State dependent dissociation of hERG channel inhibitors. Brit J Pharmacol 2007; 151: 1368-1376

Figure Legends

Figure 1: HPLC-PDA analysis of **A** cinnamon (*Cinnamomum zeylanicum*) MeOH extract, **B** guarana (*Paullinia cupana*) MeOH extract, and **C** nutmeg (*Myristica fragrans*) MeOH extract. Activity profiling of crude extracts (left column), with HPLC chromatograms and corresponding activity profiles (% inhibition of I_{hERG}) of time-based microfractions. HPLC fingerprints of tannin-depleted extracts (right column) are shown for comparison purposes. Inhibition of I_{hERG} by crude extracts and tannin-depleted extracts (100 µg/mL) is indicated on the upper right side of each chromatogram. UV traces were recorded at 254 nm.

Figure 2: HPLC-based activity profiling of black pepper (*Piper nigrum*) fruits extracts. **A** EtOAc extract. **B** MeOH extract. HPLC chromatograms (254 nm) and corresponding activity profiles (% inhibition of I_{hERG}) of time-based microfractions are shown. **C, D** Concentration-dependent inhibition of I_{hERG} by piperine (**4**). The control current is superimposed with the current traces recorded during a 1 Hz pulse train (15 pulses) in the presence of piperine (100 µM and 300 µM).

Figure 3: Structures of compounds **1**–**4** tested for hERG channel inhibitory activity.

Figure 1

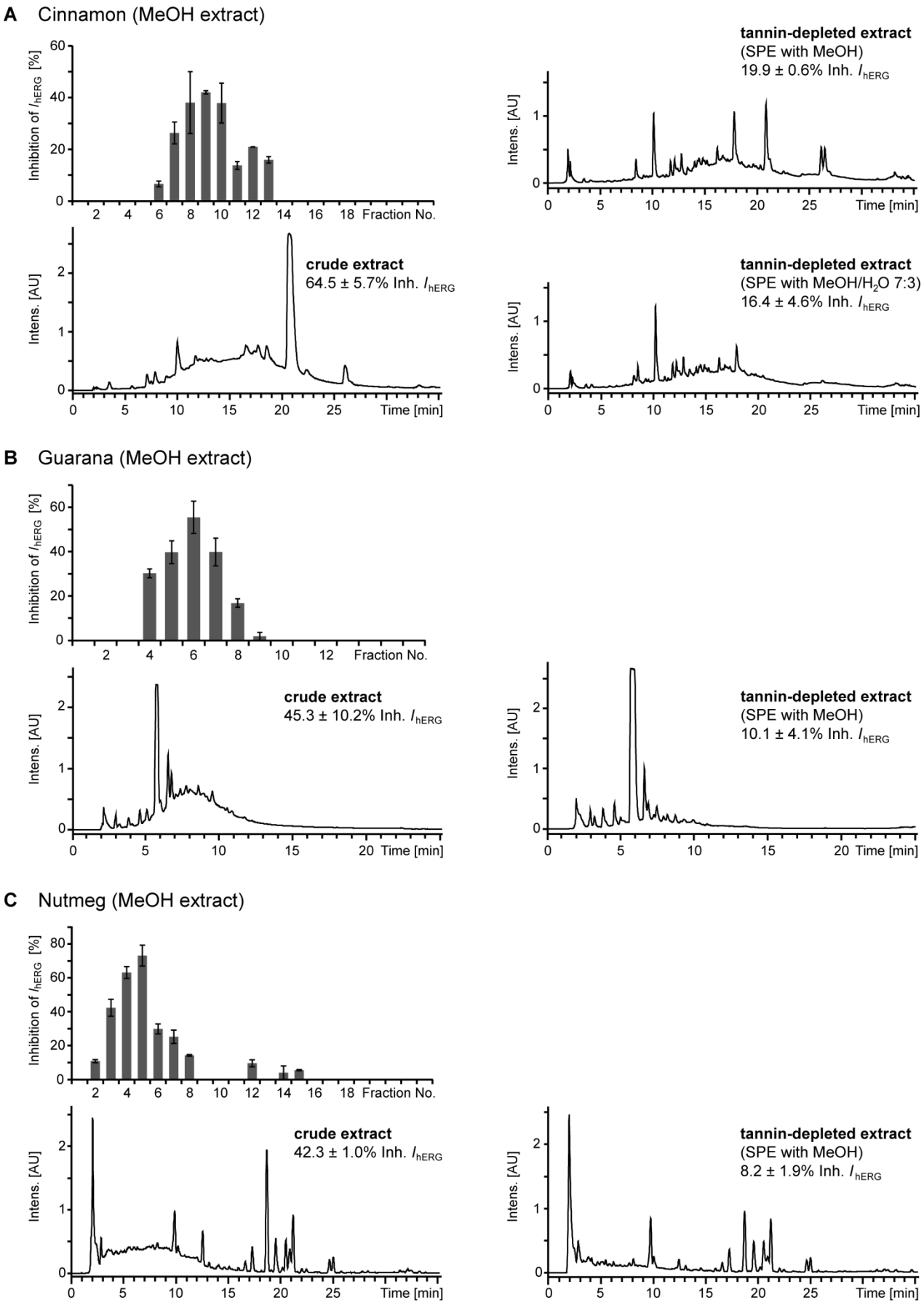
A Cinnamon (MeOH extract)
Inhibition of I_{hERG} [%]
Fraction No.
crude extract
64.5 ± 5.7% Inh. I_{hERG}
tannin-depleted extract
(SPE with MeOH)
19.9 ± 0.6% Inh. I_{hERG}
tannin-depleted extract
(SPE with MeOH/H_2O 7:3)
16.4 ± 4.6% Inh. I_{hERG}
B Guarana (MeOH extract)
crude extract
45.3 ± 10.2% Inh. I_{hERG}
tannin-depleted extract
(SPE with MeOH)
10.1 ± 4.1% Inh. I_{hERG}
C Nutmeg (MeOH extract)
crude extract
42.3 ± 1.0% Inh. I_{hERG}
tannin-depleted extract
(SPE with MeOH)
8.2 ± 1.9% Inh. I_{hERG}
Intens. [AU]
Time [min]

Figure 2

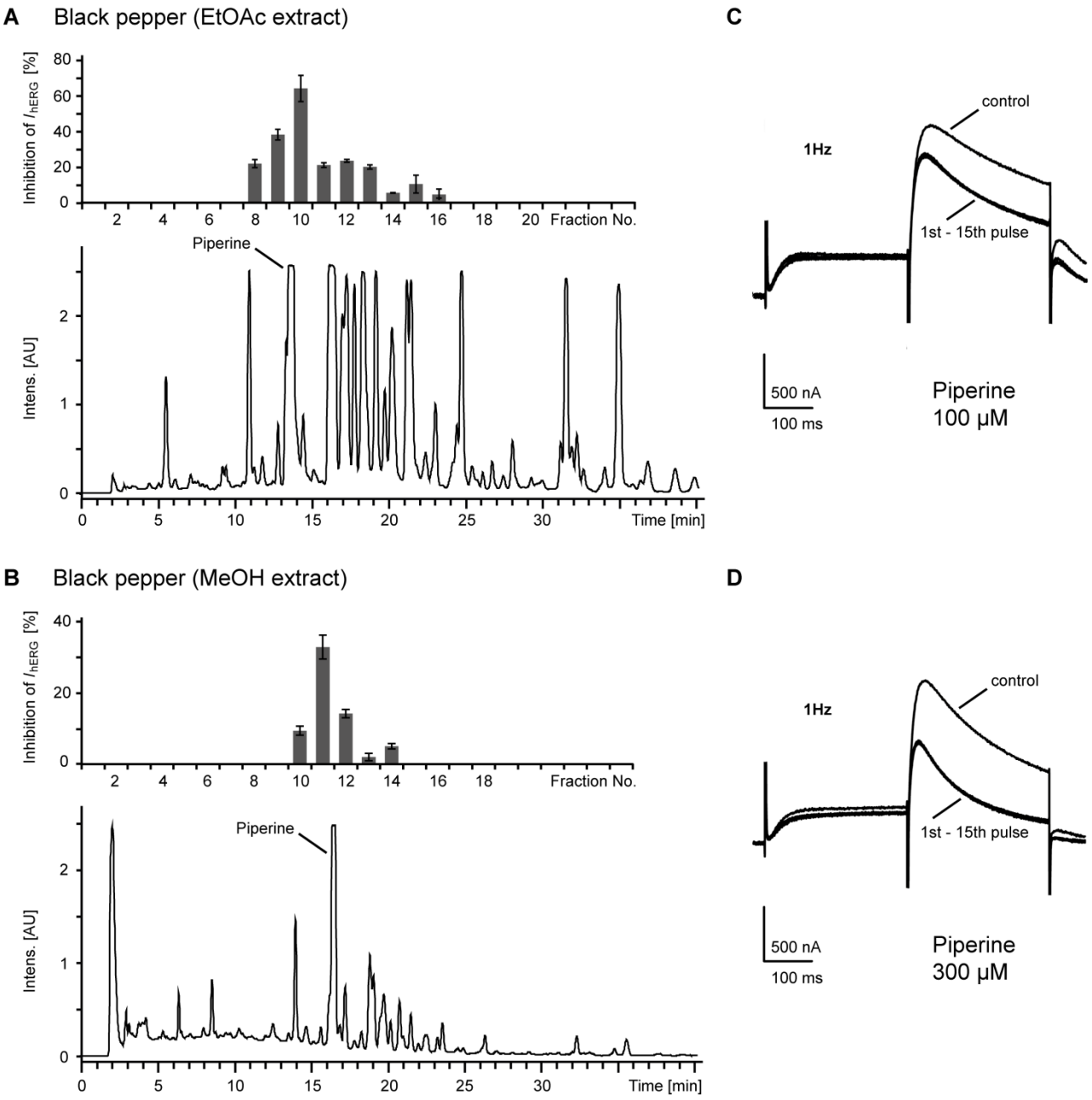
A
Black pepper (EtOAc extract)
Inhibition of I_{hERG} [%]
Fraction No.
Piperine
Intens. [AU]
Time [min]
B
Black pepper (MeOH extract)
Inhibition of I_{hERG} [%]
Fraction No.
Piperine
Intens. [AU]
Time [min]
C
control
1Hz
1st - 15th pulse
500 nA
100 ms
Piperine
100 µM
D
control
1Hz
1st - 15th pulse
500 nA
100 ms
Piperine
300 µM

Figure 3

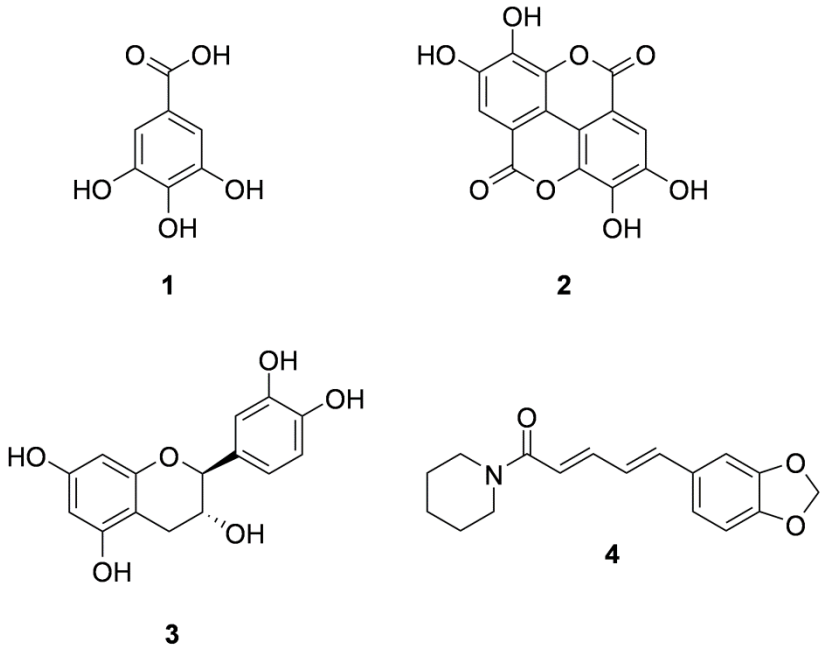

Supporting Information

Natural Products as Potential hERG Channel Inhibitors – Outcomes from a Screening of Widely Used Herbal Medicines and Edible Plants

Anja Schramm[1], Evelyn A. Jähne[1], Igor Baburin[2], Steffen Hering[2], Matthias Hamburger[1]

[1] Division of Pharmaceutical Biology, University of Basel, Klingelbergstrasse 50, 4056 Basel, Switzerland

[2] Institute of Pharmacology and Toxicology, University of Vienna, Althanstrasse 14, 1090 Vienna, Austria

Address for correspondence

Prof. Dr. Matthias Hamburger

Department of Pharmaceutical Sciences

Division of Pharmaceutical Biology

University of Basel

Klingelbergstrasse 50

CH-4056 Basel

Tel. +41 (0)61 267 14 25

Fax +41 (0)61 267 14 74

Email: Matthias.Hamburger@unibas.ch

Fig. 1S. Concentration-response relationship for the inhibition of I_{hERG} by cisapride. The IC_{50} value for hERG current inhibition at 0.3 Hz pulse frequency was 1.6 ± 0.4 μM (n = 3).

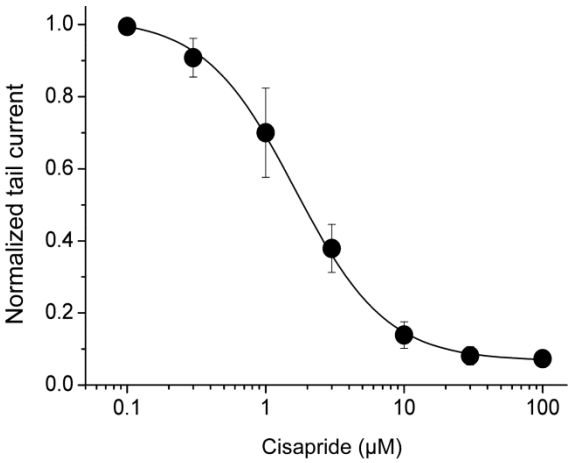

Table 1S. *In vitro* inhibition of the hERG potassium current (I_{hERG}) in *Xenopus* oocytes by medicinal plants widely used in Europe and in the United States.

Common name	Scientific name[a]	Source[b] (Lot no.)	Extract	Inhibition of I_{hERG} (%) at 100 µg/mL
Garlic	Allii sativi bulbus	A (3457001)	PE EtOAc MeOH	12.1 ± 4.7 0.0 ± 0.0 0.0 ± 0.0
Black cohosh	Cimicifugae rhizoma	B (K07.06.1999)	PE EtOAc MeOH	0.0 ± 0.0 0.0 ± 0.0 0.0 ± 0.0
Cinnamon	Cinnamomi cortex	A (3206401)	PE EtOAc MeOH	0.0 ± 0.0 0.0 ± 0.0 64.5 ± 5.7
Hawthorn	Crataegi folium cum flore	A (3510503)	PE EtOAc MeOH	0.0 ± 0.0 0.0 ± 0.0 0.0 ± 0.0
Javanese Turmeric	Curcumae xanthorrhizae rhizoma	A (3759702)	PE EtOAc MeOH	7.3 ± 3.9 9.2 ± 2.2 6.2 ± 2.7
Echinacea / Purple coneflower	Echinaceae purpureae radix	A (3584101)	PE EtOAc MeOH	0.0 ± 0.0 0.0 ± 0.0 14.7 ± 6.5
Ginkgo	Ginkgo folium	A (3460602)	PE EtOAc MeOH	0.0 ± 0.0 0.0 ± 0.0 0.0 ± 0.0
Ginseng	Ginseng radix	A	PE EtOAc MeOH	0.0 ± 0.0 0.0 ± 0.0 8.6 ± 2.4
St. John`s wort	Hyperici herba	A (3142502)	PE EtOAc MeOH	6.8 ± 3.6 0.0 ± 0.0 22.7 ± 6.9
Licorice	Liquiritiae radix	A (3400601)	PE EtOAc MeOH	0.0 ± 0.0 10.5 ± 4.3 11.4 ± 5.6
Hop strobile	Lupuli flos	C (2008.12.0312)	PE EtOAc MeOH	9.2 ± 4.4 0.0 ± 0.0 7.5 ± 3.6
Chamomile	Matricariae flos	A (3535701)	PE EtOAc MeOH	0.0 ± 0.0 0.0 ± 0.0 0.0 ± 0.0
Indian Frankincense	Olibanum indicum (gum resin)	D (3.002.007)	PE EtOAc MeOH	0.0 ± 0.0 0.0 ± 0.0 0.0 ± 0.0
Kava kava	Piperis methystici rhizoma	A (6106802)	PE EtOAc MeOH	8.7 ± 2.8 12.4 ± 6.6 8.3 ± 1.7
Senna	Sennae folium	A (3474604)	PE EtOAc MeOH	0.0 ± 0.0 23.8 ± 6.2 0.0 ± 0.0
Saw palmetto	Sabal fructus	A (3081202)	PE EtOAc MeOH	0.0 ± 0.0 0.0 ± 0.0 0.0 ± 0.0
Milk thistle	Silybi mariani fructus	A (1899605)	PE EtOAc MeOH	0.0 ± 0.0 0.0 ± 0.0 21.3 ± 7.5

Common name	Scientific name[a]	Source[b] (Lot no.)	Extract	Inhibition of I_{hERG} (%) at 100 µg/mL
Valerian	Valerianae radix	A (3031802)	PE EtOAc MeOH	0.0 ± 0.0 0.0 ± 0.0 7.3 ± 5.2

[a] Scientific names can be found in the corresponding ESCOP monographs [1,2].

[b] A: Dixa AG (St. Gallen, Switzerland); B: sinoMed GmbH & Co. (Bad Kötzting, Germany); C: Hänseler AG (Herisau, Switzerland); D: Rigoni Relax Center (Bretzwil, Switzerland).

Table 2S. *In vitro* inhibition of the hERG potassium current (I_{hERG}) in *Xenopus* oocytes by medicinal plants widely used in traditional Chinese medicine (TCM).

Common name (Chinese pinyin name)[a]	Scientific name[a]	Source[b] (Lot no.)	Extract	Inhibition of I_{hERG} (%) at 100 µg/mL
Chuanxinlian	Andrographis herba	A (P690672A)	PE EtOAc MeOH	8.3 ± 5.8 9.2 ± 2.6 0.0 ± 0.0
Baizhi	Angelicae dahuricae radix	B (0610402)	PE EtOAc MeOH	13.2 ± 2.6 0.0 ± 0.0 0.0 ± 0.0
Chaihu	Bupleuri radix	B (0901503)	PE EtOAc MeOH	0.0 ± 0.0 0.0 ± 0.0 5.4 ± 2.5
Huanglian	Coptidis rhizoma	B (0901503)	PE EtOAc MeOH	0.0 ± 0.0 0.0 ± 0.0 31.7 ± 2.0
Danshen	Salviae miltiorrhizae radix et rhizoma	B (0110202)	PE EtOAc MeOH	0.0 ± 0.0 0.0 ± 0.0 0.0 ± 0.0

[a] Pinyin names and scientific names can be found in the corresponding monographs of the Chinese Pharmacopoeia 2010 [3].

[b] A: Lian Chinaherb AG (Wollerau, Switzerland); B: Yong Quan GmbH (Ennepetal, Germany).

Table 3S. *In vitro* inhibition of the hERG potassium current (I_{hERG}) in *Xenopus* oocytes by plant-derived foods (vegetables, fruits, and spices).

Common name	Scientific plant name[a]	Source[b] (Lot no.)	Extract	Inhibition of I_{hERG} (%) at 100 µg/mL
Onion	*Allium cepa* L.	A	EtOAc MeOH	0.0 ± 0.0 0.0 ± 0.0
Leek	*Allium porrum* L.	A	EtOAc MeOH	0.0 ± 0.0 4.5 ± 1.6
Dill	*Anethum graveolens* L.	A	EtOAc MeOH	5.5 ± 3.9 7.4 ± 2.9
Celery stalks	*Apium graveolens* L. var. *dulce*	A	EtOAc MeOH	4.9 ± 2.2 3.8 ± 0.2
Celery root	*Apium graveolens* L. var. *rapaceum*	A	EtOAc MeOH	5.9 ± 1.1 4.3 ± 2.2
Horseradish	*Armoracia rusticana* P.Gaertn., Mey. & Scherb.	A	EtOAc MeOH	3.4 ± 4.5 6.7 ± 2.6
Wormwood	*Artemisia absinthium* L.	B (3518004)	EtOAc MeOH	2.9 ± 1.3 5.4 ± 2.9
Tarragon	*Artemisia dracunculus* L.	C (1602)	EtOAc MeOH	4.4 ± 5.7 1.1 ± 1.1
Rooibos tea	*Aspalathus linearis* (Burm.f.) Dahlg.	A	EtOAc MeOH	1.8 ± 1.8 1.6 ± 2.2
Asparagus	*Asparagus officinalis* L.	A	EtOAc MeOH	0.0 ± 0.0 0.0 ± 0.0
Beetroot	*Beta vulgaris* L. var. *esculenta* L.	A	EtOAc MeOH	-0.5 ± 2.2 1.8 ± 1.8
Black mustard	*Brassica nigra* (L.) Koch	C (5218)	EtOAc MeOH	6.7 ± 4.1 3.7 ± 2.6
Broccoli	*Brassica oleracea* L. var. *italica* Plenck	A	EtOAc MeOH	0.0 ± 0.0 0.0 ± 0.0
Chilli	*Capsicum frutescens* L.	B (2037101)	EtOAc MeOH	1.4 ± 2.1 8.1 ± 2.8
Lime	*Citrus aurantiifolia* (Christm.) Swingle	A	EtOAc MeOH	27.1 ± 3.2 9.4 ± 0.2
Lemon	*Citrus limon* (L.) Burm.f.	A	EtOAc MeOH	18.1 ± 5.5 9.1 ± 1.7
Grapefruit juice	*Citrus paradisi* Macfad.	A	EtOAc MeOH	0.0 ± 0.0 0.0 ± 0.0
Coffee	*Coffea arabica* L.	A	EtOAc MeOH	0.0 ± 0.0 0.0 ± 0.0
Coriander (fruits)	*Coriandrum sativum* L.	C (7335)	EtOAc MeOH	8.4 ± 1.5 0.2 ± 2.0
Coriander (leaves)	*Coriandrum sativum* L.	A	EtOAc MeOH	4.4 ± 0.8 13.5 ± 2.4
Zucchini	*Cucurbita pepo* ssp. *pepo* convar. giromontiina	A	EtOAc MeOH	0.0 ± 0.0 0.0 ± 0.0
Artichoke	*Cynara scolymus* L.	A	EtOAc MeOH	0.0 ± 0.0 0.0 ± 0.0
Cardamom	*Elettaria cardamomum* (L.) Maton	D (2005.07.0866)	EtOAc MeOH	1.7 ± 3.8 1.7 ± 2.9
Rocket	*Eruca sativa* Mill.	A	EtOAc MeOH	1.6 ± 1.6 4.4 ± 1.3

Common name	Scientific plant name[a]	Source[b] (Lot no.)	Extract	Inhibition of I_{hERG} (%) at 100 µg/mL
Acai	*Euterpe oleracea* Mart.	E	PE EtOAc MeOH	0.0 ± 0.0 4.2 ± 2.4 6.4 ± 4.2
Fig	*Ficus carica* L.	A	EtOAc MeOH	-6.0 ± 3.3 0.2 ± 0.2
Fennel	*Foeniculum vulgare* Mill. var. *azoricum*	A	EtOAc MeOH	0.0 ± 0.0 0.0 ± 0.0
Mangosteen	*Garcinia mangostana* L.	A	PE EtOAc MeOH	0.0 ± 0.0 0.0 ± 0.0 0.0 ± 0.0
Soybean	*Glycine max* (L.) Merr.	A	EtOAc MeOH	0.0 ± 0.0 0.0 ± 0.0
Mate	*Ilex paraguariensis* A. St.-Hil.	B (1544201)	EtOAc MeOH	-5.4 ± 1.7 0.0 ± 0.0
Star anise	*Illicium verum* Hook.f.	C (5901)	EtOAc MeOH	2.5 ± 2.1 6.8 ± 2.6
Bay	*Laurus nobilis* L.	B (3143300)	EtOAc MeOH	3.6 ± 0.3 8.4 ± 3.6
Lovage	*Levisticum officinale* Koch	A	EtOAc MeOH	3.4 ± 2.0 0.3 ± 2.5
Goji	*Lycium barbarum* L.	F	PE EtOAc MeOH	0.0 ± 0.0 0.0 ± 0.0 0.0 ± 0.0
Tomato	*Lycopersicon esculentum* Mill.	A	EtOAc MeOH	0.0 ± 0.0 0.0 ± 0.0
Apple	*Malus domestica* Borkh.	A	EtOAc MeOH	0.0 ± 0.0 0.0 ± 0.0
Noni	*Morinda citrifolia* L.	G	PE EtOAc MeOH	0.0 ± 0.0 0.0 ± 0.0 8.2 ± 4.3
Nutmeg	*Myristica fragrans* L.	C (0524)	EtOAc MeOH	6.2 ± 3.8 42.3 ± 1.0
Prickly pear (fruits)	*Opuntia ficus-indica* (L.) Mill.	H	PE EtOAc MeOH	0.0 ± 0.0 0.0 ± 0.0 0.0 ± 0.0
Prickly pear (leaves)	*Opuntia ficus-indica* (L.) Mill.	H	PE EtOAc MeOH	0.0 ± 0.0 0.0 ± 0.0 0.0 ± 0.0
Oregano	*Origanum vulgare* L.	C (0403)	EtOAc MeOH	8.7 ± 1.7 0.2 ± 3.5
Guarana	*Paullinia cupana* Kunth	B (3759605)	EtOAc MeOH	5.9 ± 2.9 45.3 ± 10.2
Parsley	*Petroselinum crispum* (Mill.) A.W. Hill	A	EtOAc MeOH	4.4 ± 2.2 4.4 ± 3.3
Common bean	*Phaseolus vulgaris* L.	A	EtOAc MeOH	3.3 ± 1.9 0.4 ± 2.8
Black pepper	*Piper nigrum* L.	B (3604607)	EtOAc MeOH	32.4 ± 0.5 36.9 ± 9.1
Rhubarb	*Rheum rhabarbarum* L.	A	EtOAc MeOH	2.6 ± 3.7 0.1 ± 2.3
Rosemary	*Rosmarinus officinalis* L.	C (6702)	EtOAc MeOH	8.8 ± 1.4 1.3 ± 1.7
Sage	*Salvia officinalis* L.	A	EtOAc MeOH	0.0 ± 0.0 0.0 ± 0.0

Common name	Scientific plant name[a]	Source[b] (Lot no.)	Extract	Inhibition of I_{hERG} (%) at 100 µg/mL
White mustard	*Sinapis alba* L.	B (2038801)	EtOAc MeOH	6.4 ± 0.9 4.0 ± 1.0
Spinach	*Spinacea oleracea* L.	A	EtOAc MeOH	0.0 ± 0.0 0.0 ± 0.0
Clove	*Syzygium aromaticum* (L.) Merr. & Perry	B (2076901)	EtOAc MeOH	3.8 ± 3.8 5.0 ± 3.3
Cacao bean	*Theobroma cacao* L.	I	MeOH	0.0 ± 0.0
Garden thyme	*Thymus vulgaris* L.	B (4047704)	EtOAc MeOH	0.0 ± 0.0 0.6 ± 0.6
Cranberry	*Vaccinium macrocarpon* Aiton	A	PE EtOAc MeOH	0.0 ± 0.0 0.0 ± 0.0 0.0 ± 0.0
Corn salad	*Valerianella locusta* (L.) Laterr.	A	EtOAc MeOH	0.0 ± 0.0 0.0 ± 0.0
Ginger	*Zingiber officinale* Rosc.	A	EtOAc MeOH	16.1 ± 1.2 0.0 ± 0.0

[a] Scientific plant names can be found in [4].

[b] A: Fresh plant material from local markets (Basel, Switzerland); B: Dixa AG (St. Gallen, Switzerland); C: Drogerie zum Chrüterhüsli AG (Basel, Switzerland); D: Hänseler AG (Herisau, Switzerland); E: Brasilfruits (Bern, Switzerland); F: Shanghai Institute of Materia Medica (China); G: Nature's Sunshine Products (Spanish Fork, UT, US); H: Instituto Tecnológico y de Estudios Superiores de Monterrey (Mexico); I : Confiserie Sprüngli AG (Zurich, Switzerland).

References

1 *European Scientific Cooperative on Phytotherapy*. ESCOP Monographs (second edition). Exeter/Stuttgart/New York: ESCOP/Georg Thieme Verlag/Thieme New York; 2003

2 *European Scientific Cooperative on Phytotherapy*. ESCOP Monographs (second edition, Supplement). Exeter/Stuttgart/New York: ESCOP/Georg Thieme Verlag/Thieme New York; 2009

3 *Chinese Pharmacopoeia Commission*. Pharmacopoeia of the People`s Republic of China: Volume I (English edition). Beijing: China Medical Science Press; 2010

4 *van Wyk BE*. Handbuch der Nahrungspflanzen: Ein illustrierter Leitfaden. Stuttgart: Wissenschaftliche Verlagsgesellschaft mbH; 2005

3.2. hERG channel inhibitors in extracts of Coptidis rhizoma

Schramm A, Baburin I, Hering S, Hamburger M.

Planta Med 2011; 77: 692–697

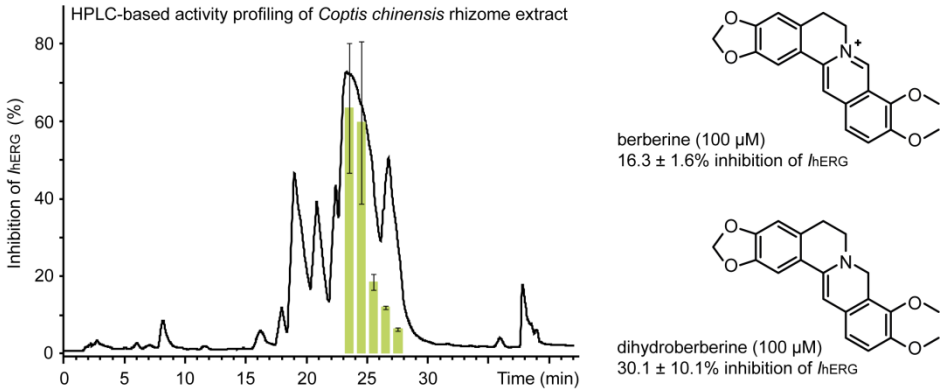

HPLC-based activity profiling was used in combination with a functional assay on *Xenopus* oocytes to localize and identify hERG channel blockers in *Coptis chinensis* rhizomes. Five quaternary protoberberines were purified, and structurally characterized by high-resolution mass spectrometry and microprobe NMR. Quaternary alkaloids, as well as di- and tetrahydroberberine were tested for their ability to reduce the hERG current. Berberine and dihydroberberine showed the highest hERG inhibitory activity.

Extraction of plant material, HPLC microfractionation, isolation of compounds, recording and interpretation of analytical data for structure elucidation (LC-PDA-ESI-TOF-MS, microprobe NMR), writing the draft of the manuscript, and preparation of figures (Fig. 2A–B, 3, 4, and 5A) were my contributions to this publication.

Anja Schramm

hERG Channel Inhibitors in Extracts of Coptidis Rhizoma

Authors: Anja Schramm[1]*, Igor Baburin[2]*, Steffen Hering[2], Matthias Hamburger[1]

Affiliations:
[1] Division of Pharmaceutical Biology, University of Basel, Basel, Switzerland
[2] Institute of Pharmacology and Toxicology, University of Vienna, Vienna, Austria

Key words
- hERG channel inhibition
- herbal extracts
- *Coptis chinensis*
- Ranunculaceae
- HPLC-based activity profiling
- protoberberine alkaloids

Abstract

Inhibition of the hERG channel delays repolarization and prolongs the QT interval and cardiac action potential which can lead to sudden death. Several drugs have been withdrawn from the market due to hERG channel inhibition. In the search of hERG channel inhibitors of natural origin, we established an HPLC-based profiling approach which combines HPLC-microfractionation and bioactivity testing on *Xenopus laevis* oocytes. The methanolic extract of the TCM herbal drug Coptidis rhizoma (*Coptis chinensis* Franch., Ranunculaceae) reduced the peak tail hERG current by 31.7 ± 2.0% at 100 µg/mL. HPLC-based activity profiling pointed towards berberine as the active constituent. However, hERG inhibition by 100 µM of a reference sample of berberine (16.3 ± 1.6%) was less pronounced than previously reported. Subsequent LC-PDA-MS analysis showed that berberine collected by microfractionation of the *Coptis* extract had been, in part, transformed to active dihydroberberine. Formic acid added to the HPLC mobile phase to reduce peak tailing of protoberberine alkaloids acted as a reducing reagent according to the mechanism of the Leuckart-Wallach reaction. Among other structurally related protoberberines tested, dihydroberberine (30.1 ± 10.1% at 100 µM) was the most potent hERG inhibitor.

Abbreviations

hERG:	human ether-a-go-go-related gene
ECG:	electrocardiogram
TdP:	torsades de pointes
TCM:	traditional Chinese medicine
ASE:	accelerated solvent extraction

received Nov. 19, 2010
revised February 11, 2011
accepted February 18, 2011

Bibliography
DOI http://dx.doi.org/10.1055/s-0030-1270920
Published online March 16, 2011
Planta Med 2011; 77: 692–697

ISSN 0032-0943

Correspondence
Prof. Dr. Matthias Hamburger
Department of Pharmaceutical Sciences
Division of Pharmaceutical Biology
University of Basel
Klingelbergstrasse 50
4056 Basel
Switzerland
Phone: + 41 6 12 67 14 25
Fax: + 41 6 12 67 14 74
Matthias.Hamburger@unibas.ch

Introduction

In the myocardium, the hERG (human ether-a-go-go-related gene) channel conducts the rapid delayed rectifier K^+ current (I_{Kr}) which accelerates the repolarization of the action potential. Channel inhibition leads to delayed repolarization and, consequently, to a prolonged action potential visible as an extended QT interval on the electrocardiogram (ECG) [1]. Class III anti-arrhythmic agents block I_{Kr}. Thus, hERG channel inhibition may be associated with pro-arrhythmic and anti-arrhythmic effects. Drug-induced QT prolongation is a risk factor for the development of *torsades de pointes* (TdP), a potentially life-threatening arrhythmia. This has led to several drug withdrawals, restrictions of use, warnings, and relabellings [2]. One of the most recent withdrawals due to an arrhythmogenic risk has been the antitussive drug clobutinol in 2007 [3]. Since both cardiac and noncardiac drugs have the potential to inhibit the repolarizing current I_{Kr}, screening for hERG channel inhibition is routinely performed in the pharmaceutical industry as part of the early pharmacological profiling of leads [4]. In contrast, virtually nothing is known about hERG channel blockers of natural origin. Naringenin is probably the best studied natural product, both *in vitro* and *in vivo*. Intake of naringenin via grapefruit juice has been shown to lead to QT prolongation in healthy humans [5–7].

To assess the risk of hERG channel inhibition by medicinal plants, we screened a library of 91 herbal extracts derived from major officinal herbal drugs of the European and Chinese Pharmacopoeias. Extracts were tested by means of an automated two-microelectrode voltage-clamp assay

* The authors contributed equally to this work.

on *Xenopus laevis* oocytes [8], at a concentration of 100 µg/mL. This concentration has been previously found to be appropriate for screening of herbal extracts in the oocyte model with other ion channel-type targets such as $GABA_A$ receptors [9,10]. Among the extracts tested, the methanolic extract of Coptidis rhizoma (*Coptis chinensis* Franch., Ranunculaceae) induced 31.7 ± 2.0% (n = 6) inhibition of the peak tail hERG current (**Fig. 1**). Coptidis rhizoma (Huanglian) is a well-known herbal drug in traditional Chinese medicine (TCM). According to the Chinese Pharmacopoeia, it is used as an antipyretic, antimicrobial, and anti-inflammatory remedy for treating fever, gastrointestinal disorders (e.g., dysentery, vomiting, and icterus), insomnia, nose bleeding, and toothache [11,12]. Quaternary protoberberine alkaloids represent the main constituents and are regarded as pharmacologically active principles of the herbal drug [12,13]. On the other hand, the alkaloids are mainly responsible for the acute toxicity of Coptidis rhizoma extract. Berberine, the most abundant alkaloid [14], also showed the strongest cytotoxicity in different cell lines [13]. The broad public considers herbal drugs to be generally safe. However, it is known that some herbs cause drug interactions or may display unwanted effects [15]. In the case of Coptidis rhizoma, respiratory failure, liver function injury, and severe arrhythmia have been reported [13]. Here, we describe the localization of hERG channel inhibitory activity of Coptidis rhizoma extract with the aid of an HPLC-based profiling protocol. HPLC-based activity profiling enables rapid identification of pharmacologically active natural products in extracts with only milligram-amounts of extracts [16].

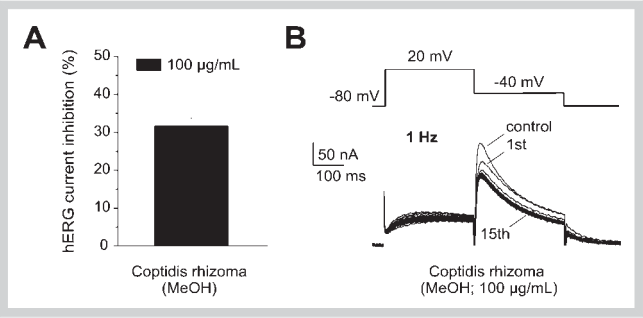

Fig. 1 Inhibition of potassium currents through hERG channels expressed in *Xenopus* oocytes by Coptidis rhizoma extract (MeOH, 100 µg/mL). **A** A mean current inhibition by 31.7 ± 2.0% (n = 6) was observed. **B** A current trace recorded in the absence (control) of the drug is superimposed with the current traces recorded in the presence of Coptidis rhizoma (MeOH; 100 µg/mL) during a 1 Hz pulse train (15 pulses) applied from −80 mV. The voltage protocol is shown above the current traces.

Materials and Methods

General experimental procedures

Analytical HPLC separations were performed with an Agilent 1100 system consisting of an autosampler, degasser, binary pump, column oven, and diode array detector. The HPLC conditions were: SunFire C18 (3.5 µm, 3.0 × 150 mm) column (Waters), water + 0.1% formic acid (solvent A), methanol + 0.1% formic acid (solvent B), gradient profile: 20% → 35% B (0–25 min), 35% → 100% B (25–26 min), 100% B (26–30 min), flow rate: 0.4 mL/min, DAD 254 nm. For LC-PDA-MS analysis, the HPLC was coupled to a micrOTOF ESI-MS system (Bruker Daltonics). Mass calibration was performed with a solution of formic acid 0.1% in 2-propanol/water (1 : 1) containing 5 mM NaOH. Mass spectra were recorded in the positive ion mode. Data acquisition and analysis were performed using HyStar 3.2 software. NMR spectra (^{1}H, COSY, HSQC, HMBC, NOESY, NOE) were recorded on a Bruker Avance III 500 MHz spectrometer (Bruker Daltonics) operating at 500.13 MHz for ^{1}H. The instrument was equipped with a 1-mm TXI microprobe. All measurements were carried out at 291.15 K. Topspin 2.1 was used to process and analyse the spectra.

Solvents and chemicals

Formic acid (98.0–100.0%), dimethylsulfoxide (DMSO), and HPLC-grade methanol were from Scharlau. Trifluoroacetic acid (≥ 98%) was purchased from Sigma-Aldrich. Solvents for the extraction and isolation process were of analytical grade whereas HPLC-grade solvents were used for HPLC separations. Berberine chloride hydrate (~ 95%), dihydroberberine (≥ 91% by HPLC), and (*R*,*S*)-tetrahydroberberine (≥ 95% by TLC and MS) were purchased from Fluka, Phytolab, and Latoxan, respectively.

Plant material

The drug Coptidis rhizoma (Huanglian) (batch no. 0901503) was purchased from Yong Quan GmbH. A voucher sample (number 00197) is preserved at the Division of Pharmaceutical Biology, University of Basel, Switzerland. Prior to extraction, the plant material was frozen with liquid nitrogen and powdered with a ZM 1 ultracentrifugal mill (sieve size 2.0 mm) (Retsch).

Extraction

The extract for the initial screening and the HPLC-based activity profiling was prepared by accelerated solvent extraction (ASE) using a Dionex ASE 200 extractor with solvent controller (Dionex). Extraction was carried out in 11 mL cartridges with the following conditions: preheat time, 1 min; static extraction cycle, 5 min; purge, 120 s with nitrogen; temperature, 70 °C; pressure, 120 bar. Extraction was successively done with petroleum ether, ethyl acetate, and methanol (3 cycles per each solvent). For isolation, the ground rhizomes (375 g) were extracted exhaustively with methanol by percolation at room temperature. After evaporation of the solvent under reduced pressure, a viscous extract (60.8 g) was obtained. All samples, including the extracts, were stored at 4 °C until use.

Microfractionation and activity profiling

Microfractionation for HPLC-based activity profiling was carried out on an Agilent 1100 system consisting of an autosampler, degasser, quaternary pump, column oven, and diode array detector. We separated 2.5 mg of the extract by semipreparative RP-HPLC into 42 one-minute microfractions. Separation was achieved on a SunFire Prep C18 (5 µm, 10 × 150 mm) column (Waters) with water + 0.1% formic acid (solvent A) and methanol + 0.1% formic acid (solvent B) using the following gradient profile: 15% → 35% B (0–35 min), 35% → 100% B (35–36 min), 100% B (36–42 min). The flow rate was 4 mL/min, and detection was at 254 nm. 50 µL of a stock solution of the extract (50 mg/mL in DMSO) was injected. Fractions were collected into glass tubes. After solvent removal (Genevac EZ-2 Plus evaporator), the dried films were redissolved in methanol, transferred to 4-mL glass vials, and dried again under N_2 gas prior to dissolution in DMSO for bioassay.

Isolation of protoberberines 1–5

For isolation of alkaloids, a portion (12.1 g) of the extract was separated by column chromatography on silica gel 60 column (63–200 µm, 9 × 31 cm i.d.). The mobile phase was a mixture of propanol, methanol, water, and formic acid (64 : 30 : 5 : 1 v/v/v/v). To elute the alkaloids, the polarity of the solvent system was increased gradually (64 : 30 : 5 : 1, 59 : 30 : 10 : 1, 54 : 30 : 15 : 1, 49 : 30 : 20 : 1, 39 : 40 : 20 : 1, 29 : 50 : 20 : 1; 2 L each). Fractions of 200 mL were collected and combined after TLC analysis (silica gel 60 F_{254} precoated Al sheets, propanol-methanol-water-formic acid 64 : 30 : 5 : 1 v/v/v/v, detection at $UV_{366\,nm}$) into 16 fractions. Final purification of quaternary protoberberines was achieved on a prep HPLC system consisting of a LC-8A preparative pump, SCL-10AVP system controller, and SPD-M10A VP PDA detector and controlled by class-VP V6.14 SP2A software (all Shimadzu). Preparative HPLC separations were performed on a SunFire Prep C18 OBD (5 µm, 30 × 150 mm) column (Waters) using water + 0.025% TFA (solvent A) and methanol + 0.025% TFA (solvent B) as eluents. The flow rate was 20 mL/min, and chromatograms were recorded at 254 nm. Separation of fraction 10 afforded **1** (t_R 11.1 min) and **5** (t_R 13.6 min) with the following gradient: 30% B (0–3 min), 30% → 55% B (3–18 min), 55% → 100% B (18–19 min), 100% B (19–23 min). Purification of fraction 5 yielded **3** (t_R 14.1 min) and **4** (t_R 15.4 min), while compound **2** (t_R 12.4 min) was isolated from fraction 16. The gradient was as follows: 30% B (0–4 min), 30% → 55% B (4–24 min), 55% → 100% B (24–26 min), 100% B (26–30 min). Compound purity was ≥ 95% by ^{1}H-NMR.

Expression of hERG channels and voltage clamp studies

Preparation of stage V–VI oocytes from *Xenopus laevis* (NASCO), synthesis of capped run-off complementary RNA (cRNA) transcripts from linearized complementary DNA (cDNA) templates, and injection of cRNA were described previously [17]. Currents through hERG channels were studied 1–4 days after microinjection of the cRNA with the two-microelectrode voltage clamp method making use of a TURBO TEC-03X amplifier (npi electronic GmbH). The bath solution contained: 96 mM 2-(N-morpholino)ethanesulphonic acid sodium salt, 2 mM 2-(N-morpholino)ethanesulphonic acid potassium salt, 1 mM CaCl2, 5 mM HEPES, and 1 mM MgCl2 adjusted to pH 7.6 with methanesulphonic acid. Voltage-recording and current-injecting microelectrodes were filled with 3 mM KCl and pulled to have resistances between 0.3 and 2 MΩ. Oocytes with maximal current amplitudes > 2 µA were discarded to exclude voltage clamp errors. The pClamp software package version 10.0 (Molecular Devices, Inc.) was used for data acquisition.

Voltage protocol

The voltage protocol (see insets in ◉ **Figs. 1B**, **2C–D**, and ◉ **5B**) was designed to simulate voltage changes during a cardiac action potential with a 300 ms depolarization to + 20 mV (analogous to plateau phase), a repolarization for 300 ms to − 40 mV (inducing a tail current) and a final step to the holding potential. The + 20 mV depolarization rapidly inactivates hERG channels, thereby limiting the amount of outward current. During the repolarization to − 40 mV, the previously activated channels open due to rapid recovery from inactivation. The decreases in the resulting tail current amplitudes were taken as a measure of block development during a pulse train.

Drug application and analysis

Drugs were applied by means of a fast ScreeningTool perfusion technique (npi electronic GmbH) [8]. ORIGIN software version 7.0 (OriginLab Corporation) was used for data analysis. Data are given as mean ± S. E. of at least two oocytes and ≥ 2 oocyte batches.

Results and Discussion

In the search for hERG channel inhibitors of natural origin, we adapted a previously developed protocol for discovery of $GABA_A$ receptor modulators [9]. For this purpose, we separated 2.5 mg of the methanolic extract of Coptidis rhizoma by semipreparative RP-HPLC into 42 one-minute microfractions which were tested in the functional bioassay. ◉ **Fig. 2** shows the HPLC chromatogram recorded at 254 nm and the corresponding activity profile. hERG inhibition was studied during 1 Hz pulse trains applied from a

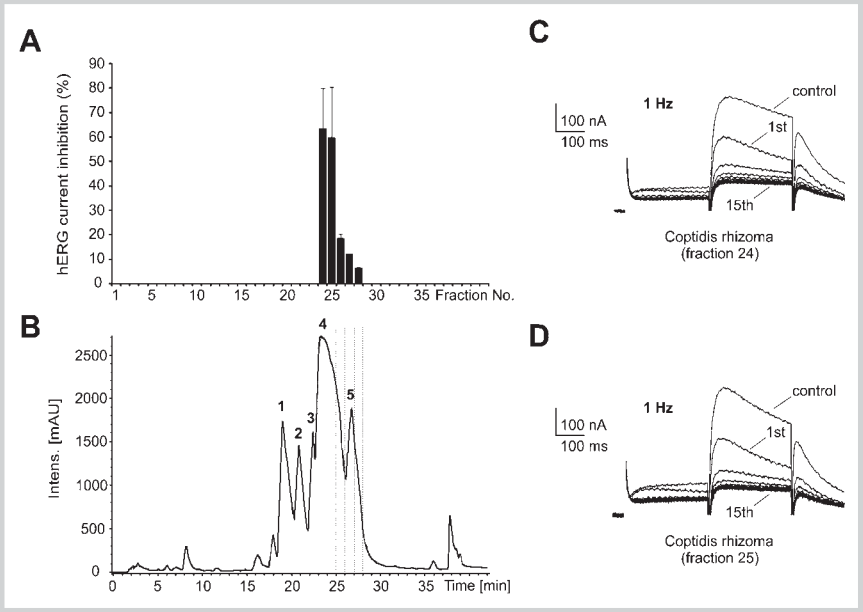

Fig. 2 Activity profiling of Coptidis rhizoma extract (MeOH) for inhibition of the hERG channel. **B** HPLC chromatogram (254 nm) of a semipreparative separation of 2.5 mg extract and (**A**) inhibition (in %) of hERG currents by 42 one-minute fractions are shown. **C, D** The control current (recorded in the absence of drug) is superimposed with the hERG currents recorded during a 1 Hz pulse train (15 pulses) in the presence of the two most active fractions (24 and 25). Same voltage protocol as in ◉ **Fig. 1**.

holding potential of − 80 mV (see Methods for details on the pulse protocol). Main activity was identified in microfractions 24 and 25 (peak tail hERG current inhibition by 63.3 ± 16.7% [n = 2] and 59.5 ± 20.9% [n = 2], respectively) which corresponded to the dominant HPLC peak. With the aid of on-line (LC-PDA-MS) and off-line (1 mm microprobe NMR of collected peak) spectroscopic data, the main peak was identified as berberine (**4**) (**Fig. 3**), a previously reported hERG channel blocker of natural origin [18, 19]. However, inhibition of the hERG current by 100 µM of a reference sample of berberine was, in our hands, less pronounced than previously reported (16.3 ± 1.6%, n = 3, but see [18, 19]).

However, subsequent LC-PDA-MS analysis showed that berberine (**4**) collected by microfractionation of the *Coptis* extract had been, in part, transformed to active dihydroberberine (**6**). This could be explained by the mechanism of the Leuckart-Wallach reaction [20], whereby formic acid added to the mobile phase to reduce peak tailing of quaternary alkaloids, acted as a reducing reagent (**Fig. 4E**). The iminium ion structure of protoberberines is sensitive to a nucleophilic attack by the hydride ion delivered by formic acid. Traces of formic acid remaining in the microfractions after evaporation of the mobile phase were apparently sufficient for the partial reduction of quaternary protoberberines at room temperature. The reaction occurred in the aprotic solvent DMSO, which is used to dissolve the fractions for bioassay, but not in the protic solvent methanol. This differential behaviour can be best explained by the solvent capability to solvate ions rather than by the solvent polarity [21]. The formation of dihydroberberine (**6**) was confirmed by comparative off-line microprobe NMR and on-line LC-PDA-MS analysis in DMSO and methanol of active microfraction 24 (**Fig. 4A–D**). However, dihydroprotoberberines are also known to auto-oxidize back to the quaternary alkaloids, especially under the influence of light [22]. Given the initial profiling protocol and the findings described above, microfractions 24 and 25 in the profiling consisted of a mixture of berberine (**4**) and dihydroberberine (**6**). When tested at 100 µM, dihydroberberine (**6**) reduced the peak tail hERG current more efficiently (30.1 ± 10.1% [n = 3, **Fig. 5**]) than the same concentration of the reference sample of berberine (16.3 ± 1.6%). We report here on the hERG channel inhibitory property of dihydroberberine for the first time.

Despite the fact that the activity profile revealed no notable activity for other peaks in the chromatogram, we isolated structurally related quaternary protoberberines for the purpose of preliminary information on structure activity relationships for this compound class. Compounds **1**–**5** (**Fig. 3**) were purified by means of open column chromatography on silica gel and preparative RP-HPLC. To avoid the above described conversion into dihydro derivatives in samples used for activity testing, trifluoroacetic acid (TFA) was used as the mobile phase additive for RP-HPLC. Quaternary alkaloids **1**–**5**, as well as dihydroberberine (**6**) and (*R,S*)-tetrahydroberberine (**7**), were tested at 100 µM for their ability to block the human hERG channel (**Fig. 5**). Quaternary protoberberines were marginally active, and substitution pattern at positions C(2), C(3), C(9), and C(10) had moderate influence on activity. Among berberine (**4**) and its derivatives **6** and **7**, dihydroberberine (**6**) showed the highest activity (peak tail hERG current inhibition by 30.1 ± 10.1%, n = 3). Berberine (**4**) displayed an inhibition (14.9 ± 1.7%, n = 3) similar to that obtained with the reference sample of berberine (see above), while tetrahydroberberine (**7**) had almost no effect (6.6 ± 5.4%, n = 3, **Fig. 5A**). These observations suggest that the double bond between C(13) and C(13a) and the resulting extended conjugated π-electron system are of importance for the inhibitory effect.

Although berberine prolongs the action potential duration, the underlying molecular mechanism remains elusive [23]. The less pronounced hERG inhibition by berberine, in our hands, may be explained by reduced channel inhibition during the shorter conditioning pre-pulses applied in our study (300 ms vs. 4 s in [18, 19]). Future studies will show if the different voltage protocols applied induce different state-dependent hERG inhibition [17]. Coptidis rhizoma preparations are mostly used internally and, therefore, the oral bioavailability of the main alkaloid, berberine,

Compound	R_1	R_2	R_3	R_4
Coptisine (**1**)	-CH_2-		-CH_2-	
Epiberberine (**2**)	CH_3	CH_3	-CH_2-	
Jatrorrhizine (**3**)	CH_3	OH	CH_3	CH_3
Berberine (**4**)	-CH_2-		CH_3	CH_3
Palmatine (**5**)	CH_3	CH_3	CH_3	CH_3

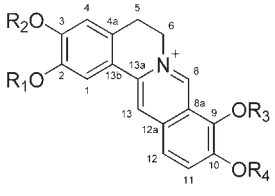

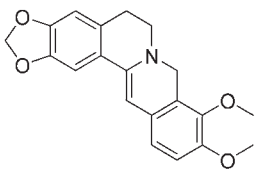

(**6**)

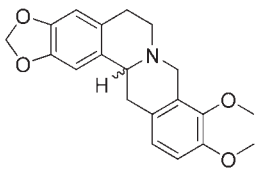

(**7**)

Fig. 3 Structures of the isolated protoberberine alkaloids **1**–**5** and the two berberine derivatives dihydroberberine (**6**) and (*R,S*)-tetrahydroberberine (**7**).

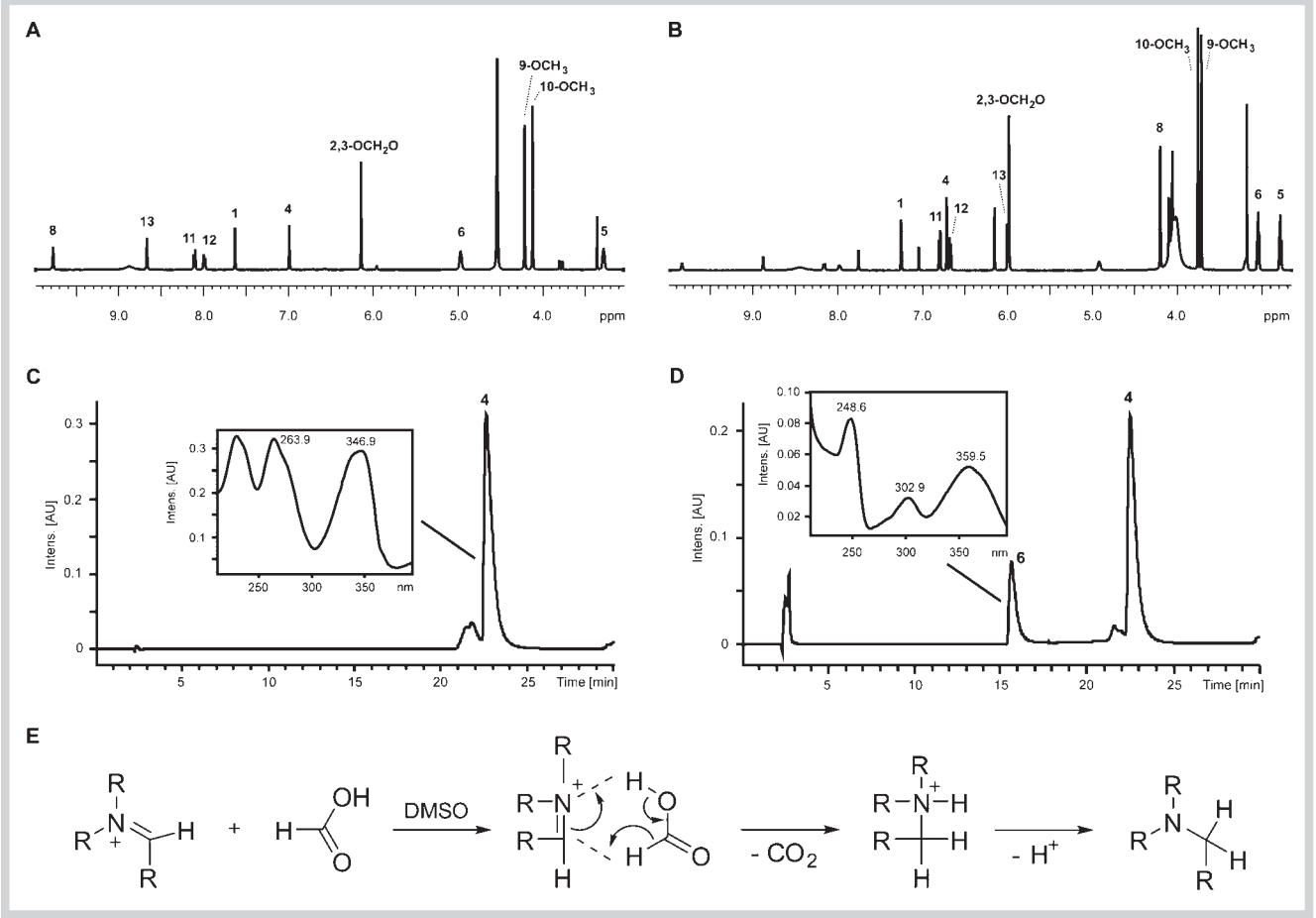

Fig. 4 Formation of dihydroberberine (**6**) from berberine (**4**) in active fraction 24 (**Fig. 1**). ^{1}H-NMR spectrum recorded in MeOH-d_4 (**A**) and in DMSO-d_6 (**B**). HPLC-PDA analysis of sample dissolved in methanol (**C**) and DMSO (**D**), with UV spectra of peaks shown as insets. (**E**) The proposed reaction mechanism for reduction of berberine (**4**) in the presence of formic acid and DMSO.

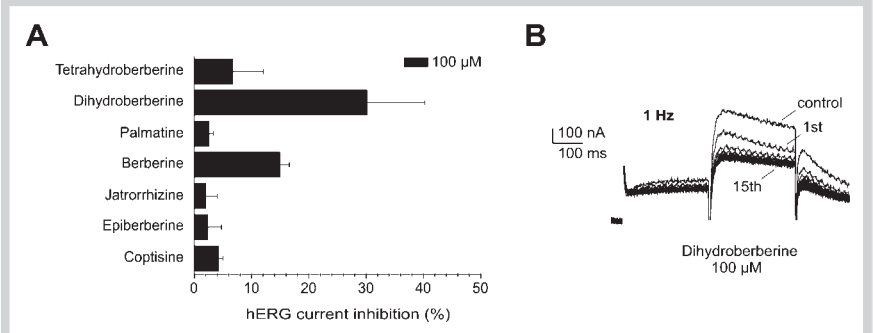

Fig. 5 Inhibition of hERG currents (in %) by compounds **1**–**7** at 100 µM. **A** A mean current inhibition by 4.2 ± 0.8 % (n = 2) for coptisine, 2.4 ± 2.4 % (n = 2) for epiberberine, 2.0 ± 2.0 % (n = 2) for jatrorrhizine, 14.9 ± 1.7 % (n = 3) for berberine, 2.5 ± 0.8 % (n = 2) for palmatine, 30.1 ± 10.1 % (n = 3) for dihydroberberine, and 6.6 ± 5.4 % (n = 2) for tetrahydroberberine was observed. **B** The current trace recorded in the absence of the drug (control) is superimposed with the currents recorded during the 1 Hz pulse train (15 pulses) in the presence of 100 µM dihydroberberine. Same pulse protocol as in **Fig. 1**.

is relevant in view of an assessment of possible undesirable effects. Daily recommended doses of Coptidis rhizoma vary from 1.5 to 9 g [24], which corresponds to a daily intake of 60 to 900 mg berberine [14]. Also, berberine, dihydroberberine, and some derivatives are currently being studied as drug candidates for treating type 2 diabetes and various neurological diseases [25, 26]. Several studies, conducted in animals and humans, demonstrated poor bioavailability of berberine after oral administration [26–28]. In human volunteers, plasma concentrations (C_{max}) after a single dose of 300 mg of berberine reached 0.39 µg/mL [26]. The comparatively high concentrations of phase I and II metabolites in human urine indicated extensive biotransformation after absorption [29, 30]. Upon intravenous administration in rats, berberine showed fast distribution into the liver and biliar excretion [31]. Oral bioavailability of dihydroberberine was higher than that of berberine, albeit also limited by the fact that the compound is prone to acidic-catalyzed aromatisation in the stomach, and the bioavailable amount of dihydroberberine is converted to berberine in the plasma [25, 32].

Identification of other hERG channel blockers in herbal drugs and means to selectively remove such compounds from herbal extracts will be reported in due course.

Acknowledgements

We thank Dr. Christian Raith and Dr. Melanie Quitschau for valuable discussions on the reactivity of protoberberines. Financial support from the Swiss National Science Foundation (Projects 31600-113109 and 205320-126888/1), the Steinegg-Stiftung, Herisau, the Fonds zur Förderung von Lehre und Forschung, Basel (M.H.), and the FWF Project P2239-B11 (S.H.) is gratefully acknowledged.

References

1 *Hancox JC, McPate MJ, El Harchi A, Zhang YH.* The hERG potassium channel and hERG screening for drug-induced torsades de pointes. Pharmacol Therapeut 2008; 119: 118–132
2 *Raschi E, Vasina V, Poluzzi E, De Ponti F.* The hERG K+ channel: target and antitarget strategies in drug development. Pharmacol Res 2008; 57: 181–195
3 *Deisemann H, Ahrens N, Schlobohm I, Kirchhoff C, Netzer R, Möller C.* Effects of common antitussive drugs on the hERG potassium channel current. J Cardiovasc Pharm 2008; 52: 494–499
4 *Polak S, Wisniowska B, Brandys J.* Collation, assessment and analysis of literature *in vitro* data on hERG receptor blocking potency for subsequent modeling of drugs' cardiotoxic properties. J Appl Toxicol 2009; 29: 183–206
5 *Scholz EP, Zitron E, Kiesecker C, Lück S, Thomas D, Kathöfer S, Kreye VAW, Katus HA, Kiehn J, Schoels W, Karle CA.* Inhibition of cardiac HERG channels by grapefruit flavonoid naringenin: implications for the influence of dietary compounds on cardiac repolarisation. Naunyn Schmiedebergs Arch Pharmacol 2005; 371: 516–525
6 *Lin CR, Ke XG, Ranade V, Somberg J.* The additive effects of the active component of grapefruit juice (naringenin) and antiarrhythmic drugs on HERG inhibition. Cardiology 2008; 110: 145–152
7 *Zitron E, Scholz E, Owen RW, Lück S, Kiesecker C, Thomas D, Kathöfer S, Niroomand F, Kiehn J, Kreye VAW, Katus HA, Schoels W, Karle CA.* QTc prolongation by grapefruit juice and its potential pharmacological basis – HERG channel blockade by flavonoids. Circulation 2005; 111: 835–838
8 *Baburin I, Beyl S, Hering S.* Automated fast perfusion of Xenopus oocytes for drug screening. Pflugers Arch Eur J Physiol 2006; 453: 117–123
9 *Kim HJ, Baburin I, Khom S, Hering S, Hamburger M.* HPLC-based activity profiling approach for the discovery of GABA(A) receptor ligands using an automated two microelectrode voltage clamp assay on *Xenopus* oocytes. Planta Med 2008; 74: 521–526
10 *Zaugg J, Baburin I, Strommer B, Kim HJ, Hering S, Hamburger M.* HPLC-based activity profiling: discovery of piperine as a positive GABA(A) receptor modulator targeting a benzodiazepine-independent binding site. J Nat Prod 2010; 73: 185–191
11 *Stöger EA, Friedl F.* Arzneibuch der Chinesischen Medizin, German edition. Stuttgart: Deutscher Apotheker Verlag; 2009
12 *Tang W, Eisenbrand G.* Chinese drugs of plant origin. Berlin: Springer-Verlag; 1992: 361–371
13 *Ma BL, Ma YM, Shi R, Wang TM, Zhang N, Wang CH, Yang Y.* Identification of the toxic constituents in Rhizoma Coptidis. J Ethnopharmacol 2010; 128: 357–364
14 *Kong WJ, Zhao YL, Xiao XH, Jin C, Li ZL.* Quantitative and chemical fingerprint analysis for quality control of rhizoma Coptidis chinensis based on UPLC-PAD combined with chemometrics methods. Phytomedicine 2009; 16: 950–959
15 *Ernst E.* Harmless herbs? A review of the recent literature. Am J Med 1998; 104: 170–178
16 *Potterat O, Hamburger M.* Natural products in drug discovery – Concepts and approaches for tracking bioactivity. Curr Org Chem 2006; 10: 899–920
17 *Stork D, Timin EN, Berjukow S, Huber C, Hohaus A, Auer M, Hering S.* State dependent dissociation of HERG channel inhibitors. Br J Pharmacol 2007; 151: 1368–1376
18 *Rodriguez-Menchaca A, Ferrer-Villada T, Lara J, Fernandez D, Navarro-Polanco RA, Sanchez-Chapula JA.* Block of hERG channels by berberine: mechanisms of voltage- and state-dependence probed with site-directed mutant channels. J Cardiovasc Pharm 2006; 47: 21–29
19 *Li BX, Yang BF, Zhou J, Xu CQ, Li YR.* Inhibitory effects of berberine on I-K1, I-K, and HERG channels of cardiac myocytes. Acta Pharmacol Sin 2001; 22: 125–131
20 *Brewer ARE.* Leuckart-Wallach reaction. In: Li JJ, Corey EJ, editors. Name reactions of functional group transformations. Hoboken, New Jersey: John Wiley & Sons, Inc.; 2007: 451–455
21 *Lukasiewicz A.* A study of the mechanism of certain chemical reactions —I: The mechanism of the leuckart-wallach reaction and of the reduction of schiff bases by formic acid. Tetrahedron 1963; 19: 1789–1799
22 *Kondo Y, Imai J, Inoue H.* Reaction of protoberberine-type alkaloids. Part 12: a facile method for regiospecific oxygenation and excited oxidative ring-cleavage of berberine alkaloids. J Chem Soc [Perkin I] 1980: 911–918
23 *Wang YX, Zheng YM.* Ionic mechanism responsible for prolongation of cardiac action-potential duration by berberine. J Cardiovasc Pharm 1997; 30: 214–222
24 *Bensky D, Clavey S, Stöger E.* Chinese herbal medicine – materia medica, 3rd edition. Seattle: Eastland Press, Inc.; 2004: 134–138
25 *Turner N, Li JY, Gosby A, To SWC, Cheng Z, Miyoshi H, Taketo MM, Cooney GJ, Kraegen EW, James DE, Hu LH, Li J, Ye JM.* Berberine and its more biologically available derivative, dihydroberberine, inhibit mitochondrial respiratory complex I – A mechanism for the action of berberine to activate AMP-activated protein kinase and improve insulin action. Diabetes 2008; 57: 1414–1418
26 *Ye MZ, Fu S, Pi RB, He F.* Neuropharmacological and pharmacokinetic properties of berberine: a review of recent research. J Pharm Pharmacol 2009; 61: 831–837
27 *Zuo F, Nakamura N, Akao T, Hattori M.* Pharmacokinetics of berberine and its main metabolites in conventional and pseudo germ-free rats determined by liquid chromatography/ion trap mass spectrometry. Drug Metab Dispos 2006; 34: 2064–2072
28 *Hua WY, Ding L, Chen Y, Gong B, He JC, Xu GL.* Determination of berberine in human plasma by liquid chromatography-electrospray ionization-mass spectrometry. J Pharm Biomed Anal 2007; 44: 931–937
29 *Yang YH, Kang N, Xia HJ, Li J, Chen LX, Qiu F.* Metabolites of protoberberine alkaloids in human urine following oral administration of coptidis Rhizoma decoction. Planta Med 2010; 76: 1859–1863
30 *Qiu F, Zhu ZY, Kang N, Piao SJ, Qin GY, Yao XS.* Isolation and identification of urinary metabolites of berberine in rats and humans. Drug Metab Dispos 2008; 36: 2159–2165
31 *Tsai PL, Tsai TH.* Hepatobiliary excretion of berberine. Drug Metab Dispos 2004; 32: 405–412
32 *Cheng Z, Chen AF, Wu F, Sheng L, Zhang HK, Gu M, Li YY, Zhang LN, Hu LH, Li JY, Li J.* 8,8-Dimethyldihydroberberine with improved bioavailability and oral efficacy on obese and diabetic mouse models. Bioorg Med Chem 2010; 18: 5915–5924

3.3. Natural products as potential human ether-a-go-go-related gene channel inhibitors – Screening of plant-derived alkaloids

Schramm A, Saxena P, Chlebek J, Cahlíková L, Baburin I, Hering S, Hamburger M.
Planta Med 2014; 80: 740–746

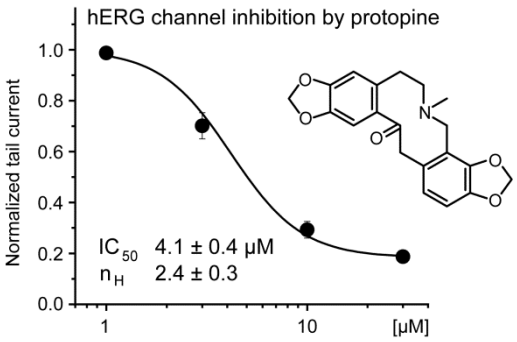

A focused plant-derived alkaloid library was screened for hERG inhibitory activity by means of a functional *Xenopus* oocyte assay. Compounds that reduced the hERG current at 100 µM by more than 50% were selected for evaluation of their concentration-response relationships. Pronounced *in vitro* hERG block was observed for some widely occurring alkaloids, such as protopine.

Semi-synthesis of 8-oxoberberine and 8-oxocoptisine (including spectral characterization by HR-ESI-TOF-MS and microprobe NMR), initial screening of 27 compounds (preparation of Xenopus oocytes, two-microelectrode voltage-clamp measurements, data analysis), writing the draft of the manuscript, and preparation of Fig. 1 were my contributions to this publication.

Anja Schramm

Natural Products as Potential Human Ether-A-Go-Go-Related Gene Channel Inhibitors – Screening of Plant-Derived Alkaloids

Authors

Anja Schramm[1]*, Priyanka Saxena[2]*, Jakub Chlebek[3], Lucie Cahlíková[3], Igor Baburin[2], Steffen Hering[2], Matthias Hamburger[1]

Affiliations

[1] Division of Pharmaceutical Biology, University of Basel, Basel, Switzerland
[2] Department of Pharmacology and Toxicology, University of Vienna, Vienna, Austria
[3] ADINACO Research Group, Department of Pharmaceutical Botany and Ecology, Charles University, Hradec Králové, Czech Republic

Key words

- natural products
- hERG channel inhibition
- *Xenopus* oocyte assay
- plant-derived alkaloids
- *in vitro* library screening

Abstract

Inhibition of the cardiac human ether-a-go-go-related gene channel is a problematic off-target pharmacological activity and, hence, a major safety liability in clinical practice. Several non-cardiac drugs have been restricted in their use, or even removed from the market due to this potentially fatal adverse effect. Comparatively little is known about the human ether-a-go-go-related gene inhibitory potential of plant-derived compounds. In the course of an ongoing human ether-a-go-go-related gene *in vitro* study, a total of 32 structurally diverse alkaloids of plant origin as well as two semi-synthetically obtained protoberberine derivatives were screened by means of an automated *Xenopus* oocyte assay. Protopine, (+)-bulbocapnine, (+)-*N*-methyllaurotetanine, (+)-boldine, (+)-chelidonine, (+)-corynoline, reserpine, and yohimbine reduced the human ether-a-go-go-related gene current by ≥ 50% at 100 µM, and were submitted to concentration-response experiments. Our data show that some widely occurring plant-derived alkaloids carry a potential risk for human ether-a-go-go-related gene toxicity.

Abbreviations

ECG:	electrocardiogram
hERG:	human ether-a-go-go-related gene
$I_{hERG:}$	hERG potassium current
TCM:	traditional Chinese medicine

Supporting information available online at http://www.thieme-connect.de/products

received February 27, 2014
revised May 2, 2014
accepted May 19, 2014

Bibliography
DOI http://dx.doi.org/10.1055/s-0034-1368590
Planta Med 2014; 80: 740–746

ISSN 0032-0943

Correspondence
Prof. Dr. Matthias Hamburger
Department of Pharmaceutical Sciences
Division of Pharmaceutical Biology
University of Basel
Klingelbergstrasse 50
4056 Basel
Switzerland
Phone: + 41 6 12 67 14 25
Fax: + 41 6 12 67 14 74
Matthias.Hamburger@unibas.ch

Introduction

Cardiotoxicity is among the most frequent reasons for the discontinuation of preclinical/clinical drug discovery programs, for serious adverse drug effects, and for withdrawal of already marketed drugs [1]. A promiscuous target with respect to cardiac safety is the hERG channel. The underlying I_{hERG} plays a pivotal role during ventricular repolarization and is, hence, an important determinant of the cardiac action potential duration. Inhibition of I_{Kr} can prolong the QT interval on the ECG and, as a consequence, may cause severe side effects, such as ventricular tachyarrhythmia (torsades de pointes arrhythmia) and sudden cardiac death [2]. Synthetic drug candidates are, therefore, routinely evaluated for hERG channel blocking properties in the early stage of lead development [3].

Natural products of plant origin exhibit a wealth of beneficial pharmacological activities, but may also have a potential for adverse drug reactions. Side effects may arise from various mechanisms, e.g., direct toxicities and/or pharmacological interactions with concomitantly administered drugs. Given that hERG block is a potential safety liability, surprisingly little is known about the hERG inhibitory potential of plant-derived compounds. So far, a number of flavonoids (e.g., acacetin, naringenin, and trimethyl-apigenin) and alkaloids (e.g., changrolin, dauricine, and lobeline) have been identified as hERG blockers *in vitro* [4–9]. These examples illustrate the need for a more comprehensive evaluation of the hERG liability of widely occurring plant secondary metabolites. We recently screened a selection of widely used herbal drugs and dietary plants by means of a functional *Xenopus* oocyte assay for

* These authors contributed equally to this work.

their ability to reduce I_{hERG}. Moderate hERG inhibitory activity was observed for the TCM herbal drug Huanglian (rhizomes of *Coptis chinensis* Franch., Ranunculaceae) and black pepper fruits (*Piper nigrum* L., Piperaceae), and successfully tracked to dihydroberberine and piperine, respectively [10,11]. Given the importance of both alkaloids, in particular of piperine as a major constituent in pepper fruits and as a starting point for the development of promising $GABA_A$ receptor modulators [12], we complemented our *in vitro* screening for hERG blockers with the evaluation of a focused alkaloid library. Compounds were selected to include structurally diverse and pharmacologically important alkaloid scaffolds, and compounds with known and relevant pharmacological activities, such as tryptanthrin, emetine, yohimbine, reserpine, and galanthamine. Their effect on hERG channel function was assessed in an automated two-microelectrode voltage-clamp assay with *Xenopus* oocytes.

Results and Discussion

A series of 32 plant-derived alkaloids and two semi-synthetic protoberberine derivatives were tested for hERG inhibitory activity *in vitro*. Alkaloids **1**–**34** (**Fig. 1**) were screened in a functional *Xenopus* oocyte assay during 1 Hz pulse trains. The initial test concentration was 100 µM (**Table 1**). Of the alkaloids tested, protopine (**16**), (+)-bulbocapnine (**18**), (+)-*N*-methyllaurotetanine (**19**), (+)-boldine (**20**), (+)-corynoline (**24**), and reserpine (**31**) reduced I_{hERG} by more than 60% (inhibition of I_{hERG} by 88.4 ± 1.9%, 72.0 ± 1.6%, 81.4 ± 2.9%, 65.8 ± 5.3%, 72.6 ± 2.4%, and 66.9 ± 0.3%, respectively). (+)-Chelidonine (**23**) and yohimbine (**30**) were somewhat less active (inhibition of I_{hERG} by 56.8 ± 8.2% and 52.6 ± 3.0%, respectively). Given the structural diversity of the alkaloids included in this study, deriving structural features critical for hERG inhibition was not possible. However, it seems that alkaloids with an aporphine (**17**–**20**) or benzophenanthridine (**21**–**24**) scaffold are particularly prone to hERG block.

For comparative purposes, we also evaluated four alkaloids for which *in vitro* data have been already published. For papaverine (**6**), we observed a mean hERG current inhibition by 33.6 ± 3.4% at a test concentration of 100 µM (**Table 1**). Reported IC_{50} values obtained with *Xenopus* oocytes range from 30.0 to 71.0 µM, whereas those from HEK293 cells vary between 0.58 and 7.3 µM [13–15]. Discrepancies between published data and our results are most likely due to differences in assay conditions, e.g., the use of different pulse protocols. Also, electrophysiological studies performed with *Xenopus* oocytes typically produce IC_{50} values that are significantly higher than those obtained in mammalian cell lines. The difference is mainly due to the large amount of lipophilic yolk in oocytes, which may adsorb lipophilic drug substances, thus lowering the effective intracellular free compound concentration [16]. Another known hERG blocker of plant origin is reserpine (**31**). Its hERG liability was previously detected in a cell-based high-throughput fluorescence assay (FluxOR thallium influx assay), and subsequently confirmed with an automated whole-cell patch-clamp assay in CHO-K1 cells (IC_{50}: 1.9 µM) [17]. In the *Xenopus* oocyte assay, the alkaloid reduced I_{hERG} by 66.9 ± 0.3% (test concentration of 100 µM) (**Table 1**). Also, the hERG inhibitory activity of galanthamine (**32**) and ephedrine had been previously reported. When assayed in HEK293 cells, galanthamine (**32**) had been classified as weak hERG blocker (IC_{50}: 760.2 µM) [18], whereas ephedrine showed no hERG block at 10 µM [15]. (−)-Ephedrine (**7**) and (−)-galanthamine (**32**) were, therefore, used as negative controls in our study and indeed induced no hERG inhibition in the oocyte assay (**Table 1**).

As a next step, we studied the concentration-response relationships for alkaloids that reduced I_{hERG} by ≥ 50% in the initial library screening. The hERG blocking effects of **16, 18**–**20, 23, 24, 30**, and **31** were determined at concentrations ranging from 0.1 to 300 µM. Increasing compound concentrations were cumulatively applied to the oocytes, and steady-state values of hERG inhibition were assessed during 0.3 Hz pulse trains. All selected alkaloids reduced I_{hERG} in a concentration-dependent manner, albeit to varying degrees (**Fig. 2**, **Table 2**). Protopine (**16**) and (+)-corynoline (**24**) were among the most potent alkaloids, with IC_{50} values of 4.1 ± 0.4 µM and 7.1 ± 0.4 µM, respectively. Representative currents illustrating concentration-dependent inhibition of I_{hERG} by **16** and **24** are shown in **Fig. 3**. Interestingly, several compounds induced a much stronger hERG block during high frequency stimulation (1 Hz) than during lower frequency pulses (0.3 Hz) when comparing the data at 100 µM (**Table 1**, **Fig. 2**). This was evident for (+)-bulbocapnine (**18**) (72.0 ± 1.6% block at 1 Hz vs. 40.5 ± 2.1% at 0.3 Hz), (+)-*N*-methyllaurotetanine (**19**) (81.4 ± 2.9% block at 1 Hz vs. 57.1 ± 3.3% at 0.3 Hz), and reserpine (**31**) (66.9 ± 0.3% block at 1 Hz vs. 47.0 ± 3.8% at 0.3 Hz). Moreover, hERG inhibition by these alkaloids was incomplete at 0.3 Hz, even at high concentrations (300 µM). These findings indicate that the hERG inhibitory activity of **18, 19**, and **31** crucially depends on the pulsing rate. Recovery from block between pulses at the lower frequency of 0.3 Hz reduces the steady-state block for some of the compounds. Such a behavior is well established for hERG and other voltage-gated ion channels. Our study highlights that hERG channel inhibition by natural products can be substantially augmented by frequent pulsing and that the frequency of membrane depolarization may thus affect the estimation of IC_{50} values (see also [19] where a stronger steady-state block at higher pulse frequencies was observed for amiodarone and cisapride, while the action of other hERG blocking drugs was less dependent on the pulsing rate).

The pronounced *in vitro* hERG blocking activity of some widely occurring alkaloids could represent a risk for cardiotoxicity. Further studies are warranted to assess potential hERG-related safety aspects, and to explore the clinical relevance of our findings. For example, protopine (**16**) is a major constituent of California poppy (*Eschscholzia californica*; Papaveraceae), a well-known medicinal plant from North America. In folk medicine, the herb has been used as an analgesic and sedative remedy [20]. Protopine (**16**) has been reported to inhibit multiple cardiac ion currents (e.g., I_{Na}, $I_{Ca,L}$, I_{K1}, and I_K) in isolated guinea pig ventricular myocytes. Moreover, the alkaloid has been shown to shorten the ventricular action potential duration [21]. It is, to the best of our knowledge, still unclear whether the intake of protopine with *Eschscholzia*-containing herbal preparations is toxicologically relevant. Further studies are certainly needed to evaluate its cardiac safety profile. The same applies for other hERG blocking alkaloids identified in this study. The cardiac safety of these alkaloids will depend on their oral bioavailability, clinically achieved free plasma concentrations, and the hERG blocking potency of their metabolites. Future pharmacodynamic/pharmacokinetic studies should, however, not only be performed with the hERG blocking alkaloids, but also with their corresponding herbal extracts, in order to evaluate a possible influence of other extract constituents.

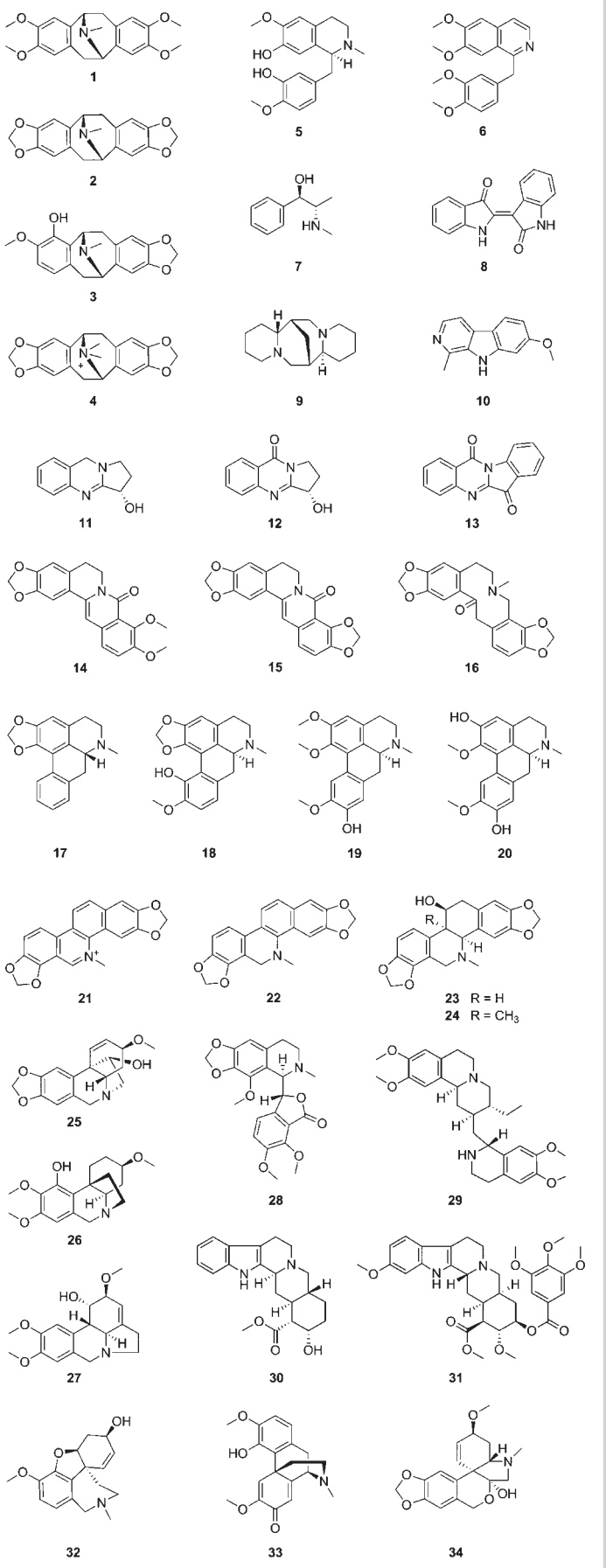

Fig. 1 Structures of alkaloids **1**–**34** tested for human ether-a-go-go-related gene inhibitory activity.

Table 1 Alkaloid library screening for human ether-a-go-go-related gene *in vitro* inhibition (in %). The hERG inhibitory potential of alkaloids **1**–**34** was assessed at 100 µM in a functional assay with *Xenopus* oocytes. Inhibition of I_{hERG} was determined during 1 Hz pulse trains applied from − 80 mV.

Compound	I_{hERG} inhibition (%) at 100 µM
(−)-Argemonine (**1**)	10.0 ± 0.8
(−)-Eschscholtzine (**2**)	14.6 ± 2.0
(−)-Neocaryachine (**3**)	9.8 ± 0.4
(−)-Californidine (**4**)	0.0 ± 0.0
(+)-Reticuline (**5**)	28.1 ± 2.0
Papaverine (**6**)	33.6 ± 3.4
(−)-Ephedrine (**7**)	0.0 ± 0.0
Indirubin (**8**)	0.0 ± 0.0
(−)-Sparteine (**9**)	0.0 ± 0.0
Harmine (**10**)	27.5 ± 3.1
Vasicine (**11**)	2.2 ± 0.3
Vasicinone (**12**)	0.0 ± 0.0
Tryptanthrin (**13**)	0.0 ± 0.0
8-Oxoberberine (**14**)	3.7 ± 1.9
8-Oxocoptisine (**15**)	0.9 ± 0.9
Protopine (**16**)	88.4 ± 1.9
(−)-Remerine (**17**)	42.7 ± 7.3
(+)-Bulbocapnine (**18**)	72.0 ± 1.6
(+)-*N*-methyllaurotetanine (**19**)	81.4 ± 2.9
(+)-Boldine (**20**)	65.8 ± 5.3
Sanguinarine (**21**)	34.8 ± 12.1
Dihydrosanguinarine (**22**)	22.5 ± 4.3
(+)-Chelidonine (**23**)	56.8 ± 8.2
(+)-Corynoline (**24**)	72.6 ± 2.4
(+)-Haemanthamine (**25**)	0.0 ± 0.0
(+)-Hippeastidine (**26**)	28.2 ± 1.1
(−)-Galanthine (**27**)	1.3 ± 0.3
Noscapine (**28**)	6.8 ± 3.0
Emetine (**29**)	3.3 ± 1.9
Yohimbine (**30**)	52.6 ± 3.0
Reserpine (**31**)	66.9 ± 0.3
(−)-Galanthamine (**32**)	0.7 ± 0.5
(+)-Salutaridine (**33**)	22.4 ± 1.6
(+)-Tazettine (**34**)	3.6 ± 1.1

Materials and Methods

Chemicals

Noscapine (98% by TLC) and (−)-remerine hydrochloride (95% by TLC) were purchased from Latoxan. (+)-Boldine (ROTICHROM® ~CHR) was from Carl Roth GmbH. (+)-Chelidonine monohydrate (≥ 95% by ^{1}H NMR), harmine (98% by TLC), sanguinarine chloride (≥ 98% by HPLC), and tryptanthrin (≥ 95% by ^{1}H NMR) were purchased from Sigma-Aldrich.

Emetine dihydrochloride, (−)-ephedrine hydrochloride, papaverine hydrochloride, reserpine, (−)-sparteine sulfate, and yohimbine hydrochloride were from the Institute of Pharmaceutical Biology, University of Jena (purities ≥ 95% by ^{1}H NMR).

Vasicine (> 95% by ^{1}H NMR) and vasicinone (> 95% by ^{1}H NMR) were isolated from leaves and twigs of *Peganum harmala* (Zygophyllaceae) [22] (Supporting Information).

(−)-Argemonine, (−)-californidine iodide, (−)-eschscholtzine, (−)-neocaryachine, (+)-*N*-methyllaurotetanine, protopine, (+)-reticuline, and (+)-salutaridine were isolated from aerial parts and roots of *E. californica* [23]. (+)-Bulbocapnine and (+)-corynoline were isolated from tubers of *Corydalis cava* (Fumariaceae) [24]. (−)-Galanthamine, (−)-galanthine, (+)-haemanthamine, (+)-hippeastidine, and (+)-tazettine were isolated from the bulbs of *Zephyranthes robusta* (Amaryllidaceae) [25]. Dihydrosanguinarine was isolated from a commercial extract of *Macleaya cordata* (Papaveraceae) (Supporting Information). Purities of isolated compounds were ≥ 95% (TLC).

Indirubin (≥ 95% by ^{1}H NMR) had been previously synthesized according to published procedures [26,27].

8-Oxoberberine (≥ 95% by ^{1}H NMR) and 8-oxocoptisine (≥ 95% by ^{1}H NMR) were prepared according to an established procedure [28], with minor modifications (Supporting Information).

Electrophysiological bioassay: expression of human ether-a-go-go-related gene channels in *Xenopus* oocytes and voltage-clamp experiments

Oocyte preparation: Oocytes from the South African clawed frog, *Xenopus laevis*, were prepared as follows: After 15 min exposure of female *Xenopus laevis* to the anesthetic (0.2% solution of MS-222; Sigma-Aldrich), parts of the ovary tissue were surgically removed. Defolliculation was achieved by enzymatical treatment with 2 mg/mL collagenase type 1A (Sigma-Aldrich). Stage V–VI oocytes were selected and injected with the hERG-encoding cRNA. Injected oocytes were stored at 18 °C in ND96 bath solution containing 1% penicillin-streptomycin solution (Sigma-Aldrich). ND96 bath solution contained 96 mM NaCl, 2 mM KCl, 1 mM $MgCl_2 \times 6H_2O$, 1.8 mM $CaCl_2 \times 2H_2O$, and 5 mM HEPES (pH 7.4).

Automated two-microelectrode voltage-clamp studies: Currents through hERG channels were studied with the two-microelectrode voltage-clamp technique using a Turbo TEC-03X amplifier (npi electronic GmbH). Electrophysiological experiments were performed one to three days after cRNA injection. Voltage-recording and current-injecting microelectrodes (Harvard Apparatus) were filled with 3 M KCl and had resistances between 0.5 and 2 MΩ. Oocytes with maximal current amplitudes > 4 µA were discarded to avoid voltage-clamp errors. For the initial compound screening, the following voltage protocol was used: From a holding potential of − 80 mV, the cell membrane was initially depolarized to + 20 mV (300 ms) in order to achieve channel activation and subsequent rapid inactivation. During following repolarization to − 50 mV (300 ms), channels recover from inactivation and elicit I_{hERG}. A final step to the holding potential ensured that channels returned to the closed state. The protocol was applied in 1-s intervals (1 Hz pulse frequency). Cumulative concentration-response experiments were performed with the same voltage protocol as described above, with minor modifications: the holding potential was − 100 mV, and pulse frequency was 0.3 Hz. Measurements were started after the initial current "run up" (slow increase of hERG current amplitudes during repetitive pulsing) reached a steady baseline. The automated fast perfusion system ScreeningTool (npi electronic GmbH, see [29] for details) was used to apply the test solutions to the oocyte. Sample stock solutions (prepared in DMSO) were freshly diluted every day with ND96 bath solution. Steady-state block of I_{hERG} was evaluated at ambient temperature (20–24 °C). Decreases in tail current amplitudes were taken as a measure of block development during repetitive pulsing. The final maximum DMSO concentration (1%) in test solutions did not affect hERG currents (data not shown). Cisapride (Sigma-Aldrich; purity ≥ 98%) was used as positive control. The IC_{50} value for hERG current inhibition at 0.3 Hz pulse frequency was 1.6 ± 0.4 µM (n = 3, ◉ **Table 2**, see also [19] for comparison). Data acquisition and processing were per-

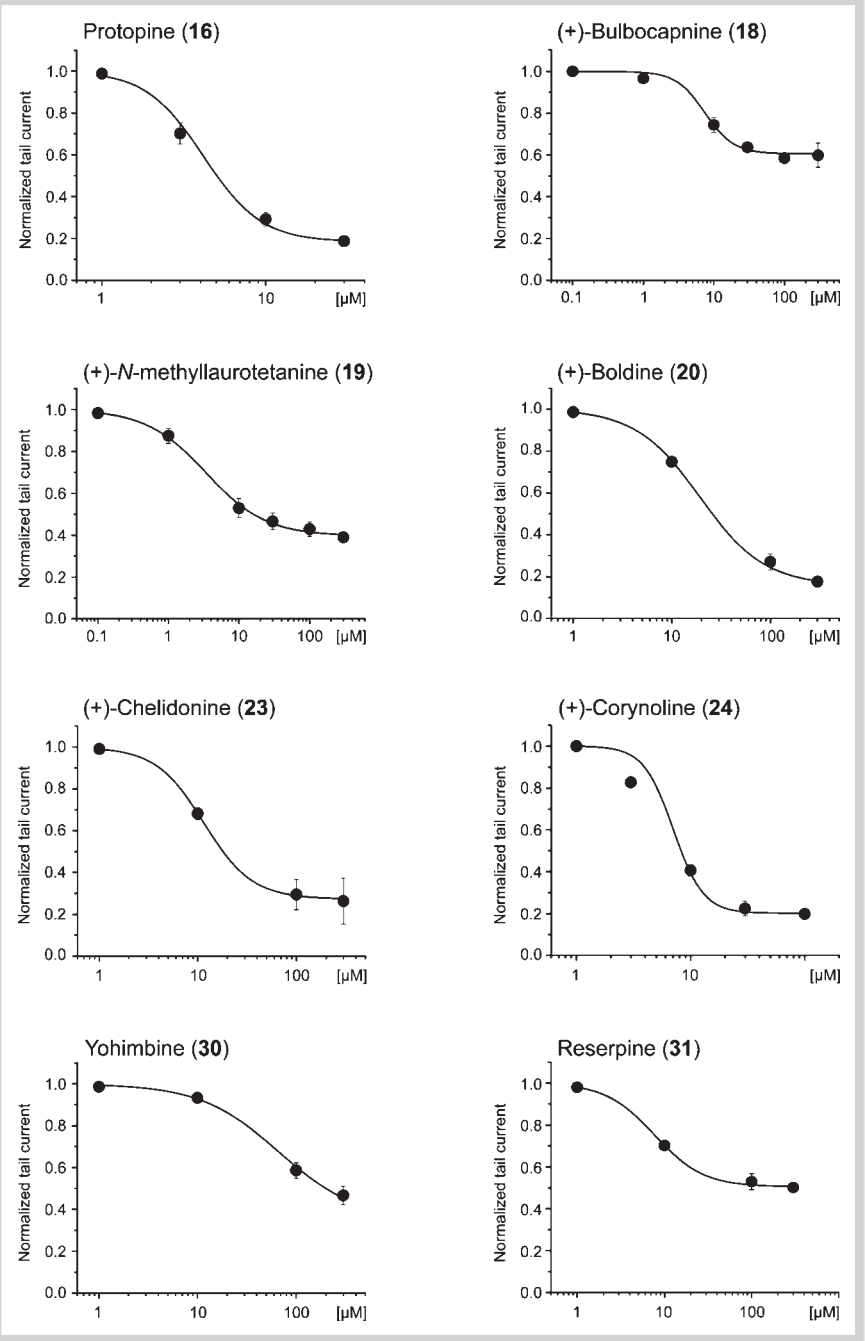

Fig. 2 Concentration-response relationships for the inhibitory effects of selected alkaloids on human ether-a-go-go-related gene potassium current in transfected *Xenopus* oocytes. Steady-state inhibition of I_{hERG} at the indicated concentrations was estimated during 0.3 Hz pulse trains applied from − 100 mV.

formed using pCLAMP 10.0 software and Clampfit 10.2 software, respectively.

Data analysis

Data were analyzed using Origin software 7.0 (OriginLab Corporation). Data from cumulative concentration-response experiments were fitted using the Hill equation

$$I_{(hERG,comp)}/I_{(hERG,ctrl)} = (100 - A)/(1 + [C/IC_{50}]^{nH}) + A$$

where $I_{(hERG,comp)}$ is the current amplitude in the presence of a given compound, $I_{(hERG,ctrl)}$ is the control current amplitude, IC_{50} is the concentration at which hERG current inhibition is half-maximal, C is the applied compound concentration, A is the fraction of hERG current that is not blocked, and n_H is the Hill coefficient. Each data point represents the mean ± SE from at least three oocytes and two oocyte batches.

Supporting information

Protocols for the isolation of vasicine and dihydrosanguinarine, as well as details on the semi-synthesis and spectral characterization of 8-oxoberberine and 8-oxocoptisine are available as Supporting Information.

Acknowledgments

The project was conducted within the International Research Staff Exchange Scheme (IRSES), project "hERG Related Risk Assessment of Botanicals" PIRSES-GA-2011–295 174 Marie Curie

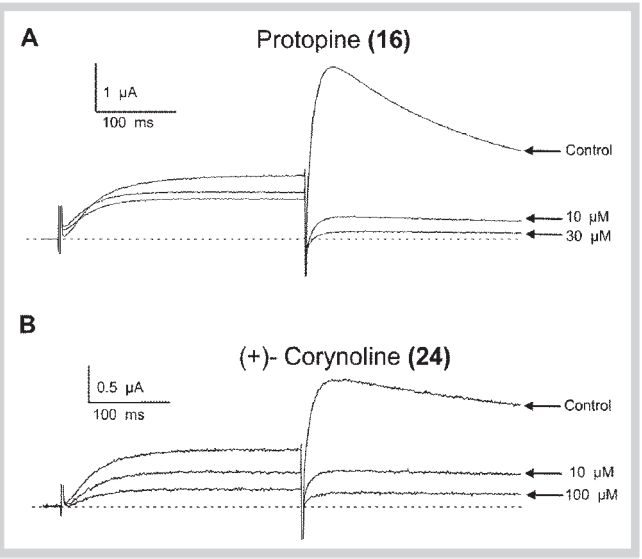

Fig. 3 Representative currents illustrating concentration-dependent inhibition of human ether-a-go-go-related gene potassium current by (**A**) protopine (**16**) and (**B**) (+)-corynoline (**24**). Superimposed current traces recorded in the absence (control) and after attaining steady-state block with increasing concentrations of **16** and **24** are shown. Steady-state inhibition of I_{hERG} was studied during 0.3 Hz pulse trains applied from − 100 mV.

Table 2 Collated IC_{50} values calculated from the Hill plots in ◉ **Fig. 2**.

Compound	IC_{50} (µM)	Hill coefficient (n_H)	n[a]
Protopine (**16**)	4.1 ± 0.4	2.4 ± 0.3	4
(+)-Bulbocapnine (**18**)	7.4 ± 1.5	2.1 ± 0.6	3
(+)-*N*-methyllaurotetanine (**19**)	3.4 ± 1.0	1.0 ± 0.1	3
(+)-Boldine (**20**)	19.3 ± 2.7	1.3 ± 0.1	4
(+)-Chelidonine (**23**)	11.5 ± 1.6	1.7 ± 0.1	4
(+)-Corynoline (**24**)	7.1 ± 0.4	3.3 ± 0.4	3
Yohimbine (**30**)	67.1 ± 34.8	1.1 ± 0.1	3
Reserpine (**31**)	7.6 ± 0.9	1.5 ± 0.1	4
Cisapride[b]	1.6 ± 0.4	1.3 ± 0.3	3

[a] *n*: number of experiments; [b] positive control

Actions funded under the 7th Framework Programme of the European Commission. Financial support was provided by the Swiss National Science Foundation (Project 205320–126888) (M.H.), the Freiwillige Akademische Gesellschaft Basel (A.S.), and by the programs SVV-2010–261–002 and UNCE 204026/2012 of Charles University in Prague. We thank Patrick Grabher for the isolation of vasicine and vasicinone. This work was supported by FWF grant P22395. Priyanka Saxena is a student of FWF doctoral program "Molecular drug targets" W1232.

Conflict of Interest

The authors declare no conflict of interest.

References

1 *Laverty HG, Benson C, Cartwright EJ, Cross MJ, Garland C, Hammond T, Holloway C, McMahon N, Milligan J, Park BK, Pirmohamed M, Pollard C, Radford J, Roome N, Sager P, Singh S, Suter T, Suter W, Trafford A, Volders PGA, Wallis R, Weaver R, York M, Valentin JP.* How can we improve our understanding of cardiovascular safety liabilities to develop safer medicines? Br J Pharmacol 2011; 163: 675–693
2 *Vandenberg JI, Perry MD, Perrin MJ, Mann SA, Ke Y, Hill AP.* HERG K^+ channels: Structure, function, and clinical significance. Physiol Rev 2012; 92: 1393–1478
3 *Kaczorowski GJ, Garcia ML, Bode J, Hess SD, Patel UA.* The importance of being profiled: Improving drug candidate safety and efficacy using ion channel profiling. Front Pharmacol 2011; 2: 78
4 *Li GR, Wang HB, Qin GW, Jin MW, Tang Q, Sun HY, Du XL, Deng XL, Zhang XH, Chen JB, Chen L, Xu XH, Cheng LC, Chiu SW, Tse HF, Vanhoutte PM, Lau CP.* Acacetin, a natural flavone, selectively inhibits human atrial repolarization potassium currents and prevents atrial fibrillation in dogs. Circulation 2008; 117: 2449–2457
5 *Zitron E, Scholz E, Owen RW, Lück S, Kiesecker C, Thomas D, Kathöfer S, Niroomand F, Kiehn J, Kreye VAW, Katus HA, Schoels W, Karle CA.* QTc prolongation by grapefruit juice and its potential pharmacological basis: hERG channel blockade by flavonoids. Circulation 2005; 111: 835–838
6 *Liu Y, Xu XH, Liu Z, Du XL, Chen KH, Xin X, Jin ZD, Shen JZ, Hu Y, Li GR, Jin MW.* Effects of the natural flavone trimethylapigenin on cardiac potassium currents. Biochem Pharmacol 2012; 84: 498–506
7 *Chen WH, Wang WY, Zhang J, Yang D, Wang YP.* State-dependent blockade of human ether-a-go-go-related gene (hERG) K^+ channels by changrolin in stably transfected HEK293 cells. Acta Pharmacol Sin 2010; 31: 915–922
8 *Zhao J, Lian Y, Lu CF, Jing L, Yuan HT, Peng SQ.* Inhibitory effects of a bisbenzylisoquinline alkaloid dauricine on hERG potassium channels. J Ethnopharmacol 2012; 141: 685–691
9 *Jeong I, Choi BH, Hahn SJ.* Effects of lobeline, a nicotinic receptor ligand, on the cloned Kv1.5. Pflugers Arch 2010; 460: 851–862
10 *Schramm A, Baburin I, Hering S, Hamburger M.* hERG channel inhibitors in extracts of Coptidis rhizoma. Planta Med 2011; 77: 692–697
11 *Schramm A, Jähne EA, Baburin I, Hering S, Hamburger M.* Natural products as potential hERG channel inhibitors: Outcomes from a screening of widely used herbal medicines and edible plants. Planta Med, in press
12 *Khom S, Strommer B, Schöffmann A, Hintersteiner J, Baburin I, Erker T, Schwarz T, Schwarzer C, Zaugg J, Hamburger M, Hering S.* $GABA_A$ receptor modulation by piperine and a non-TRPV1 activating derivative. Biochem Pharmacol 2013; 85: 1827–1836
13 *Kim YJ, Hong HK, Lee HS, Moh SH, Park JC, Jo SH, Choe H.* Papaverine, a vasodilator, blocks the pore of the hERG channel at submicromolar concentration. J Cardiovasc Pharmacol 2008; 52: 485–493
14 *Kim CS, Lee N, Son SJ, Lee KS, Kim HS, Kwak YG, Chae SW, Lee S, Jeon BH, Park JB.* Inhibitory effects of coronary vasodilator papaverine on heterologously-expressed hERG currents in *Xenopus* oocytes. Acta Pharmacol Sin 2007; 28: 503–510
15 *Wible BA, Hawryluk P, Ficker E, Kuryshev YA, Kirsch G, Brown AM.* HERG-Lite®: A novel comprehensive high-throughput screen for drug-induced hERG risk. J Pharmacol Toxicol Methods 2005; 52: 136–145
16 *Witchel HJ, Milnes JT, Mitcheson JS, Hancox JC.* Troubleshooting problems with *in vitro* screening of drugs for QT interval prolongation using hERG K^+ channels expressed in mammalian cell lines and *Xenopus* oocytes. J Pharmacol Toxicol Methods 2002; 48: 65–80
17 *Xia MH, Shahane SA, Huang RL, Titus SA, Shum E, Zhao Y, Southall N, Zheng W, Witt KL, Tice RR, Austin CP.* Identification of quaternary ammonium compounds as potent inhibitors of hERG potassium channels. Toxicol Appl Pharmacol 2011; 252: 250–258
18 *Vigneault P, Bourgault S, Kaddar N, Caillier B, Pilote S, Patoine D, Simard C, Drolet B.* Galantamine (Reminyl®) delays cardiac ventricular repolarization and prolongs the QT interval by blocking the hERG current. Eur J Pharmacol 2012; 681: 68–74
19 *Stork D, Timin EN, Berjukow S, Huber C, Hohaus A, Auer M, Hering S.* State dependent dissociation of hERG channel inhibitors. Br J Pharmacol 2007; 151: 1368–1376
20 *Rolland A, Fleurentin J, Lanhers MC, Younos C, Misslin R, Mortier F, Pelt JM.* Behavioural effects of the American traditional plant *Eschscholzia californica*: Sedative and anxiolytic properties. Planta Med 1991; 57: 212–216

21 *Song LS, Ren GJ, Chen ZL, Chen ZH, Zhou ZN, Cheng HP.* Electrophysiological effects of protopine in cardiac myocytes: Inhibition of multiple cation channel currents. Br J Pharmacol 2000; 129: 893–900
22 *Grabher P, Durieu E, Kouloura E, Halabalaki M, Skaltsounis LA, Meijer L, Hamburger M, Potterat O.* Library-based discovery of DYRK1A/CLK1 inhibitors from natural product extracts. Planta Med 2012; 78: 951–956
23 *Cahlíková L, Macáková K, Kuneš J, Kurfürst M, Opletal L, Cvačka J, Chlebek J, Blunden G.* Acetylcholinesterase and butyrylcholinesterase inhibitory compounds from *Eschscholzia californica* (Papaveraceae). Nat Prod Commun 2010; 5: 1035–1038
24 *Chlebek J, Macáková K, Cahlíková L, Kurfürst M, Kuneš J, Opletal L.* Acetylcholinesterase and butyrylcholinesterase inhibitory compounds from *Corydalis cava* (Fumariaceae). Nat Prod Commun 2011; 6: 607–610
25 *Kulhánková A, Cahlíková L, Novák Z, Macáková K, Kuneš J, Opletal L.* Alkaloids from *Zephyranthes robusta* BAKER and their acetylcholinesterase- and butyrylcholinesterase-inhibitory activity. Chem Biodivers 2013; 10: 1120–1127
26 *Hoessel R, Leclerc S, Endicott JA, Nobel MEM, Lawrie A, Tunnah P, Leost M, Damiens E, Marie D, Marko D, Niederberger E, Tang W, Eisenbrand G, Meijer L.* Indirubin, the active constituent of a Chinese antileukaemia medicine, inhibits cyclin-dependent kinases. Nat Cell Biol 1999; 1: 60–67
27 *Friedländer P, Roschdestwensky N.* Über ein Oxidationsprodukt des Indigoblaus. Ber Dtsch Chem Ges 1915; 48: 1841–1847
28 *Dostál J, Potáček M, Man S, Humpa O.* Non-aromatic derivatives of berberine. Scr Med (Brno) 1999; 72: 3–8
29 *Baburin I, Beyl S, Hering S.* Automated fast perfusion of *Xenopus* oocytes for drug screening. Pflugers Arch 2006; 453: 117–123

Supporting Information

Natural Products as Potential Human Ether-A-Go-Go-Related Gene Channel Inhibitors – Screening of Plant-Derived Alkaloids

Anja Schramm[1*], Priyanka Saxena[2*], Jakub Chlebek[3], Lucie Cahlíková[3], Igor Baburin[2], Steffen Hering[2], Matthias Hamburger[1]

[*] These authors contributed equally to the work.

Affiliations

[1]Division of Pharmaceutical Biology, University of Basel, Basel, Switzerland

[2]Department of Pharmacology and Toxicology, University of Vienna, Vienna, Austria

[3]ADINACO Research Group, Department of Pharmaceutical Botany and Ecology, Charles University, Hradec Králové, Czech Republic

Correspondence

Prof. Dr. Matthias Hamburger

Department of Pharmaceutical Sciences

Division of Pharmaceutical Biology

University of Basel

Klingelbergstrasse 50

CH-4056 Basel

Switzerland

Phone: +41 61 267 14 25

Fax: +41 61 267 14 74

Matthias.Hamburger@unibas.ch

 · DOI 10.1055/s-0034-1368590 · Planta Med · Schramm A et al.

Experimental details

General experimental procedures:

HR-TOF-ESI-MS data were obtained on a micrOTOF ESI-MS spectrometer (Bruker Daltonics). A solution of 0.1% formic acid in 2-propanol/water (1:1 v/v) containing 5 mM NaOH was used for mass calibration. Data acquisition and analysis were performed using HyStar 3.2 software. NMR spectra were recorded at 291.15 K on a Bruker Avance III spectrometer (Bruker Daltonics) operating at 500.13 MHz for ^{1}H. A 1 mm TXI microprobe was used for 1D and 2D NMR experiments (^{1}H, COSY, HSQC, HMBC). Topspin 2.1 software was used for spectra analysis and processing.

Isolation of vasicine:

Vasicine was isolated from the CH_2Cl_2 extract of *Peganum harmala* L. (Zygophyllaceae). Briefly, a portion of the crude extract (2.0 g) was suspended in CH_2Cl_2 and partitioned with 0.25 M H_2SO_4. Alkalinization of the aqueous phase to pH 12 with 26% NH_4OH and subsequent extraction with CH_2Cl_2 yielded an alkaloid-enriched fraction. Final purification by semi-preparative HPLC (Agilent 1100 system, SunFire C18 column [10 × 150 mm i.d., 5 µm], flow rate 4 mL/min, PDA 254 nm) with a gradient of 5–35% MeCN in aqueous 0.5% formic acid in 20 min afforded vasicine (11.1 mg). Vasicine was identified by ESI-MS (Esquire 3000 plus ion trap mass spectrometer, Bruker Daltonics), 1D and 2D NMR spectroscopy, and comparison with literature data [1]. Purity was > 95% (^{1}H NMR).

Isolation of dihydrosanguinarine:

Dihydrosanguinarine was isolated from a commercial extract of *Macleaya cordata* (*Macleaya cordata* extract 60%; Organic Herb Inc., China). The alkaloidal extract (10 g) was dissolved in MeOH and filtered over 10 g of aluminum oxide. The effluent was collected, evaporated to dryness, and tested for alkaloids by means of TLC analysis (silica gel 60 F_{254} pre-coated Al sheets [Merck], toluene/Et_2NH [95:5 v/v], Dragendorff's reagent). The concentrated alkaloidal extract (8.5 g) was fractionated by open column chromatography on aluminum oxide. Elution was done with a step gradient of petroleum ether/$CHCl_3$ (9:1, 8:2, 7:3, 6:4, 1:1, 4:6, 3:7, 2:8, 1:9; 500 mL each), followed by a step gradient of $CHCl_3$/EtOH (1:1, 1:2, 1:3, 1:4, 1:5; 500 mL each). Fractions of 150 mL were collected and combined after TLC analysis. Six subfractions were obtained (I–VI). Dihydrosanguinarine (53 mg) was recrystallized in EtOH from subfraction I (95 mg).

Synthesis of protoberberine derivatives:

8-Oxoberberine was synthesized according to a published procedure [2], with minor modifications. To a solution of berberine chloride hydrate (~ 95%, Fluka; 50.7 mg dissolved in 4 mL of hot water), a 30% aqueous solution of NaOH (4 mL) was added dropwise under stirring. The mixture was heated under reflux for 3 h. After cooling to ambient temperature, the collected precipitate was washed with water and treated with 3% hydrochloric acid (25 mL) by heating the mixture on the water bath for 10 min. The precipitate was filtered off and washed with hot 3% hydrochloric acid. Crystallization from EtOH afforded 7.1 mg of yellow crystals of 8-oxoberberine (HR-ESI-TOF-MS *m/z* 374.1004 $[M+Na]^+$, calcd. for $C_{20}H_{17}NNaO_5$: 374.0999; ^1H and ^{13}C NMR data, see **Table 1S**).

8-Oxocoptisine was obtained as described above. Coptisine (50.6 mg) was isolated from rhizomes of *Coptis chinensis* Franch. (Ranunculaceae) [3]. Crystallization from EtOH yielded 9.6 mg of orange crystals of 8-oxocoptisine (HR-ESI-TOF-MS *m/z* 358.0679 $[M+Na]^+$, calcd. for $C_{19}H_{13}NNaO_5$: 358.0686; ^1H and ^{13}C NMR data, see **Table 2S**). Purity of both products was ≥ 95% (^1H NMR).

Table 1S NMR spectroscopic data for 8-oxoberberine ($CDCl_3$, 500 MHz, δ in ppm).

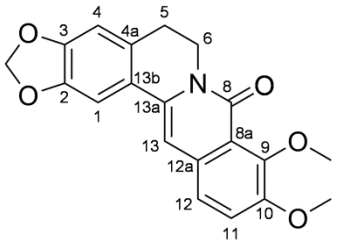

Position	δ_H (J in Hz)	δ_C[a]
1	7.22, s	104.6
2		147.5
3		148.5
4	6.70, s	107.8
4a		130.1
5	2.90, t (6.1)	28.6
6	4.30, t (6.1)	39.3
7		
8		159.9
8a		119.4
9		149.8
10		151.5
11	7.32, d (8.7)	119.3
12	7.26, d (8.7)	122.0
12a		132.5
13	6.71, s	101.1
13a		135.6
13b		123.5
2,3-OCH_2O	6.00, s	101.2
9-OCH_3	4.03, s	61.5
10-OCH_3	3.95, s	57.0

[a] ^{13}C shifts deduced from HSQC and HMBC experiments.

δ_H reference data measured in $CDCl_3$ can be found in [2].

δ_H and δ_C reference data measured in DMSO-d_6 can be found in [4].

Table 2S NMR spectroscopic data for 8-oxocoptisine ($CDCl_3$, 500 MHz, δ in ppm).

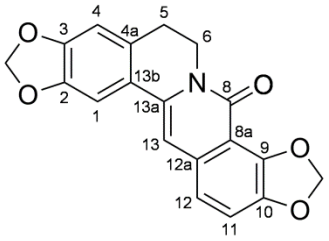

Position	δ_H (J in Hz)	δ_C[a]
1	7.17, s	104.7
2		147.6
3		148.1
4	6.67, s	107.8
4a		129.9
5	2.86, t (6.2)	28.6
6	4.25, t (6.2)	39.1
7		
8		159.5
8a		110.6
9		146.5
10		146.2
11	7.12, d (8.2)	113.6
12	7.00, d (8.2)	119.0
12a		131.8
13	6.70, s	101.9
13a		135.2
13b		123.8
2,3-OCH_2O	5.97, s	101.0
9,10-OCH_2O	6.18, s	102.3

[a] ^{13}C shifts deduced from HSQC and HMBC experiments.

δ_H and δ_C reference data measured in DMSO-d_6 can be found in [4].

References

1 *Joshi BS, Bai YL, Puar MS, Dubose KK, Pelletier SW*. ^{1}H- and ^{13}C-NMR assignments for some pyrrolo[2,1b]-quinazoline alkaloids of *Adhatoda vasica*. J Nat Prod 1994; 57: 953-962

2 *Dostál J, Potáček M, Man S, Humpa O*. Non-aromatic derivatives of berberine. Scripta Medica (Brno) 1999; 72: 3-8

3 *Schramm A, Baburin I, Hering S, Hamburger M*. hERG channel inhibitors in extracts of Coptidis rhizoma. Planta Med 2011; 77: 692-697

4 *Dostál J, Man S, Sečkářová P, Hulová D, Nečas M, Potáček M, Toušek J, Dommisse R, Van Dongen W, Marek R*. Berberine and coptisine free bases. J Mol Struct 2004; 687: 135-142

3.4. Gram-scale purification of dehydroevodiamine from *Evodia rutaecarpa* fruits, and a procedure for selective removal of quaternary indoloquinazoline alkaloids from *Evodia* extracts

Schramm A, Hamburger M.

Fitoterapia 2014; 94: 127–133

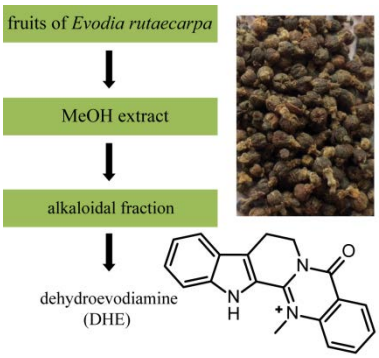

A two-step procedure for the gram-scale isolation of dehydroevodiamine (DHE) from *Evodia rutaecarpa* fruits was developed. DHE was selectively enriched by cation-exchange solid phase extraction, and further purified by preparative RP-HPLC. A method for the selective removal of quaternary indoloquinazoline alkaloids from *Evodia* extracts was developed. The DHE content in commercially available *Evodia* products was assessed by HPLC-PDA analysis.

Selective removal of quaternary indoloquinazoline alkaloids from Evodia extracts, developing a protocol for the gram-scale purification of dehydroevodiamine, quantitative analysis of dehydroevodiamine in commercially available Evodia products, writing the draft of the manuscript, and preparation of figures were my contributions to this publication.

Anja Schramm

Fitoterapia 94 (2014) 127–133

Contents lists available at ScienceDirect

Fitoterapia

journal homepage: www.elsevier.com/locate/fitote

Gram-scale purification of dehydroevodiamine from *Evodia rutaecarpa* fruits, and a procedure for selective removal of quaternary indoloquinazoline alkaloids from *Evodia* extracts

Anja Schramm, Matthias Hamburger *

Division of Pharmaceutical Biology, University of Basel, Klingelbergstrasse 50, 4056 Basel, Switzerland

ARTICLE INFO

Article history:
Received 1 November 2013
Accepted in revised form 12 February 2014
Available online 19 February 2014

Keywords:
Evodia rutaecarpa
Dehydroevodiamine
Gram-scale isolation
Cation-exchange chromatography
Preparative HPLC
Quantitative analysis

ABSTRACT

Dehydroevodiamine (DHE) is a major bioactive constituent in the traditional Chinese herbal drug Evodiae fructus (Wu zhu yu). The compound has been shown to possess pronounced cardiovascular and neuropharmacological activities in vitro and in vivo. For quality control purposes and follow-up studies assessing potential safety risks of DHE, we developed a simple and efficient two-step protocol for gram-scale purification of DHE. An alkaloidal fraction was obtained by cation-exchange solid phase extraction, and DHE and the minor alkaloid hortiamine were purified by isocratic preparative RP-HPLC. The DHE content in different commercial batches of Evodiae fructus, and in a series of commercially available *Evodia*-containing TCM products was assessed. A daily intake of up to mg amounts of DHE was calculated from recommended doses of these products. A method for the selective removal of quaternary indoloquinazoline alkaloids from *Evodia* extracts was developed.

1. Introduction

Numerous studies in the field of herbal medicines report on promising in vitro activities of pure compounds, including molecular modes of action. However, follow-up studies assessing in vivo pharmacological properties, pharmacokinetic profiles, and toxicological risks are rarely performed [1]. A major limiting factor for such studies is the access to compounds of required purity in larger amounts. Common plant-derived compounds can be obtained from commercial sources, but the costs may be prohibitive if multi-gram amounts are needed, e.g., for in vivo pharmacological and toxicological studies. Less common natural products are typically not available from commercial suppliers, and they need to be purified in multi-gram amounts by the scientists who wish to carry out such in vivo studies. Purification of gram amounts of a desired compound in high purity (>95%) is challenging. Factors such as simplicity, robustness, scalability, and process efficiency become increasingly important, and a careful balance has to be found between purity and throughput [2]. Gram-scale purification protocols have been developed for a broad range of rare natural products, e.g., triterpenoid esters from marigold [3], catechins from green tea [4], the iridoid glycoside geniposide from *Gardenia jasminoides* [5,6], the phenolic acid salvianolic acid B from *Salvia miltiorrhiza* [7], the coumarin scoparone from *Artemisia scoparia* [8], and flavonolignans from milk thistle [9].

Evodiae fructus (Wu zhu yu) consists of the nearly ripe, dried fruit of *Evodia rutaecarpa* (Juss.) Benth. (Rutaceae), and is among the most popular herbal drugs in traditional Chinese medicine (TCM). It is widely used as an analgesic, anti-emetic, and astringent remedy for the treatment of headaches, gastrointestinal disorders, and menstrual complaints, and also for treating mouth ulcers [10,11]. Indoloquinazoline and quinolone alkaloids, flavonoids, and limonoids have been identified in the drug [11–15]. The quaternary indoloquinazoline

Abbreviations: DHE, dehydroevodiamine; TCM, traditional Chinese medicine.

* Corresponding author. Tel.: +41 61 267 14 25; fax: +41 61 267 14 74.
E-mail address: matthias.hamburger@unibas.ch (M. Hamburger).

http://dx.doi.org/10.1016/j.fitote.2014.02.005
0367-326X/

alkaloid dehydroevodiamine (DHE, 1) (Fig. 1) is a major constituent that has been intensively studied from a pharmacological point of view. DHE has been shown to exhibit pronounced anti-amnesic effects in vivo [16], and moderate acetylcholinesterase inhibition in vitro [16,17]. In addition, hypotensive, bradycardiac, and vasorelaxant effects have been reported [18,19]. Electrophysiological studies in isolated guinea pig cardiomyocytes revealed that DHE inhibited several cardiac ion currents (e.g., I_{Na}, $I_{Ca,L}$, and I_K) and prolonged duration of the atrial and ventricular action potential [20].

Cardiovascular safety liabilities are, however, of utmost importance in drug discovery, drug development, and clinical practice [21]. Similar considerations also have to be applied to herbal products containing potent active constituents. Hence, an assessment of the cardiac safety and pharmacokinetic properties of DHE is needed. As DHE is not commercially available, a simple, robust, and scalable procedure for purification of DHE at the gram-scale was required. In parallel, we also devised a procedure for the selective removal of DHE from *Evodia* extracts, for the case that cardiac liabilities of DHE should be substantiated.

2. Experimental

2.1. General experimental procedures

Silica gel 60 F_{254} pre-coated Al sheets (Merck, Darmstadt, Germany) were used for TLC analysis (ethyl acetate–methanol–formic acid [69:30:1 v/v/v], detection at 366 nm). Analytical HPLC separations were carried out on a SunFire C18 column (3 × 150 mm i.d., 3.5 μm). LC-PDA analyses were performed with a Waters Alliance 2695 separation module equipped with a 996 PDA detector. Data acquisition and analysis were performed using Empower Pro 2 software. NMR spectra were recorded in methanol-d_4 on a Bruker Avance III spectrometer (Bruker Daltonics) operating at 500 MHz and 125 MHz for ^{1}H and ^{13}C, respectively. A 1 mm TXI microprobe was used for 1D and 2D NMR experiments (^{1}H, NOE difference, COSY, HSQC, HMBC). The ^{13}C spectrum of hortiamine (2) was recorded with a 5 mm BBO-probe. Topspin 2.1 software was used for spectra analysis and processing.

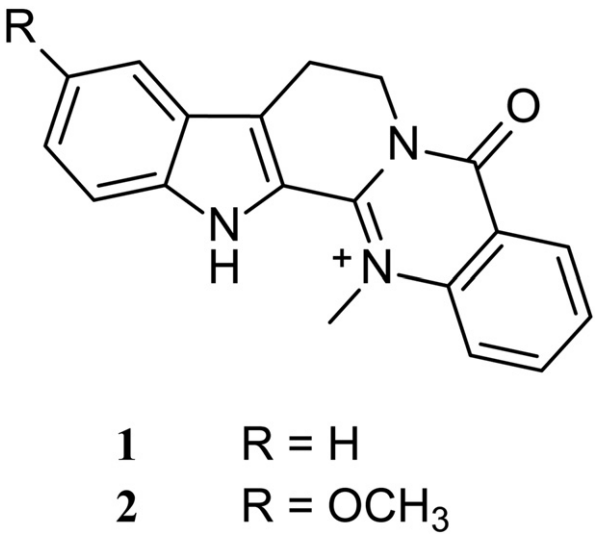

1 R = H

2 R = OCH_3

Fig. 1. Structures of DHE (1) and hortiamine (2).

2.2. Solvents and chemicals

Methanol used for extraction and cation-exchange chromatography was of technical grade, whereas HPLC-grade solvents were used for HPLC separations. HPLC-grade water was obtained by an EASY-pure II water purification system. HPLC-grade methanol and HPLC-grade acetonitrile were from Scharlau (Barcelona, Spain). Formic acid (98.0–100.0%), dimethylsulfoxide (DMSO), and trifluoroacetic acid (TFA, ≥98%) were purchased from Sigma-Aldrich. Dehydroevodiamine chloride (purity > 95% by ^{1}H NMR and HPLC) had been previously synthesized at the Department of Pharmaceutical/Medicinal Chemistry, University of Jena, Germany. Lewatit® cation exchange resins were kindly provided by Chemia Brugg AG (Brugg, Switzerland).

2.3. Plant material

Evodiae fructus (fruits of *E. rutaecarpa*) (batch no. 70588813) were purchased from Yong Quan GmbH (Ennepetal, Germany). A voucher specimen (number 00 465) has been deposited at the Division of Pharmaceutical Biology, University of Basel, Switzerland.

2.4. Extraction

Dried fruits were ground in a ZM 1 ultracentrifugal mill (sieve size of 2.0 mm; Retsch, Haan, Germany) under cooling with liquid nitrogen. The powdered fruits (526 g) were exhaustively percolated at room temperature with methanol. Solvent evaporation under reduced pressure afforded a dark brown viscous residue (108.8 g).

2.5. LC-PDA analysis

Analyses were carried out on an Alliance 2695 instrument (Waters). Separations were achieved with 0.1% aqueous formic acid (solvent A) and acetonitrile containing 0.1% formic acid (solvent B). The gradient profile was as follows: 5% B to 30% B in 25 min, 30% B to 100% B in 5 min, 100% B for 6 min. The flow rate was 0.5 mL/min, and the injection volume was 10 μL. The samples were dissolved in DMSO at a concentration of 7.5 mg/mL for extracts (crude *E. rutaecarpa* extract and alkaloid-depleted extracts), and 1 mg/mL for the alkaloid-enriched fraction. Detection was at 365 nm, while PDA spectra were recorded from 210 to 400 nm.

2.6. LC-PDA-ESI-TOF-MS analyses

HR-ESI-TOF-MS data were recorded on a micrOTOF ESI-MS spectrometer (Bruker Daltonics) coupled via a 1:10 splitter to an Agilent 1100 system consisting of an autosampler, degasser, binary pump, column oven, and PDA detector. Data acquisition and analysis were performed using HyStar 3.2 software. A solution of formic acid 0.1% in 2-propanol/water (1:1 v/v) containing 5 mM NaOH was used for mass calibration.

Separation conditions were identical as those described in Section 2.5. Typical mass accuracy was ± 2 ppm.

2.7. Cation-exchange solid phase extraction

2.7.1. Selection of ion-exchange resin

Three strongly acidic resins (Lewatit® MonoPlus SP 112, K 1221, and S 100 G1) and three weakly acidic resins (Lewatit® CNP 80, CNP 80 WS, and S 8528) were tested for their ability to selectively retain the quaternary alkaloids. For this purpose, the resins (suspended in methanol) were packed into glass columns of 1.7 cm diameter to give bed heights of approximately 10 cm. Columns were washed with methanol until the effluent appeared colorless. A portion (0.5 g) of methanolic *E. rutaecarpa* extract was dissolved in methanol (50 mL), applied to the column, and allowed to percolate with a flow rate of 1 mL/min. Columns were then washed with 300 mL of methanol. The alkaloid-depleted effluents were collected, evaporated to dryness, and submitted to LC-PDA analysis.

2.7.2. Process optimization

The strong exchange resin Lewatit® MonoPlus SP 112 was selected for further work. Conditions were optimized with respect to sample loading and sample elution. Alkaloid retention and breakthrough were monitored by means of TLC analysis of collected fractions. The extract was dissolved in methanol at a concentration of 10 mg/mL, and the maximum loading ratio was 20% (1 g of crude extract with 5 g of resin). The flow rate was 1 mL/min. Upon completion of sample introduction, the column was washed with methanol until the effluent appeared colorless. For recovery of alkaloids, the resin was transferred to a vessel and extracted under stirring with a solution of sodium chloride 5% in methanol/water (1:1 v/v). Exhaustive alkaloid recovery was achieved by repeating the washing step until the supernatant was colorless. The combined supernatants were evaporated to dryness under reduced pressure. The residue was suspended in water and exhaustively partitioned with chloroform. The alkaloidal fraction was obtained by evaporation of the organic phase on a rotary evaporator.

2.8. Preparative HPLC

Preparative HPLC separation was performed with a system consisting of two LC-8A preparative pumps, a SCL-10AVP system controller, and SPD-M10A VP PDA detector (all Shimadzu). A 1 mL loop was used for injection. Data acquisition and analysis were performed using class-VP V6.14 SP2A software. Separation was carried out on a Waters SunFire Prep C18 OBD (30 × 150 mm i.d., 5 μm) column. The mobile phase consisted of water containing 0.025% TFA (solvent C) and methanol containing 0.025% TFA (solvent D). The flow rate was 20 mL/min. Detection was at 365 and 420 nm. Separation of alkaloids was carried out in isocratic mode (73% C, 27% D) over 36 min. A stock solution of the alkaloidal fraction was prepared (40 mg/mL in DMSO/methanol [9:1 v/v]) and repeatedly injected. The injection volume was 1 mL. Fractions corresponding to peaks of DHE and hortiamine were collected and evaporated with a Multivapor P-12 evaporator equipped with a vacuum pump V-700 and a vacuum controller V-855 (all Büchi).

2.9. Quantitative determination of DHE in Evodia-containing products

Quantification by HPLC-UV was carried out on an Alliance 2695 instrument (Waters). The mobile phase consisted of water containing 0.025% TFA (solvent E) and acetonitrile containing 0.025% TFA (solvent F). The gradient profile was as follows: 10% F to 40% F in 20 min, 40% F to 100% F in 2 min, 100% F for 8 min. The flow rate was 0.5 mL/min, and detection was at 365 nm. The injection volume was 10 μL, unless otherwise stated. A stock solution of dehydroevodiamine chloride (reference compound) was prepared in DMSO (1 mg/mL). Calibration solutions covering a concentration range of 10 to 200 μg/mL were prepared from the stock solution by dilution with DMSO. A linear calibration curve ($y = 8.12 * 10^7\ x + 5.59 * 10^4$; $R^2 = 0.9999$) was obtained. Limit of detection (LOD; S/N ratio ≥ 3), and limit of quantification (LOQ; S/N ratio ≥ 10) were determined by serial dilution of the stock solution. The LOD and LOQ (amount of compound injected) were 0.8 ng and 2 ng, respectively. In the range of 10 to 200 μg/mL, intra-day precision (repeatability) and inter-day precision (between-day precision) were assessed in the course of the analysis with calibration samples, quality control samples, and two *Evodia* extract samples demonstrating that the method is precise (for details, see Supporting Information). Analyses were performed in triplicate, and at ambient temperature (20–24 °C).

2.9.1. Unprocessed E. rutaecarpa fruits

Dried *E. rutaecarpa* fruits were purchased from Yong Quan GmbH (Ennepetal, Germany) (Lot no. 70588813), Lian Chinaherb AG (Wollerau, Switzerland) (Lot no. Y410377A), and Complemedis AG (Trimbach, Switzerland) (Lot no. 905). Voucher specimens (number 00 465, 00 611, and 00 612, respectively) have been deposited at the Division of Pharmaceutical Biology, University of Basel, Switzerland. The macroscopic characteristics of *E. rutaecarpa* fruits were confirmed with the aid of the corresponding monograph of the Chinese Pharmacopeia and other literature [22,23]. Methanolic extracts were prepared by pressurized liquid extraction (PLE) using a Dionex ASE 200 instrument connected to a solvent controller (Dionex). Ground plant material (ZM 1 ultracentrifugal mill, Retsch; sieve size 2.0 mm) was packed into steel cartridges (11 mL; Dionex) and consecutively extracted with solvents of increasing polarity (petroleum ether, ethyl acetate, and methanol). Extraction temperature was at 70 °C, and the pressure was set at 120 bar. Duration of a static extraction cycle was 5 min, and 3 extraction cycles were used for each solvent to obtain exhaustive extraction [24,25]. Extracts were dried under reduced pressure, and dissolved in DMSO at a concentration of 3.5 mg/mL.

2.9.2. Commercial Evodia-containing TCM products

The following five TCM products were purchased and analyzed: “Wu zhu yu” (Guangdong Yifang Pharmaceutical Co., Ltd., China), “Wu zhu yu zhi” (Plantasia, Oberndorf, Austria), “Wu zhu yu tang” (Euroherbs BV, EZ Westervoort, The Netherlands), “Wen jing tang” (Euroherbs BV, EZ Westervoort, The Netherlands), and “Si shen wan” (Eagle Herbs, Santa Monica, CA, USA). Powdered granules were macerated exhaustively with methanol at room temperature. Pooled extracts

were filtered through a standard laboratory filter, concentrated under reduced pressure, and lyophilized. Dried extracts were dissolved in DMSO at a concentration of 10 mg/mL. The injection volume was 10 μL, except for "Si shen wan" (25 μL).

3. Results and discussion

Small-scale preparative purification (multi-mg amounts) of DHE was achieved by a combination of normal-phase and reverse-phase column chromatography. However, this approach was clearly not applicable for purification at the gram-scale (data not shown). Isolation of the structurally related minor alkaloid hortiamine (2) (Fig. 1), e.g., for pharmacological and toxicological studies, also required an efficient large-scale purification procedure.

Since DHE and hortiamine are both quaternary alkaloids, enrichment of an alkaloidal fraction on a cation-exchange resin, followed by an HPLC separation of the alkaloids, seemed to be an efficient two-stage approach. Therefore, we first tested various strongly and weakly acidic Lewatit®

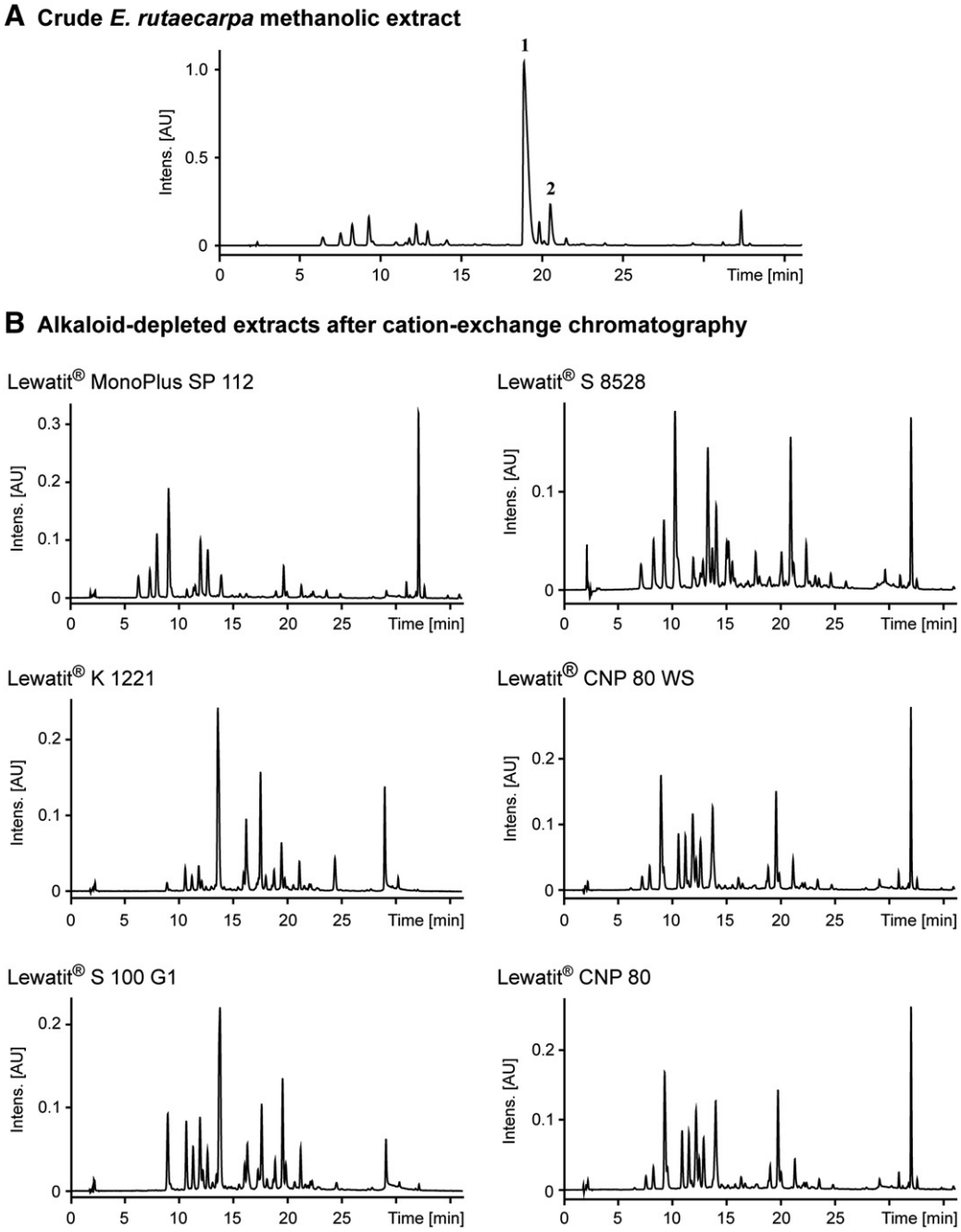

Fig. 2. LC-PDA fingerprints of crude *E. rutaecarpa* methanolic extract (A) and alkaloid-depleted extracts (B). Three strongly (left column) and three weakly (right column) acidic resins were tested for their potential of selective alkaloid retention. Peak numbering denotes alkaloids 1 and 2. HPLC traces were recorded at 365 nm.

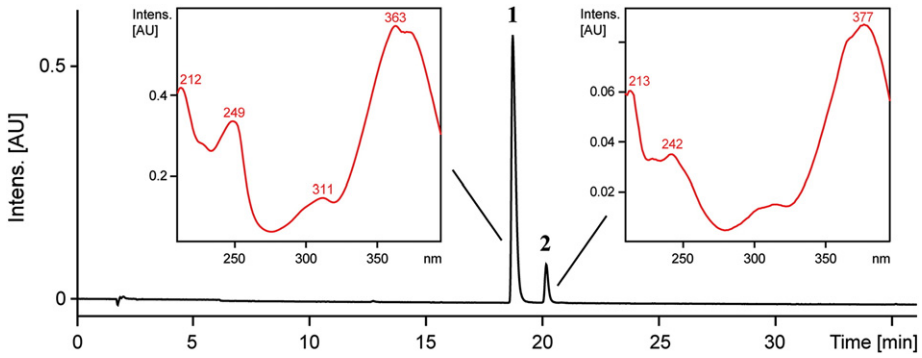

Fig. 3. Analytical HPLC chromatogram (365 nm) of the alkaloidal fraction obtained by enrichment on Lewatit® MonoPlus SP 112 resin. Peak numbering denotes alkaloids 1 and 2, with UV spectra of peaks shown as insets.

resins for their ability to selectively retain the quaternary alkaloids. LC-PDA analysis of the alkaloid-containing methanolic extract, and alkaloid-depleted extracts revealed that alkaloid retention (i) was successful with all resins and, (ii) was not influenced by the counterion of the resin. However, significant differences in the chromatographic fingerprints of the alkaloid-depleted extracts were observed. Representative HPLC chromatograms are shown in Fig. 2. The strong exchange resin Lewatit® MonoPlus SP 112 showed the best selectivity with respect to alkaloid retention, without significant modification of the non-alkaloidal fraction. Hence, this resin was selected for further work. Next, conditions for sample loading and sample elution were optimized. With respect to alkaloid extraction, removal via a packed column was more effective than batch extraction in a resin suspension under stirring (data not shown). The extract could be dissolved in methanol at a maximum concentration of 10 mg/mL, as higher sample concentrations (15 and 25 mg/mL) led to insoluble residues. For further process optimization, the capacity of the resin was determined by serial sample loading and parallel monitoring of breakthrough. Satisfactory alkaloid retention with minimal bleeding was achieved with a loading ratio up to 20% (1 g of extract on 5 g of resin). Moreover, the effect of different flow rates (0.5, 1.0, and 2.0 mL/min) for elution of the column was investigated. Flow rates up to 1.0 mL/min gave good retention of alkaloids, and a flow rate of 1 mL/min was thus selected for achieving highest possible throughput. Quaternary alkaloids were eluted from the cation-exchange resin by increasing the ionic strength with the aid of a solution of sodium chloride 5% in methanol/water (1:1 v/v). The alkaloidal fraction was readily desalted by solvent partitioning, and further characterized by LC-PDA analysis and ^{1}H NMR spectroscopy. In summary, cation-exchange solid phase extraction afforded a highly enriched alkaloidal fraction composed of DHE (1) and the accompanying minor alkaloid hortiamine (2) in a ratio of 91:9 (^{1}H NMR and HPLC). A representative analytical HPLC chromatogram of the alkaloidal fraction is shown in Fig. 3.

The optimized cation-exchange solid phase extraction procedure was then upscaled for gram-scale purification of DHE. A linear scale up was done, and the alkaloid enrichment was reproducible at preparative scale, as an alkaloidal fraction with 91% of DHE (^{1}H NMR and HPLC) was obtained. Several attempts to separate DHE (1) and hortiamine (2) by crystallization failed. Purification of alkaloids 1 and 2 was finally achieved by isocratic preparative RP-HPLC. Conditions were optimized with respect to sample loading, resolution, and

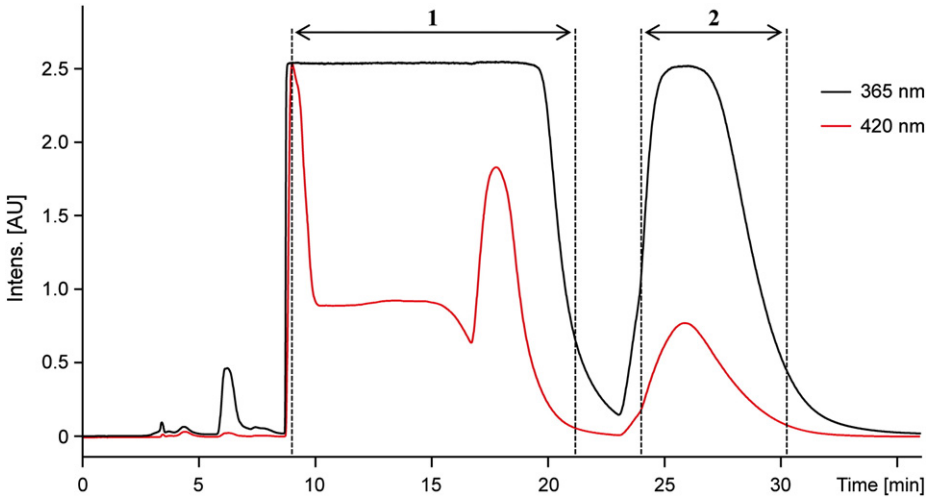

Fig. 4. Preparative HPLC chromatogram of the alkaloidal fraction. HPLC traces of a separation of 40 mg of alkaloidal fraction are shown. Dashed lines denote collected fractions.

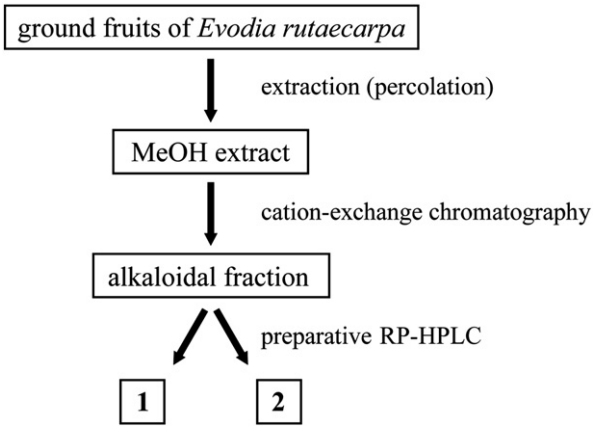

Fig. 5. Procedure for the large-scale purification of DHE (1) from crude *E. rutaecarpa* extract.

separation time. Increasing both sample volume and sample concentration caused a noticeable column overload and led to peak broadening and saturation of the detector signal. However, amounts of up to 40 mg of alkaloidal fraction could be separated in a single HPLC run, without significant loss of separation performance (Fig. 4). Repeated injections combined with automated solvent evaporation of collected fractions afforded 200 mg of DHE per day. The structurally related alkaloid hortiamine was isolated for the first time from *E. rutaecarpa* fruits. The identity of compounds was confirmed by comprehensive analysis of on-line (LC-PDA-ESI-TOF-MS) and off-line (microprobe 1D and 2D NMR) spectroscopic data, and comparison with published literature [26–28]. Hortiamine has been previously reported from *Hortia arborea* Engl. and *Hortia brasiliana* Vand. ex DC., but no NMR spectral data were recorded at that time [28,29]. The ^{1}H and ^{13}C NMR spectroscopic data of hortiamine are listed in Table S2 of the Supplementary data. Final purities of alkaloids 1 and 2 were ≥95%, as determined by LC-PDA analysis and ^{1}H NMR spectroscopy (for ^{1}H NMR spectra see Supplementary data).

The purification strategy used for the gram-scale isolation of DHE from the methanolic *Evodia* extract is summarized in Fig. 5. The procedure involved two steps, namely cation-exchange solid phase extraction and RP-HPLC. Due to the ionic nature of the target compounds, an enrichment of the alkaloidal fraction was readily achieved with a cation-exchange resin. Careful selection of an appropriate cation-exchange resin was critical for a selective enrichment of the alkaloidal fraction with minimal non-alkaloidal contaminants. Given the purity of the alkaloidal fraction, isocratic HPLC conditions could be used for separation of DHE and hortiamine, without need for column washing between runs. Hence, a medium sample throughput could be achieved. A major advantage is that ion-exchange resins can be easily regenerated and are amenable to repeated use. There is, however, room for further optimization of the purification procedure, e.g., unattended operation of the HPLC by an automated MS-triggered fractionation. Also, chloroform could be replaced as the organic phase in the partitioning step by a more eco-friendly solvent.

Postharvest processing of herbs is a unique feature of TCM, and is believed to enhance the efficacy and/or reduce the toxicity of crude herbal drugs [30]. According to Bensky et al., unprocessed *Evodia* fruits are only used externally, while for internal administration various processing methods are described. The minimum requirement is that the fruits are soaked in water and subsequently sun-dried. Different processing methods are used for producing different therapeutic effects according to TCM concepts [31]. From a scientific perspective, processing may lead to significant qualitative and quantitative changes in the metabolite pattern. This is of particular importance for pharmacologically/toxicologically critical compounds in TCM drugs, such as DHE. Therefore, we determined the DHE content in different commercial batches of dried *E. rutaecarpa* fruits, and in a series of commercially available processed TCM products, and we then calculated the intake of DHE in recommended daily doses for these products (Table 1). DHE was detected in all herbal drug samples and processed TCM products, but quantitative differences were observed. The daily intake in DHE with the crude herbal drug is significantly higher (12 to 43 mg) than with processed *Evodia*-containing preparations (6.7 to 7.3 mg considering manufacturers' recommendations). However, the amounts of DHE consumed in the latter type of products could still be toxicologically relevant. If the DHE intake should indeed turn out to be toxicologically critical, the alkaloid would have to be removed from *Evodia* products, even if the pharmacological activity of the herbal drug would be linked to the compound. A selective removal of quaternary indoloquinazoline alkaloids with the cation-exchange resin Lewatit® MonoPlus SP 112, as demonstrated with our experiments (Fig. 2), could be a viable approach for their removal from *Evodia* extracts without altering the fingerprint of the non-alkaloidal portion.

4. Conclusions

An efficient two-step protocol for the gram-scale isolation of DHE from a crude *E. rutaecarpa* extract has been developed.

Table 1
Content of DHE in commercial *Evodia* products[1].

Supplier of crude Evodiae fructus	DHE content in RDD[2] (1.5–4.5 g fruits [22,31])	Processed TCM product[3]	DHE content in 1 g of formulation/RDD[2]
Lian Chinaherb AG	12.0–36.0 mg	Wu zhu yu	7.3 mg/7.3 mg
Complemedis AG	12.4–37.3 mg	Wu zhu yu zhi	6.5 mg/nd
Yong Quan GmbH	14.4–43.2 mg	Wu zhu yu tang	3.2 mg/nd
		Wen jing tang	1.1 mg/nd
		Si shen wan	0.5 mg/6.7 mg

nd: not determined (no RDD given by the supplier).
[1] Contents are expressed as dehydroevodiamine chloride and represent the mean from three injections.
[2] RDD: recommended daily dose.
[3] For details on the composition of the investigated preparations, see Supporting Information.

The approach is based on a combination of cation-exchange chromatography and preparative RP-HPLC. Gram amounts of DHE could be purified for quality control purposes and further evaluation of its in vivo pharmacological and toxicological properties. A quantitative analysis of DHE in commercially available *Evodia* products provided valuable information about the exposure to this alkaloid. These data are of considerable relevance from a clinical point of view, e.g., for evaluating the potential of DHE for pharmacological/pharmacokinetic interactions with other phytomedicines, dietary supplements, or drugs. We developed a procedure for the selective removal of quaternary indoloquinazoline alkaloids from *Evodia* extracts which could be upscaled for production of DHE-depleted *Evodia* products.

Conflict of interest

The authors declare no conflict of interest.

Acknowledgments

This project was supported by the Swiss National Science Foundation (grant no. 205320_126888), and by the Marie Curie Action "hergAccess". The authors are grateful to Chemia Brugg AG (Brugg, Switzerland) for the gift of Lewatit® ion-exchange resins. We also thank Dr. M. Decker for synthesizing dehydroevodiamine chloride, Dr. M. Oufir for the valuable discussions on analytical method validation, and Orlando Fertig for the technical assistance.

Appendix A. Supplementary data

Supplementary data to this article can be found online at http://dx.doi.org/10.1016/j.fitote.2014.02.005.

References

[1] Butterweck V, Nahrstedt A. What is the best strategy for preclinical testing of botanicals? A critical perspective. Planta Med 2012;78:747–54.
[2] Martin SM, Kau DA, Wrigley SK. Scale-up of natural product isolation. In: Sarker SD, Latif Z, Gray AI, editors. Natural product isolation. 2nd ed. Totowa, New Jersey: Humana Press Inc.; 2005. p. 439–61.
[3] Hamburger M, Adler S, Baumann D, Förg A, Weinreich B. Preparative purification of the major anti-inflammatory triterpenoid esters from marigold (*Calendula officinalis*). Fitoterapia 2003;74:328–38.
[4] Baumann D, Adler S, Hamburger M. A simple isolation method for the major catechins in green tea using high-speed countercurrent chromatography. J Nat Prod 2001;64:353–5.
[5] Zhou TT, Fan GR, Hong ZY, Chai YF, Wu YT. Large-scale isolation and purification of geniposide from the fruit of *Gardenia jasminoides* Ellis by high-speed counter-current chromatography. J Chromatogr A 2005;1100:76–80.
[6] Zhou M, Zhuo JX, Wei WX, Zhu JW, Ling XR. Simple and effective large-scale preparation of geniposide from fruit of *Gardenia jasminoides* Ellis using a liquid–liquid two-phase extraction. Fitoterapia 2012;83:1558–61.
[7] Lee HJ, Lee KH, Park KH, Moon JH. Large scale isolation and purification of salvianolic acid B in high purity from roots of Dansham (*Salvia miltiorrhiza* Bunge). Food Sci Biotechnol 2010;19:497–502.
[8] Ma CH, Ke W, Sun ZL, Peng JY, Li ZX, Zhou X, et al. Large-scale isolation and purification of scoparone from *Herba artemisiae scopariae* by high-speed counter-current chromatography. Chromatographia 2006;64:83–7.
[9] Graf TN, Wani MC, Agarwal R, Kroll DJ, Oberlies NH. Gram-scale purification of flavonolignan diastereoisomers from *Silybum marianum* (milk thistle) extract in support of preclinical in vivo studies for prostate cancer chemoprevention. Planta Med 2007;73:1495–501.
[10] Chinese Pharmacopoeia Commission. Pharmacopoeia of the People's Republic of China — Volume I. English ed. Beijing: China Medical Science Press; 2010.
[11] Tang W, Eisenbrand G. Handbook of Chinese medicinal plants: chemistry, pharmacology, toxicology. Weinheim: Wiley-VCH; 2011.
[12] Huang X, Li W, Yang XW. New cytotoxic quinolone alkaloids from fruits of *Evodia rutaecarpa*. Fitoterapia 2012;83:709–14.
[13] Wang XX, Zan K, Shi SP, Zeng KW, Jiang Y, Guan Y, et al. Quinolone alkaloids with antibacterial and cytotoxic activities from the fruits of *Evodia rutaecarpa*. Fitoterapia 2013;89:1–7.
[14] Sugimoto T, Miyase T, Kuroyanagi M, Ueno A. Limonoids and quinolone alkaloids from *Evodia rutaecarpa* Bentham. Chem Pharm Bull 1988;36:4453–61.
[15] Wang YF, Liu YN, Hu LM, Pan GX, Gao XM. A qualitative and quantitative assessment of eight constituents in *Fructus Evodiae* by HPLC-DAD-ESI-MS/MS. J Liq Chromatogr R T 2011;34:408–20.
[16] Park CH, Kim SH, Choi W, Lee YJ, Kim JS, Kang SS, et al. Novel anticholinesterase and antiamnesic activities of dehydroevodiamine, a constituent of *Evodia rutaecarpa*. Planta Med 1996;62:405–9.
[17] Decker M. Novel inhibitors of acetyl- and butyrylcholinesterase derived from the alkaloids dehydroevodiamine and rutaecarpine. Eur J Med Chem 2005;40:305–13.
[18] Yang MCM, Wu SL, Kuo JS, Chen CF. The hypotensive and negative chronotropic effects of dehydroevodiamine. Eur J Pharmacol 1990;182:537–42.
[19] Chiou WF, Liao JF, Chen CF. Comparative study on the vasodilatory effects of three quinazoline alkaloids isolated from *Evodia rutaecarpa*. J Nat Prod 1996;59:374–8.
[20] Loh SH, Lee AR, Huang WH, Lin CI. Ionic mechanisms responsible for the antiarrhythmic action of dehydroevodiamine in guinea-pig isolated cardiomyocytes. Brit J Pharmacol 1992;106:517–23.
[21] Laverty HG, Benson C, Cartwright EJ, Cross MJ, Garland C, Hammond T, et al. How can we improve our understanding of cardiovascular safety liabilities to develop safer medicines? Brit J Pharmacol 2011;163:675–93.
[22] Stöger EA, Friedl F. Arzneibuch der Chinesischen Medizin. German ed. Stuttgart: Deutscher Apotheker Verlag; 2009.
[23] Zhongzhen Z. An illustrated Chinese Materia medica in Hong Kong. Hong Kong: School of Chinese Medicine, Hong Kong Baptist University; 2004.
[24] Basalo C, Mohn T, Hamburger M. Are extraction methods in quantitative assays of pharmacopoeia monographs exhaustive? A comparison with pressurized liquid extraction. Planta Med 2006;72:1157–62.
[25] Benthin B, Danz H, Hamburger M. Pressurized liquid extraction of medicinal plants. J Chromatogr A 1999;837:211–9.
[26] King CL, Kong YC, Wong NS, Yeung HW, Fong HHS, Sankawa U. Uterotonic effect of *Evodia rutaecarpa* alkaloids. J Nat Prod 1980;43:577–82.
[27] Lin LC, Li SH, Wu YT, Kuo KL, Tsai TH. Pharmacokinetics and urine metabolite identification of dehydroevodiamine in the rat. J Agr Food Chem 2012;60:1595–604.
[28] Pachter IJ, Raffauf RF, Ullyot GE, Ribeiro O. The alkaloids of *Hortia arborea* Engl. J Am Chem Soc 1960;82:5187–93.
[29] Pachter IJ, Mohrbacher RJ, Zacharias DE. Chemistry of hortiamine and 6-methoxyrhetsinine. J Am Chem Soc 1961;83:635–42.
[30] Zhao ZZ, Liang ZT, Chan K, Lu GH, Lee ELM, Chen HB, et al. A unique issue in the standardization of Chinese Materia Medica: processing. Planta Med 2010;76:1975–86.
[31] Bensky D, Clavey S, Stöger E. Chinese herbal medicine: materia medica. 3rd ed. Seattle: Estland Press, Inc.; 2004.

Supplementary data

Gram-scale purification of dehydroevodiamine from *Evodia rutaecarpa* fruits, and a procedure for selective removal of quaternary indoloquinazoline alkaloids from *Evodia* extracts

Anja Schramm, Matthias Hamburger*

Division of Pharmaceutical Biology, University of Basel, Klingelbergstrasse 50, 4056 Basel, Switzerland

* Corresponding author. Tel.: +41 (0)61 267 14 25; fax: +41 (0)61 267 14 74

E-mail address: matthias.hamburger@unibas.ch (M. Hamburger)

Analytical data of dehydroevodiamine (DHE, 1)

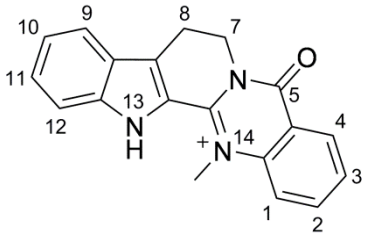

HR-ESI-TOF-MS *m/z* 302.1291 [M^+] (calcd for $C_{19}H_{16}N_3O$: 302.1288)

Table S1. NMR spectroscopic data (MeOH-d_4, 500 MHz, δ in ppm).

Position	δ_H (*J* in Hz)	δ_C[a]
1	8.06, br d (8.4)	117.7
2	8.11, ddd (8.6, 7.2, 1.5)	136.2
3	7.79, ddd (8.0, 7.2, 0.9)	128.3
4	8.44, dd (7.9, 1.5)	127.9
4a		118.9
5		158.7
7	4.61, t (7.1)	41.9
8	3.42, t (7.1)	18.6
8a		131.8
8b		123.9
9	7.85, br d (8.2)	121.1
10	7.31, ddd (8.5, 7.1, 1.0)	121.8
11	7.55, ddd (8.5, 7.2, 1.0)	129.3
12	7.67, br d (8.5)	113.0
12a		142.4
13a		119.9
13b		150.3
14a		139.9
14-NCH_3	4.45, s	39.9

[a] ^{13}C shifts deduced from HSQC and HMBC experiments.

δ_H reference data measured in MeOH-d_4 can be found in [1,2].

δ_H and δ_C reference data measured in DMSO-d_6 can be found in [3].

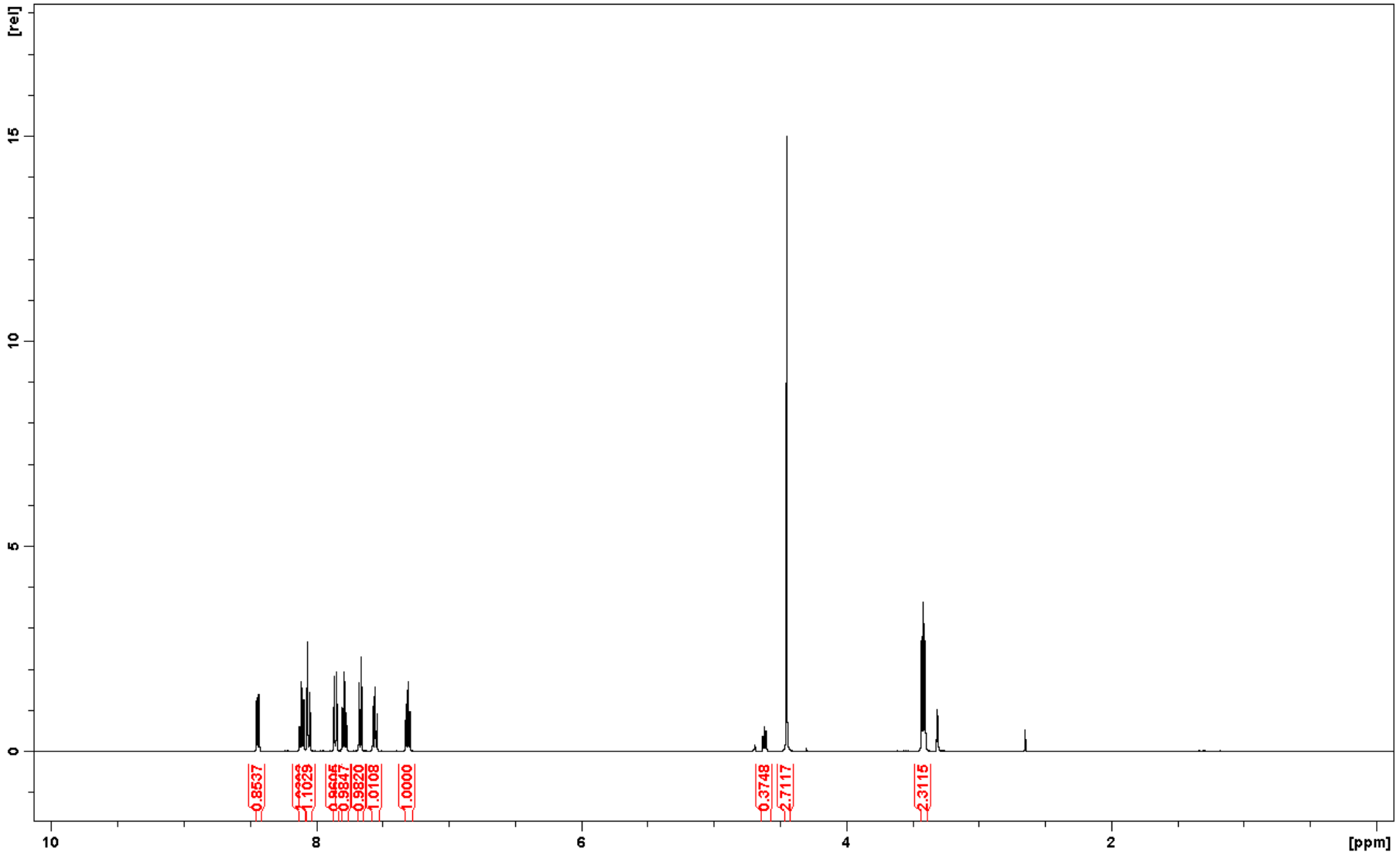

Figure S1. ^{1}H NMR spectrum of DHE (**1**) in MeOH-d_4 (recorded with water suppression).

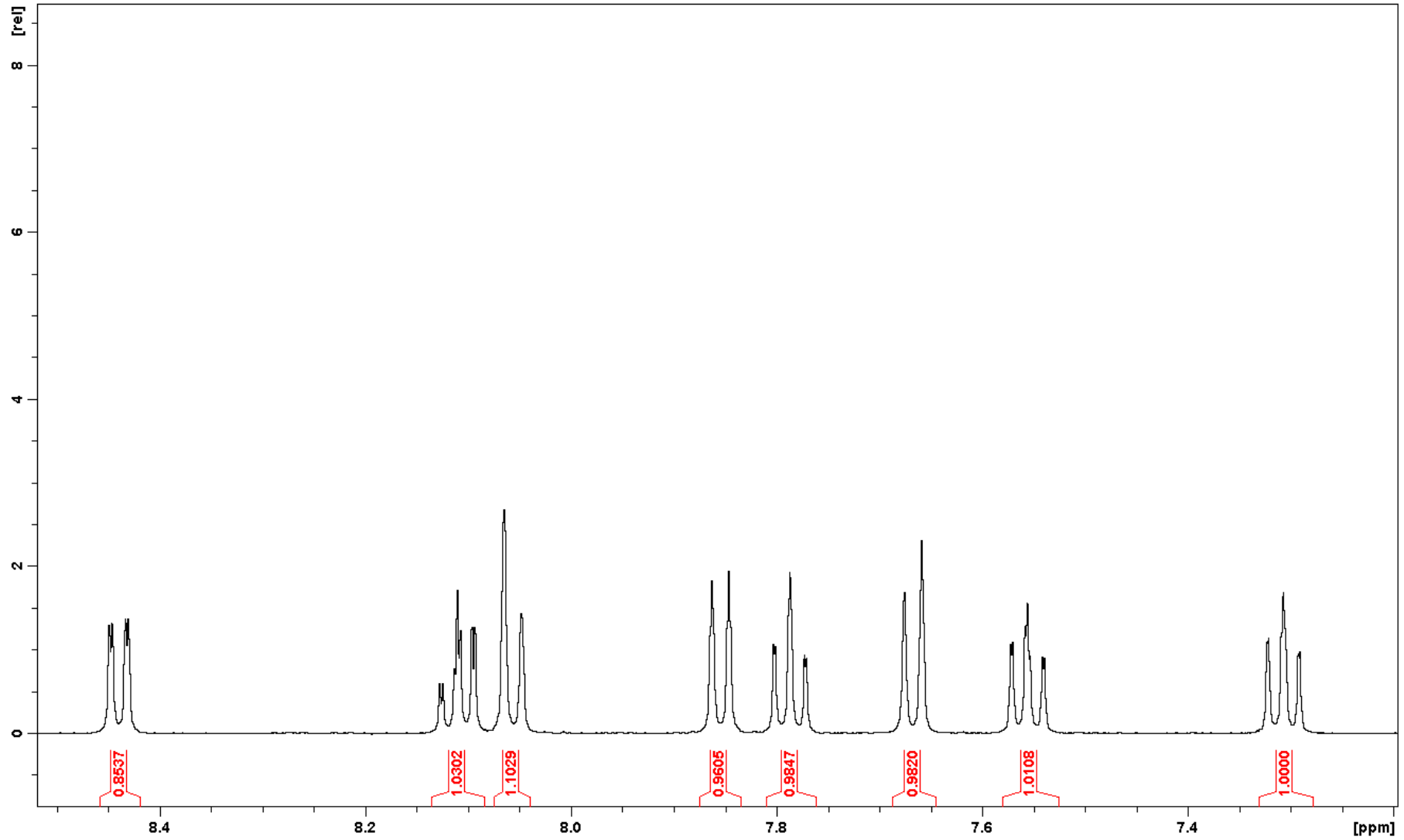

Figure S2. ^{1}H NMR spectrum of DHE (**1**). Expansion of the region 7.2–8.5 ppm.

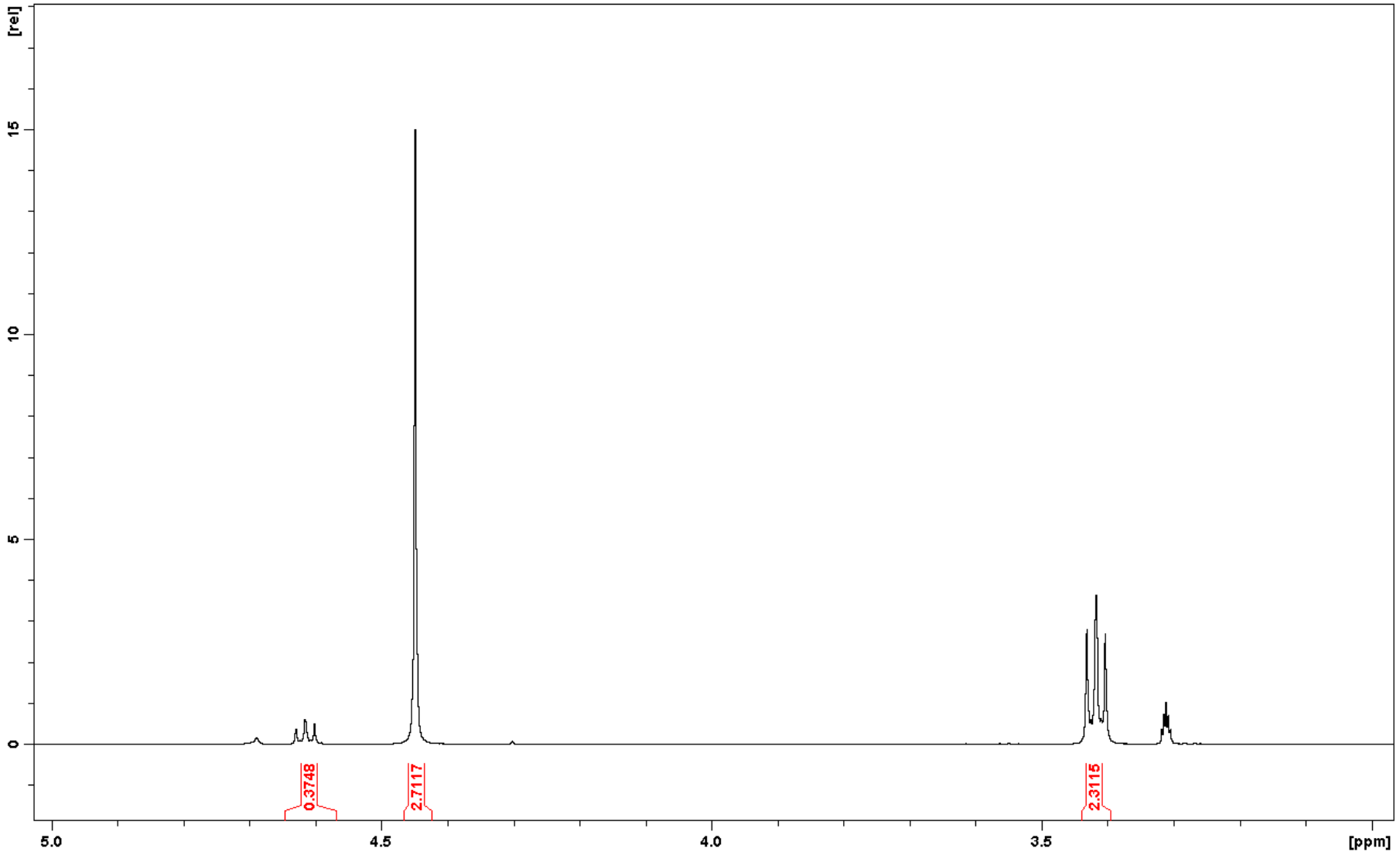

Figure S3. ^{1}H NMR spectrum of DHE (**1**). Expansion of the region 3.0–5.0 ppm. Water suppression caused decreased signal intensities for δ_H 4.61 (H-7) and δ_H 4.45 (14-NCH_3).

Analytical data of hortiamine (2)

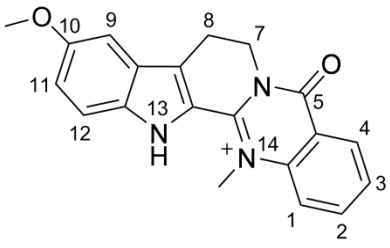

HR-ESI-TOF-MS *m/z* 332.1389 [M^+] (calcd for $C_{20}H_{18}N_3O_2$: 332.1394)

Table S2. NMR spectroscopic data (MeOH-d_4, 500 MHz for δ_H, 125 MHz for δ_C, δ in ppm).

Position	δ_H (*J* in Hz)	δ_C[a]	δ_C
1	8.02, br d (8.6)	117.6	119.3
2	8.09, ddd (8.4, 7.1, 1.2)	136.4	138.0
3	7.76, dd (8.1, 7.3)	128.2	129.9
4	8.41, dd (7.9, 1.2)	127.9	129.6
4a		118.6	120.5
5		158.3	159.7
7	4.58, t (7.0)	42.0	43.6
8	3.36, t (7.0)	18.7	20.2
8a		131.1	132.2
8b		124.2	125.7
9	7.20, d (2.0)	99.6	100.9
10		155.8	157.3
11	7.18, dd (9.0, 2.1)	122.2	123.8
12	7.55, d (9.0)	114.0	115.6
12a		138.4	139.7
13a		119.7	121.2
13b		150.2	151.5
14a		140.0	141.5
14-NCH_3	4.42, s	39.8	41.4
10-OCH_3	3.88, s	54.8	56.3

[a] ^{13}C shifts deduced from HSQC and HMBC experiments.

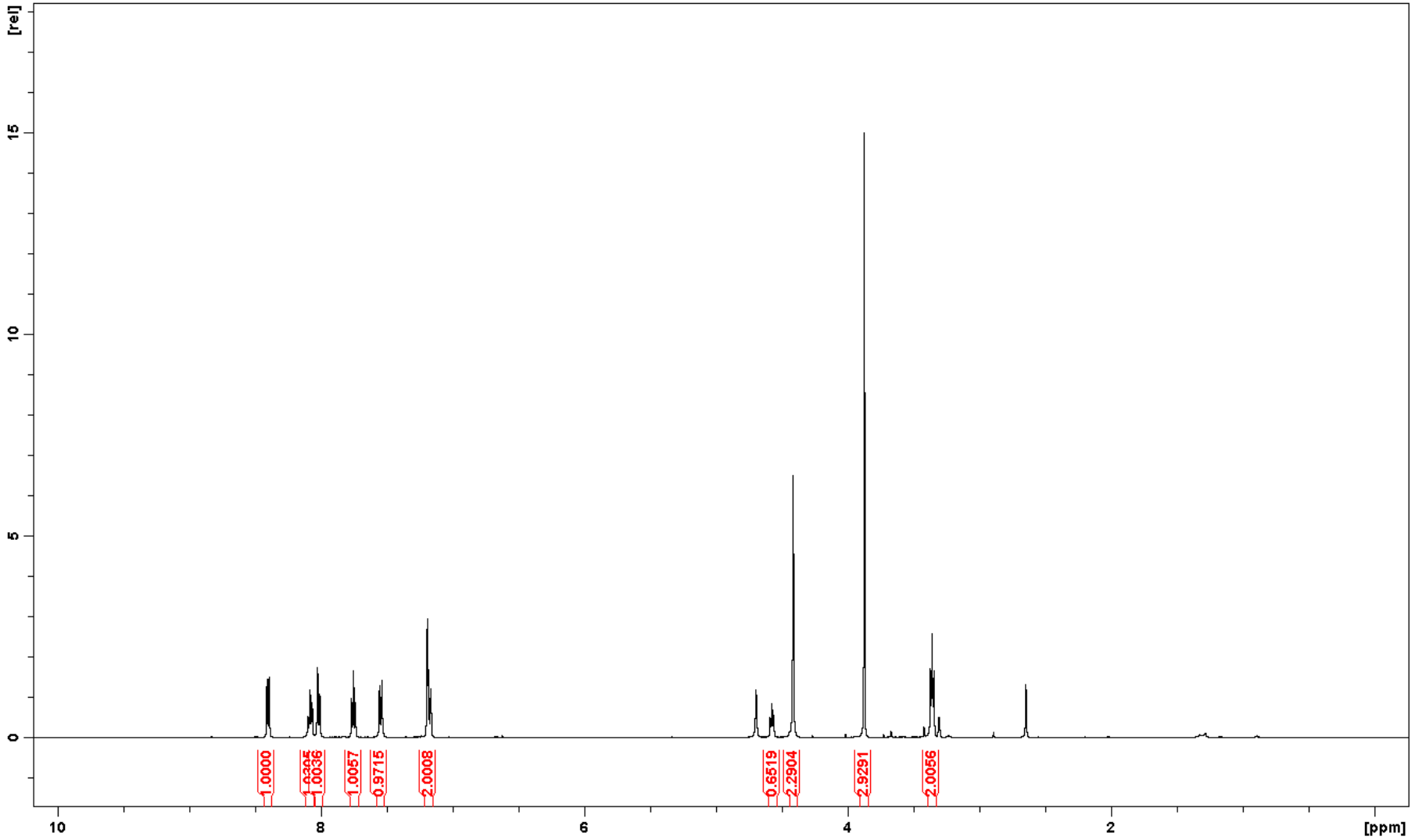

Figure S4. ^{1}H NMR spectrum of hortiamine (**2**) in MeOH-d_4 (recorded with water suppression).

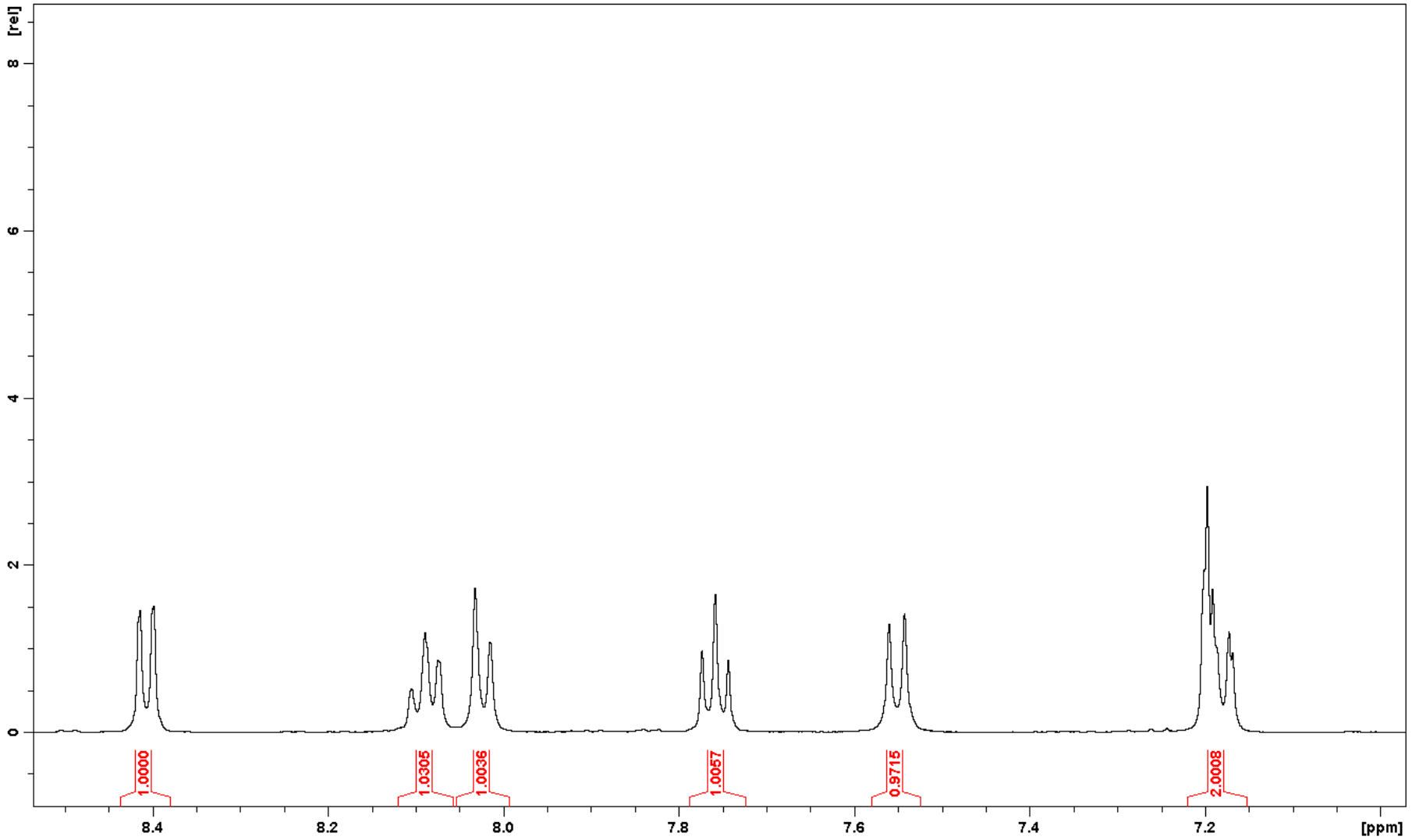

Figure S5. ^{1}H NMR spectrum of hortiamine (**2**). Expansion of the region 7.0–8.5 ppm.

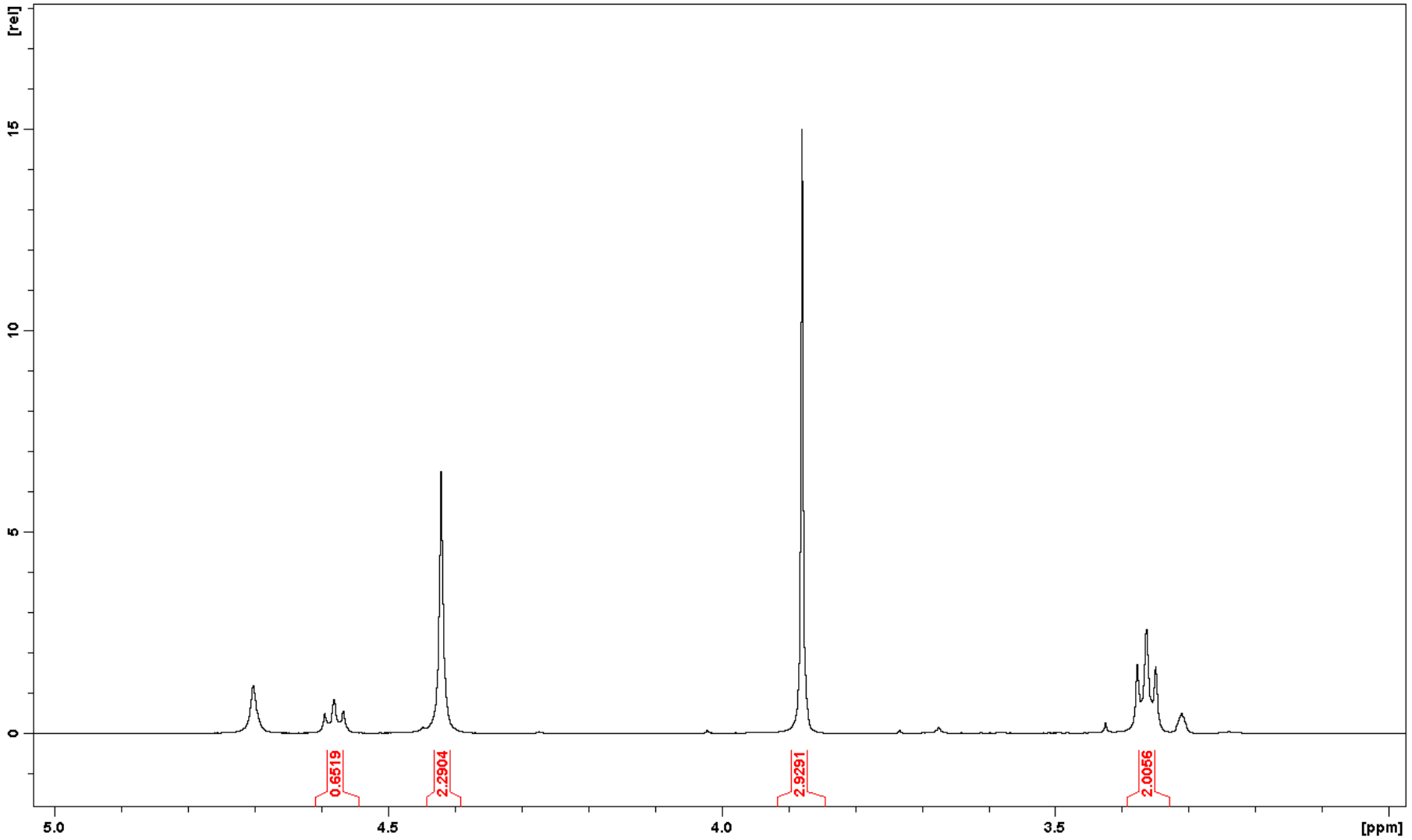

Figure S6. ^{1}H NMR spectrum of hortiamine (**2**). Expansion of the region 3.0–5.0 ppm. Water suppression caused decreased signal intensities for δ_H 4.58 (H-7) and δ_H 4.42 (14-NCH_3).

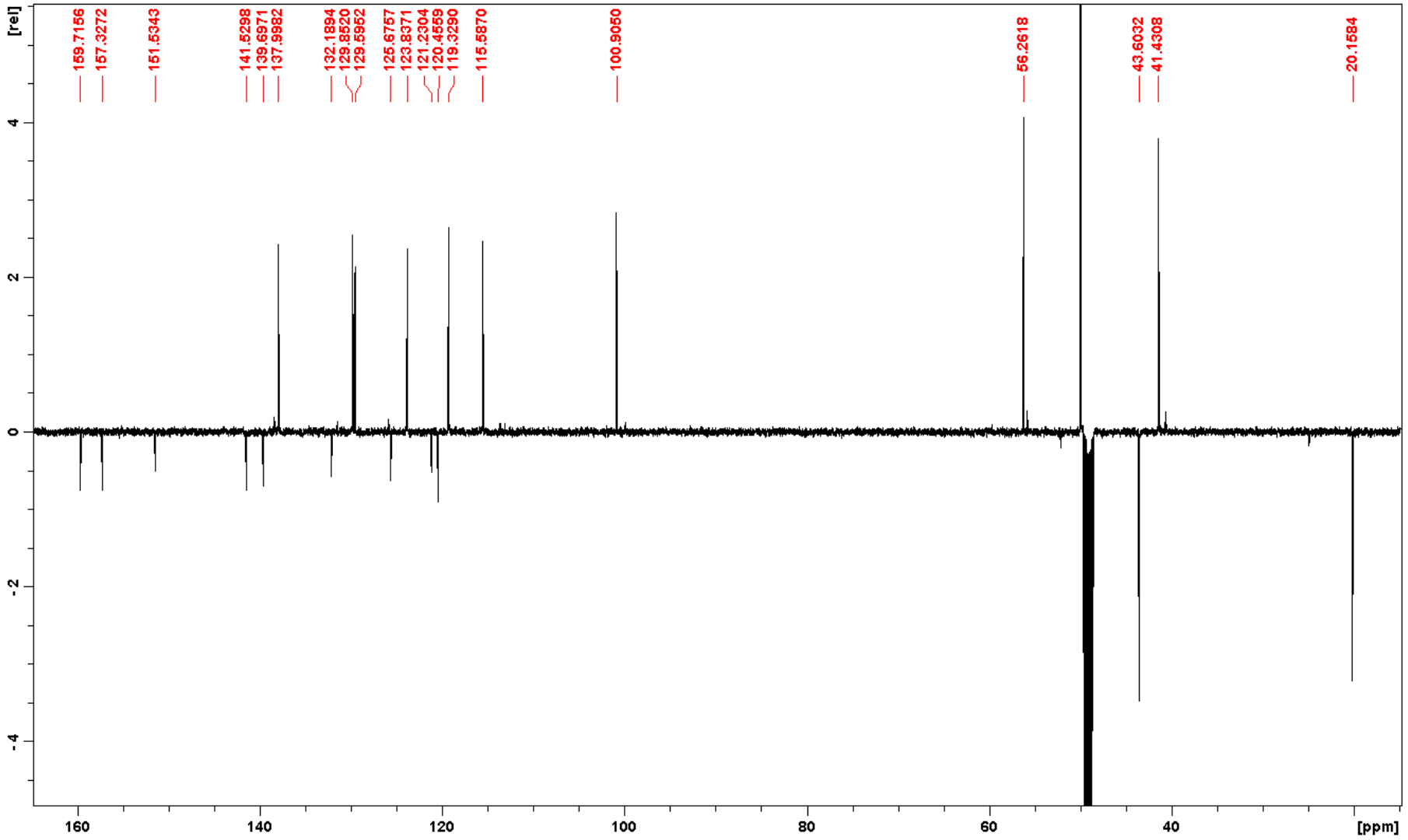

Figure S7. DEPT NMR spectrum of hortiamine (**2**) in MeOH-d_4.

Additional information on processed *Evodia*-containing TCM products

"Wu zhu yu"
Supplier: This product was purchased through the Internet.
Manufacture: Guangdong Yifang Pharmaceutical Co., Ltd., China
Lot no.: 0908053
Recommended daily dose: 0.5 g of the granule (equivalent to 3 g of crude herbal drug) twice a day
Ingredient: Evodiae fructus

"Wu zhu yu zhi"
Supplier: Plantasia, Oberndorf, Austria
Manufacture: Tianjiang Pharmaceutical Co., Ltd., China
Lot no.: 0710519
Recommended daily dose: no information given
Ingredient: Evodiae fructus (prepared)

"Wu zhu yu tang"
Supplier: Euroherbs BV, EZ Westervoort, The Netherlands
Manufacture: Kaiser Pharmaceutical
Lot no.: 423756
Recommended daily dose: no information given

Contents per 100 g:	Zingiberis rhizoma recens	33
	Evodiae fructus	28
	Jujubae fructus	22
	Ginseng radix et rhizoma	17

“Wen Jing Tang”

Supplier: Euroherbs BV, EZ Westervoort, The Netherlands
Manufacture: Kaiser Pharmaceutical
Lot no.: 433556
Recommended daily dose: no information given

Contents per 100 g:		
	Pinelliae rhizoma	13
	Ophiopogonis radix	13
	Evodiae fructus	10
	Zingiberis rhizoma recens	10
	Angelicae sinensis radix	7
	Cnidii fructus	7
	Paeoniae radix alba	7
	Ginseng radix et rhizoma	7
	Cinnamomi ramulus	7
	Moutan cortex	7
	Glycyrrhizae radix et rhizoma	6
	Asini corii colla	6

“Si Shen Wan”

Supplier: Eagle Herbs, Santa Monica, CA, USA
Manufacture: no information given
Lot no.: no information given
Recommended daily dose: ½–1 teaspoon of the granule, up to three times daily

Ingredients:
Psoraleae fructus
Myristicae semen
Schisandrae chinensis fructus
Evodiae fructus
Jujubae fructus
Zingiberis rhizoma recens
Chebulae fructus
(quantities of ingredients are not listed)

Quantitative determination of DHE

Intra-day precision (repeatability) and inter-day precision (between-day precision) were assessed with calibration samples (Cal), quality control samples (QC), and two *Evodia* extract samples. The intra- and inter-series imprecisions (expressed as CV %) were calculated for each level (Cal, QC, and extract sample) as follows: CV % = 100 x (standard deviation / mean measured concentration).

1. Intra-day imprecision

Compound: DHE

Units: µg/mL

Matrix: DMSO

	Cal1	QC1	QC2	QC3	Cal5
Theoretical concentration	**10.0 µg/mL**	**20.0 µg/mL**	**100 µg/mL**	**160 µg/mL**	**200 µg/mL**
Run number	**Measured conc.**	**Measured conc.**	**Measured conc.**	**Measured conc.**	**Measured conc.**
1	6.93	18.2	104	163	196
	7.17	18.2	104	162	197
Intra-run Mean	7.05	18.2	104	163	196
Intra-run S.D.	0.17	0.06	0.18	0.18	0.64
Intra-run CV %	2.44	0.32	0.17	0.11	0.33

The intra-day imprecision was between 0.11% and 2.44%.

2. Inter-day imprecision

Compound: DHE

Units: µg/mL

Matrix: DMSO

	Cal1	QC1	QC2	QC3	Cal5
Theoretical concentration	**10.0 µg/mL**	**20.0 µg/mL**	**100 µg/mL**	**160 µg/mL**	**200 µg/mL**
Run number	**Measured conc.**	**Measured conc.**	**Measured conc.**	**Measured conc.**	**Measured conc.**
1	6.93	18.2	104	163	196
	7.17	18.2	104	162	197
Mean	7.05	18.2	104	163	196
S.D.	0.17	0.06	0.18	0.18	0.64
CV %	2.44	0.32	0.17	0.11	0.33
Run number	**Measured conc.**	**Measured conc.**	**Measured conc.**	**Measured conc.**	**Measured conc.**
2	7.25	18.5	104	161	198
	7.37	18.2	104	162	195
Mean	7.31	18.4	104	161	196
S.D.	0.08	0.18	0.09	0.65	1.75
CV %	1.15	0.99	0.09	0.40	0.89
Run number	**Measured conc.**	**Measured conc.**	**Measured conc.**	**Measured conc.**	**Measured conc.**
3	7.39	18.5	* 61	158	195
	7.35	17.7	104	* 94	197
Mean	7.37	18.1	83	126	196
S.D.	0.03	0.61	30.05	45.00	1.57
CV %	0.41	3.35	36.36	35.79	0.80
Inter-run Mean	7.24	18.2	97	150	196
Inter-run S.D.	0.10	0.28	10.11	15.28	1.32
Inter-run CV %	1.33	1.55	12.21	12.10	0.67

* LC injection issue, values used for calculations

The inter-day imprecision was between 0.67% and 12.21%.

3. *Evodia* extract samples

Compound: DHE

Units: µg/mL

Matrix: Methanolic extracts were dissolved in DMSO at a concentration of 3.5 mg/mL.

	Extract 1 [a]	Extract 2 [b]
Run number	**Measured conc.**	**Measured conc.**
1	135	87
	135	86
Mean	135	86
S.D.	0.25	0.55
CV %	0.18	0.64
Run number	**Measured conc.**	**Measured conc.**
2	131	88
	130	89
Mean	130	88
S.D.	0.66	0.66
CV %	0.51	0.75
Run number	**Measured conc.**	**Measured conc.**
3	137	84
	133	85
Mean	135	84
S.D.	2.95	0.79
CV %	2.18	0.94
Inter-run Mean	133	86
Inter-run S.D.	1.29	0.67
Inter-run CV %	0.96	0.77

[a] Dried *E. rutaecarpa* fruits were from Lian Chinaherb AG (Wollerau, Switzerland).
[b] Dried *E. rutaecarpa* fruits were from Complemedis AG (Trimbach, Switzerland).

For both *Evodia* extract samples, the inter-day imprecision was between 0.77% and 0.96%.

References

[1] King CL, Kong YC, Wong NS, Yeung HW, Fong HHS, Sankawa U. Uterotonic effect of *Evodia rutaecarpa* alkaloids. J Nat Prod 1980;43:577-82.

[2] Lin LC, Li SH, Wu YT, Kuo KL, Tsai TH. Pharmacokinetics and urine metabolite identification of dehydroevodiamine in the rat. J Agr Food Chem 2012;60:1595-604.

[3] Arisawa M, Horiuchi T, Hayashi T, Tezuka Y, Kikuchi T, Morita N. Studies on constituents of *Evodia rutaecarpa* (Rutaceae). I. Constituents of the leaves. Chem Pharm Bull 1993;41:1472-4.

3.5. Phytochemical profiling of *Curcuma kwangsiensis* rhizome extract, and identification of labdane diterpenoids as positive $GABA_A$ receptor modulators

Schramm A, Ebrahimi SN, Raith M, Zaugg J, Rueda DC, Hering S, Hamburger M.
Phytochemistry 2013; 96: 318–329

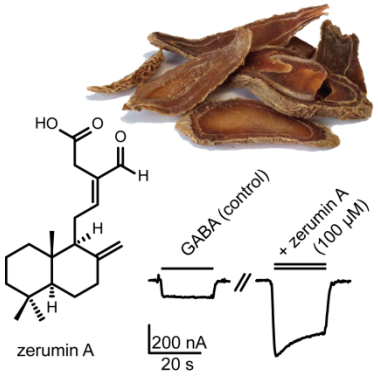

Labdane diterpenoids from *Curcuma kwangsiensis* rhizomes were identified as positive $\alpha_1\beta_2\gamma_{2S}$ $GABA_A$ receptor modulators with the aid of HPLC-based activity profiling. Eleven compounds, including four new natural products, were obtained. Structures were elucidated by high resolution mass spectrometry and microprobe NMR. The absolute configuration of diterpenoids was assigned by ECD. Modulation of the GABA-induced chloride current was assessed in a functional assay on *Xenopus* oocytes. The highest efficiency was observed for zerumin A.

Extraction of plant material, HPLC microfractionation, isolation of compounds, recording and interpretation of analytical data for structure elucidation (LC-PDA-ESI-TOF-MS, microprobe NMR, optical rotation), electrophysiological studies on pure compounds (preparation of Xenopus oocytes, two-microelectrode voltage-clamp measurements, data analysis), writing the draft of the manuscript, and preparation of figures (except for Fig. 5, 7, and 8) were my contributions to this publication.

Anja Schramm

Phytochemistry 96 (2013) 318–329

Contents lists available at ScienceDirect

Phytochemistry

journal homepage: www.elsevier.com/locate/phytochem

Phytochemical profiling of *Curcuma kwangsiensis* rhizome extract, and identification of labdane diterpenoids as positive $GABA_A$ receptor modulators

Anja Schramm [a], Samad Nejad Ebrahimi [a,b], Melanie Raith [a], Janine Zaugg [a], Diana C. Rueda [a], Steffen Hering [c], Matthias Hamburger [a,*]

[a] Division of Pharmaceutical Biology, University of Basel, Klingelbergstrasse 50, 4056 Basel, Switzerland
[b] Department of Phytochemistry, Medicinal Plants and Drugs Research Institute, Shahid Beheshti University, G. C. Evin, Tehran, Iran
[c] Institute of Pharmacology and Toxicology, University of Vienna, Althanstrasse 14, 1090 Vienna, Austria

ARTICLE INFO

Article history:
Received 7 May 2013
Received in revised form 29 July 2013
Available online 3 September 2013

Keywords:
Curcuma kwangsiensis
Zingiberaceae
Xenopus oocyte assay
$GABA_A$ receptor modulation
HPLC-based activity profiling
Labdane diterpenoids
Electronic circular dichroism (ECD)

ABSTRACT

An ethyl acetate extract of *Curcuma kwangsiensis* S.G. Lee & C.F. Liang (Zingiberaceae) rhizomes (100 μg/ml) enhanced the GABA-induced chloride current (I_{GABA}) through $GABA_A$ receptors of the $\alpha_1\beta_2\gamma_{2S}$ subtype by 79.0 ± 7.0%. Potentiation of I_{GABA} was measured using the two-microelectrode voltage-clamp technique and *Xenopus laevis* oocytes. HPLC-based activity profiling of the crude extract led to the identification of 11 structurally related labdane diterpenoids, including four new compounds. Structure elucidation was achieved by comprehensive analysis of on-line (LC-PDA-ESI-TOF-MS) and off-line (microprobe 1D and 2D NMR) spectroscopic data. The absolute configuration of the compounds was established by comparison of experimental and calculated ECD spectra. Labdane diterpenes represent a new class of plant secondary metabolites eliciting positive $GABA_A$ receptor modulation. The highest efficiency was observed for zerumin A (maximum potentiation of I_{GABA} by 309.4 ± 35.6%, and EC_{50} of 24.9 ± 8.8 μM).

1. Introduction

Worldwide, anxiety and sleep difficulties, especially insomnia, are common and highly prevalent healthcare problems (Ringdahl et al., 2004; Uhde et al., 2009). A crucial target for anxiolytics, sedatives, hypnotics, anticonvulsants, and muscle relaxants is the gamma-aminobutyric acid type A ($GABA_A$) receptor, a ligand-gated ion channel that mediates inhibitory neurotransmission in the central nervous system (CNS). The $GABA_A$ receptor has a heteropentameric structure and can be assembled from 19 different subunits (α_{1-6}, β_{1-3}, γ_{1-3}, δ, ε, π, ρ_{1-3}, and θ). The most abundant $GABA_A$ receptor in the mammalian brain consists of two α_1, two β_2, and one γ_{2S} subunits (Olsen and Sieghart, 2008). Despite the broad range of drugs that are clinically in use to treat anxiety and sleep disorders, there is an increasing demand for herbal preparations with such properties. Herbal products have become increasingly important during the last decades, owing to positive consumer acceptance (Biesalski, 2002). In addition to synthetic drug candidates, a wide range of plant-derived natural products have been shown to modulate the function of $GABA_A$ receptors (Johnston et al., 2006). Given the continued importance of natural products in drug discovery and development (Newman and Cragg, 2012), plant-derived compounds may provide inspiration for new scaffolds of $GABA_A$ receptor modulators.

In the search for positive $GABA_A$ receptor modulators of natural origin, we screened an in-house plant extract library, comprising major officinal herbal drugs of the European and Chinese Pharmacopoeias, for the ability to potentiate GABA-induced chloride currents. Extracts were tested with an automated two-microelectrode voltage clamp assay in *Xenopus laevis* oocytes expressing recombinant $\alpha_1\beta_2\gamma_{2S}$ $GABA_A$ receptors, at a concentration of 100 μg/ml. A previously validated HPLC profiling protocol for the discovery of new $GABA_A$ receptor modulating natural products was applied to identify the active constituents (Kim et al., 2008). Using this approach, we successfully identified various plant secondary metabolites including alkaloids (Zaugg et al., 2010), lignans (Zaugg et al., 2011a), terpenes (Zaugg et al., 2011b,d), coumarins (Zaugg

Abbreviations: GABA, gamma-aminobutyric acid; I_{GABA}, GABA-induced chloride current; TCM, traditional Chinese medicine; ECD, electronic circular dichroism; TDDFT, time-dependent density function theory; CE, Cotton effect; OPLS, optimized potential for liquid simulations; CPCM, conductor-like polarizable continuum model; SCRF, self-consistent reaction field.

* Corresponding author. Tel.: +41 (0)61 267 14 25; fax: +41 (0)61 267 14 74.
E-mail address: matthias.hamburger@unibas.ch (M. Hamburger).

0031-9422/$ - see front matter © 2013 Elsevier Ltd. All rights reserved.
http://dx.doi.org/10.1016/j.phytochem.2013.08.004

et al., 2011c), sanggenons (Kim et al., 2012), and flavonoids (Yang et al., 2011) as positive $GABA_A$ receptor modulators.

In the course of our *in vitro* screening, an ethyl acetate extract from rhizomes of *Curcuma kwangsiensis* S.G. Lee & C.F. Liang (Zingiberaceae) displayed positive $GABA_A$ receptor modulation. While the activity was only moderate, the extract was selected for further investigation based on chemotaxonomic considerations and the fact that none of the typical metabolites of the genus *Curcuma* was reported to exhibit $GABA_A$ receptor modulating activity. Curcumae rhizoma (Ezhu) is the dried rhizome of *C. kwangsiensis* S.G. Lee & C.F. Liang, *C. wenyujin* Y.H. Chen & C. Ling, or *C. phaeocaulis* Val., and belongs to the best known herbs in traditional Chinese medicine (TCM). Ezhu is widely used as a digestive and analgesic agent, and also for the treatment of menstrual disorders (Chinese Pharmacopoeia Commission, 2010; Tang and Eisenbrand, 2011). The genus *Curcuma* counts approximately 100 species, among which only about one fifth have been studied extensively from a phytochemical viewpoint. Known compounds from *Curcuma* species belong to three major classes of plant secondary metabolites, including diphenylalkanoids, phenylpropanoids, and terpenoids (Nahar and Sarker, 2007). The phytochemistry of *C. kwangsiensis* is poorly studied compared to other *Curcuma* species. The rhizome is known to contain a number of structurally related diarylheptanoids (Li et al., 2011, 2010), and various mono- and sesquiterpenes which are the main components of the essential oil (Zeng et al., 2009).

We here describe the identification of $GABA_A$ receptor modulating labdane diterpenes via an HPLC-based discovery platform, along with the structure elucidation and *in vitro* pharmacological evaluation of the isolated compounds. The absolute configuration of the diterpenoids was established by comparing experimental and TDDFT simulated electronic circular dichroism (ECD) spectra.

2. Results and discussion

2.1. Isolation and structure elucidation

In a screening for new $GABA_A$ receptor modulators, an ethyl acetate extract from *C. kwangsiensis* rhizomes enhanced I_{GABA} by 79.0 ± 7.0% when tested at 100 µg/ml. To track the active principles responsible for positive $GABA_A$ receptor modulation, the extract was submitted to a process referred to as HPLC-based activity profiling. This approach combines physicochemical data recorded on-line with biological information obtained in parallel from time-based microfractionation (Potterat and Hamburger, 2006). An aliquot of the extract (5 mg) was separated by semi-preparative RP-HPLC, and collected peak-based microfractions were retested in the oocyte assay. Fig. 1 shows the active time window of the HPLC chromatogram (254 nm) and the activity of peak-based microfractions a–r. The activity was dispersed over a broad time window, suggesting that the activity of the extract was due to several related compounds. The highest activity was found in microfraction k (potentiation of I_{GABA} by 164.7 ± 47.6%), while other microfractions were less or only marginally active. By means of LC-PDA-ESI-TOF-MS analysis of the extract, in combination with off-line NMR data recorded after peak-based collection, the compound eluting at 42.5 min was readily identified as coronarin D (**6**), a labdane diterpene previously reported from *Hedychium coronarium* (Itokawa et al., 1988). Several HPLC peaks in the active time window exhibited UV and MS spectra similar to those of **6**, indicating structurally related compounds. Targeted preparative purification by a combination of flash chromatography on silica gel and semi-preparative RP-HPLC afforded a series of 11 labdane diterpenes (**1**–**11**) (Fig. 2), including four new natural products (**2**, **4**, **9**, and **11**). Structure elucidation was achieved by comprehensive analysis

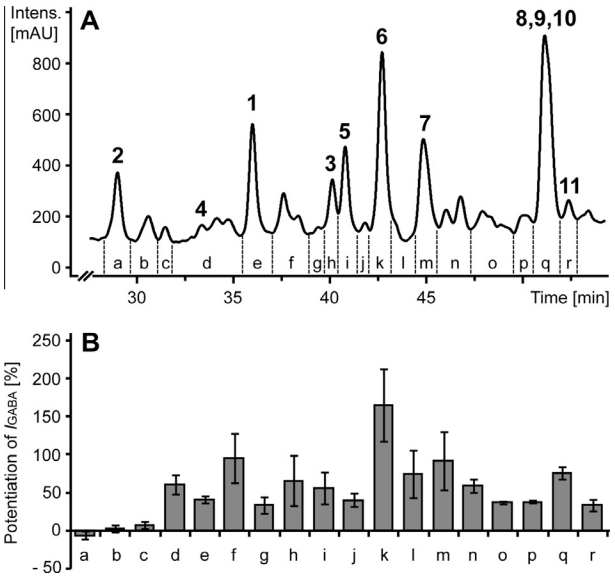

Fig. 1. Activity profiling of *C. kwangsiensis* rhizome extract for $GABA_A$ receptor modulating activity. (A) HPLC chromatogram (254 nm) of a semi-preparative separation of 5 mg extract. (B) Activity profile of collected peak-based microfractions a–r tested for I_{GABA} modulation. Peak labeling in the HPLC chromatogram refers to the isolated compounds **1**–**11**.

of on-line (LC-PDA-ESI-TOF-MS) and off-line (microprobe 1D and 2D NMR) spectroscopic data, and comparison with literature data. The relative configuration of compounds was established by NOESY and NOE difference experiments, while the absolute configuration was determined by comparison of experimental and calculated ECD spectra.

The ^1H and ^{13}C NMR data of compound **1** (Tables 1 and 2) were in agreement with the data published for curcuminol D, a diterpene isolated from *Curcuma wenyujin* (Zhang et al., 2008) and *Curcuma zedoaria* (Park et al., 2012). However, the relative configuration of curcuminol D was established only for the decalin ring system, whereas the configuration at C-15 remained undefined. We here report the unequivocal determination of the relative and absolute configuration of compound **1** based on NMR spectral assignments and ECD spectroscopy. Assignment of the relative configuration of the *trans*-decalin system was supported by NOESY correlation between H-5 and H-9, and between CH_3-20 and H-2β. Hence, H-5, H-9, and CH_3-20 were in an axial position, indicative for two possible absolute configurations of the decalin ring system (5*R*,9*R*,10*R* or 5*S*,9*S*,10*S*). In addition, 1D NOE difference experiments were performed to assign the relative configuration at C-15 (Fig. 3). Presaturation of H-15 resulted in the enhancement of H-14a, H-16a, and H-16b. Irradiation of H-14b enhanced H-14a, H-9, and H-16a, while no enhancement of H-15 was observed. A selective 1D TOCSY experiment was used to unambiguously determine the multiplicities of H-14a, H-14b, H-16a, and H-16b (Table 1). Excitation of H-15 unraveled H-14b as a doublet of doublet with coupling constants J = 13.7, and 12.6 Hz, indicative for the *trans*-orientation of both protons. Consequently, the hydroxyl group at C-15 had to be in α-orientation. This was further corroborated by the vicinal coupling constants between H-14a/H-15 ($^3J_{H-H}$ = 4.1 Hz), H-16a/H-15 ($^3J_{H-H}$ = <4.0 Hz), and H-16b/H-15 ($^3J_{H-H}$ = 3.1 Hz) which corresponded to dihedral angles of approx. 50°, 50–60°, and 60°, respectively.

In order to establish the absolute configuration of **1**, ECD spectra were calculated for two stereoisomers (5*S*,9*S*,10*S*,15*S* and 5*S*,9*S*,10*S*,15*R*). Conformational analysis using OPLS 2005 molecular mechanic force field in H_2O revealed nine and eight conformers,

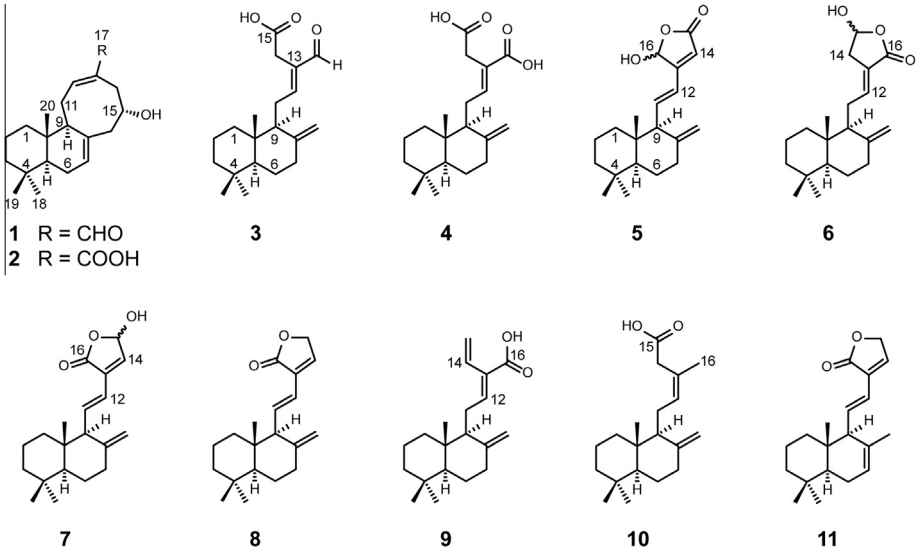

Fig. 2. Structures of compounds **1**–**11**.

Table 1
^{1}H NMR spectroscopic data for compounds **1**, **2**, **4**, and **4a** (500 MHz, δ in ppm, J in Hz).

Position	**1** ($CDCl_3$)	**2** ($CDCl_3$)	**2** (C_6D_6)	**4** ($CDCl_3$)	**4a** (C_6D_6)
1α	0.95, ddd (13.3, 13.3, 3.5)	0.99, ddd (12.9, 12.9, 3.5)	0.73, ddd (12.9, 12.9, 3.0)	1.06, ddd (12.8, 12.8, 3.1)	0.85[a]
1β	1.84, br d (13.6)	1.88, br d (12.6)	1.58, br d (12.6)	1.67[a]	1.51[a]
2α	1.47, m	1.50, m	1.37[a]	1.50, m	1.36[a]
2β	1.54, m	1.56, m	1.45, m	1.55, m	1.46[a]
3α	1.14, ddd (13.3, 13.3, 2.4)	1.18, ddd (13.2, 13.2, 3.1)	1.09, ddd (13.4, 13.4, 3.3)	1.18, ddd (13.2, 13.2, 3.5)	1.08, ddd (13.3, 13.3, 3.7)
3β	1.40, br d (13.3)	1.44, br d (13.2)	1.36[a]	1.39, br d (13.2)	1.31[a]
4					
5	1.29, dd (12.0, 4.1)	1.30, dd (12.1, 4.3)	1.15, dd (12.0, 4.4)	1.11, dd (12.5, 2.1)	0.91, dd (12.6, 2.8)
6α	2.12[a]	2.12[a]	1.94, br d (17.7)	1.72[a]	1.55[a]
6β	1.91, br d (13.9)	1.93, br d (13.6)	1.75, dd (17.7, 12.0)	1.32, dddd (12.9, 12.9, 12.9, 4.1)	1.20, dddd (12.6, 12.6, 12.6, 4.3)
7α	5.62, br s	5.65, br s	5.56, br s	2.01, ddd (12.7, 12.7, 4.5)	1.86, ddd (12.9, 12.9, 5.1)
7β				2.38[a]	2.27[a]
8					
9	2.51, br d (12.5)	2.47[a]	2.28[a]	1.87, br d (10.4)	1.69, br d (10.7)
10					
11a	2.76, dd (19.7, 4.9)	2.64, dd (18.7, 6.2)	2.28[a]	2.40[a]	2.28[a]
11b	2.26[a]	2.16[a]	1.84, m	2.24, m	2.16[a]
12	6.76, br s	7.27, dd (6.2, 6.2)	7.31, dd (6.1, 6.1)	7.03, dd (6.4, 6.4)	7.10, dd (6.2, 6.2)
13					
14a	3.06, dd (12.6, 4.1)	3.00, dd (13.6, 4.9)	3.20, dd (13.8, 4.4)	3.36, m	3.43, m
14b	2.22, dd (12.6, 13.7)[b]	2.47[a]	2.49, dd (14.1, 13.1)		
15	3.68, m	3.85, m	3.91, m		
16a	2.36, br d (14.2)	2.49[a]	2.39, br d (13.9)		
16b	2.06, dd (14.2, 3.1)[b]	2.09[a]	2.05, dd (13.9, 4.7)		
17a	9.29, s			4.82, br s	4.86, d (1.0)
17b				4.38, br s	4.53, d (1.0)
18	0.85, s	0.89, s	0.83[a]	0.87, s	0.81, s
19	0.87, s	0.91, s	0.83[a]	0.81, s	0.75, s
20	0.75, s	0.79, s	0.66, s	0.71, s	0.65, s
15-OCH3					3.37, s
16-OCH3					3.39, s

[a] Multiplicities of overlapped signals are omitted.
[b] Signals were resolved by 1D selective TOCSY experiment.

respectively, within a 2 kcal/mol energy window from the particular global minimum. These conformers were subjected to geometrical optimization and energy calculation using density function theory (DFT) with B3LYP using the 6-31G** basis set in the gas phase. Vibrational frequency calculations were carried out to confirm these minima. No imaginary frequencies were found. Conformational analysis using relative free energies indicated the presence of five and four stable conformers for 5*S*,9*S*,10*S*,15*S* and 5*S*,9*S*,10*S*,15*R* stereoisomers, respectively. The four low-energy structures of the 5*S*,9*S*,10*S*,15*R* stereoisomer are represented in Fig. S34 of the Supplementary data. The experimental ECD spectrum of **1** showed three negative cotton effects (CEs) at around 320, 240, and 210 nm (Fig. 5). The calculated ECD spectrum of the 5*S*,9*S*,10*S*,15*R* stereoisomer showed good agreement with the overall pattern of the experimental ECD spectrum. The negative CE around 320 nm was due to the n→π* transition of the α,β-unsaturated aldehyde, and the CE around 240 nm to a π→π* transition. The difference between calculated and experimental spectra

Table 2
^{13}C NMR spectroscopic data for compounds **1**, **2**, **4**, and **4a** (125 MHz, δ in ppm).

Position	**1**[a] ($CDCl_3$)	**2** ($CDCl_3$)	**2**[a] (C_6D_6)	**4** ($CDCl_3$)	**4a**[a] (C_6D_6)
1	39.5	39.7	39.4	39.4	38.9
2	18.8	19.1	18.9	19.5	19.3
3	42.0	42.2	42.1	42.2	42.1
4	33.0	32.7	32.8	33.8	33.4
5	50.0	50.4	50.3	55.5	55.1
6	24.2	24.4	24.1	24.3	24.1
7	128.4	128.9	128.1	38.0	37.9
8	131.9	132.9	133.0	148.2	147.4
9	51.5	51.2	nd	56.5	56.3
10	36.5	36.7	36.3	39.7	39.4
11	30.7	30.6	29.5	24.6	24.1
12	157.6	147.6	146.6	150.5	146.5
13	138.9	127.2	127.5	124.3	125.3
14	29.6	32.6	33.0	32.6	32.5
15	69.7	70.4	70.8	177.6	170.6
16	41.1	41.0	42.1	172.7	166.9
17	194.6	173.7	173.1	108.2	107.8
18	33.2	33.3	33.2	33.8	33.4
19	21.7	22.0	21.9	22.0	21.8
20	13.1	13.2	13.6	14.6	14.2
15-OCH_3					51.1
16-OCH_3					51.1

nd: not detected.
[a] ^{13}C shifts deduced from HSQC and HMBC experiments.

may have resulted from an overestimation of the UV absorbance in the calculations, or from minor differences between calculated and solution conformers (Zaugg et al., 2011a). The calculated ECD spectrum of the 5*S*,9*S*,10*S*,15*S* stereoisomer (Fig. 5) was clearly different from the experimental data, with two positive CEs at around 300 and 250 nm, and one negative CE at around 230 nm. Thus, we conclude that the absolute configuration of compound **1** is 5*S*,9*S*,10*S*,15*R*.

The molecular formula of compound **2** was established as $C_{20}H_{30}O_3$ from the pseudomolecular ion peak at *m*/*z* 341.2080 $[M+Na]^+$ in the HR-ESI-TOF-MS spectrum. The UV spectrum showed an absorption maximum at 217 nm and was similar to that of **1** (λ_{max} 219 nm). Analysis of the ^{1}H NMR data (Table 1) showed strong similarities with **1**, except for the downfield shift of H-12 (δ_H 7.27, *dd*, *J* = 6.2, 6.2 Hz in **2**; δ_H 6.76, br *s* in **1**) and the absence of an aldehyde proton (δ_H 9.29, *s*, H-17 in **1**). The COSY and HMBC correlations were in agreement with those observed for **1** and confirmed the presence of an uncommon 6/6/8 carbon ring skeleton. Remarkable differences in the ^{13}C NMR shifts (Table 2) were observed for C-12 (δ_C 147.6 in **2**; δ_C 157.6 in **1**), C-13 (δ_C 127.2 in **2**; δ_C 138.9 in **1**), and C-17 (δ_C 173.7 in **2**; δ_C 194.6 in **1**). The carbon signal at δ_C 173.7 was assigned to a carboxylic group which caused a shielding of C-12 and C-13. Thus, the planar structure of **2** differed from **1** in the oxidation state of C-17. The relative configuration of **2** was established with the aid of ^3J NMR coupling constants

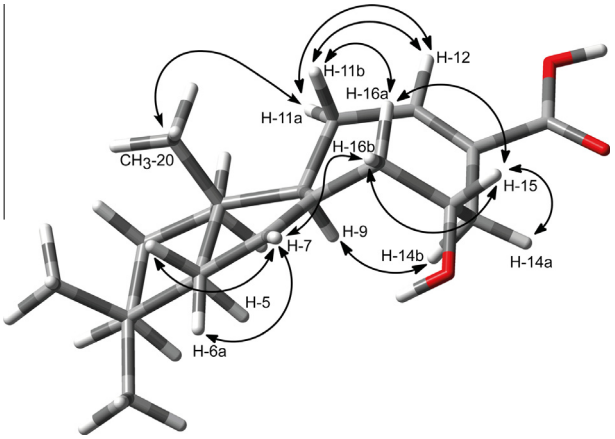

Fig. 4. Geometrically optimized 3D structure of the most stable conformer of 5*S*,9*S*,10*S*,15*R*-(−)-curcuminol H (**2**). Key NOESY correlations for corroborating the configuration at C-15 are indicated with arrows.

in the ^{1}H NMR spectrum, and by NOESY correlations. Measurements were performed in the anisotropic solvent benzene-d_6 to resolve overlapping signals appearing in $CDCl_3$ (Table 1). The observed vicinal coupling constants and estimated dihedral angles were comparable with those observed for compound **1**. Fig. 4 shows the 3D optimized structure of the most stable conformer of the 5*S*,9*S*,10*S*,15*R* stereoisomer and key NOESY correlations. H-15 showed NOESY cross-peaks with H-16a, H-16b, and H-14a, but not with H-14b. Hence, the hydroxyl group at C-15 was also in α-position, and the relative configuration of **2** is identical with that of **1**.

The absolute configuration of **2** was investigated by comparison of experimental and calculated ECD spectra. Conformational analysis, geometry optimization, and calculation of ECD spectra of the conformers were performed as described above. Conformational analysis of the 5*S*,9*S*,10*S*,15*S* and 5*S*,9*S*,10*S*,15*R* stereoisomers revealed 15 and 17 conformers, respectively, within a 2 kcal/mol energy window from the particular global minimum. Conformational analysis using relative free energies indicated the presence of six and eight stable conformers, respectively. The eight low-energy structures of the 5*S*,9*S*,10*S*,15*R* stereoisomer are represented in Fig. S36 of the Supplementary data. The conformers exhibited differences with respect to the orientation of the carboxylic acid moiety and the hydroxyl group. For the 5*S*,9*S*,10*S*,15*R* stereoisomer, the ECD spectrum showed two negative CEs around 240 and 210 nm (Fig. 5). The negative CE at around 240 nm was likely due to a $\pi \rightarrow \pi^*$ transition of the α,β-unsaturated acid chromophore. There was excellent agreement of the overall patterns of the calculated and experimental ECD spectra. In contrast, the ECD spectrum calculated for the 5*S*,9*S*,10*S*,15*S* stereoisomer significantly differed

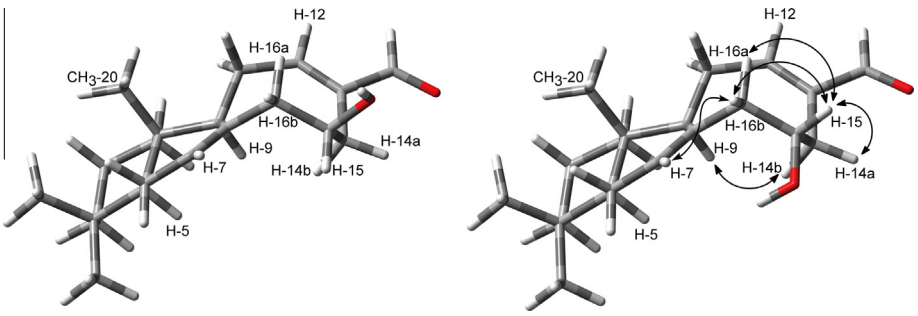

Fig. 3. The most predominant conformers of two possible stereoisomers, 5*S*,9*S*,10*S*,15*S* (left) and 5*S*,9*S*,10*S*,15*R* (right), of (−)-curcuminol D (**1**). The structural information derived from vicinal coupling constants and key NOE correlations (indicated with arrows) were in accord only with the 5*S*,9*S*,10*S*,15*R* stereoisomer.

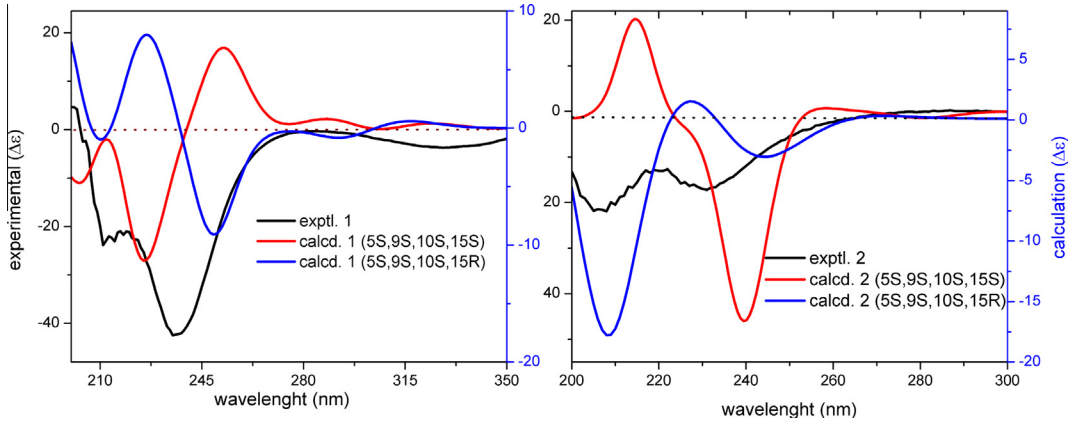

Fig. 5. Comparison of experimental and calculated ECD spectra of **1** (left) and **2** (right). The calculations were performed with TDDFT at the B3LYP/6–31G** level with MeCN as solvent.

from the experimental data, with one negative and one positive CE at around 240 and 215 nm, respectively. The 5*S*,9*S*,10*S*,15*R* configuration of **2** is further supported by the obvious biogenetic relationship between **1** and **2**. We propose to name the new compound **2** as (−)-curcuminol H.

For compound **3**, a molecular formula of $C_{20}H_{30}O_3$ was calculated from its HR-ESI-TOF-MS spectrum. On the basis of spectroscopic data, including 1D and 2D NMR data, optical rotation, and UV absorption maximum, compound **3** was identified as zerumin A. This diterpenoid has been reported from the seeds of *Alpinia zerumbet* (Xu et al., 1996). The relative configuration of **3** was confirmed by NOESY data.

Compound **4** has a molecular formula of $C_{20}H_{30}O_4$, as calculated from the pseudomolecular ion peak at *m*/*z* 357.2048 $[M+Na]^+$ in the HR-ESI-TOF-MS spectrum. Comparison of ^1H and ^{13}C NMR spectra of **4** (Tables 1 and 2) with those of **3** (Table S1 of the Supplementary data) revealed that both compounds were closely related. Differences were observed for the signals of the side chains of **3** and **4**. The olefinic proton at C-12 in **4** (δ_H 7.03, *dd*, *J* = 6.4, 6.4 Hz) was shifted downfield compared to **3** (δ_H 6.60, *dd*, *J* = 6.0, 6.0 Hz), while the signal of the aldehyde proton (δ_H 9.29, *s*, H-16) in **3** was absent in the ^1H NMR spectrum of **4**. The ^{13}C signal assigned to C-16 (δ_C 194.1 in **3**; δ_C 172.7 in **4**) indicated the presence of a second carboxylic group in **4**. Thus, compound **4** was the diacid congener of zerumin A (**3**). While for compound **3** the *E*-geometry of the double bond of the side chain was verified by HMBC and NOESY correlations, no unambiguous assignment was possible for **4** on the basis of both NOESY and NOE difference experiments. The labdadienedioic acid **4** was previously semi-synthetically obtained as a 3:2 mixture of *E*/*Z* isomers, but unfortunately no attempts were made to assign the NMR resonances of the two isomers (González et al., 2010). The geometry of the double bond was established with the aid of the dimethyl ester derivative **4a** (Tables 1 and 2, and Fig. 6). The HMBC spectrum confirmed that the methoxy groups at δ_H 3.37 and δ_H 3.39 were located at C-15 and C-16, respectively. The NOESY spectrum showed a diagnostic cross-peak between H-12/16-OCH_3, and indicated a spatial proximity of H-14, H-11a, and H-11b. Hence, the *E*-configuration of the double bond between C-12/C-13 was established, which is in accord with the configuration of the related aldehyde **3**.

The ECD spectrum of **4** (Fig. 7B) showed a positive CE around 218 nm and two negative CEs at around 200 and 250 nm. The positive CE at 218 nm was probably due to a $\pi\rightarrow\pi^*$ transition of the α,β-unsaturated acid moiety, whereas the negative CE at 200 nm was attributed to a $\pi\rightarrow\pi^*$ transition of the olefinic group. A molecular model of **4** was built based on the relative configuration represented in Fig. 7A, and the 3D structure subjected to

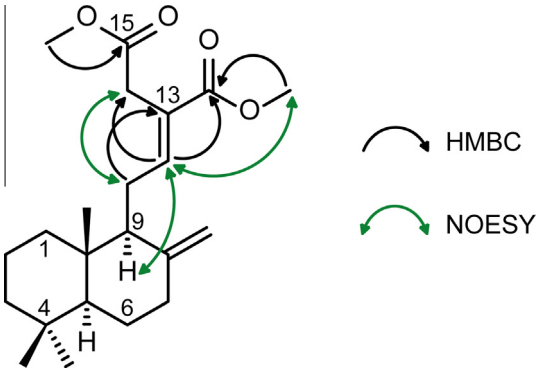

Fig. 6. Structure of dimethyl-(*E*)-labda-8(17),12-diene-15,16-dioate (**4a**) with key HMBC and NOESY correlations.

conformational analysis and geometry optimization as described above. For the 5*S*,9*S*,10*S* stereoisomer, the DFT energy minimized at B3LYP/6-31G** level of theory yielded 26 relevant conformers within a 2 kcal/mol range from the global minimum. The conformers could be divided into three core conformers which differed in the orientation of the side chain. Minor differences of superimposed conformers resulted from free rotation of the C-15 carboxylic group (Fig. 7A). The calculated ECD spectrum exhibited two positive CEs at around 210 and 240 nm, along with a negative CE at around 200 nm, and was in excellent agreement with the experimental ECD spectrum (Fig. 7B). The differences between calculated and experimental spectra were likely due to minor conformational differences in solution. Thus, we conclude that the absolute configuration of compound **4** is 5*S*,9*S*,10*S*. Compounds **4** and **3** differ only in the degree of oxidation at C-16. The experimental ECD spectra for both compounds were similar (Fig. 7B). The slight blue shift of the ECD spectrum of **4** could be explained with the chromophore group at C-16, changing from an α,β-unsaturated aldehyde in **3** to an α,β-unsaturated carboxylic acid in **4**. The similarity of the ECD spectra led to the conclusion that the absolute configuration of **3** is also 5*S*,9*S*,10*S*.

The known labdane diterpenes **5**–**7** were identified from their HR-ESI-TOF-MS, 1D and 2D NMR data as (*E*)-16-hydroxylabda-8(17),11,13-trien-15,16-olide (Margaros and Vassilikogiannakis, 2007; Mohamad et al., 2005), coronarin D (Itokawa et al., 1988), and (*E*)-15-hydroxylabda-8(17),11,13-trien-16,15-olide (Margaros and Vassilikogiannakis, 2007; Sy and Brown, 1997), respectively. These compounds contain a cyclic hemiacetal moiety which is

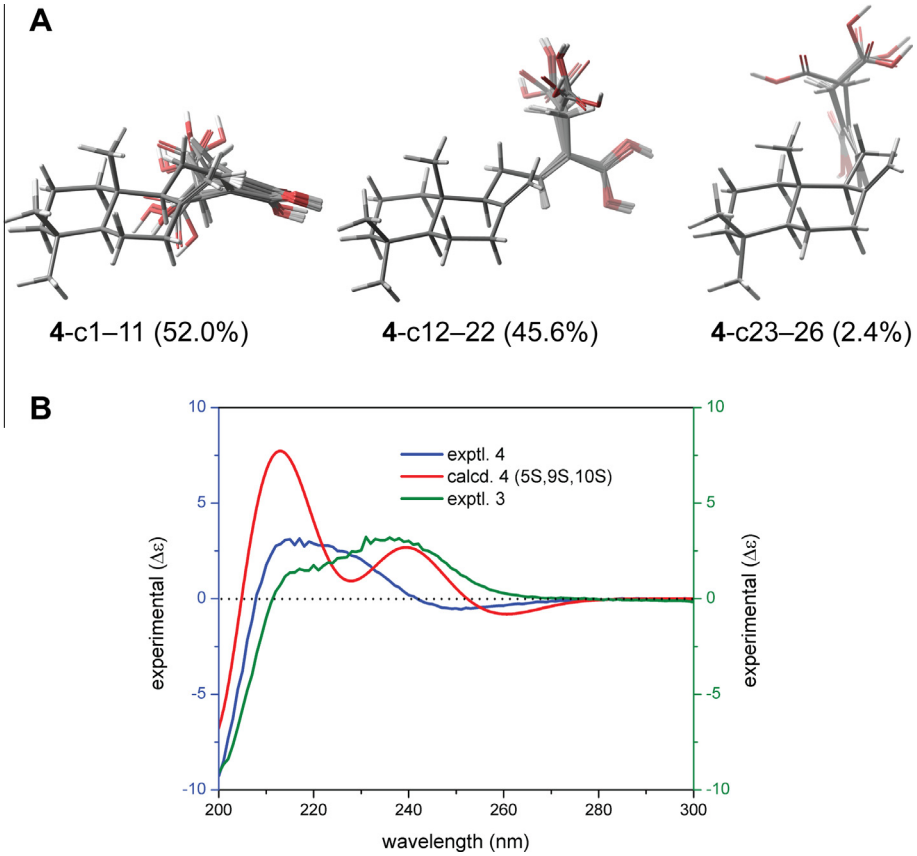

Fig. 7. (A) Superimposed lowest energy conformers (within a 2 kcal/mol range from the global minimum) of **4.** Compound **4** showed three core conformers which differed in the orientation of the side chain, whereby c1–26 refers to the 26 conformers. (B) Comparison of experimental spectra of compounds **3** and **4**, with the calculated ECD spectrum of **4**. The calculation was performed with TDDFT at the B3LYP/6–31G** level with MeCN as solvent. Comparison of **3** and **4** was justified by the close structural relationship of the compounds.

prone to epimerization. Therefore, we did not analyze the configuration of these compounds further.

Compound **8** was identified as (*E*)-labda-8(17),11,13-trien-16,15-olide from its UV, optical rotation, HR-ESI-TOF-MS, and NMR spectroscopic data, which were in good agreement with those reported in the literature (Nakatani et al., 1994). Analysis of vicinal coupling constants and NOESY experiments confirmed the relative configuration as established. Since CD data and absolute configuration have not been reported so far, we submitted compound **8** to ECD analysis. The experimental ECD spectrum of compound **8** showed a negative CE around 205 nm and a positive CE at 219 nm (Fig. 8B). The positive CE at 219 nm was due to a $\pi\rightarrow\pi^*$ transition of the diene group. Conformational analysis of the 3D model of the 5*S*,9*S*,10*S* stereoisomer and energy minimization revealed two stable conformers (Fig. 8A) which differed in the orientation of the lactone ring. The simulated ECD spectrum showed a negative CE around 205 nm along with a positive CE around 220 nm. The excellent agreement between simulated and experimental ECD spectra established the absolute configuration of compound **8** as 5*S*,9*S*,10*S*.

The HR-ESI-TOF-MS data of compound **9** revealed a molecular formula of $C_{20}H_{30}O_2$ (found *m*/*z* 325.2155 $[M+Na]^+$), implying six degrees of unsaturation. The HSQC and HMBC spectra confirmed the presence of five quaternary carbons, four methine, eight methylene, and three methyl groups. The signal patterns and shift values of the carbon and proton signals (Table 3) were similar to those of **4**. The ^{1}H NMR spectrum showed three characteristic downfield-shifted protons, namely an olefinic proton at δ_H 6.48 (*dd*, *J* = 17.7, 11.7 Hz, H-14) and two olefinic methylene protons at δ_H 5.63 (*dd*, *J* = 17.7, 1.3 Hz, H-15a) and δ_H 5.41 (br *d*, *J* = 11.7 Hz, H-15b), indicating the presence of a terminal double bond. The most deshielded carbon signal at δ_C 172.6 (C-16) was attributed to a carboxlic acid. The observed long-range HMBC correlations between C-16 and the olefinic protons H-12 (^3J) and H-14 (^3J) revealed that, when compared to **4**, the additional double bond was located at C-14/C-15. Diagnostic NOESY contacts between H-9 and H-12, as well as between H-14 and both H-11a and H-11b, indicated an *E*-configured double bond between C-12/C-13. Thus, the structure of the new labdane diterpenoid **9** was established as (*E*)-labda-8(17),12,14-trien-16-oic acid. Since **9** could only be purified up to 90% (^{1}H NMR), optical rotation and CD data were not determined. On-line LC-PDA-ESI-TOF-MS analysis revealed the presence of a co-eluting impurity with a pseudomolecular ion peak at *m*/*z* 327.2305 $[M+Na]^+$, corresponding to the molecular formula $C_{20}H_{32}O_2$. Compound **10** co-eluted with **9** and could only be obtained as a mixture of **9** and **10** in a ratio of 64:36 (^{1}H NMR). The ^{13}C NMR spectrum of this mixture showed virtually duplicated carbon signals which could be readily assigned to both compounds according to their distinct signal intensities. By comprehensive analysis of HR-ESI-TOF-MS and 1D and 2D NMR data, and comparison with published data, compound **10** was identified as calcaratarin B (Kong et al., 2000).

For compound **11**, the HR-ESI-TOF-MS data revealed a molecular formula of $C_{20}H_{28}O_2$ (found *m*/*z* 323.1979 $[M+Na]^+$), accounting for seven degrees of unsaturation. Both the ^{1}H NMR data and observed COSY correlations indicated that the structure of **11** was closely related to that of **8**. Notable differences were in the presence of a methyl group (δ_H 1.49, δ_C 22.4, C-17) and an olefinic

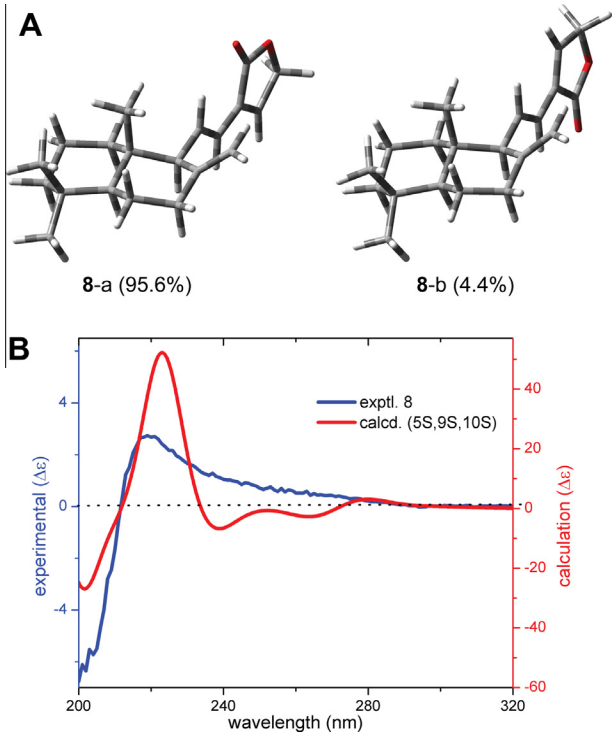

Fig. 8. (A) Low-energy conformers (within a 2 kcal/mol range from the global minimum) of **8**. Compound **8** showed two stable conformers. The predominance of conformer **8**-a (95.6%) was corroborated by a NOESY correlation between H-12 and H-14 (data not shown). (B) Comparison of experimental and calculated ECD spectra of **8**. The calculation was performed with TDDFT at the B3LYP/6–31G** level with MeCN as solvent.

methine (δ_H 5.49, δ_C 122.3, H-7), indicating that the exocyclic double bond in **8** was replaced in **11** by a methyl group, and the double bond shifted to C-7/C-8. These findings were confirmed by key COSY and HMBC correlations (Fig. 9). The relative configuration was assigned on the basis of NOESY correlations. H-9 showed cross-peaks with H-1α, H-5, and H-12. The structural similarity to **8** was further supported by the NOESY correlation between H-12 and H-14. Thus, the structure of the new labdane diterpenoid **11** was established as (*E*)-labda-7,11,13-trien-16,15-olide. Since the compound could only be purified up to 80% (^{1}H NMR), optical rotation and CD data were not determined.

2.2. $GABA_A$ receptor modulation

Modulation of GABA-induced chloride currents (I_{GABA}) were studied in an automated two-microelectrode voltage-clamp assay with transfected *Xenopus leavis* oocytes expressing recombinant $\alpha_1\beta_2\gamma_{2S}$ $GABA_A$ receptors. Potentiation of I_{GABA} by diterpenes **1**–**11** was initially assessed at 100 μM (Table 4). Zerumin A (**3**) displayed the highest efficiency (324.2 ± 46.2%, $n = 6$), whereas replacement of the aldehyde group at C-16 by a carboxylic moiety, as in **4**, resulted in a total loss of activity. The eight-membered ring, as in **1** and **2**, appears unfavorable for I_{GABA} potentiation, since both compounds showed comparatively low efficiencies. Despite the close structural relationship of **1**–**11**, further structure–activity considerations regarding I_{GABA} modulation remain rather speculative at present.

Concentration–response experiments were performed for zerumin A (**3**) and the major labdane diterpene, coronarin D (**6**). Both compounds enhanced GABA-induced chloride currents in a concentration-dependent manner (Fig. 10A–D). In the absence of GABA, application of saturating concentrations of **3** and **6** (100 μM) induced only small chloride currents (Fig. 11). The weak direct agonistic activity on $\alpha_1\beta_2\gamma_{2S}$ $GABA_A$ receptors hence

Table 3
^{1}H and ^{13}C NMR spectroscopic data for compounds **9** and **11** ($CDCl_3$, 500 MHz for δ_H, 125 MHz for δ_C, δ in ppm).

Position	**9**			**11**	
	δ_H (*J* in Hz)	δ_C[a]	δ_C	δ_H (*J* in Hz)	δ_C[a]
1α	1.08, ddd (13.0, 13.0, 2.8)	39.3	39.5	0.98, ddd (13.1, 13.1, 3.6)	40.4
1β	1.71[b]			1.57, br d (13.1)	
2α	1.51, m	19.3	19.5	1.38[b]	18.7
2β	1.58, m			1.49[b]	
3α	1.19, ddd (13.3, 13.3, 3.7)	42.0	42.3	1.16[b]	42.3
3β	1.41, br d (13.2)			1.40[b]	
4		33.5	33.8		33.1
5	1.13, dd (12.6, 2.5)	55.4	55.5	1.19, dd (12.1, 4.6)	49.7
6α	1.72[b]	24.1	24.3	2.00, m	23.7
6β	1.33, dddd (12.9, 12.9, 12.9, 4.2)			1.90, m	
7α	2.01, ddd (12.9, 12.9, 4.6)	37.9	38.1	5.49, br s	122.3
7β	2.38[b]				
8		148.2	148.4		132.5
9	1.87, br d (10.4)	56.8	57.0	2.42, d (10.5)	60.8
10		38.3	39.7		36.4
11a	2.52, m	24.6	24.8	6.62, dd (15.8, 10.7)	138.5
11b	2.39[b]				
12	6.86, dd (6.7, 6.7)	148.1	148.9	6.10, d (15.8)	120.9
13		128.6	128.8		129.5
14	6.48, dd (17.7, 11.7)	128.8	129.1	7.13, dd (2.0, 2.0)	141.9
15a	5.63, dd (17.7, 1.3)	119.8	120.3	4.77, br s	69.4
15b	5.41, br d (11.7)				
16		172.4	172.6		172.2
17a	4.81, s	107.6	108.1	1.49[b]	22.4
17b	4.35, s				
18	0.88, s	33.5	33.8	0.85, s	33.2
19	0.81, s	21.8	22.0	0.88, s	21.8
20	0.73, s	14.4	14.7	0.86, s	14.9

[a] ^{13}C shifts deduced from HSQC and HMBC experiments.
[b] Multiplicities of overlapped signals are omitted.

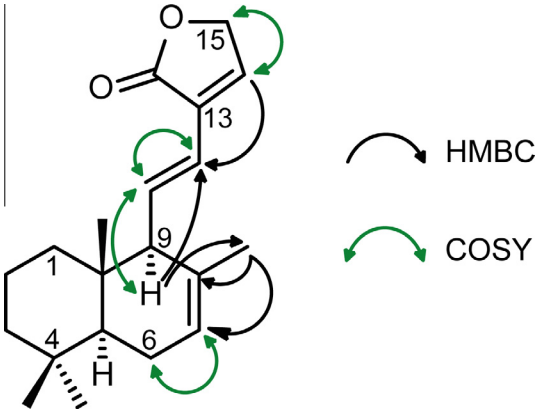

Fig. 9. Key COSY and HMBC correlations observed for (*E*)-labda-7,11,13-trien-16,15-olide (**11**).

Table 4
Mean potentiation of I_{GABA} through $\alpha_1\beta_2\gamma_{2S}$ $GABA_A$ receptors (GABA EC_{3-10}) by compounds **1–11** (100 μM).

Compound	Potentiation of I_{GABA} (%)	n[a]
1	54.7 ± 7.8	4
2	2.5 ± 4.8	5
3	324.2 ± 46.2	6
4	12.1 ± 5.9	5
5	209.5 ± 10.4	4
6	199.7 ± 42.0	5
7	116.7 ± 23.0	4
8	53.6 ± 11.7	4
9/10[b]	68.6 ± 14.6	3
11	81.2 ± 17.2	3
Diazepam (10 μM)[c]	191.9 ± 9.5	10

[a] *n*: number of experiments.
[b] Inseparable mixture of **9** and **10**.
[c] Positive control.

suggested positive allosteric receptor modulation as the underlying mechanism of action. The observed EC_{50} values of 24.9 ± 8.8 μM for **3** and 35.7 ± 8.8 μM for **6** (Table 5) are of comparable potencies to known plant-derived modulators, such as piperine (EC_{50} = 52.4 ± 9.4 μM), zuihonin A (EC_{50} = 21.8 ± 7.5 - μM), sandaracopimaric acid (EC_{50} = 33.3 ± 8.7 μM) (Zaugg et al., 2010, 2011a, 2011d), or honokiol (EC_{50} = 36.2 ± 14.7 μM) (Taferner et al., 2011). However, their efficiencies (309.4 ± 35.6% for **3** and 211.0 ± 26.0% for **6**) were not significantly higher than those of the clinically used benzodiazepines midazolam and triazolam (maximum potentiation of the GABA-induced chloride current of 342 ± 64% and 253 ± 12%, respectively) (Khom et al., 2006).

To the best of our knowledge, oral biovailability and CNS penetration of labdane diterpenes have not been studied up to now. Given the high lipophilicity of these compounds (clogP values of compounds are given in Table S2 of the Supplementary data), absorption in the small intestine and passage through the blood–brain barrier appears possible (Lipinski et al., 1997; Pajouhesh and Lenz, 2005). Another important attribute is the number of H-bond acceptors in the compounds, and the ratio of H-bond acceptors/donors. These physicochemical features are not only relevant for tissue permeability and, thus, bioavailability of a compound (Lipinski et al., 1997), but also for the binding mode of a molecule to its site of action. Similar to **3**, compounds **5**, **6**, and **7** potentiated I_{GABA} by more than 100%, all containing H-bond acceptors/donors in the ratio 3:1. Further investigations are needed to substantiate the therapeutic potential of labdane diterpenes as

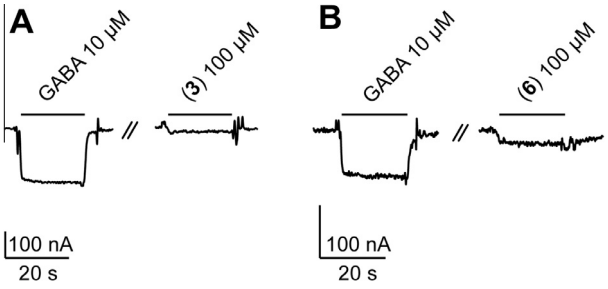

Fig. 11. Representative currents illustrating weak direct activation of $\alpha_1\beta_2\gamma_{2S}$ $GABA_A$ receptors by (A) zerumin A (**3**) and (B) coronarin D (**6**). The current amplitudes induced by a saturating concentration (100 μM) of **3** and **6** did not exceed the current amplitudes elicited by GABA control samples (EC_{3-10}).

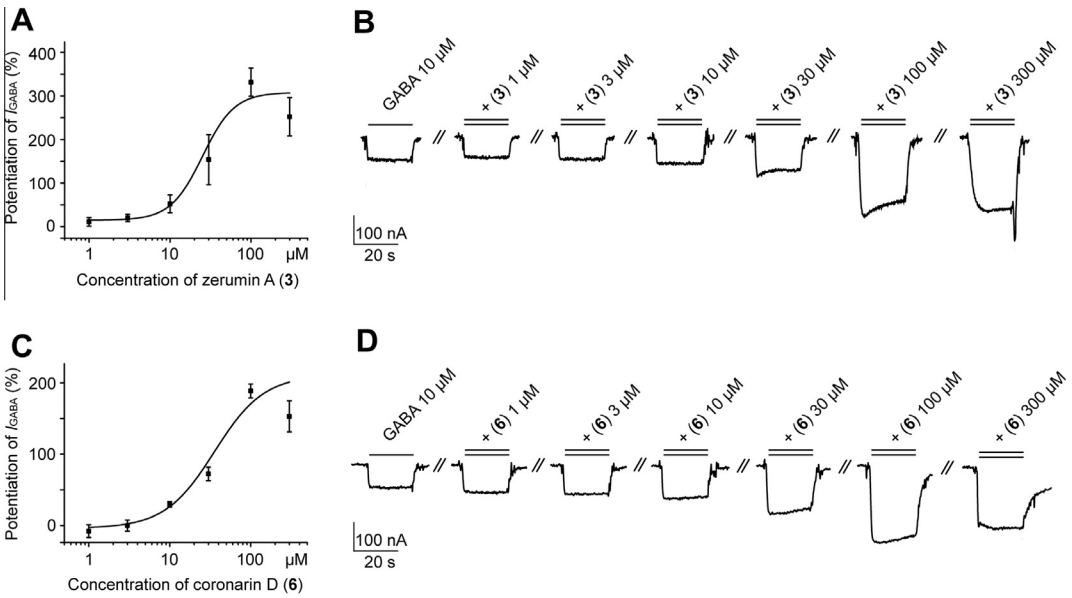

Fig. 10. Concentration–response curves for I_{GABA} enhancement by (A) zerumin A (**3**) and (C) coronarin D (**6**). Representative currents through $\alpha_1\beta_2\gamma_{2S}$ $GABA_A$ receptors in the presence of GABA (EC_{3-10}, single bar, control), and during co-application (double bar) of GABA (EC_{3-10}) and different concentrations of compounds **3** (B) and **6** (D) are shown.

Table 5
Summary of potencies (EC_{50}) and efficiencies (maximum potentiation of I_{GABA}) of compounds **3** and **6**.

Compound	EC_{50} (μM)	Max. Potentiation of I_{GABA} (%)	Hill coefficient (n_H)	n[a]
3	24.9 ± 8.8	309.4 ± 35.6	2.2 ± 1.0	4
6	35.7 ± 8.8	211.0 ± 26.0	1.4 ± 0.3	5

[a] *n*: number of experiments.

positive modulators of $GABA_A$ receptors in the central nervous system. Several constituents from the genus *Curcuma* have been reported to possess pharmacological properties with a possible link to the GABAergic system. Curcumin showed *in vivo* effects against seizures and cognitive impairment (Mehla et al., 2010), as well as anxiolytic-like activity (Chimakurthy and Talasila, 2010). Very recently, the anticonvulsant-like effect of bisabolene sesquiterpenoids from *Curcuma longa* rhizome was demonstrated in zebrafish and mouse models (Orellana-Paucar et al., 2012).

It is noteworthy that the Chinese Pharmacopoeia does not list any potentially GABA-related indication for Curcumae rhizome (Ezhu). However, the closely related herbal drug Curcumae radix (Yujin; dried root tuber of *C. kwangsiensis* S.G. Lee & C.F. Liang, *C. wenyujin* Y.H. Chen & C. Ling, *C. phaeocaulis* Val., or *C. longa* L.) is used, among others, as an anti-epileptic and sedative agent (Chinese Pharmacopoeia Commission, 2010; Tang and Eisenbrand, 2011).

3. Conclusions

With the aid of an HPLC-based activity profiling approach, labdane diterpenoids were identified as a new class of plant secondary metabolites eliciting positive $GABA_A$ receptor modulation. From a phytochemical point of view, this is the first report of diterpenoids **1**–**11** in the TCM herb *C. kwangsiensis*. A total of four labdane diterpenoids were thereby isolated for the first time. Further pharmacological studies are needed, at least for the most active diterpene zerumin A (**3**), to assess its $GABA_A$ receptor subtype-selectivity, binding properties, and possible *in vivo* effects.

4. Experimental

4.1. General experimental procedures

Solvents used for extraction and flash column chromatography were of analytical grade. HPLC-grade solvents (Scharlau, Barcelona, Spain) were used for HPLC separations. HPLC-grade water was obtained by an EASY-pure II water purification system. Formic acid (98.0–100.0%), dimethylsulfoxide (DMSO), and glacial acetic acid were purchased from Sigma–Aldrich. Flash chromatography was performed on a Sepacore® chromatography system (Büchi Labortechnik, Flawil, Switzerland) consisting of two C 605 pump modules, a C 620 control unit, and a C 660 fraction collector. Prepacked silica gel 60 cartridges (40 × 150 mm, 40–63 μm, Büchi) were used for all separations. Liquid injection was performed by means of a 6-way valve with a 20 ml loop. The flow rate was 15 ml/min, and 1 min fractions were collected, unless otherwise stated. Analytical TLC analysis was carried out with silica gel 60 F_{254} pre-coated Al sheets (Merck, Darmstadt, Germany). Detection was at 254 nm, and after spraying with vanillin-sulphuric acid reagent and heating for 5–10 min at 110 °C. Analytical and semi-preparative HPLC separations were carried out on SunFire C_{18} columns (3 × 150 mm, 3.5 μm and 10 × 150 mm, 5 μm, respectively) using H_2O + 0.1% formic acid (solvent A) and MeCN + 0.1% formic acid (solvent B) as mobile phase. HR-ESI-TOF-MS data were recorded on a micrOTOF ESI-MS spectrometer (Bruker Daltonics) coupled via a 1:10 splitter to an Agilent 1100 system consisting of an autosampler, degasser, binary pump, column oven, and PDA detector. Separation was achieved with a gradient of 55% to 80% B in 35 min at a flow rate of 0.5 ml/min. A solution of formic acid 0.1% in 2-propanol/water (1:1) containing 5 mM NaOH was used for mass calibration. Semi-preparative HPLC was performed on an Agilent 1100 system consisting of an autosampler, quaternary pump with degasser module, column thermostat, and PDA detector. Data acquisition and processing was controlled by HyStar 3.2 software. NMR spectra were recorded in $CDCl_3$ or benzene-d_6 on a Bruker Avance III spectrometer (Bruker Daltonics) operating at 500 MHz and 125 MHz for ^1H and ^{13}C, respectively. A 1 mm TXI microprobe was used for 1D and 2D NMR experiments (^1H, NOE difference, COSY, HSQC, HMBC, 2D-NOESY), whereas ^{13}C spectra were recorded with a 5 mm BBO-probe. Topspin 2.1 software was used for spectra analysis and processing. UV spectra were recorded on an Agilent 8453 UV–visible spectrophotometer. Optical rotation was measured with a Perkin Elmer 341 polarimeter using a 10 cm microcell and $CHCl_3$ as solvent. CD spectra were recorded in MeCN on an AVIV CD spectrometer (model 62A DS) and analyzed with AVIV 60DS V4.1 software.

4.2. Plant material

The rhizomes of *C. kwangsiensis* were collected by D. Yang in the area of Guang Xi, China in 2005 and identified by one of the authors (M.H.). A voucher specimen (nr. 293) has been deposited at the Division of Pharmaceutical Biology, University of Basel, Switzerland.

4.3. Extraction

The rhizome material was powdered in a ZM 1 ultracentrifugal mill (sieve size 2.0 mm; Retsch, Haan, Germany) cooled with liquid nitrogen. The library extract (ethyl acetate extract) used for screening and HPLC-based activity profiling was prepared with an ASE 200 instrument connected to a solvent controller (Dionex, Sunnyvale, USA). The conditions were as follows: temperature 70 °C; pressure 120 bar; three extraction cycles of 5 min each, 11 ml steel cartridges. For compound purification, the powdered rhizome material (385 g) was percolated exhaustively at room temperature with ethyl acetate. Solvent evaporation under reduced pressure afforded a dark brown viscous residue (3.8 g).

4.4. HPLC-based activity profiling

Microfractionation for activity profiling was performed according to a validated protocol (Kim et al., 2008). Briefly, an aliquot (5 mg) of the crude extract was separated by semi-preparative RP-HPLC, and peak-based microfractions were collected manually into glass tubes. A gradient of 30% to 90% B in 60 min was used. The flow rate was 5 ml/min and 100 μl of extract (50 mg/ml in DMSO/methanol [1:3 v/v]) were injected. Microfractions were evaporated with a Genevac EZ-2 Plus vacuum evaporator. For pharmacological testing, the dried fractions were re-dissolved in 30 μl of DMSO, and then diluted with 2.97 ml of bath solution containing GABA EC_{3-10}.

4.5. Isolation

Preliminary separation was performed by flash chromatography. A portion of the extract (1 g) was adsorbed to silica gel 60 (40–63 μm, 3 g) and packed into a PrepElut cartridge. This cartridge was then connected to the top of the separation cartridge. A *n*-hexane/ethyl acetate gradient (100:0 to 0:100 in 4 h, followed by 0:100 for 30 min) was used for separation. Fractions (15 ml

each) were combined based on TLC analysis (*n*-hexane/ethyl acetate [1:1 v/v]) into ten fractions (A–J). Fractions used for compound isolation were separated by semi-preparative RP-HPLC with different gradients of H_2O + 0.1% formic acid (solvent A) and MeCN + 0.1% formic acid (solvent B). The flow rate was set at 4 ml/min. Final purification of fractions G (86.4 mg) and H (52.0 mg) with a gradient of 50% to 70% B in 25 min afforded **2** (2.2 mg, t_R 15.6 min) and **4** (1.8 mg, t_R 18.9 min), respectively. Compound **5** (0.5 mg, t_R19.7 min) was isolated from fraction E (60.7 mg) using a gradient of 60% to 75% B in 30 min. Fractions C (48.1 mg) and D (68.4 mg) were combined and separated by flash chromatography on silica gel, using a gradient of chloroform/ethyl acetate (100:0 to 90:10 in 2 h). Three fractions (CD1–CD3) were combined on the basis of TLC patterns (chloroform/ethyl acetate [95:5 v/v]). Separation of fraction CD1 (5.6 mg) with a gradient of 65% to 90% B in 35 min, yielded **8** (2.7 mg, t_R 24.1 min) and **11** (0.4 mg, t_R 25.7 min), while fraction CD3 (18.0 mg) under the same conditions afforded **9** and **10** as an inseparable mixture (1.0 mg, t_R 23.8 min). Flash chromatography on silica gel of a portion (108.3 mg) of fraction *F* (200.1 mg), using a chloroform/acetone gradient (100:0 to 95:5 in 1 h, followed by 95:5 to 50:50 in 1 h; fraction volume: 10 ml) afforded six subfractions (*F*1–*F*6). Final purification of fractions was achieved with a gradient of 60% to 75% B in 30 min. Compound **6** (2.2 mg, t_R 22.0 min) and **7** (0.3 mg, t_R 24.5 min) were obtained from fraction *F*3 (10.9 mg), while fraction *F*4 (20.1 mg) gave additional **6** (6.3 mg). Fraction *F*1 (48.1 mg) afforded compound **1** (2.1 mg, t_R 15.9 min), and fraction *F*5 (15.2 mg) yielded compound **3** (1.0 mg, t_R 19.0 min). To obtain sufficient amounts for structure elucidation and pharmacological testing, the isolation procedure was repeated once with the same extract amount. Purities of isolated compounds were determined by ^{1}H NMR. Purities of compounds **1**–**8** were >95%. Compound **9** was obtained as a mixture with **10** in the ratio 64:36. Purity of **11** was 80%.

4.6. Methylation of **4**

To a solution of **4** (1 mg, dissolved in chloroform/methanol [3:2 v/v]), a 2 M solution of trimethylsilyldiazomethane in diethyl ether (Sigma) was added dropwise under stirring until a yellow coloration of the reaction mixture appeared. The mixture was further stirred for 1 h at room temperature. Then, glacial acetic acid was added dropwise until complete disappearance of the yellow color. Evaporation to dryness afforded the dimethyl ester **4a**: HR-ESI-TOF-MS *m*/*z* 385.2361 $[M+Na]^+$ (calcd for $C_{22}H_{34}NaO_4$: 385.2349); ^{1}H and ^{13}C NMR data, see Tables 1 and 2.

4.7. Characterization of isolates

4.7.1. 5S,9S,10S,15R-(−)-curcuminol D (**1**)

White needles; $[\alpha]^{23}_D$: −22.4 ($CHCl_3$, *c* = 0.10); CD (MeCN, $c = 1.82 \times 10^{-4}$ M, 1 cm pathlength): $[\theta]_{211}$ −12 018, $[\theta]_{236}$ −23 810, $[\theta]_{283}$ −116, $[\theta]_{326}$ −2 048; UV (MeCN) λ_{max} (log ε) 219 (4.20); ^{1}H and ^{13}C NMR data, see Tables 1 and 2; HR-ESI-TOF-MS *m*/*z* 325.2118 $[M+Na]^+$ (calcd for $C_{20}H_{30}NaO_2$: 325.2138).

4.7.2. 5S,9S,10S,15R-(−)-curcuminol H (**2**)

Colorless oil; $[\alpha]^{23}_D$: −11.8 ($CHCl_3$, *c* = 0.10); CD (MeCN, $c = 1.41 \times 10^{-4}$ M, 1 cm pathlength): $[\theta]_{200}$ −9 377, $[\theta]_{208}$ −15 495, $[\theta]_{222}$ −8 969, $[\theta]_{231}$ −12 178, $[\theta]_{287}$ + 156; UV (MeCN) λ_{max} (log ε) 217 (4.01); ^{1}H and ^{13}C NMR data, see Tables 1 and 2; HR-ESI-TOF-MS *m*/*z* 341.2080 $[M + Na]^+$ (calcd for $C_{20}H_{30}NaO_3$: 341.2087).

4.7.3. 5S,9S,10S-(+)-zerumin A (**3**)

$[\alpha]^{23}_D$: +12.4 ($CHCl_3$, *c* = 0.08); CD (MeCN, $c = 1.55 \times 10^{-4}$ M, 1 cm pathlength): $[\theta]_{200}$ −30 033, $[\theta]_{220}$ + 5 799, $[\theta]_{231}$ + 10 664, $[\theta]_{236}$ + 10 529; UV (MeCN) λ_{max} (log ε) 230 (4.14); HR-ESI-TOF-MS *m*/*z* 317.2118 $[M-H]^-$ (calcd for $C_{20}H_{29}O_3$: 317.2122).

4.7.4. 5S,9S,10S-(+)-(E)-labda-8(17),12-diene-15,16-dioic acid (**4**)

Colorless oil; $[\alpha]^{23}_D$: +2.0 ($CHCl_3$, *c* = 0.10); CD (MeCN, $c = 1.53 \times 10^{-4}$ M, 1 cm pathlength): $[\theta]_{200}$ −30 571, $[\theta]_{217}$ + 10 398, $[\theta]_{251}$ −1 828; UV (MeCN) λ_{max} (log ε) 217 (4.01), ^{1}H and ^{13}C NMR data, see Tables 1 and 2; HR-ESI-TOF-MS *m*/*z* 357.2048 $[M+Na]^+$ (calcd for $C_{20}H_{30}NaO_4$: 357.2036).

4.7.5. 5S,9S,10S-(−)-(E)-labda-8(17),11,13-trien-16,15-olide (**8**)

$[\alpha]^{23}_D$: −8.1 ($CHCl_3$, *c* = 0.15); CD (MeCN, $c = 1.65 \times 10^{-4}$ M, 1 cm pathlength): $[\theta]_{200}$ −22 304, $[\theta]_{202}$ −20 963, $[\theta]_{204}$ −18 881, $[\theta]_{219}$ +9 024; UV (MeCN) λ_{max} (log ε) 249 (3.85); HR-ESI-TOF-MS *m*/*z* 301.2164 $[M+H]^+$ (calcd for $C_{20}H_{29}O_2$: 301.2162).

4.7.6. (E)-labda-8(17),12,14-trien-16-oic acid (**9**)

Colorless oil, as mixture with **10**; ^{1}H and ^{13}C NMR data see Table 3; HR-ESI-TOF-MS *m*/*z* 325.2155 $[M+Na]^+$ (calcd for $C_{20}H_{30}NaO_2$: 325.2138).

4.7.7. (E)-labda-7,11,13-trien-16,15-olide (**11**)

Colorless oil; ^{1}H and ^{13}C NMR data, see Table 3; HR-ESI-TOF-MS *m*/*z* 323.1979 $[M+Na]^+$ (calcd for $C_{20}H_{28}NaO_2$: 323.1982).

4.8. Conformational analysis, geometrical optimization, and ECD calculation

Conformational analysis of compounds **1**, **2**, **4**, and **8** were performed with Schrödinger MacroModel 9.1 software (Schrödinger, LLC, New York) using the OPLS 2005 (Optimized Potential for Liquid Simulations) force field in H_2O. Conformers occurring within a 2 kcal/mol energy window from the particular global minimum were chosen for the gas phase geometrical optimization and energy calculation using the density function theory (DFT) with the B3LYP functional and the 6-31G** basis set as implemented in the gas phase with the Gaussian 09 program package (Frisch et al., 2009). Vibrational analysis was performed at the same level to confirm stability of minima. Time-dependent density function theory TDDFT/B3LYP/6-31G** in MeCN using the "self-consistent reaction field" method (SCRF) with the conductor-like polarizable continuum model (CPCM) was employed to calculate excitation energy (denoted by wavelength in nm) and rotatory strength R in dipole velocity (R_{vel}) and dipole length (R_{len}) forms. ECD curves were calculated based on rotatory strengths using half bandwidth of 0.2 eV with conformers of **1**, **2**, **4**, and **8** using SpecDis version 1.53 (Bruhn et al., 2012). The spectra were constructed based on the Boltzmann-weighting according to their population contribution.

4.9. Electrophysiological bioassay: expression of $GABA_A$ receptors in Xenopus oocytes and voltage-clamp experiments

4.9.1. Oocyte preparation

Oocytes derived from the South African clawed frog, *Xenopus leavis*, were prepared as follows: after 15 min exposure of female *Xenopus leavis* to the anaesthetic (0.2% solution of MS-222; the methane sulfonate salt of 3-aminobenzoic acid ethyl ester; Sigma), parts of the ovary tissue were surgically removed. Defolliculation was achieved by enzymatical treatment with 3 mg/ml collagenase type 1A (Sigma). Stage V–VI oocytes were selected and injected with the desired subunit-encoding cRNAs. To ensure the incorporation of the

γ-subunit, the cRNAs of α_1, β_2, and γ_{2S} were mixed in the ratio 1:1:10, respectively. Injected oocytes were stored at 18 °C in ND96 bath solution containing 1% penicillin–streptomycin solution (Sigma). ND96 bath solution contained 96 mM NaCl, 2 mM KCl, 1 mM $MgCl_2 \cdot 6H_2O$, 1.8 mM $CaCl_2 \cdot 2H_2O$, and 5 mM HEPES (pH 7.4).

4.9.2. Automated two-microelectrode voltage-clamp studies

Currents through $GABA_A$ receptors were studied with the two-microelectrode voltage-clamp technique using a TURBO TEC-03X amplifier (npi electronic GmbH, Germany). Experiments were performed at a holding potential of −70 mV and at room temperature (20–24 °C). Voltage-recording and current-injecting microelectrodes (Harvard Apparatus) were filled with 3 M KCl and had resistances between 1 and 3 MΩ. The automated fast perfusion system ScreeningTool (npi electronic GmbH, see Baburin et al., 2006 for details) was used to apply the test solutions to the oocyte. Modulation of the GABA-induced chloride current (I_{GABA}) was measured with a GABA concentration eliciting 3 to 10% of the maximum current amplitude (EC_{3-10}) and corresponded to 3–10 μM GABA. The EC_{3-10} was determined at the beginning of each experiment. Successful expression of the γ-subunit was confirmed by measuring I_{GABA} after co-application of GABA EC_{3-10} and 10 μM diazepam (Sigma). Diazepam was used as positive control. Sample stock solutions (prepared in DMSO) were freshly diluted every day with ND96 bath solution containing GABA EC_{3-10}. To exclude current inhibition in the presence of DMSO, equal amounts of DMSO (1%) were present in both control and sample-containing solutions. Electrophysiological experiments were performed one to three days after cRNA injection. Oocytes with maximal current amplitudes >4 μA after application of 1 mM GABA were discarded to avoid voltage-clamp errors. Data acquisition and processing were performed using pCLAMP 10.0 software and Clampfit 10.2 software, respectively.

4.9.3. Data analysis

Enhancement of I_{GABA} was defined as $(I_{(GABA+Comp)}/I_{GABA}) - 1$, where $I_{(GABA+Comp)}$ is the current response in the presence of the indicated test material (extract, fraction, or pure compound), and I_{GABA} is the GABA-induced control current. Concentration–response curves were generated, and the data analyzed using Origin software 7.0 (OriginLab Corporation, Northampton, MA, USA). Data were fitted to the equation $1/[1 + (EC_{50}/[Comp])^{nH}]$, where EC_{50} is the concentration of the compound that increases the amplitude of the GABA-evoked current by 50% of the compound-induced maximum response, and n_H is the Hill coefficient. Each data point represents the mean ± S.E. from at least three oocytes and two oocyte batches.

Acknowledgments

Financial support by the Swiss National Science Foundation (Project 31600-113109), the Steinegg-Stiftung, Herisau, and the Fonds zur Förderung von Lehre und Forschung, Basel (M.H.) is gratefully acknowledged. A.S. was recipient of a research scholarship from the Freiwillige Akademische Gesellschaft, Basel. The authors thank Dr. H.J. Kim for the initial screening of the *C. kwangsiensis* extract and D. Yang for collecting the plant material.

Appendix A. Supplementary data

Supplementary data associated with this article can be found, in the online version, at http://dx.doi.org/10.1016/j.phytochem.2013.08.004.

References

Baburin, I., Beyl, S., Hering, S., 2006. Automated fast perfusion of *Xenopus* oocytes for drug screening. Pflug. Arch. Eur. J. Phy. 453, 117–123.
Biesalski, H.K., 2002. Nutraceuticals: the link between nutrition and medicine. J. Toxicol. Cutan. Ocul. Toxicol. 21, 9–30.
Bruhn, T., Schaumlöffel, A., Hemberger, Y., Bringmann, G., 2012. SpecDis version 1.53, University of Würzburg, Germany.
Chimakurthy, J., Talasila, M., 2010. Effects of curcumin on pentylenetetrazole-induced anxiety-like behaviors and associated changes in cognition and monoamine levels. Psychol. Neurosci. 3, 239–244.
Chinese Pharmacopoeia Commission, 2010. Pharmacopoeia of the People's Republic of China, vol. I. China Medical Science Press, Beijing (English edition).
Frisch, M.J., Trucks, G.W., Schlegel, H.B., Scuseria, G.E., Robb, M.A., Cheeseman, J.R., Scalmani, G., Barone, V., Mennucci, B., Petersson, G.A., Nakatsuji, H., Caricato, M., Li, X., Hratchian, H.P., Izmaylov, A.F., Bloino, J., Zheng, G., Sonnenberg, J.L., Hada, M., Ehara, M., Toyota, K., Fukuda, R., Hasegawa, J., Ishida, M., Nakajima, T., Honda, Y., Kitao, O., Nakai, H., Vreven, T., Montgomery, J.A., Peralta, J.E., Ogliaro, F., Bearpark, M., Heyd, J.J., Brothers, E., Kudin, K.N., Staroverov, V.N., Kobayashi, R., Normand, J., Raghavachari, K., Rendell, A., Burant, J.C., Iyengar, S.S., Tomasi, J., Cossi, M., Rega, N., Millam, J.M., Klene, M., Knox, J.E., Cross, J.B., Bakken, V., Adamo, C., Jaramillo, J., Gomperts, R., Stratmann, R.E., Yazyev, O., Austin, A.J., Cammi, R., Pomelli, C., Ochterski, J.W., Martin, R.L., Morokuma, K., Zakrzewski, V.G., Voth, G.A., Salvador, P., Dannenberg, J.J., Dapprich, S., Daniels, A.D., Farkas, O., Foresman, J.B., Ortiz, J.V., Cioslowski, J., Fox, D.J., 2009. Gaussian 09, Revision A02. Gaussian, Inc., Wallingford, CT.
González, M.A., Mancebo-Aracil, J., Tangarife-Castaño, V., Agudelo-Goméz, L., Zapata, B., Mesa-Arango, A., Betancur-Galvis, L., 2010. Synthesis and biological evaluation of (+)-labdadienedial, derivatives and precursors from (+)-sclareolide. Eur. J. Med. Chem. 45, 4403–4408.
Itokawa, H., Morita, H., Katou, I., Takeya, K., Cavalheiro, A.J., de Oliveira, R.C.B., Ishige, M., Motidome, M., 1988. Cytotoxic diterpenes from the rhizomes of *Hedychium coronarium*. Planta Med. 54, 311–315.
Johnston, G.A.R., Hanrahan, J.R., Chebib, M., Duke, R.K., Mewett, K.N., 2006. Modulation of ionotropic GABA receptors by natural products of plant origin. Adv. Pharmacol. 54, 285–316.
Khom, S., Baburin, I., Timin, E.N., Hohaus, A., Sieghart, W., Hering, S., 2006. Pharmacological properties of GABA(A) receptors containing gamma 1 subunits. Mol. Pharmacol. 69, 640–649.
Kim, H.J., Baburin, I., Khom, S., Hering, S., Hamburger, M., 2008. HPLC-based activity profiling approach for the discovery of GABA(A) receptor ligands using an automated two microelectrode voltage clamp assay on *Xenopus* oocytes. Planta Med. 74, 521–526.
Kim, H.J., Baburin, I., Zaugg, J., Ebrahimi, S.N., Hering, S., Hamburger, M., 2012. HPLC-based activity profiling – discovery of sanggenons as GABA(A) receptor modulators in the traditional Chinese drug Sang bai pi (*Morus alba* root bark). Planta Med. 78, 440–447.
Kong, L.Y., Qin, M.J., Niwa, M., 2000. Diterpenoids from the rhizomes of *Alpinia calcarata*. J. Nat. Prod. 63, 939–942.
Li, J., Liao, C.R., Wei, J.Q., Chen, L.X., Zhao, F., Qiu, F., 2011. Diarylheptanoids from *Curcuma kwangsiensis* and their inhibitory activity on nitric oxide production in lipopolysaccharide-activated macrophages. Bioorg. Med. Chem. Lett. 21, 5363–5369.
Li, J., Zhao, F., Li, M.Z., Chen, L.X., Qiu, F., 2010. Diarylheptanoids from the rhizomes of *Curcuma kwangsiensis*. J. Nat. Prod. 73, 1667–1671.
Lipinski, C.A., Lombardo, F., Dominy, B.W., Feeney, P.J., 1997. Experimental and computational approaches to estimate solubility and permeability in drug discovery and development settings. Adv. Drug Deliver. Rev. 23, 3–25.
Margaros, I., Vassilikogiannakis, G., 2007. Synthesis of chinensines A–E. J. Org. Chem. 72, 4826–4831.
Mehla, J., Reeta, K.H., Gupta, P., Gupta, Y.K., 2010. Protective effect of curcumin against seizures and cognitive impairment in a pentylenetetrazole-kindled epileptic rat model. Life Sci. 87, 596–603.
Mohamad, H., Lajis, N.H., Abas, F., Ali, A.M., Sukari, M.A., Kikuzaki, H., Nakatani, N., 2005. Antioxidative constituents of *Etlingera elatior*. J. Nat. Prod. 68, 285–288.
Nahar, L., Sarker, S.D., 2007. Phytochemistry of the genus *Curcuma*. In: Ravindran, P.N., NirmalBabu, K., Sivaraman, K. (Eds.), Tumeric – The genus *Curcuma*. CRC Press, pp. 71–106.
Nakatani, N., Kikuzaki, H., Yamaji, H., Yoshio, K., Kitora, C., Okada, K., Padolina, W.G., 1994. Labdane diterpenes from rhizomes of *Hedychium coronarium*. Phytochemistry 37, 1383–1388.
Newman, D.J., Cragg, G.M., 2012. Natural products as sources of new drugs over the last 30 years from 1981 to 2010. J. Nat. Prod. 75, 311–335.
Olsen, R.W., Sieghart, W., 2008. International Union of Pharmacology. LXX. Subtypes of gamma-aminobutyric acid(A) receptors: classification on the basis of subunit composition, pharmacology, and function. Update Pharmacol. Rev. 60, 243–260.
Orellana-Paucar, A.M., Serruys, A.S.K., Afrikanova, T., Maes, J., De Borggraeve, W., Alen, J., León-Tamariz, F., Wilches-Arizábala, I.M., Crawford, A.D., de Witte, P.A.M., Esguerra, C.V., 2012. Anticonvulsant activity of bisabolene sesquiterpenoids of *Curcuma longa* in zebrafish and mouse seizure models. Epilepsy Behav. 24, 14–22.
Pajouhesh, H., Lenz, G.R., 2005. Medicinal chemical properties of successful central nervous system drugs. NeuroRx 2, 541–553.
Park, G.G., Eun, S., Shim, S.H., 2012. Chemical constituents from *Curcuma zedoaria*. Biochem. Syst. Ecol. 40, 65–68.

Potterat, O., Hamburger, M., 2006. Natural products in drug discovery – concepts and approaches for tracking bioactivity. Curr. Org. Chem. 10, 899–920.
Ringdahl, E.N., Pereira, S.L., Delzell, J.E., 2004. Treatment of primary insomnia. J. Am. Board Fam. Pract. 17, 212–219.
Sy, L.K., Brown, G.D., 1997. Labdane diterpenoids from *Alpinia chinensis*. J. Nat. Prod. 60, 904–908.
Taferner, B., Schuehly, W., Huefner, A., Baburin, I., Wiesner, K., Ecker, G.F., Hering, S., 2011. Modulation of GABA(A)-receptors by honokiol and derivatives: subtype selectivity and structure–activity relationship. J. Med. Chem. 54, 5349–5361.
Tang, W., Eisenbrand, G., 2011. Handbook of Chinese Medicinal Plants – Chemistry, Pharmacology. Toxicology, Wiley-VCH, Weinheim.
Uhde, T.W., Cortese, B.M., Vedeniapin, A., 2009. Anxiety and sleep problems: emerging concepts and theoretical treatment implications. Curr. Psychiatry Rep. 11, 269–276.
Xu, H.X., Dong, H., Sim, K.Y., 1996. Labdane diterpenes from *Alpinia zerumbet*. Phytochemistry 42, 149–151.
Yang, X., Baburin, I., Plitzko, I., Hering, S., Hamburger, M., 2011. HPLC-based activity profiling for GABA(A) receptor modulators from the traditional Chinese herbal drug Kushen (*Sophora flavescens* root). Mol. Divers. 15, 361–372.
Zaugg, J., Baburin, I., Strommer, B., Kim, H.J., Hering, S., Hamburger, M., 2010. HPLC-based activity profiling: discovery of piperine as a positive GABA(A) receptor modulator targeting a benzodiazepine-independent binding site. J. Nat. Prod. 73, 185–191.
Zaugg, J., Ebrahimi, S.N., Smiesko, M., Baburin, I., Hering, S., Hamburger, M., 2011a. Identification of GABA A receptor modulators in *Kadsura longipedunculata* and assignment of absolute configurations by quantum-chemical ECD calculations. Phytochemistry 72, 2385–2395.
Zaugg, J., Eickmeier, E., Ebrahimi, S.N., Baburin, I., Hering, S., Hamburger, M., 2011b. Positive GABA(A) receptor modulators from *Acorus calamus* and structural analysis of (+)-dioxosarcoguaiacol by 1D and 2D NMR and molecular modeling. J. Nat. Prod. 74, 1437–1443.
Zaugg, J., Eickmeier, E., Rueda, D.C., Hering, S., Hamburger, M., 2011c. HPLC-based activity profiling of *Angelica pubescens* roots for new positive GABA(A) receptor modulators in *Xenopus* oocytes. Fitoterapia 82, 434–440.
Zaugg, J., Khom, S., Eigenmann, D., Baburin, I., Hamburger, M., Hering, S., 2011d. Identification and characterization of GABA(A) receptor modulatory diterpenes from *Biota orientalis* that decrease locomotor activity in mice. J. Nat. Prod. 74, 1764–1772.
Zeng, J.H., Xu, G.B., Chen, X., 2009. Application of the chromatographic fingerprint for quality control of essential oil from GuangXi *Curcuma kwangsiensis*. Med. Chem. Res. 18, 158–165.
Zhang, P., Huang, W., Song, Z., Zhang, M., Cheng, L., Cheng, Y., Qu, H., Ma, Z., 2008. Cytotoxic diterpenes from the radix of *Curcuma wenyujin*. Phytochem. Lett. 1, 103–106.

Supplementary data

Phytochemical profiling of *Curcuma kwangsiensis* rhizome extract, and identification of labdane diterpenoids as positive $GABA_A$ receptor modulators

Anja Schramm[a], Samad Nejad Ebrahimi[a,b], Melanie Raith[a], Janine Zaugg[a], Diana C. Rueda[a], Steffen Hering[c], Matthias Hamburger[a,*]

[a] Division of Pharmaceutical Biology, University of Basel, Klingelbergstrasse 50, 4056 Basel, Switzerland

[b] Department of Phytochemistry, Medicinal Plants and Drugs Research Institute, Shahid Beheshti University, G. C., Evin, Tehran, Iran

[c] Institute of Pharmacology and Toxicology, University of Vienna, Althanstrasse 14, 1090 Vienna, Austria

[*] Corresponding author. Tel.: +41 (0)61 267 14 25; fax: +41 (0)61 267 14 74

E-mail address: matthias.hamburger@unibas.ch (M. Hamburger)

Table S1. ^{1}H and ^{13}C NMR spectroscopic data for compound **3** ($CDCl_3$, 500 MHz, δ in ppm).

Position	**Zerumin A** (**3**)	
	δ_H (*J* in Hz)	δ_C[a]
1α	1.05, ddd (12.6, 12.6, 3.1)	39.2
1β	1.71[b]	
2α	1.48, m	19.2
2β	1.55, m	
3α	1.17, ddd (13.4, 13.4, 3.7)	42.0
3β	1.39, br d (13.2)	
4		33.7
5	1.12, dd (12.6, 1.7)	55.4
6α	1.73[b]	24.1
6β	1.32, dddd (12.8, 12.8, 12.8, 4.1)	
7α	2.00, ddd (13.1, 13.1, 4.7)	37.8
7β	2.39[b]	
8		148.0
9	1.89, br d (10.7)	56.4
10		39.9
11a	2.56, m	24.6
11b	2.39[b]	
12	6.60, dd (6.0, 6.0)	159.0
13		136.2
14	3.25, m	30.6
15		nd
16	9.29, s	194.1
17a	4.81, s	107.8
17b	4.38, s	
18	0.87, s	33.4
19	0.80, s	21.7
20	0.72, s	14.4

[a] ^{13}C shifts deduced from HSQC and HMBC experiments.

[b] Multiplicities of overlapped signals are omitted.

nd: not detected.

(δ_H and δ_C reference data can be found in Xu, H. X., Dong, H., Sim, K. Y., 1996. Labdane diterpenes from *Alpinia zerumbet*. Phytochemistry 42, 149-151.)

Table S2. Calculated logP values for compounds **1**–**11**.

Compound	clogP[a]
1	4.25 ± 0.37
2	4.19 ± 0.43
3	4.51 ± 0.69
4	4.40 ± 0.65
5	4.34 ± 0.62
6	4.62 ± 0.56
7	4.45 ± 0.68
8	4.94 ± 0.61
9	5.56 ± 0.91
10	5.57 ± 0.90
11	5.04 ± 0.57

[a] logP values were calculated using ALOGPA 2.1 software (VCCLAB, Virtual Computational Chemistry Laboratory, http://www.vcclab.org, 2005).

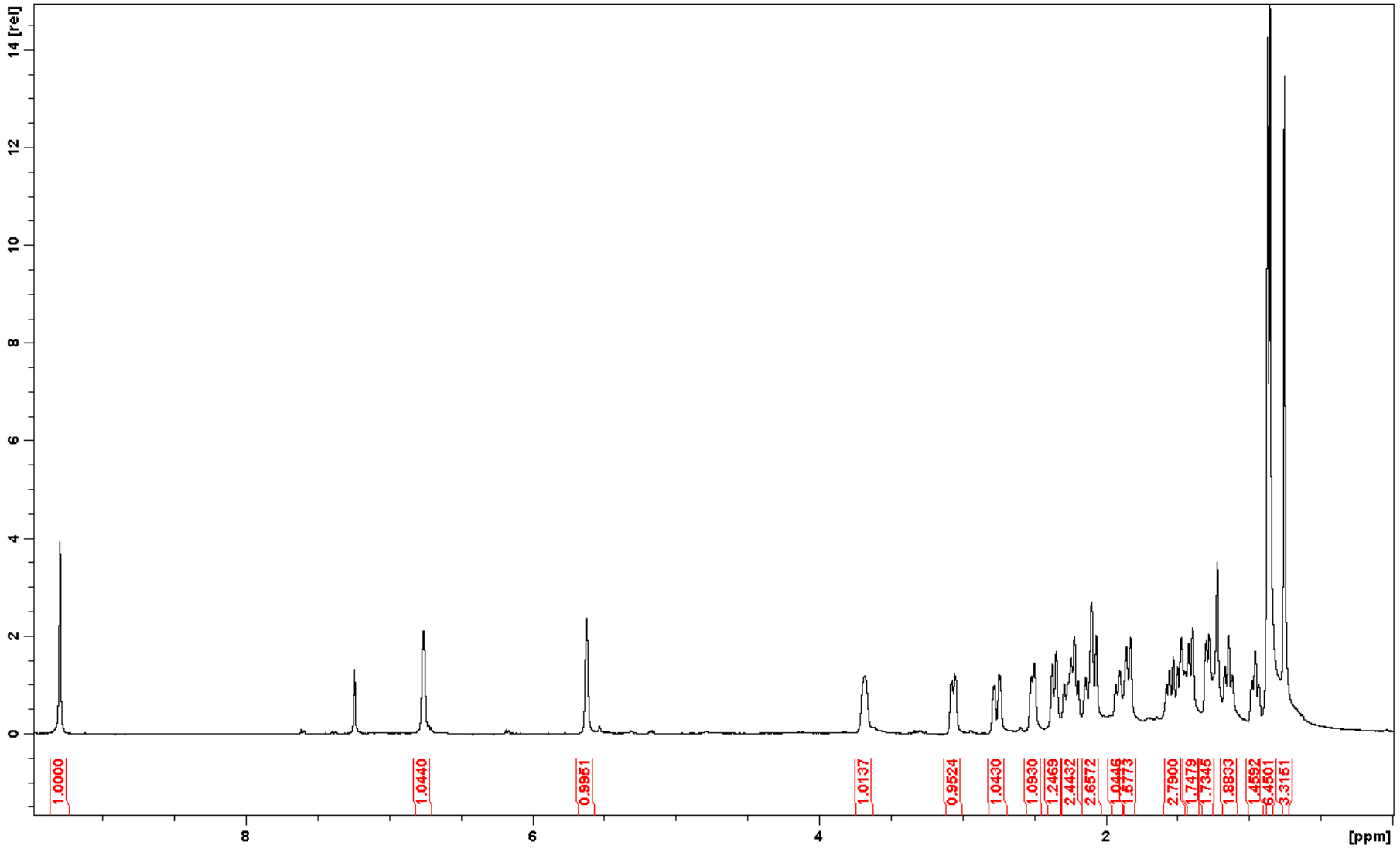

Figure S1. ^{1}H NMR spectrum of compound **1** (recorded in $CDCl_3$).

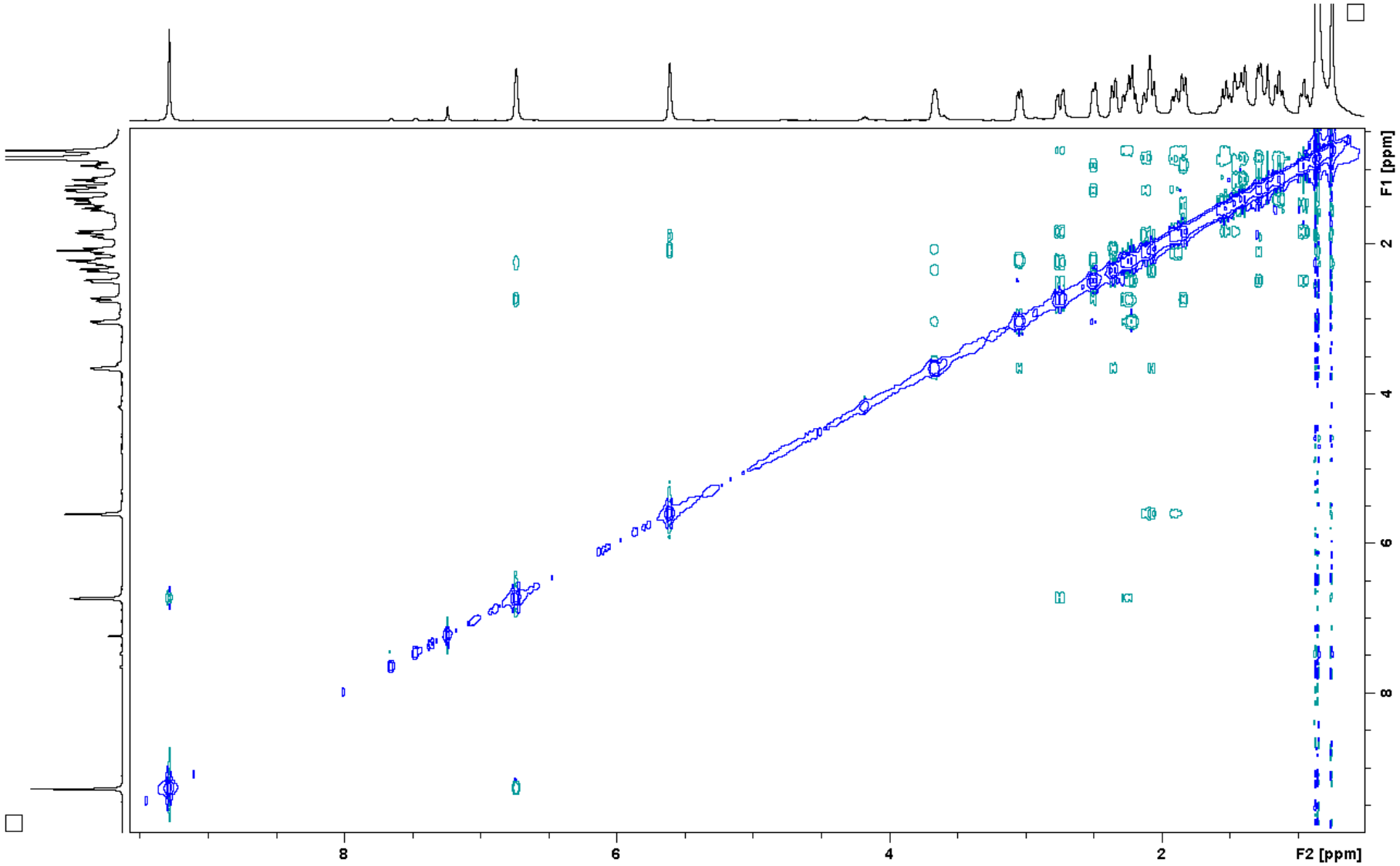

Figure S2. NOESY NMR spectrum of compound **1** (recorded in $CDCl_3$).

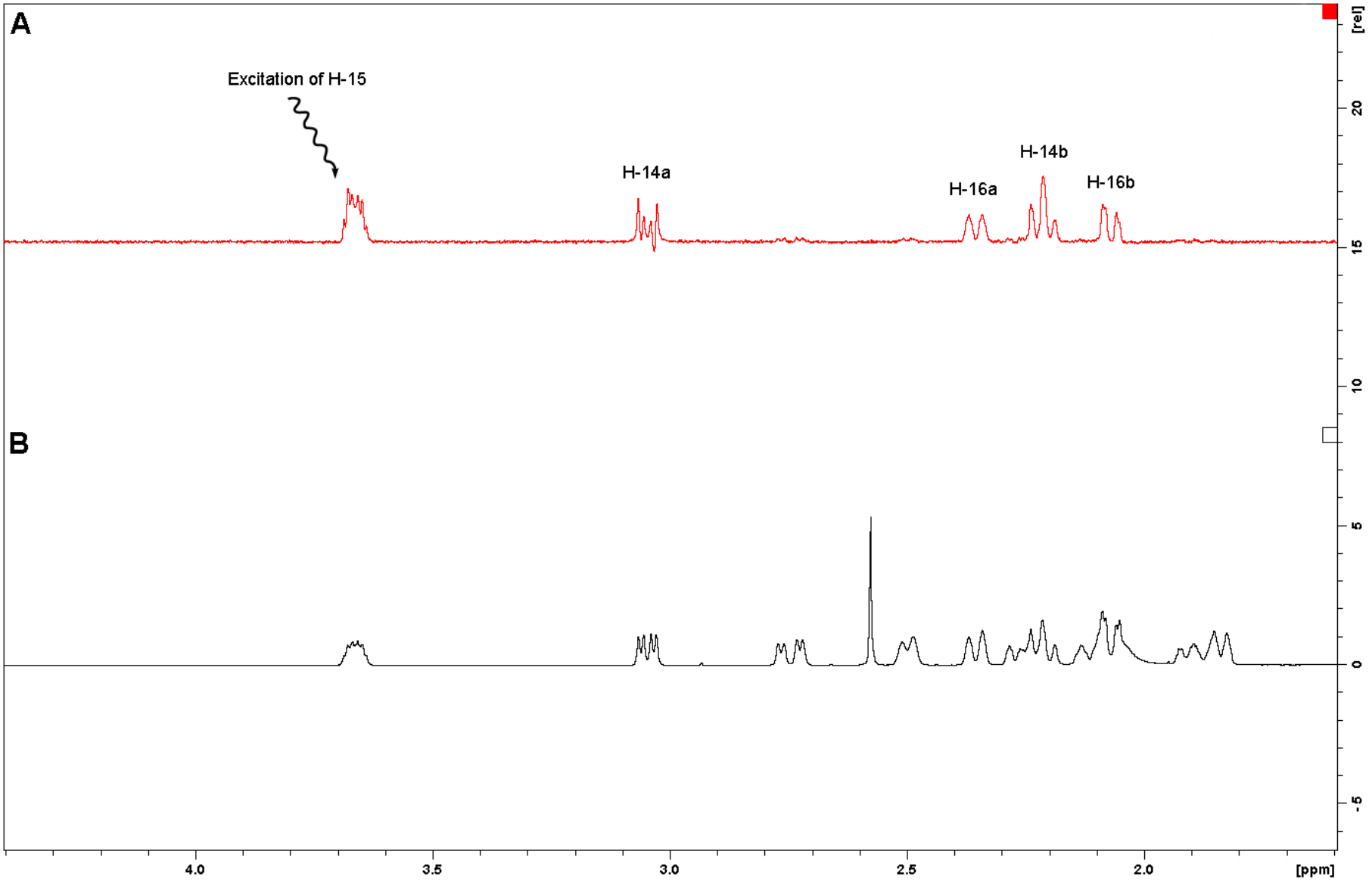

Figure S3. 1D TOCSY NMR experiment applied to compound **1** (recorded in $CDCl_3$). (**B**) The critical range of the ^1H NMR spectrum and (**A**) the selective excitation of the H-15 resonance are shown.

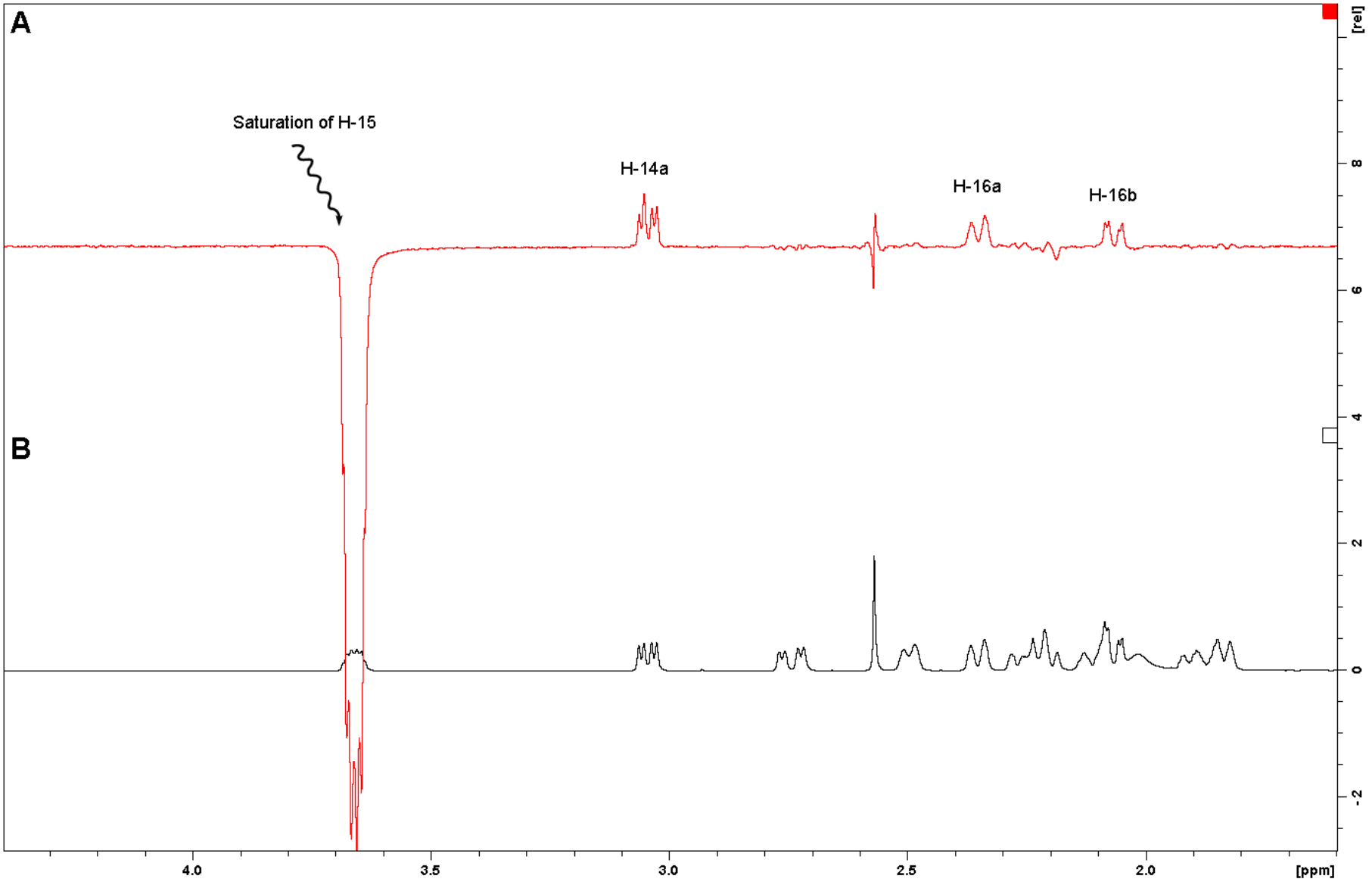

Figure S4. 1D NOE experiment applied to compound **1** (recorded in $CDCl_3$). (**B**) The critical range of the ^1H NMR spectrum and (**A**) the NOE difference NMR spectrum are shown. Saturating the H-15 resonance increased the intensities of the signals H-14a, H-16a, and H-16b.

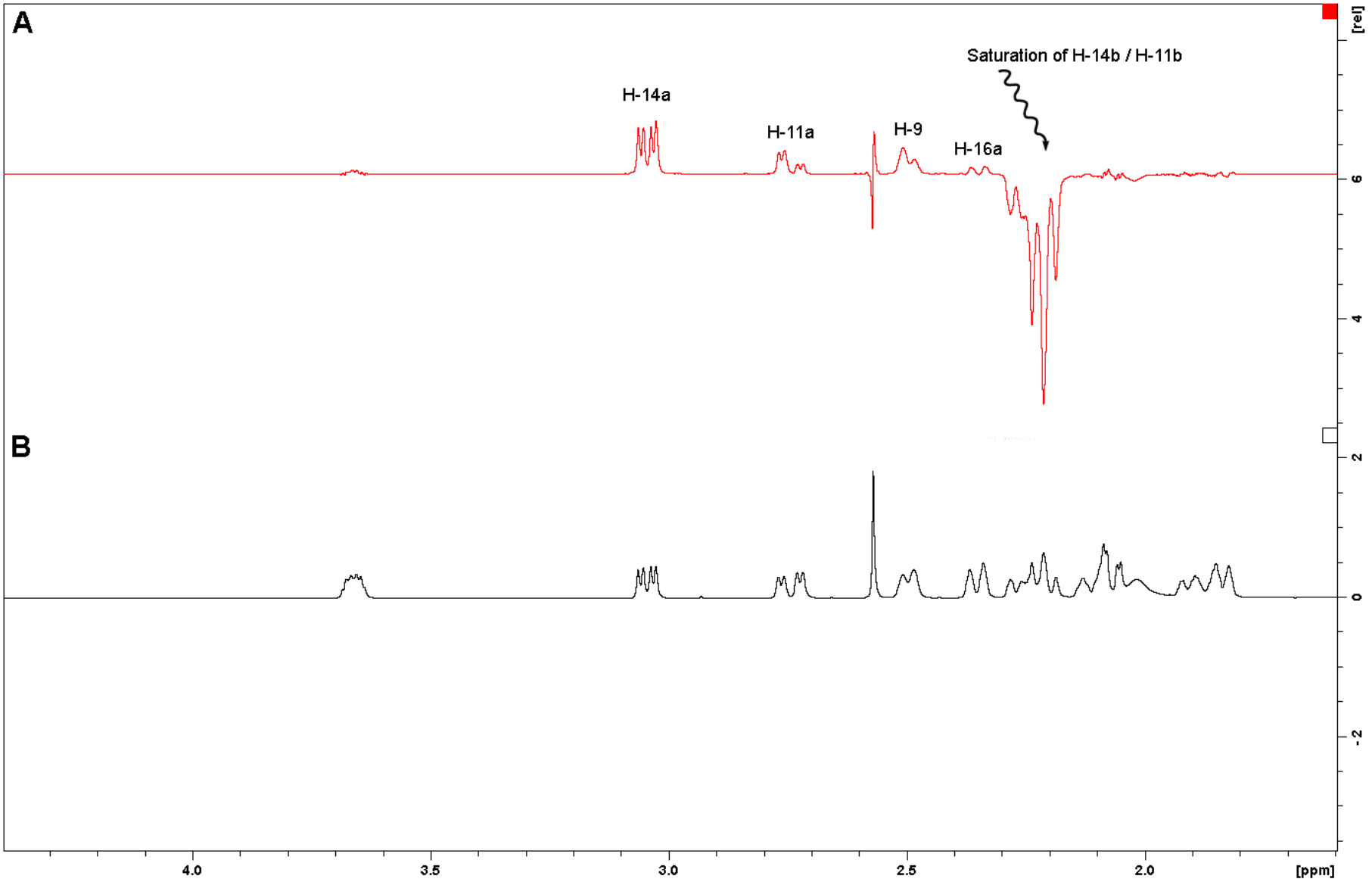

Figure S5. 1D NOE experiment applied to compound **1** (recorded in $CDCl_3$). (**B**) The critical range of the ^1H NMR spectrum and (**A**) the NOE difference NMR spectrum are shown. Saturating the H-14b resonance increased the intensities of the signals H-14a, H-9, and H-16a. The H-11b resonance was partially saturated by the irradiating frequency, and thus, resulted in a positive NOE for the H-11a signal.

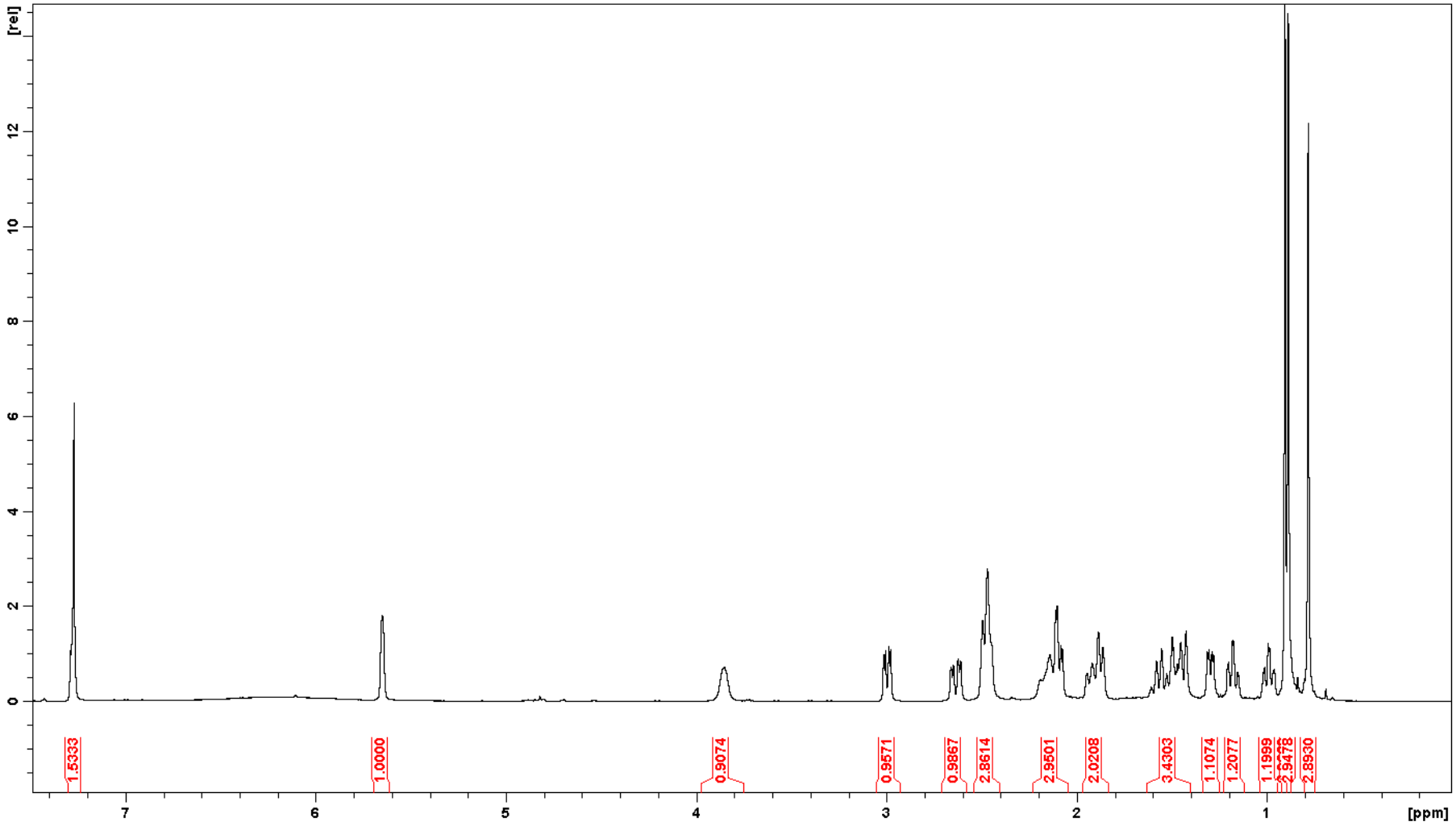

Figure S6. ^{1}H NMR spectrum of compound **2** (recorded in $CDCl_3$).

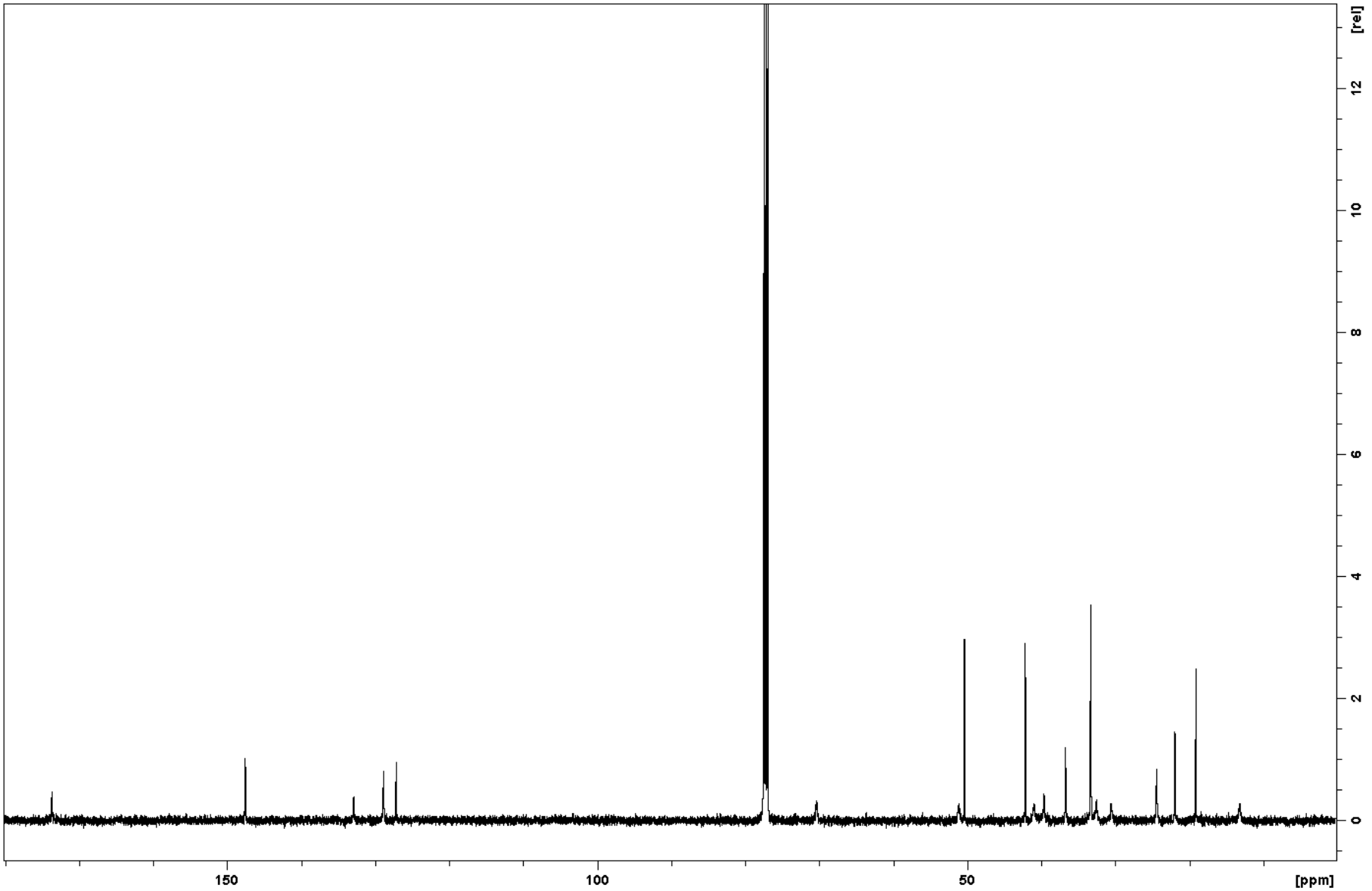

Figure S7. ^{13}C NMR spectrum of compound **2** (recorded in $CDCl_3$).

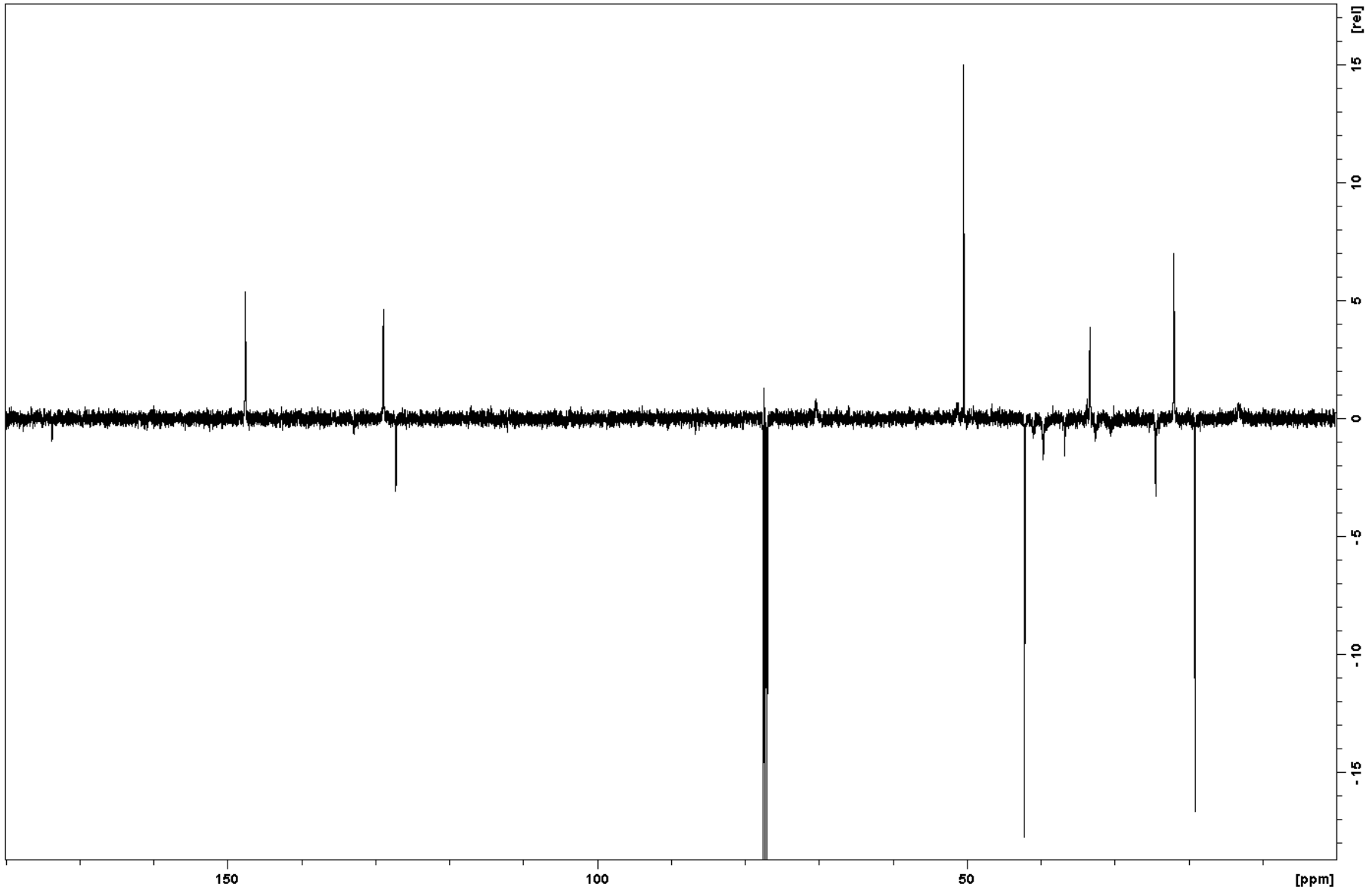

Figure S8. DEPT NMR spectrum of compound **2** (recorded in $CDCl_3$).

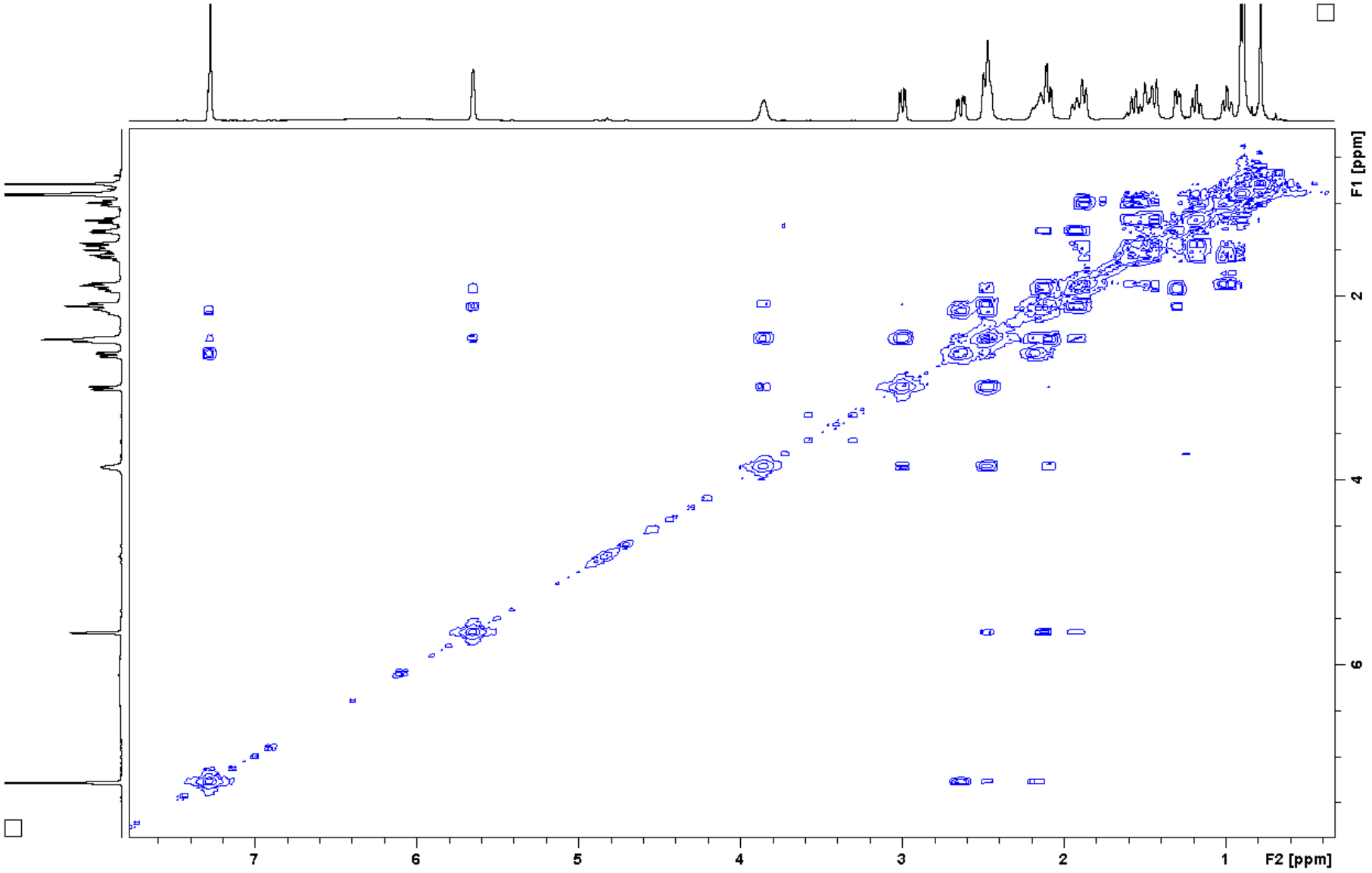

Figure S9. COSY NMR spectrum of compound **2** (recorded in $CDCl_3$).

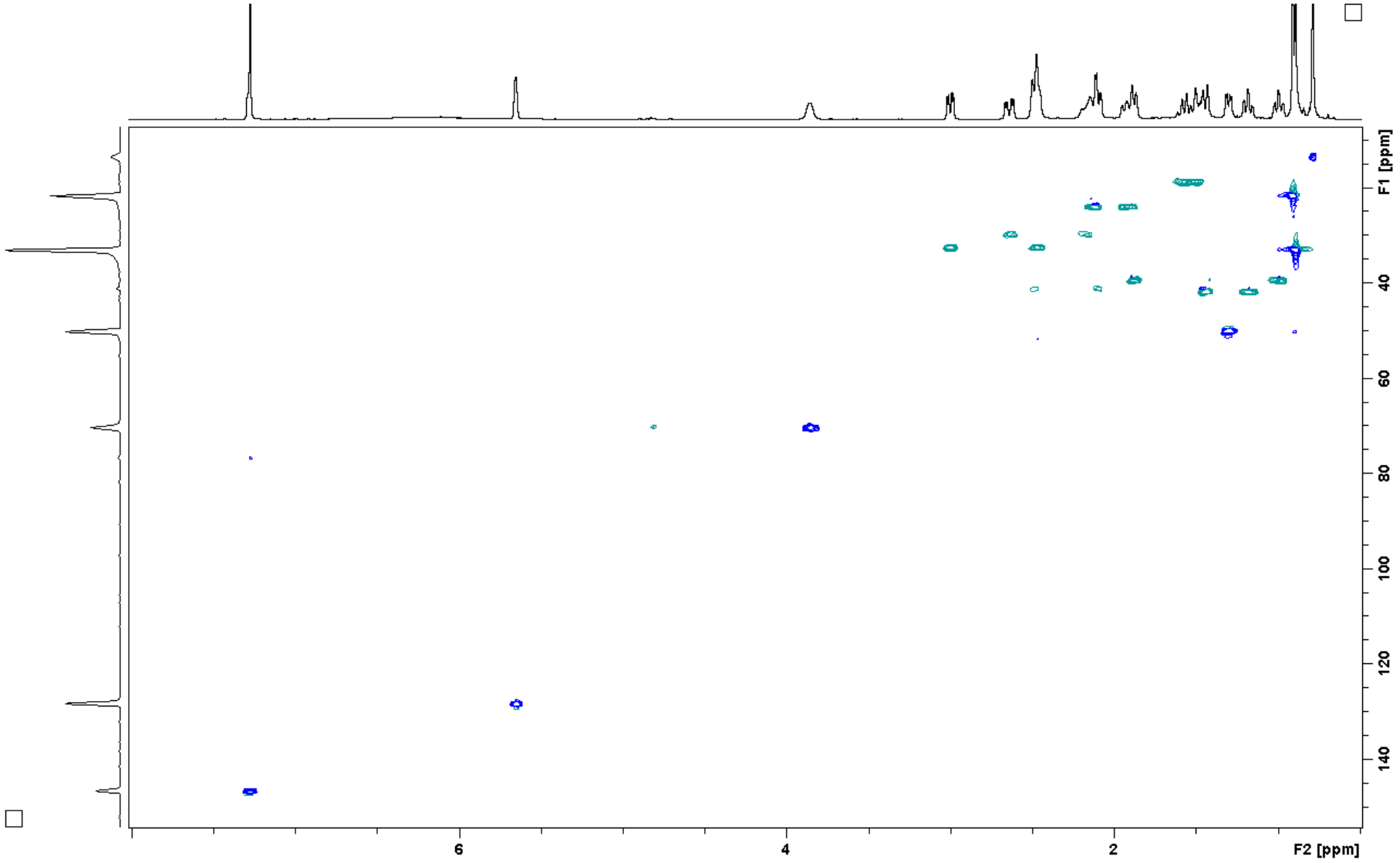

Figure S10. HSQC NMR spectrum of compound **2** (recorded in $CDCl_3$).

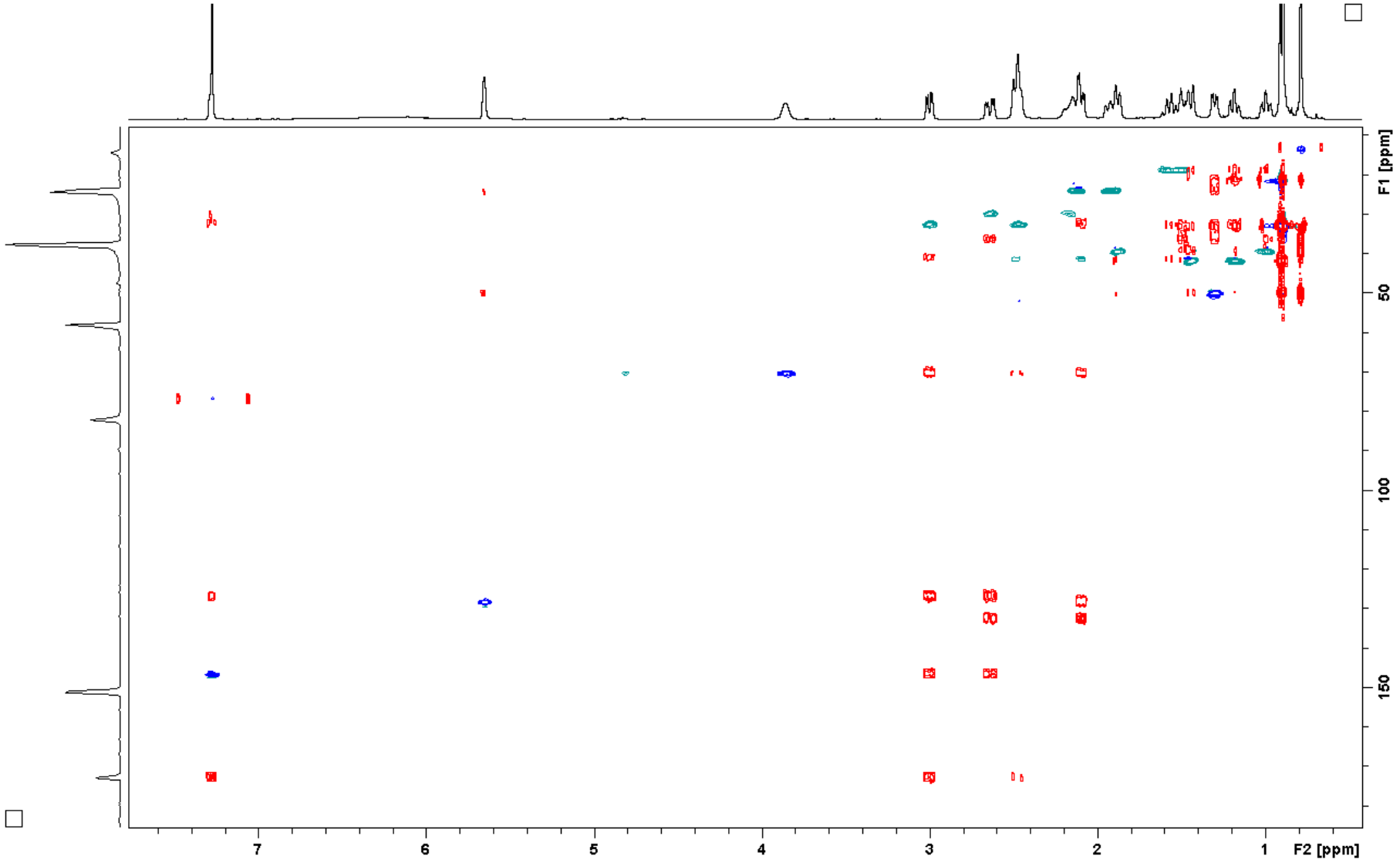

Figure S11. Overlay of HSQC and HMBC NMR spectra of compound **2** (recorded in $CDCl_3$).

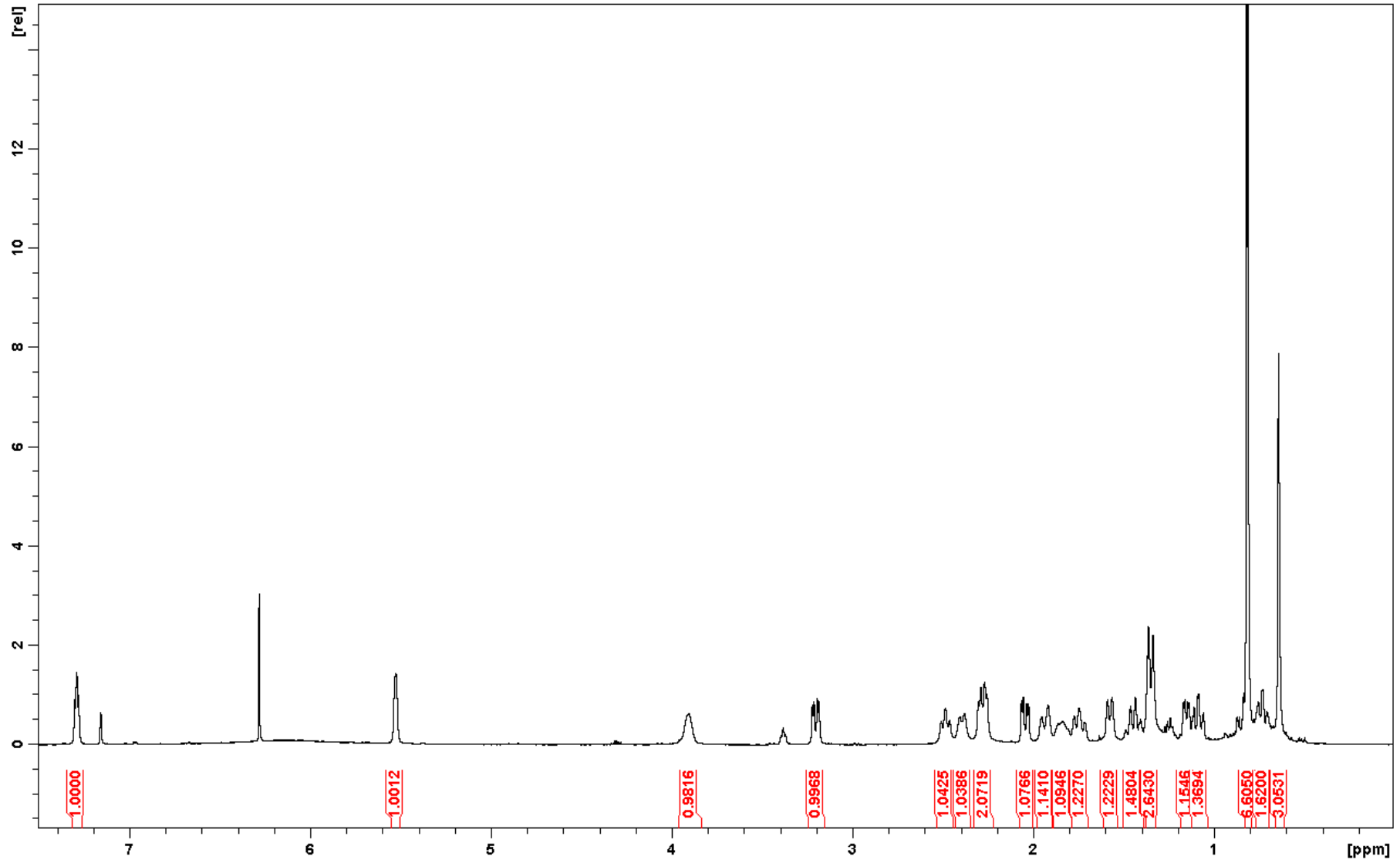

Figure S12. ^{1}H NMR spectrum of compound **2** (recorded in C_6D_6).

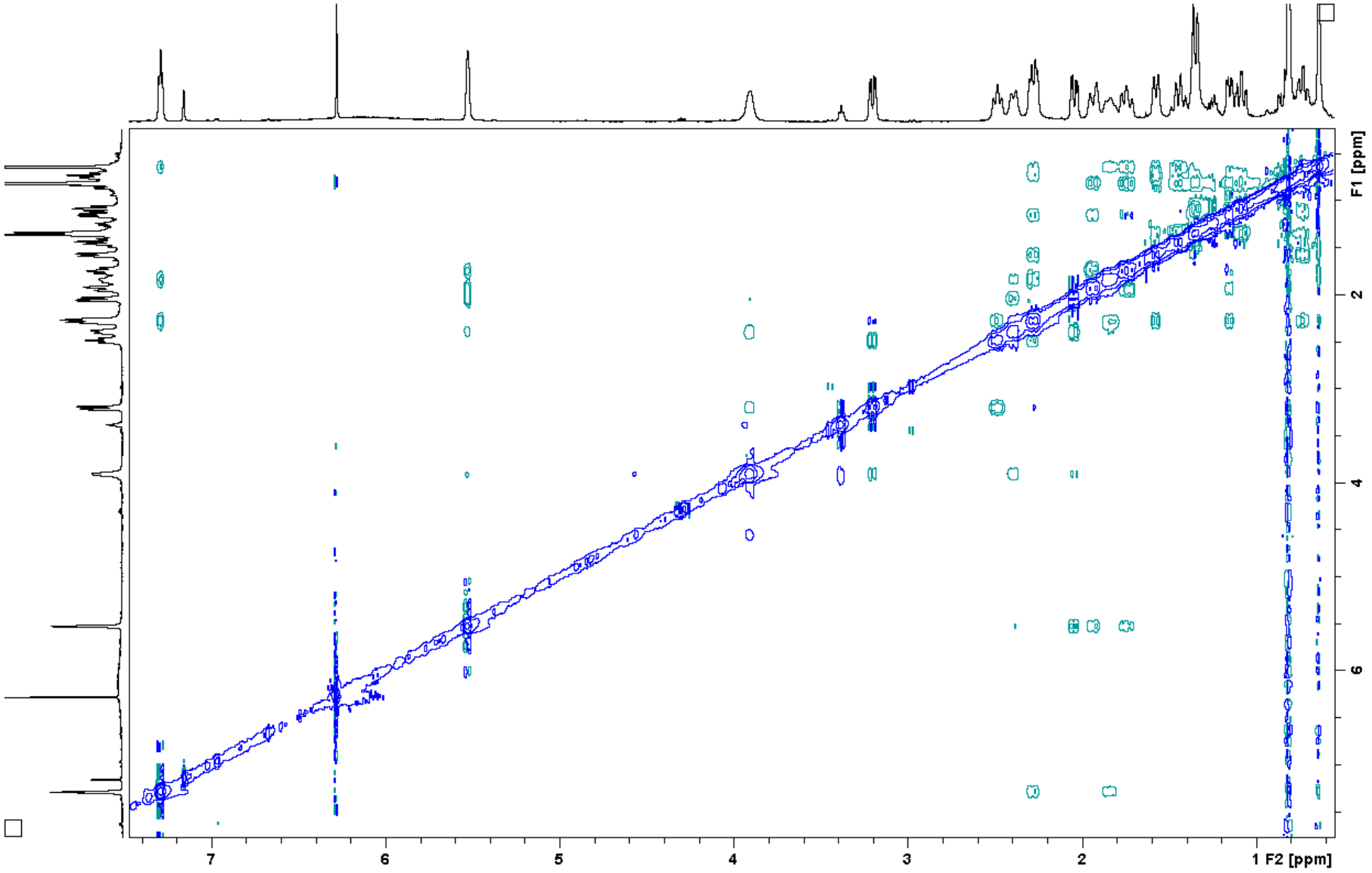

Figure S13. NOESY NMR spectrum of compound **2** (recorded in C_6D_6).

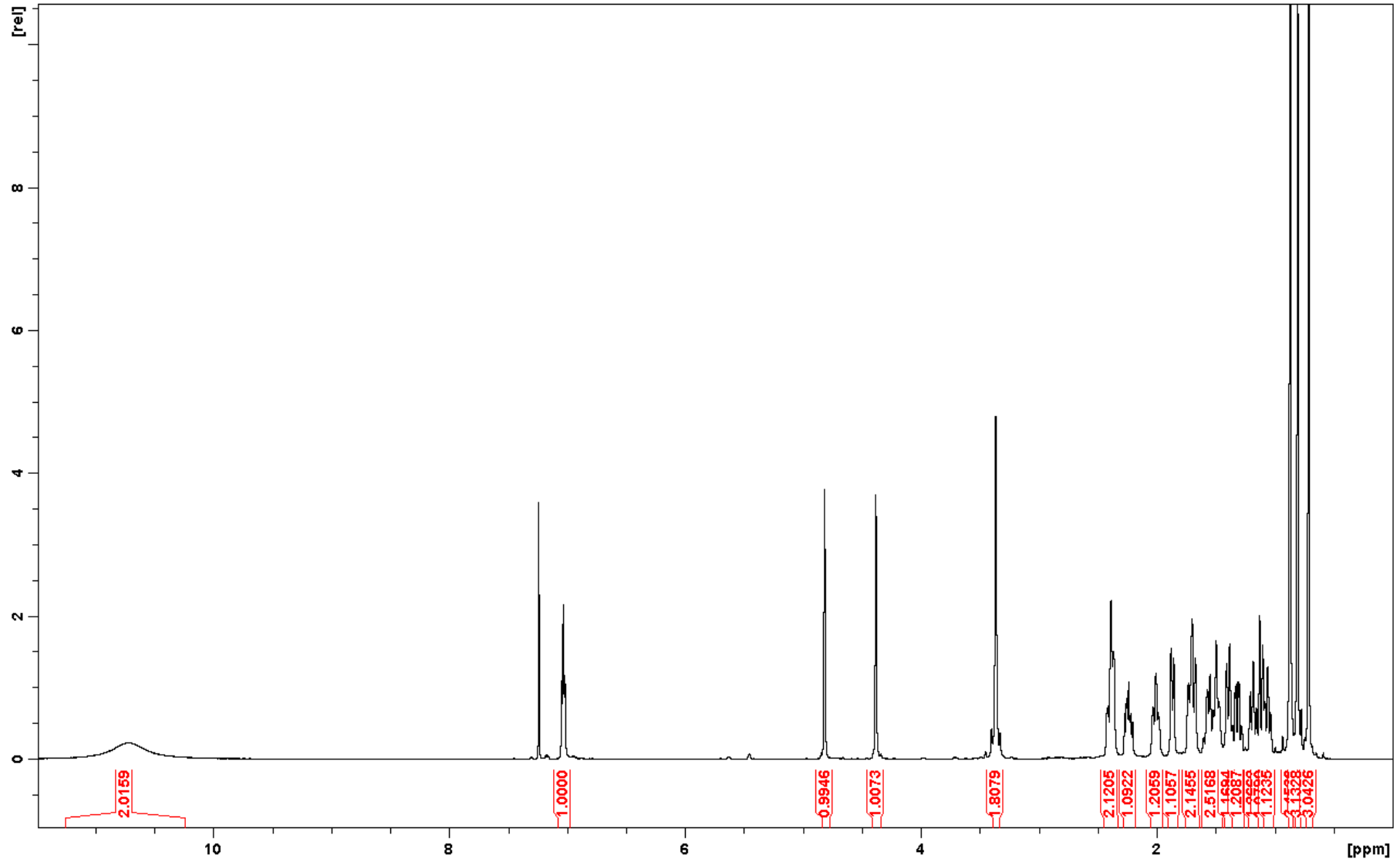

Figure S14. ^{1}H NMR spectrum of compound **4** (recorded in $CDCl_3$).

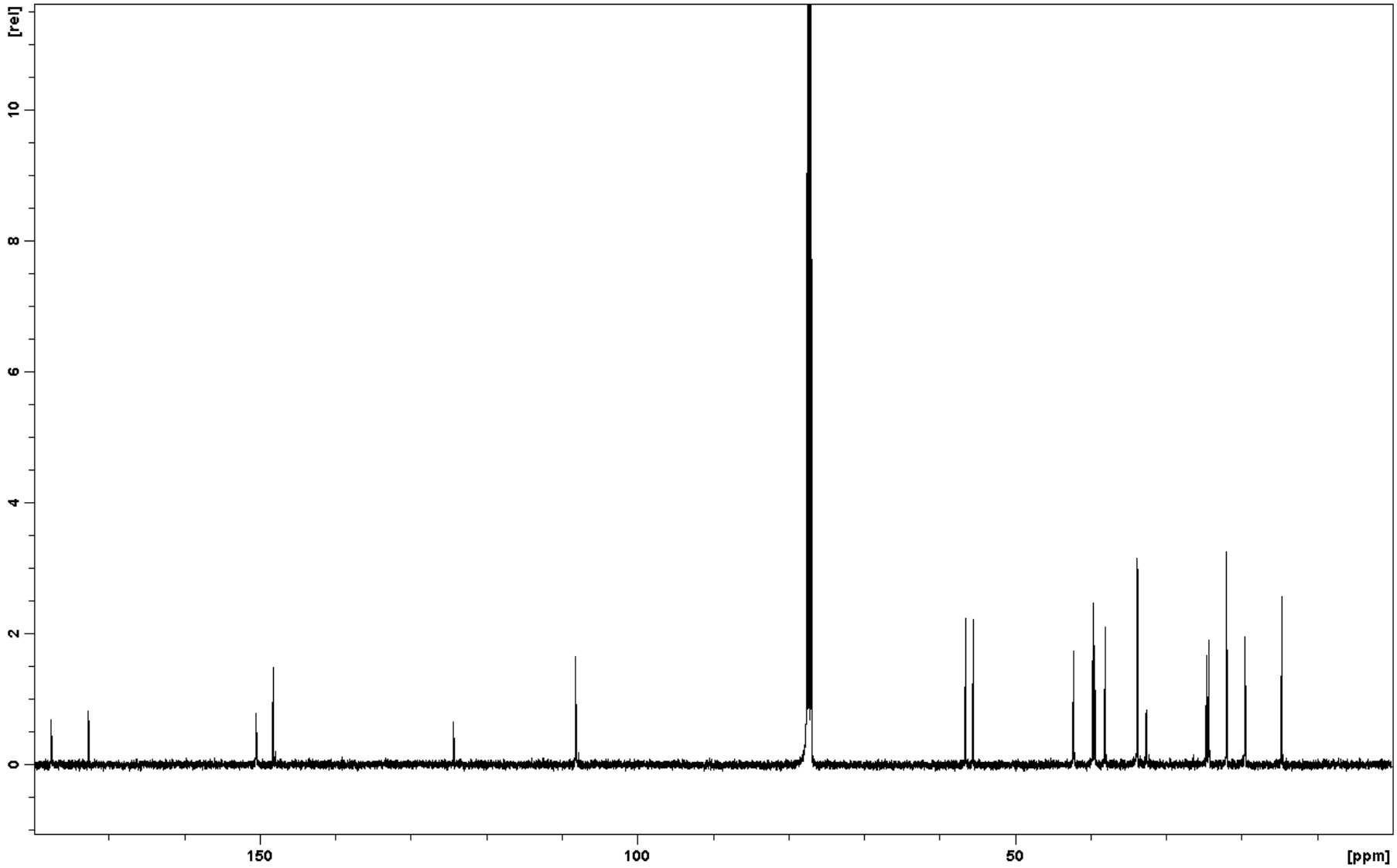

Figure S15. ^{13}C NMR spectrum of compound **4** (recorded in $CDCl_3$).

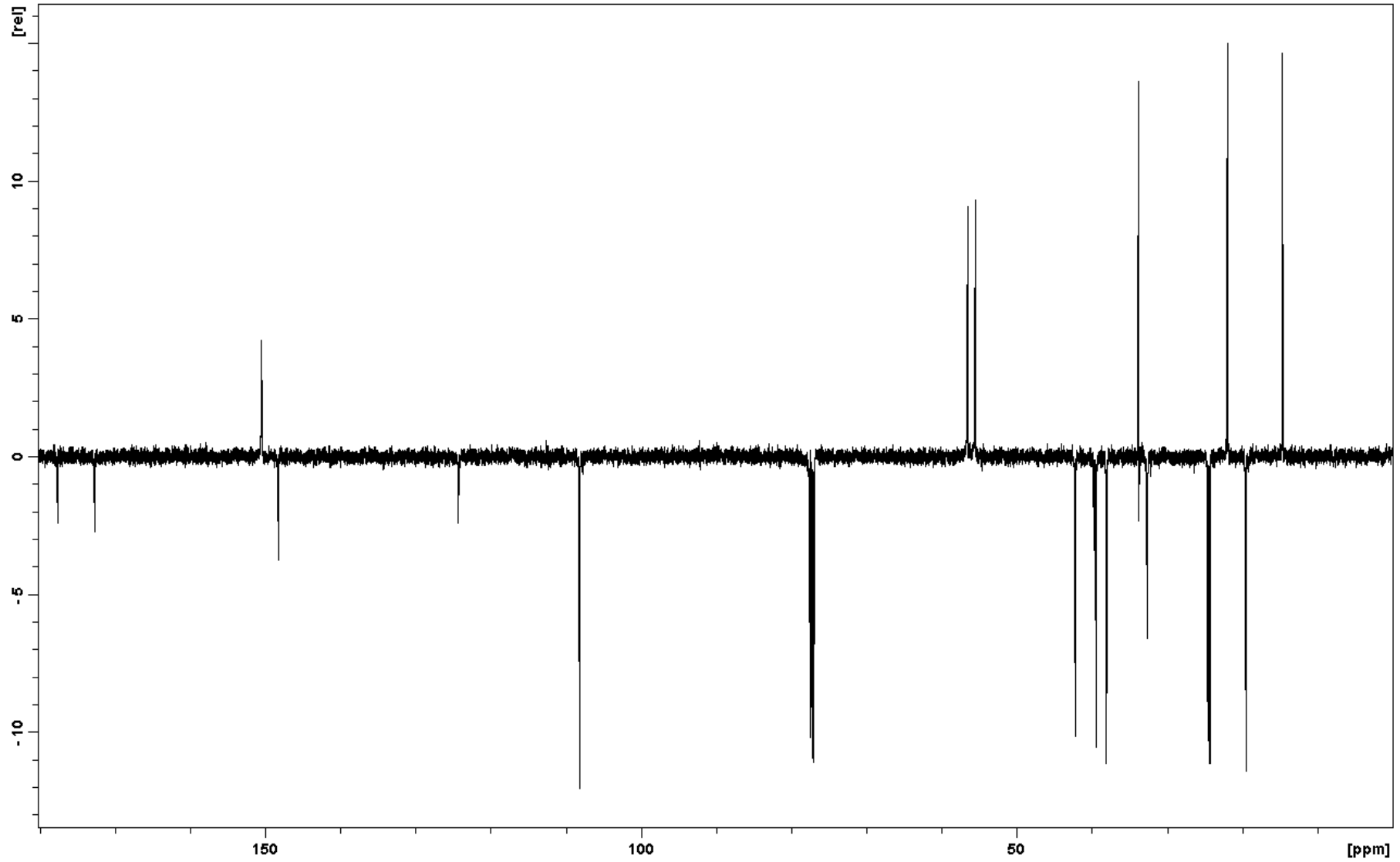

Figure S16. DEPT NMR spectrum of compound **4** (recorded in $CDCl_3$).

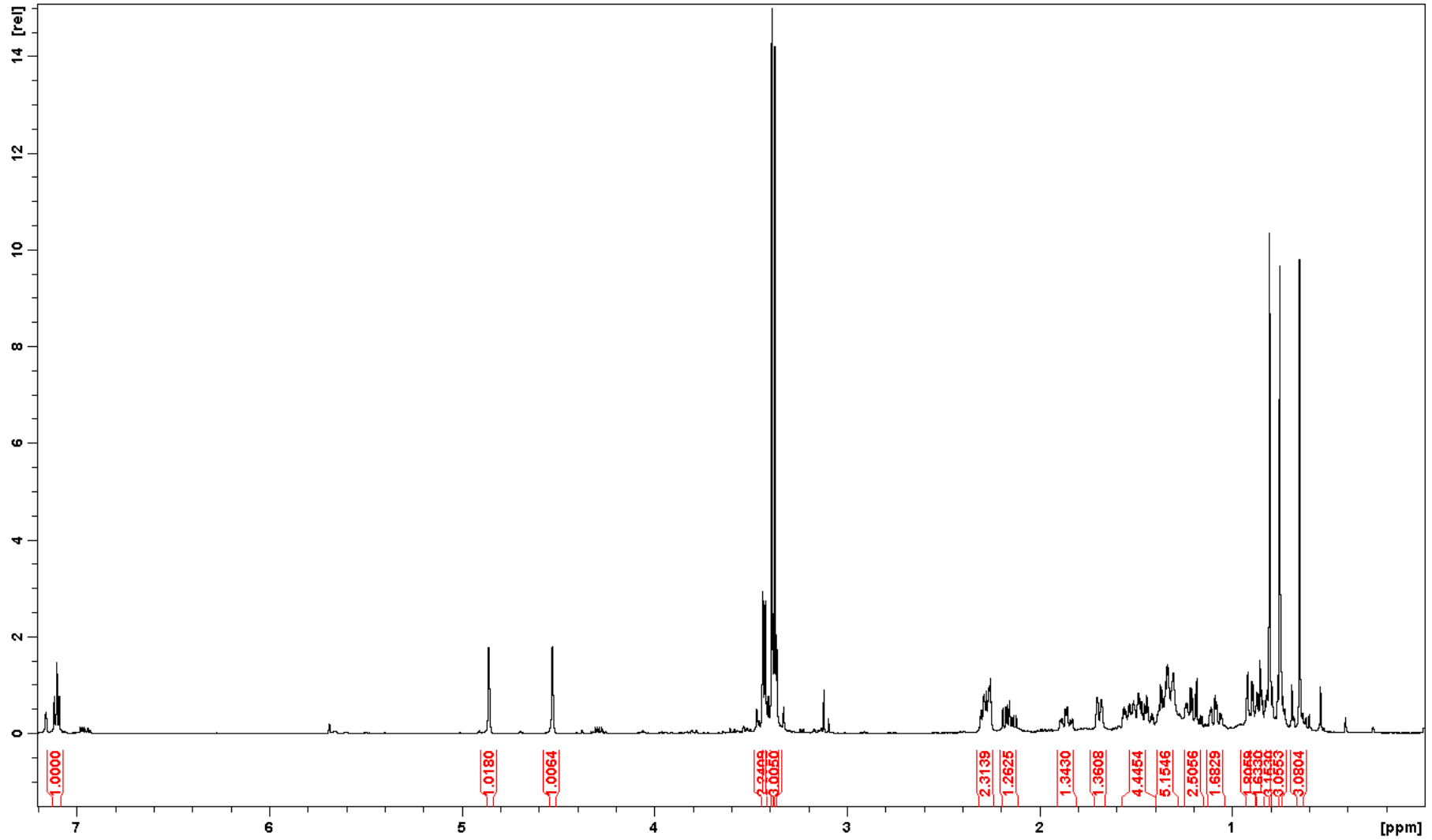

Figure S17. ^{1}H NMR spectrum of compound **4a** (recorded in C_6D_6).

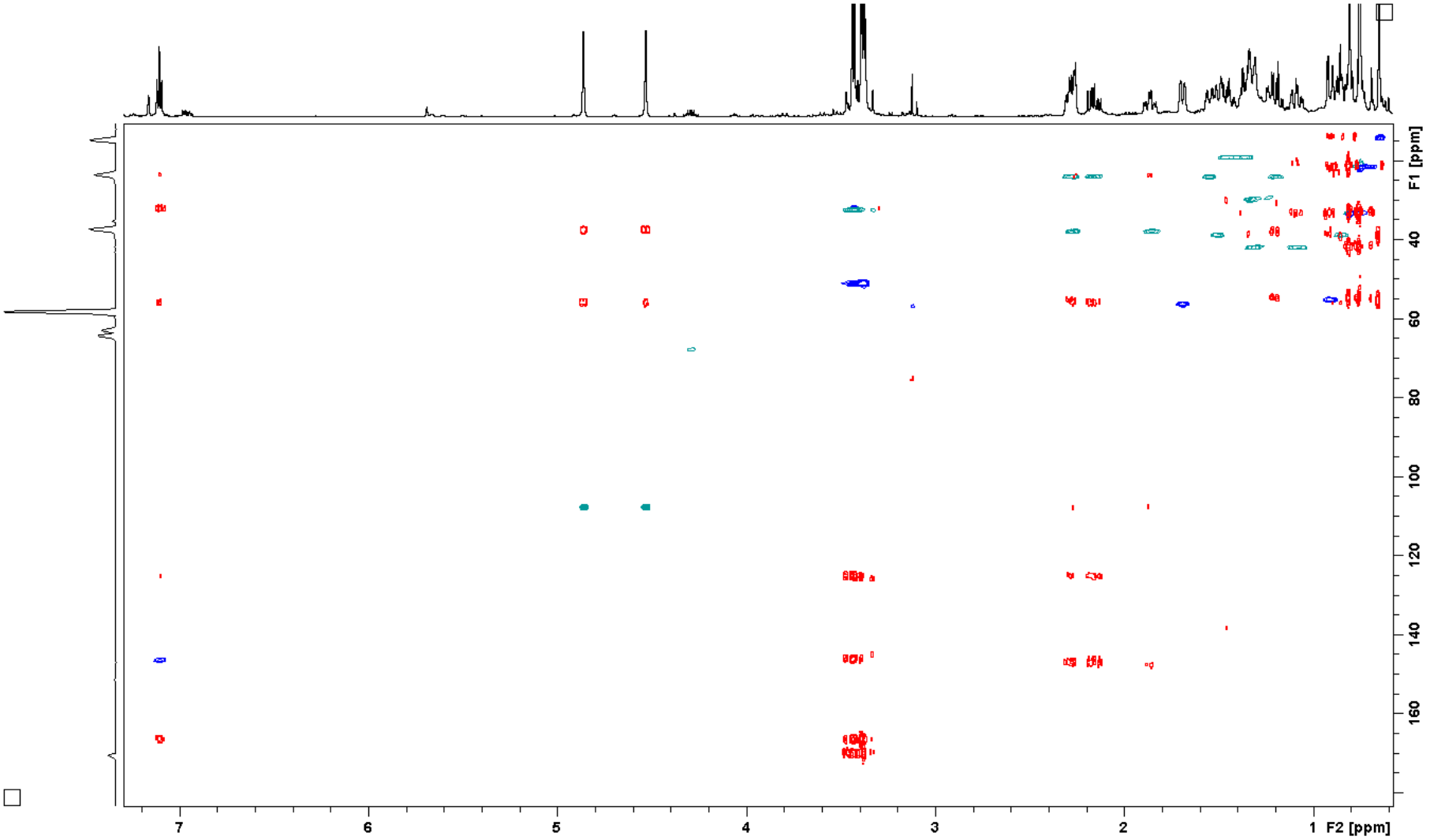

Figure S18. Overlay of HSQC and HMBC NMR spectra of compound **4a** (recorded in C_6D_6).

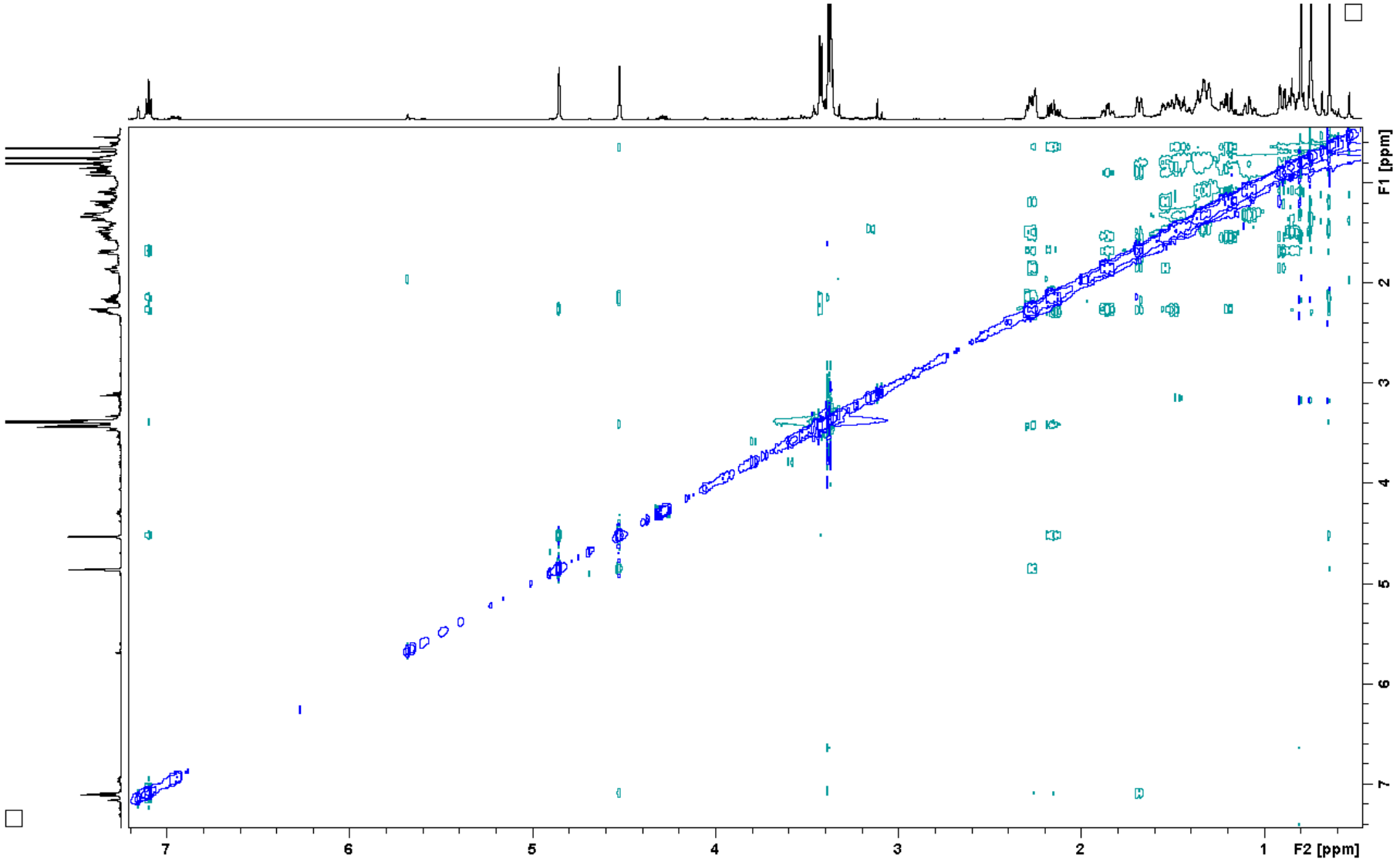

Figure S19. NOESY NMR spectrum of compound **4a** (recorded in C_6D_6).

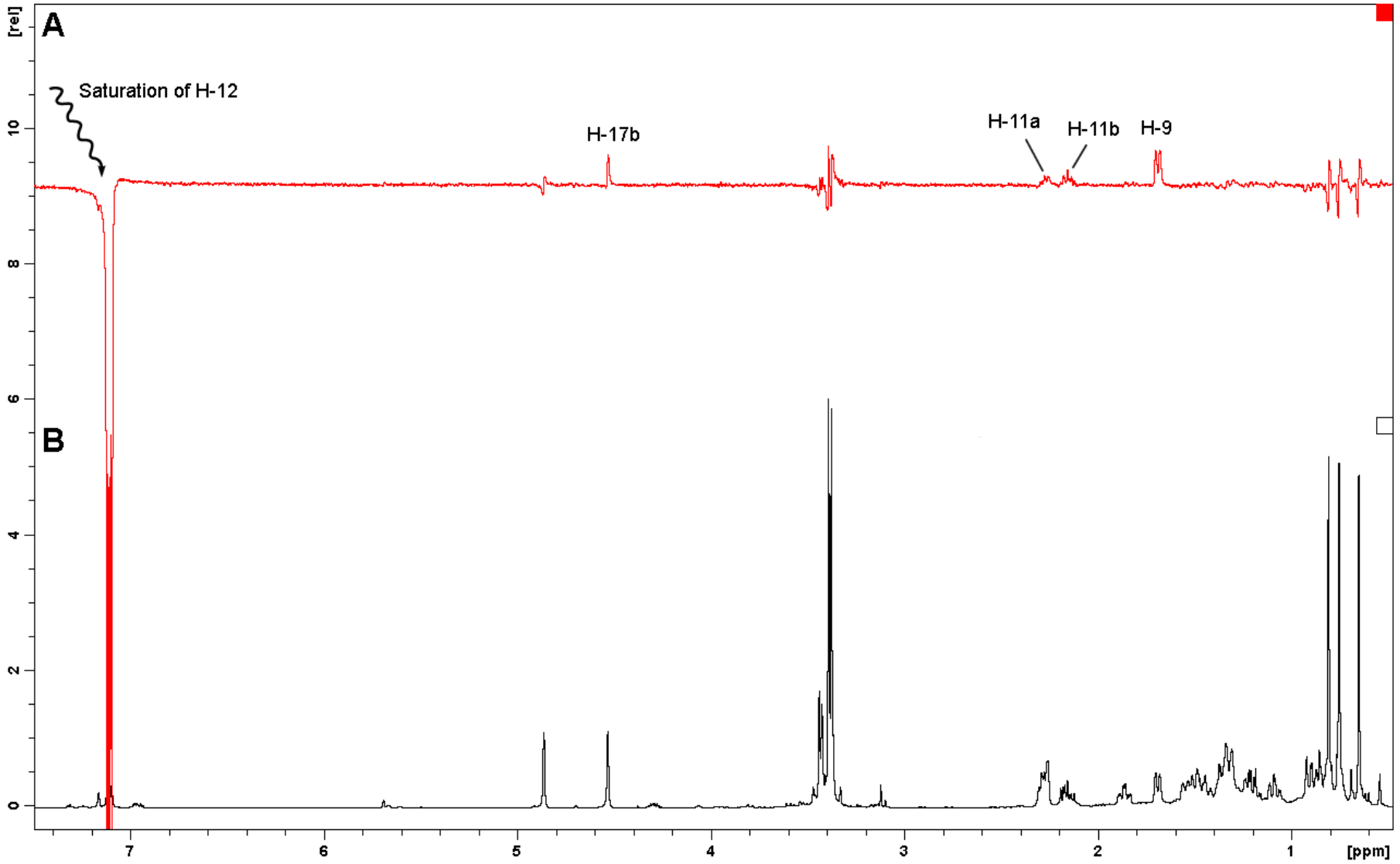

Figure S20. 1D NOE experiment applied to compound **4a** (recorded in C_6D_6). (**B**) The ^{1}H NMR spectrum and (**A**) the NOE difference NMR spectrum are shown. Saturating the H-12 resonance increased the intensities of the signals H-17b, H-11a, H-11b, and H-9.

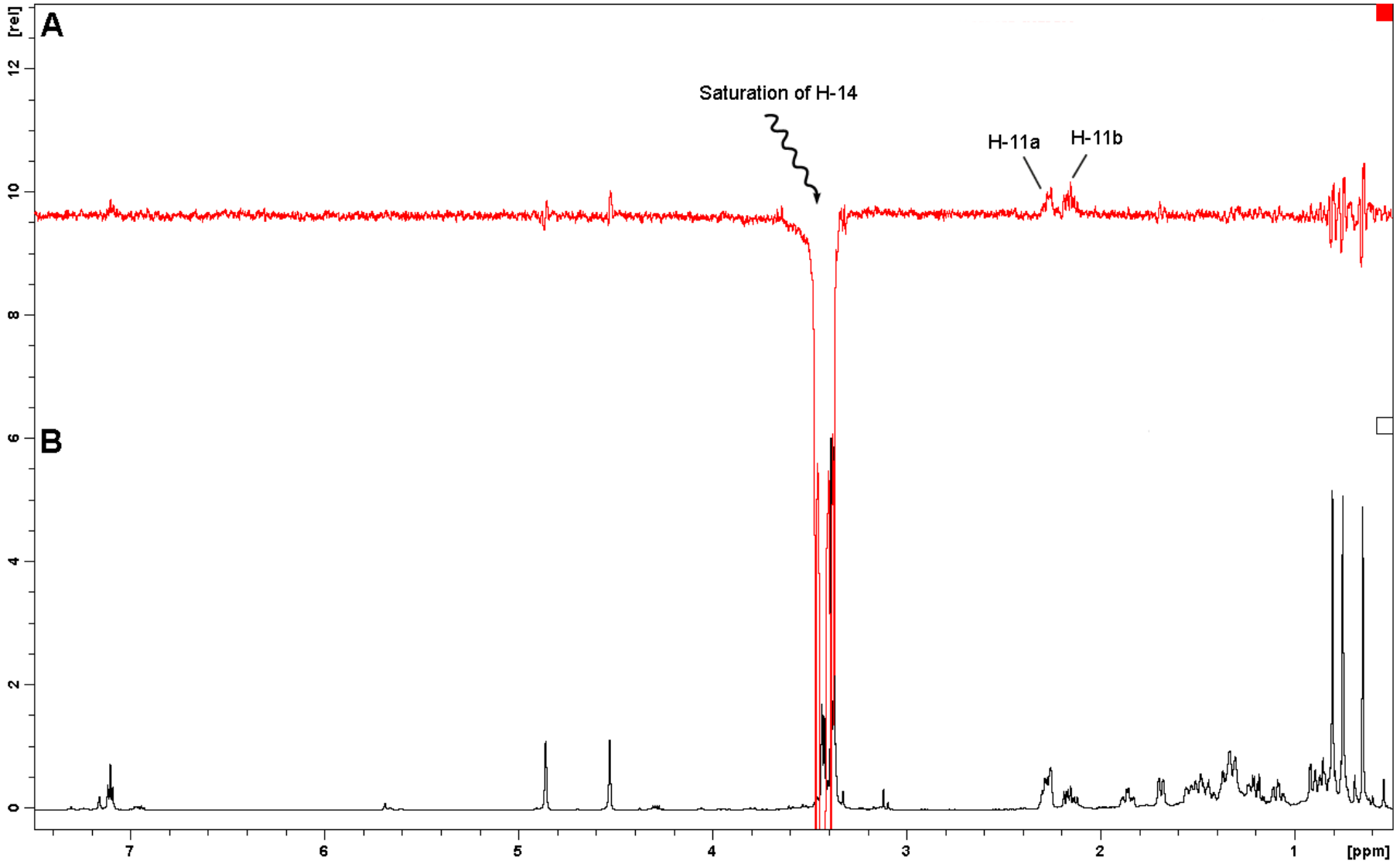

Figure S21. 1D NOE experiment applied to compound **4a** (recorded in C_6D_6). (**B**) The ^{1}H NMR spectrum and (**A**) the NOE difference NMR spectrum are shown. Saturating the H-14 resonance increased the intensities of the signals H-11a and H-11b.

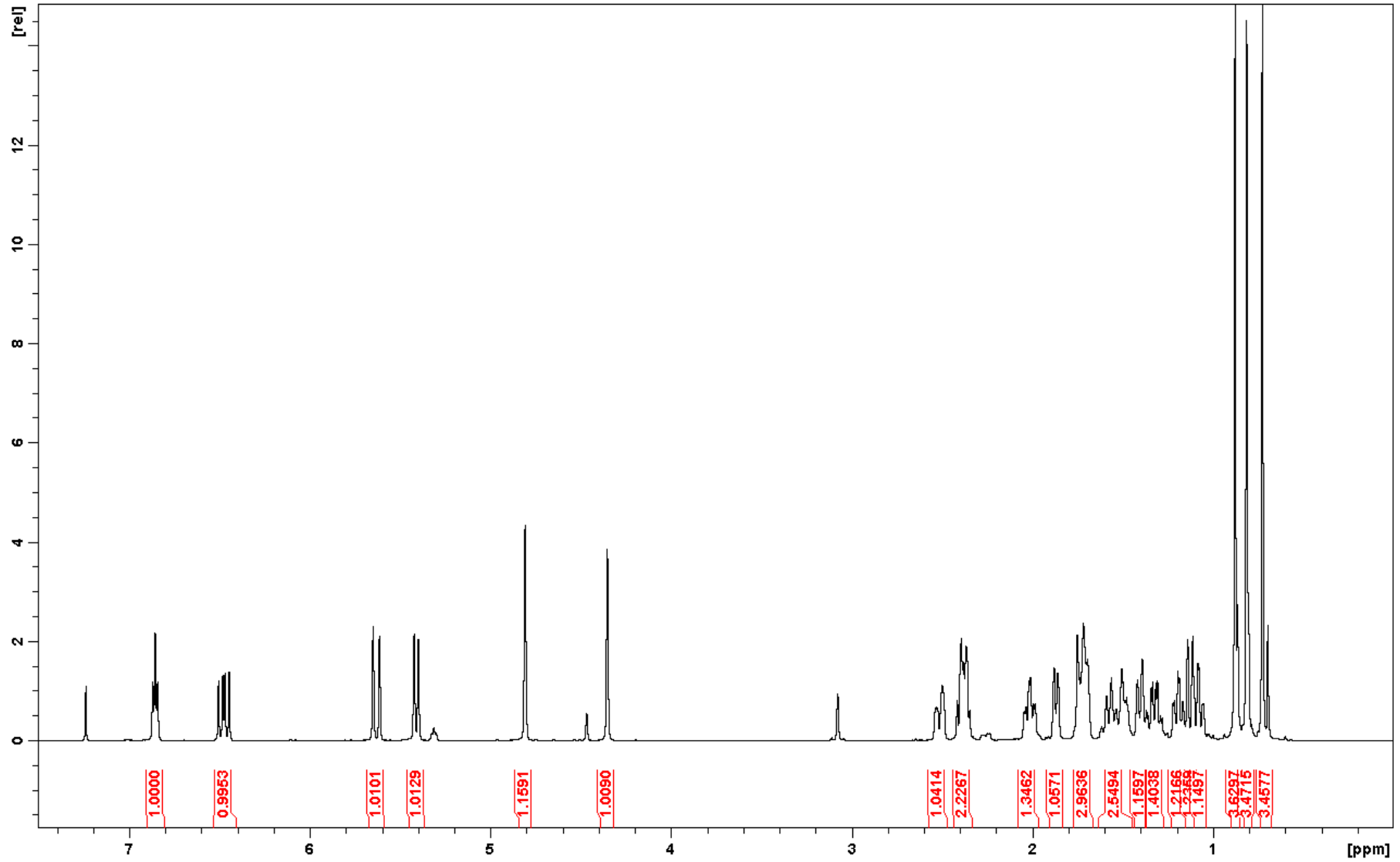

Figure S22. ^{1}H NMR spectrum of compound **9** (with 10% impurity of **10**, recorded in $CDCl_3$).

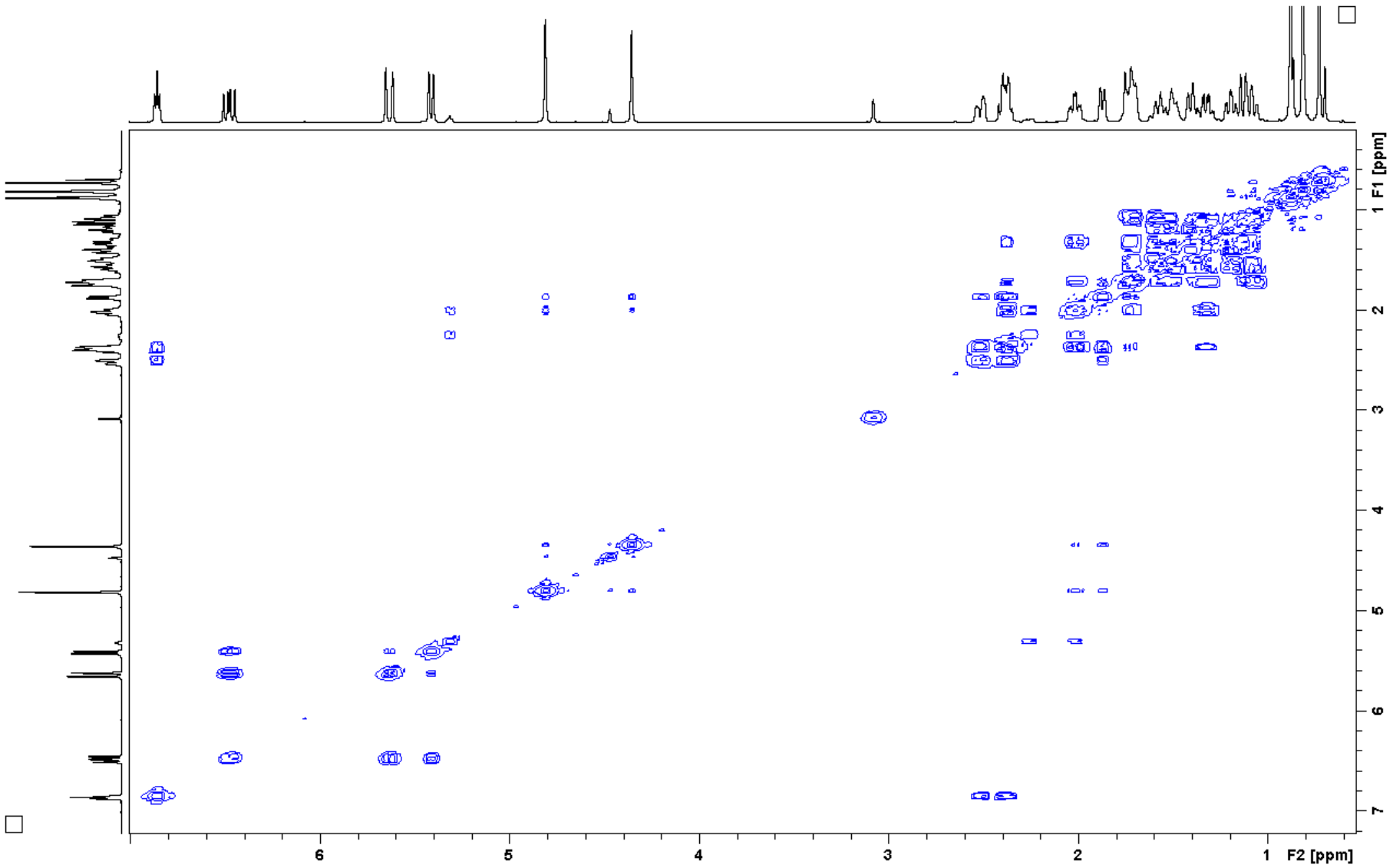

Figure S23. COSY NMR spectrum of compound **9** (with 10% impurity of **10**, recorded in $CDCl_3$).

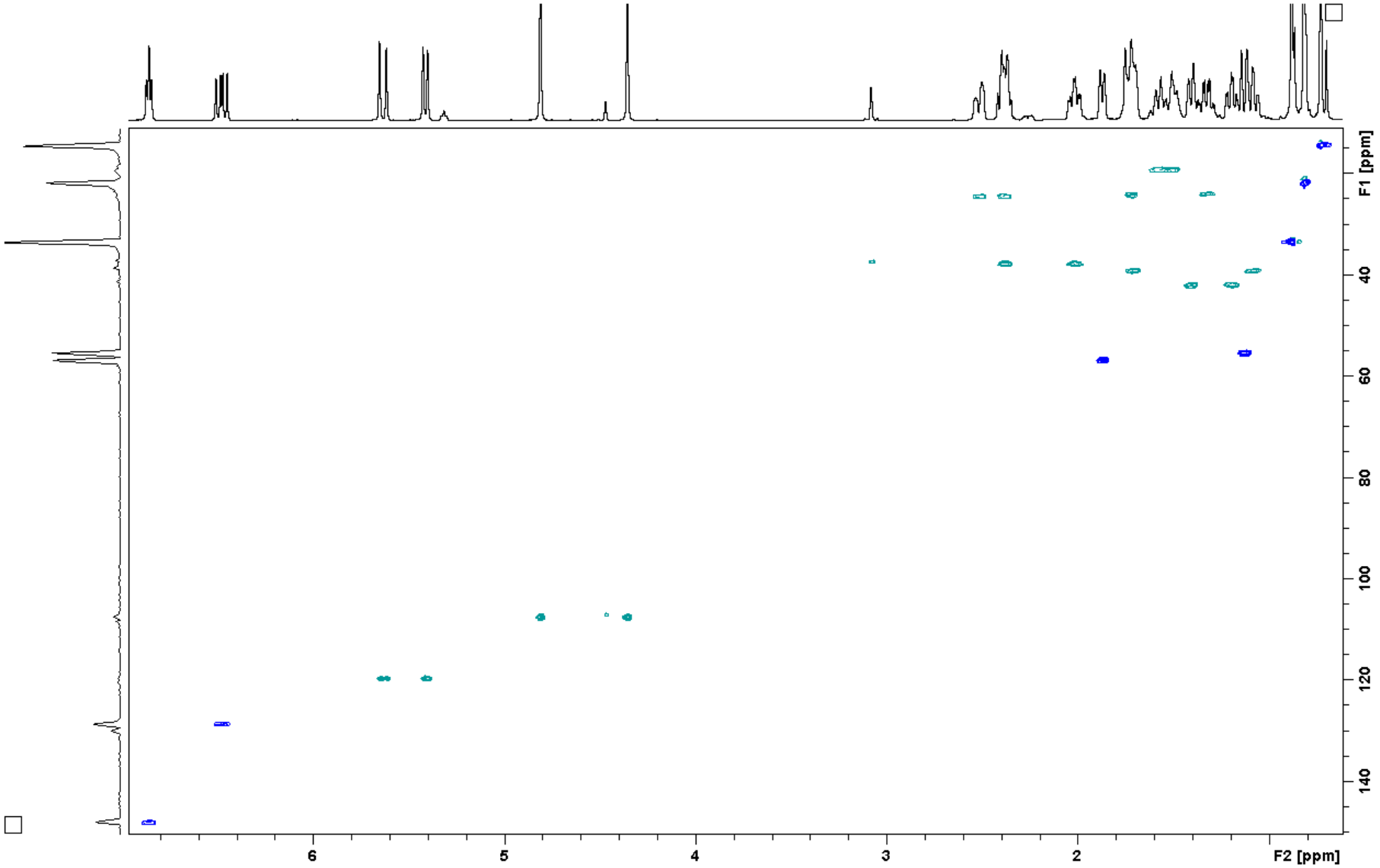

Figure S24. HSQC NMR spectrum of compound **9** (with 10% impurity of **10**, recorded in $CDCl_3$).

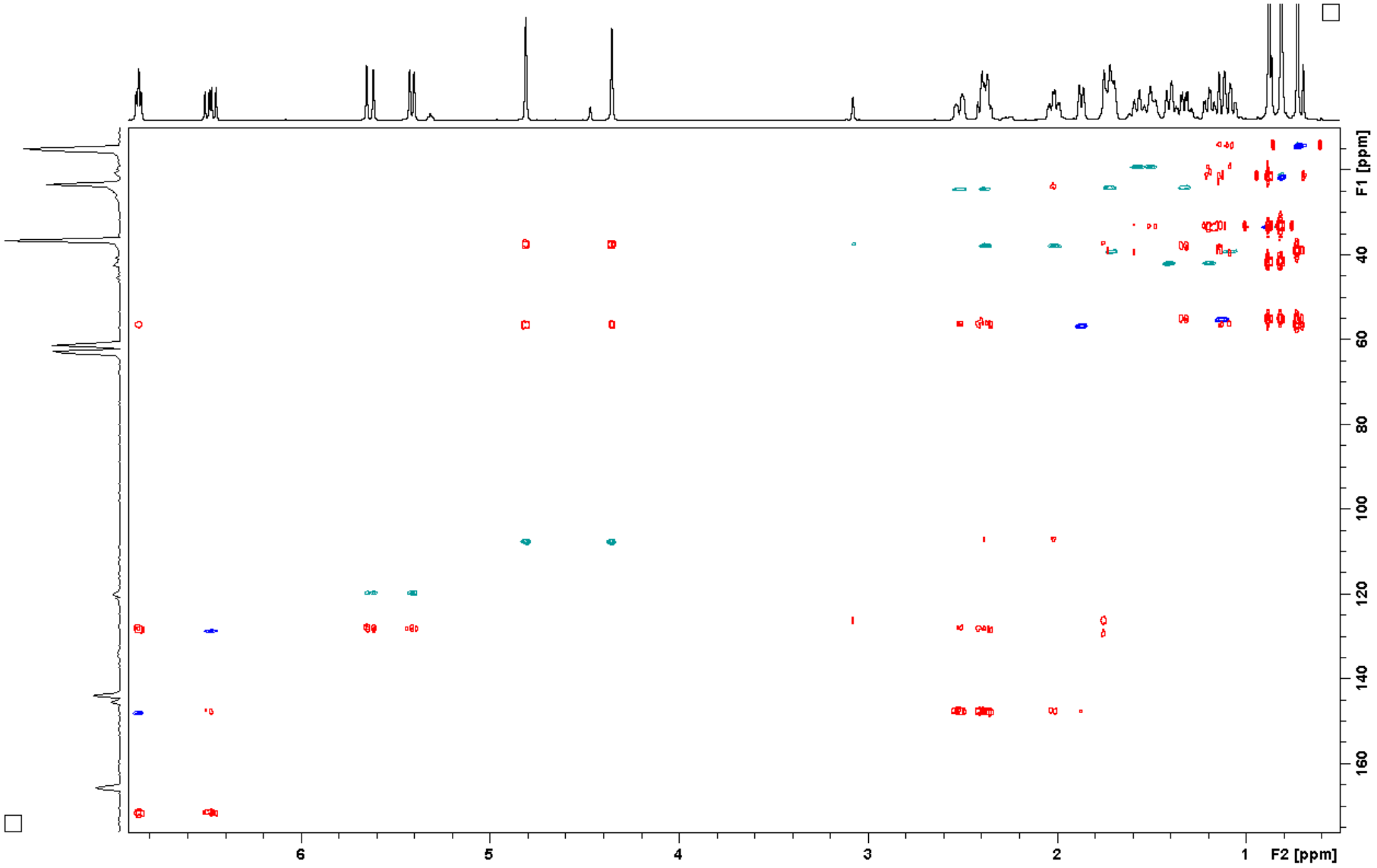

Figure S25. Overlay of HSQC and HMBC NMR spectra of compound **9** (with 10% impurity of **10**, recorded in $CDCl_3$).

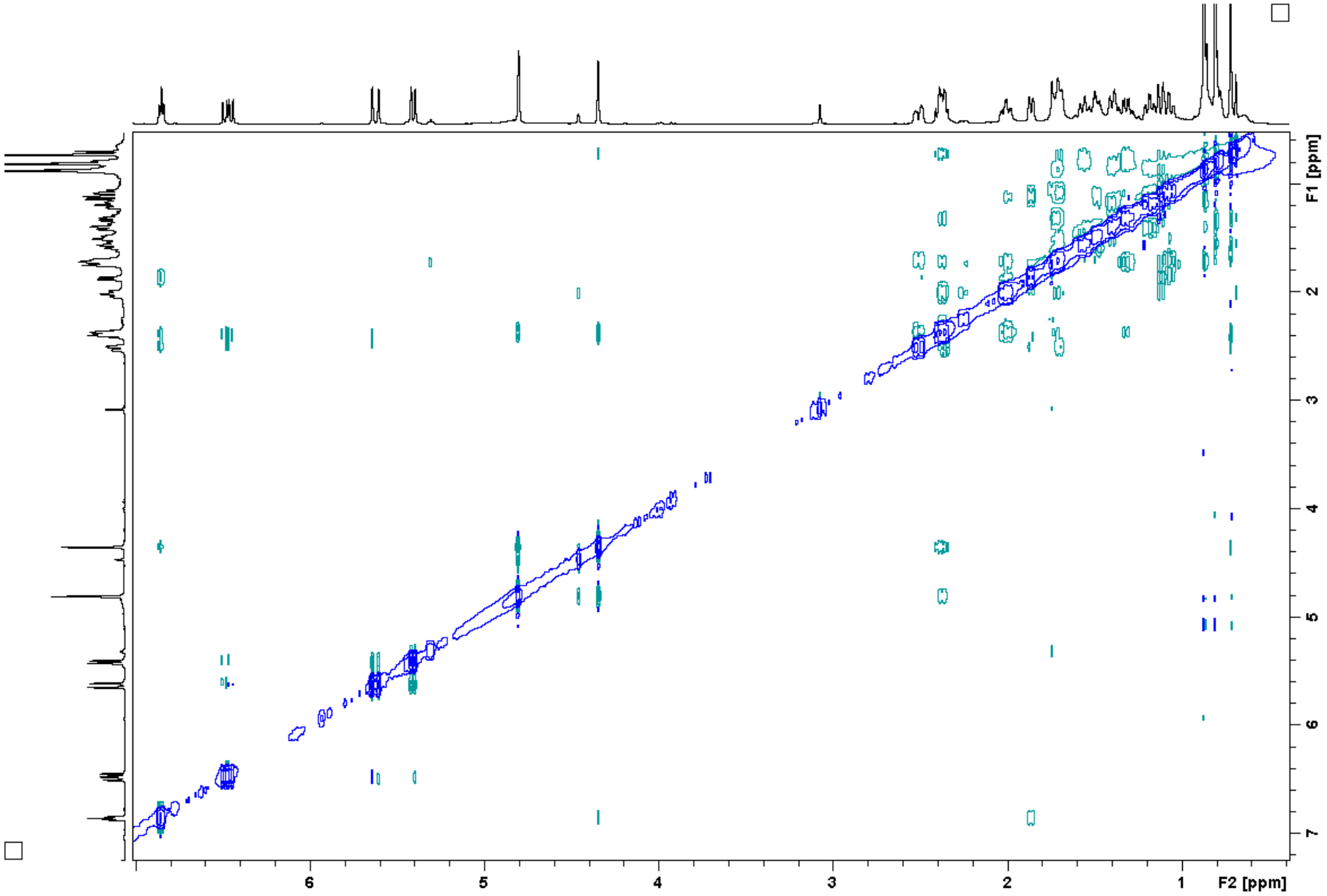

Figure S26. NOESY NMR spectrum of compound **9** (with 10% impurity of **10**, recorded in $CDCl_3$).

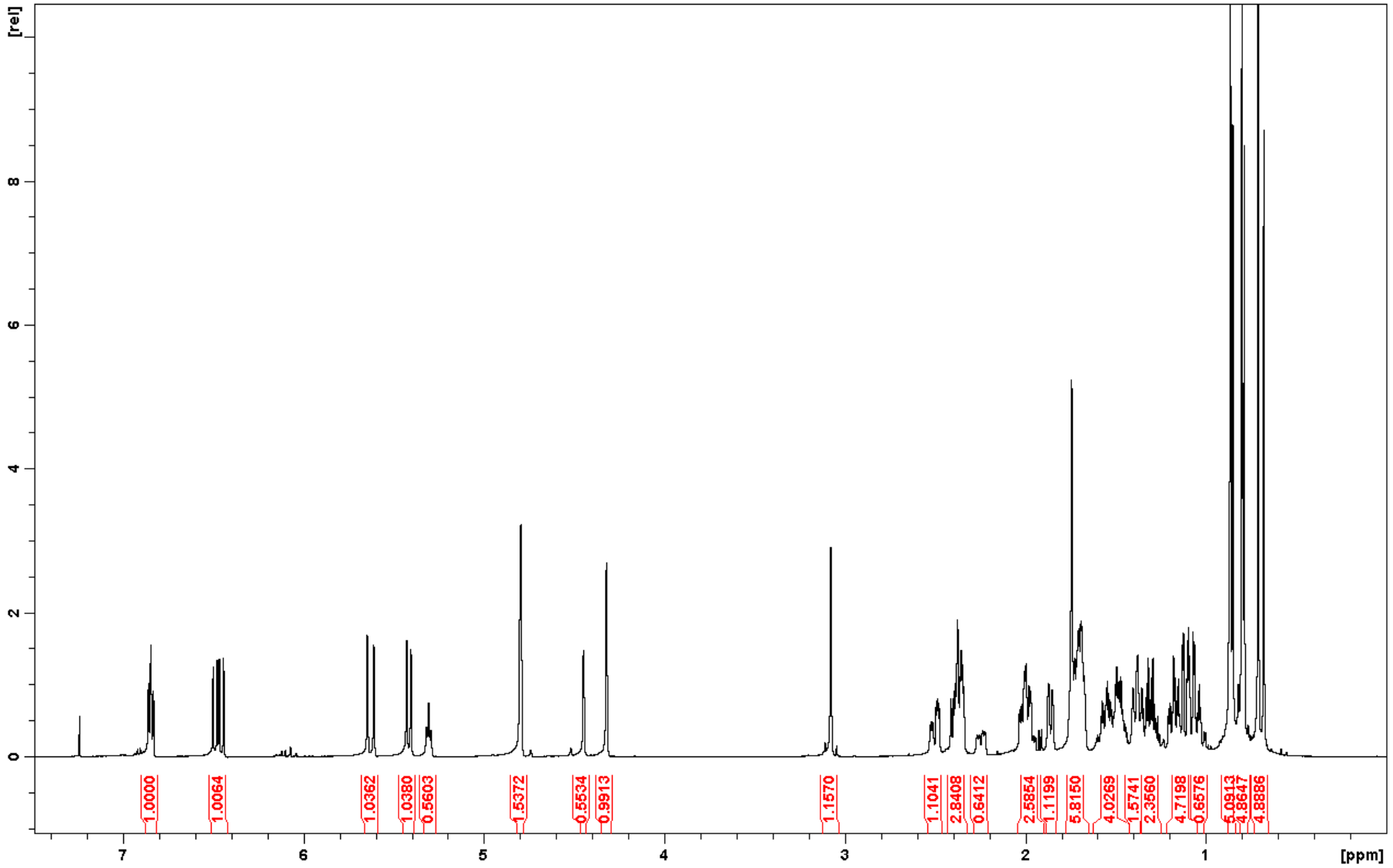

Figure S27. ^{1}H NMR spectrum of the mixture **9**/**10** (existing in a ratio of 64:36, recorded in $CDCl_3$).

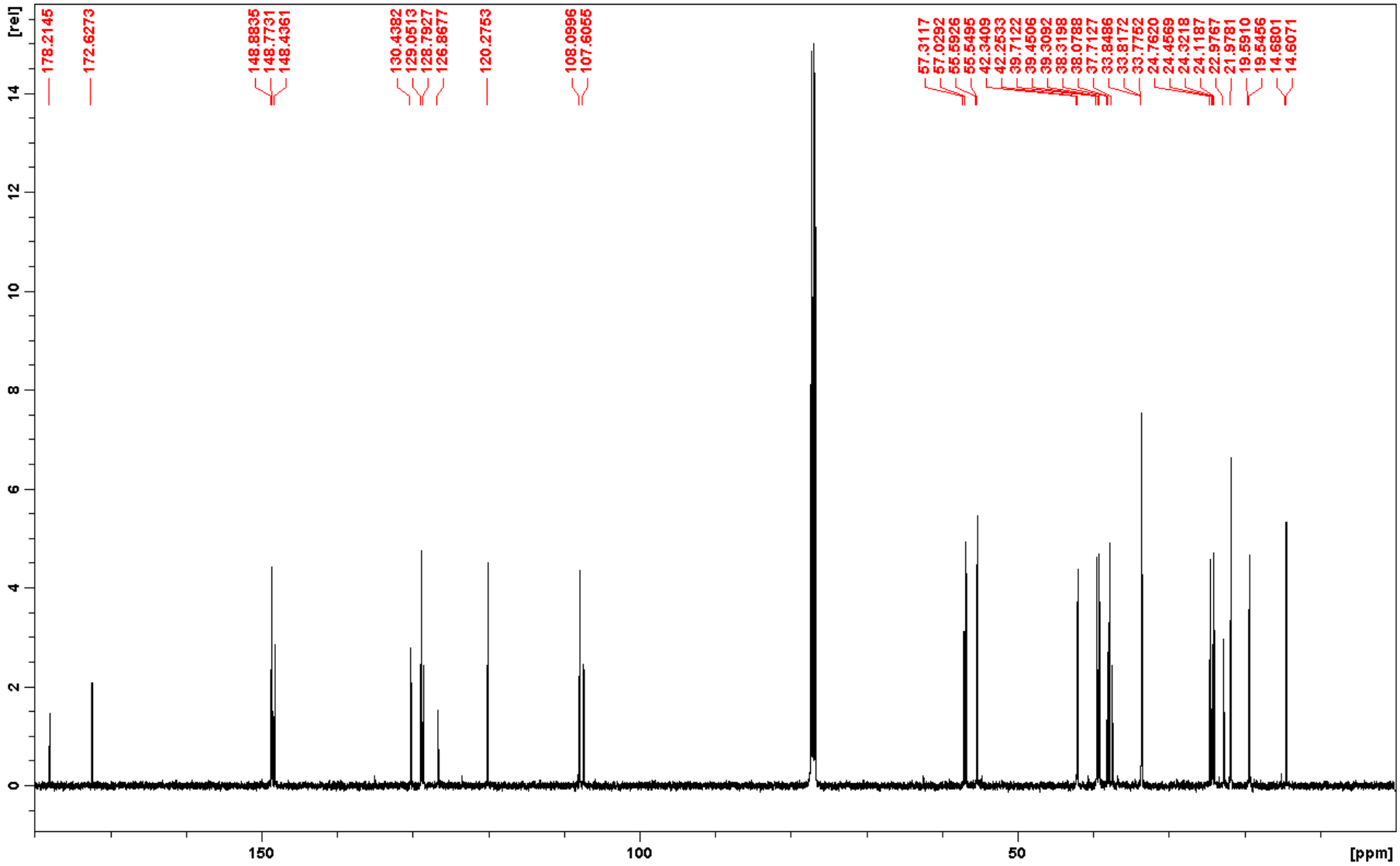

Figure S28. ^{13}C NMR spectrum of the mixture **9**/**10** (existing in a ratio of 64:36, recorded in $CDCl_3$).

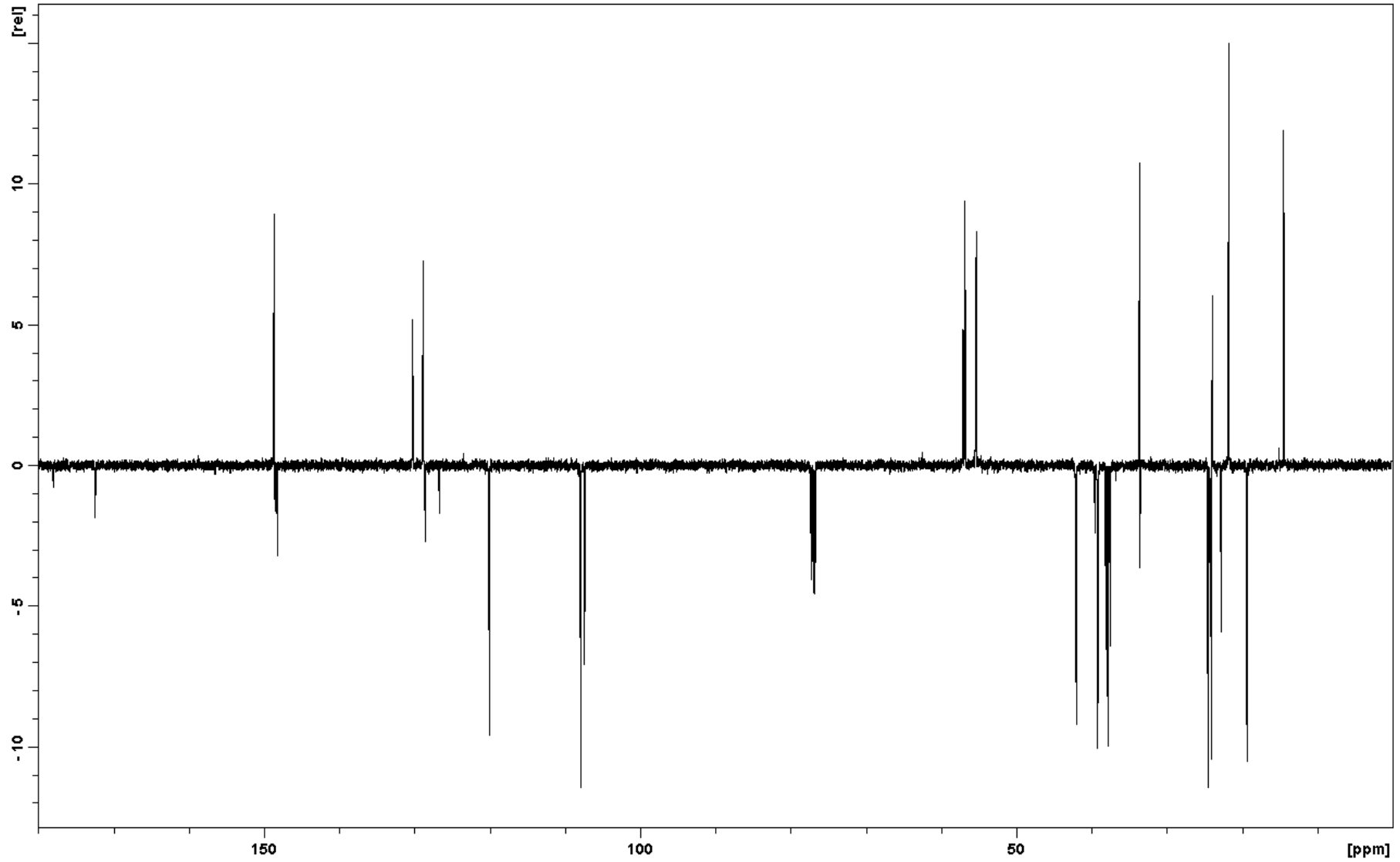

Figure S29. DEPT NMR spectrum of the mixture **9**/**10** (existing in a ratio of 64:36, recorded in $CDCl_3$).

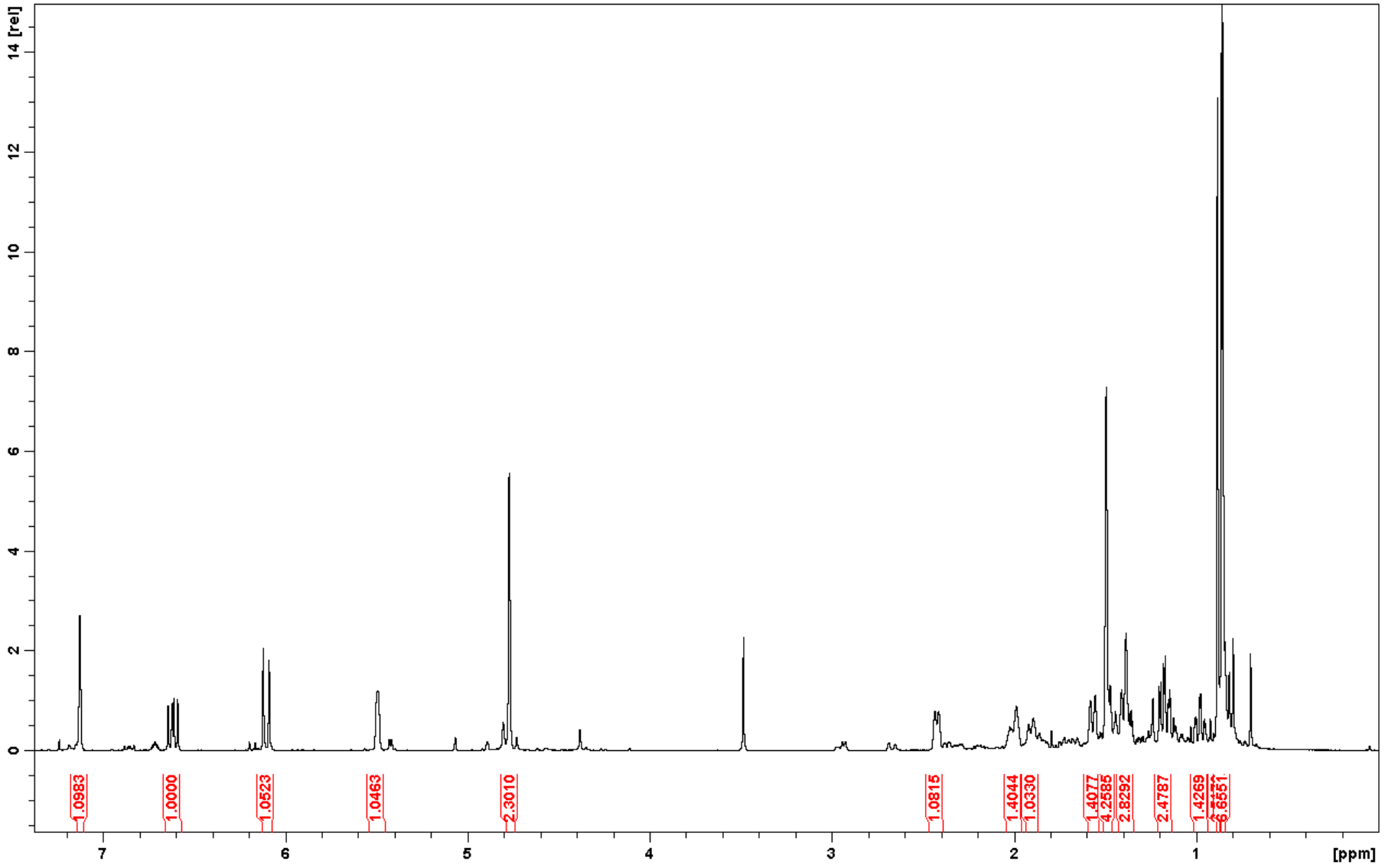

Figure S30. ^{1}H NMR spectrum of compound **11** (with 20% impurity, recorded in $CDCl_3$).

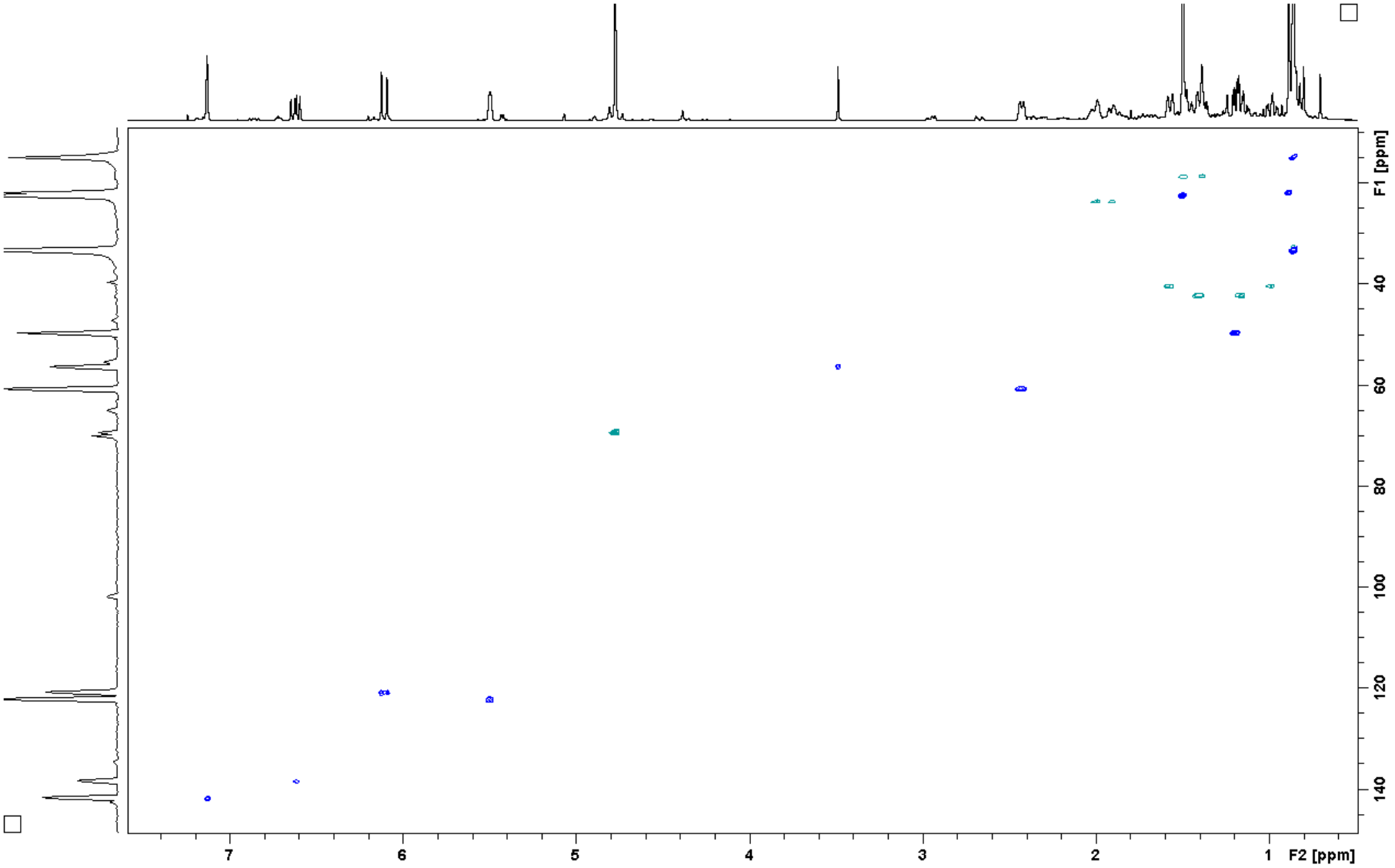

Figure S31. HSQC NMR spectrum of compound **11** (with 20% impurity, recorded in $CDCl_3$).

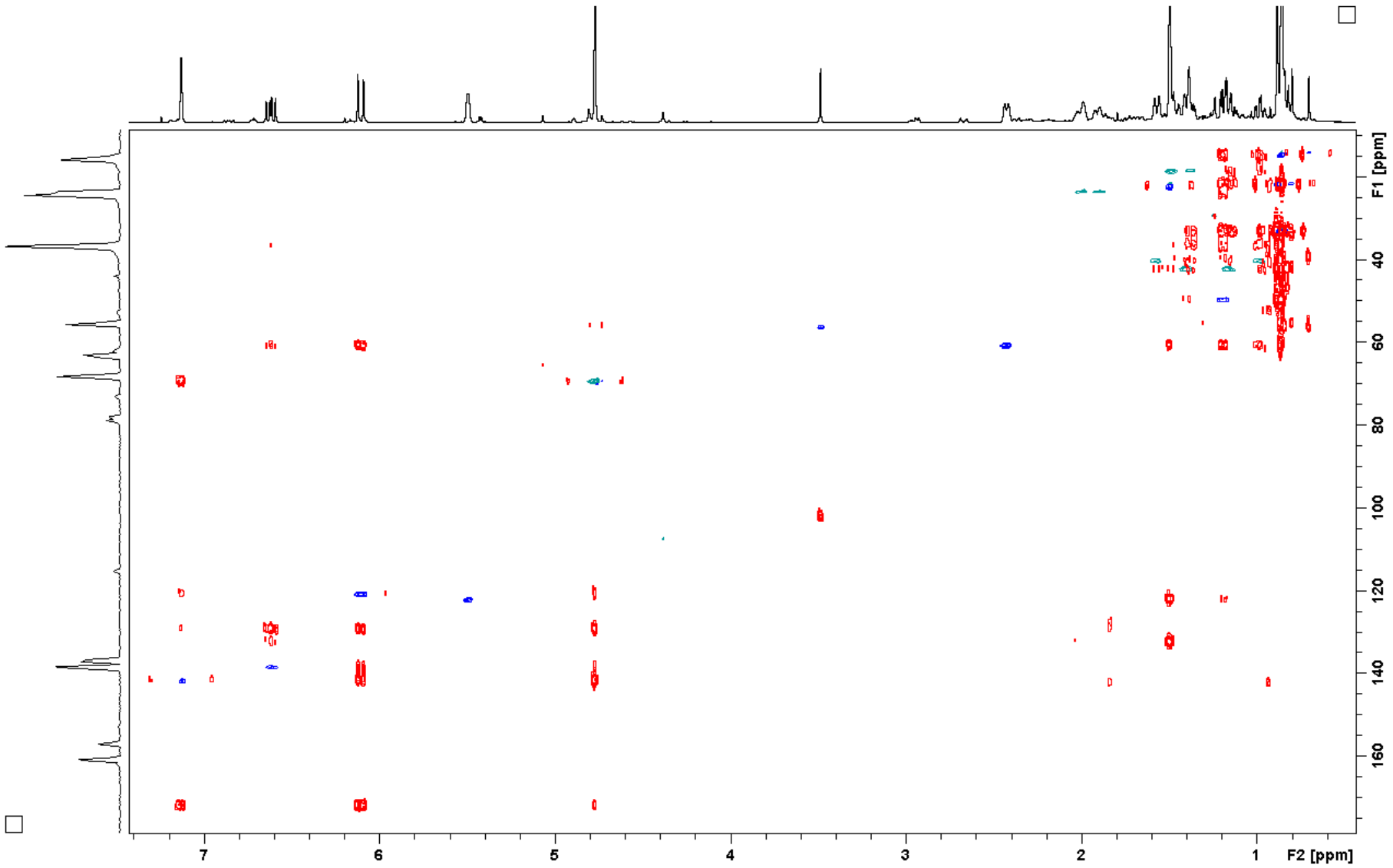

Figure S32. Overlay of HSQC and HMBC NMR spectra of compound **11** (with 20% impurity, recorded in $CDCl_3$).

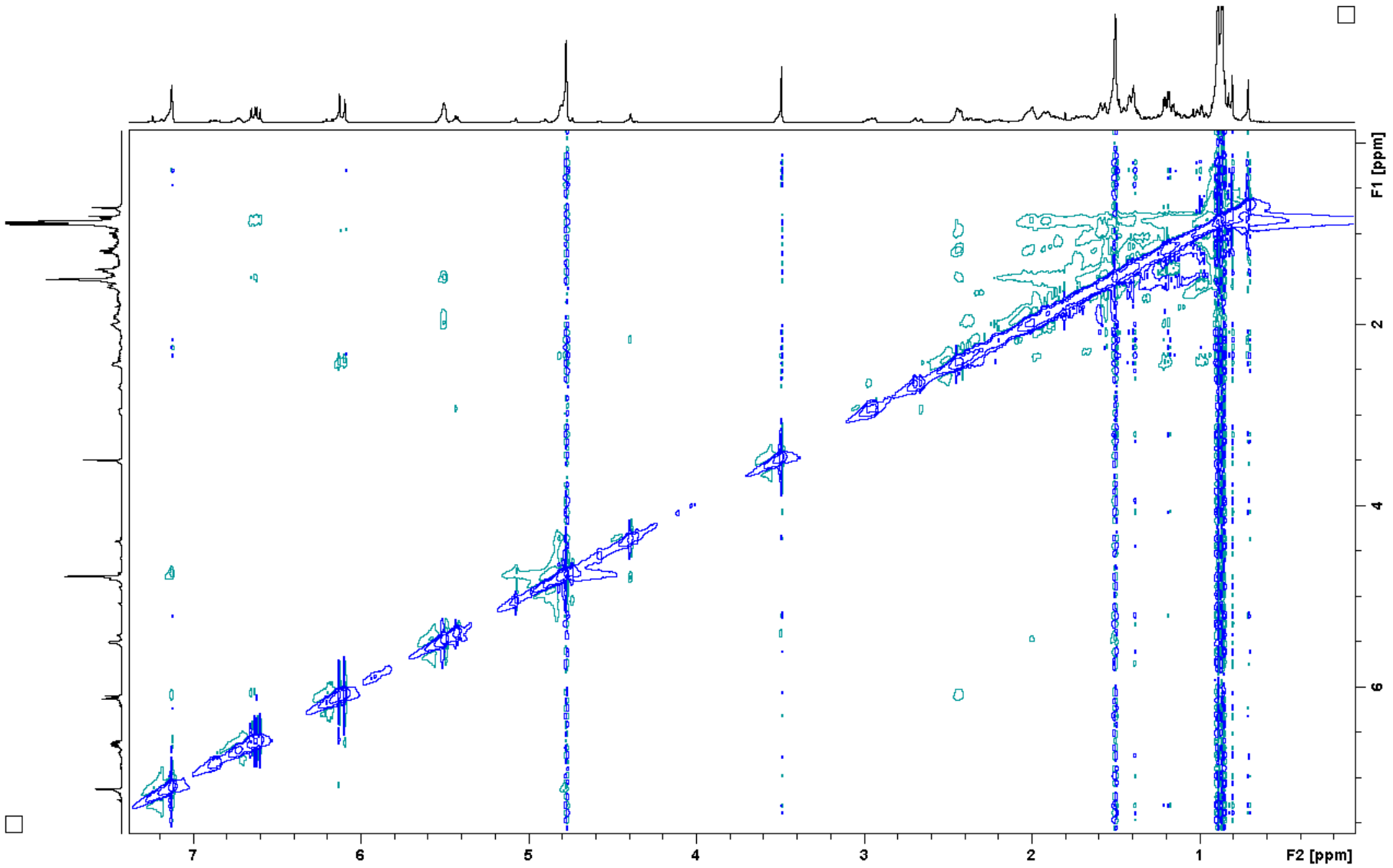

Figure S33. NOESY NMR spectrum of compound **11** (with 20% impurity, recorded in $CDCl_3$).

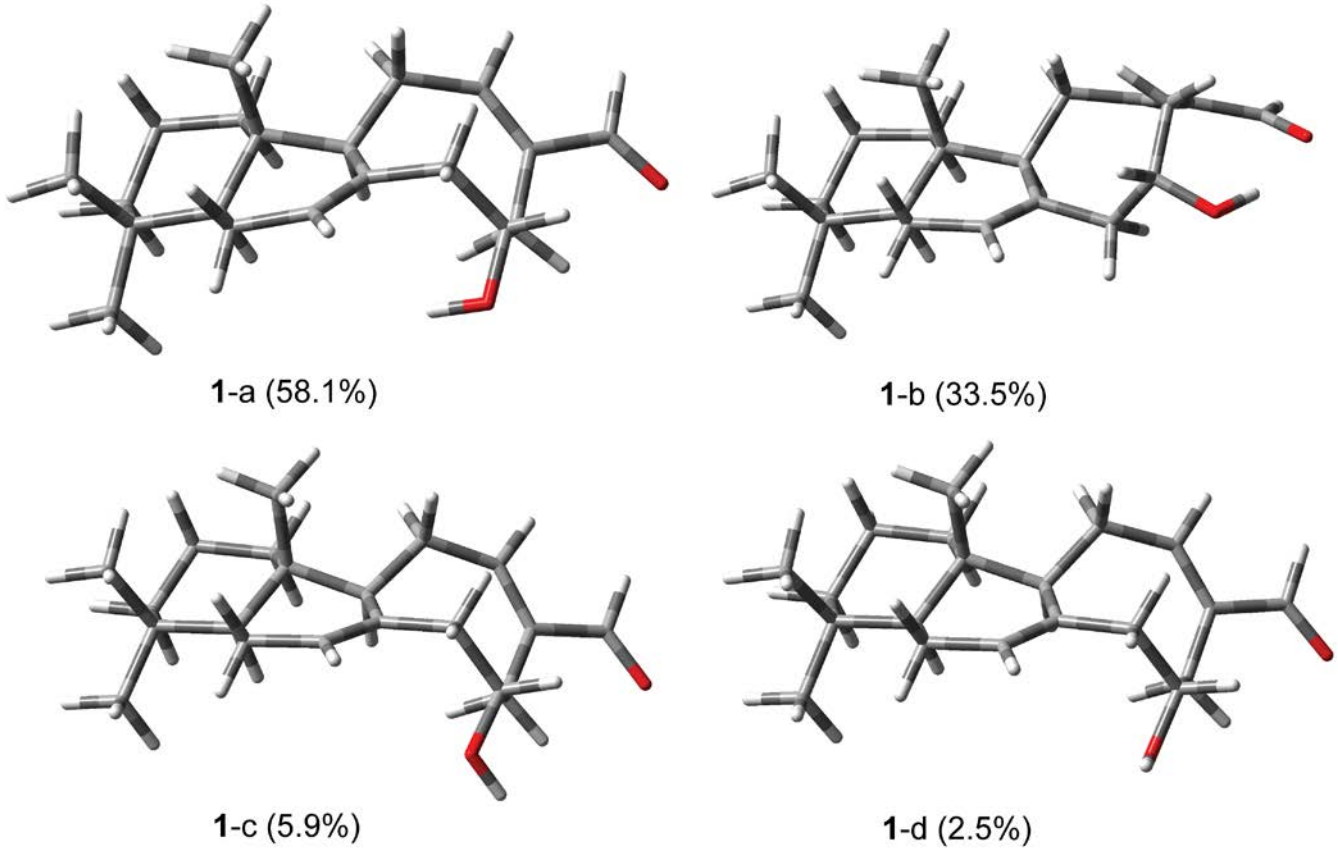

Figure S34. Minimized conformers of (5*S*,9*S*,10*S*,15*R*)-**1** in the gas phase using DFT at the B3LYP/6-31G** level. Four conformers (**1**-a–d) occurred within a 2 kcal/mol range from the global minima.

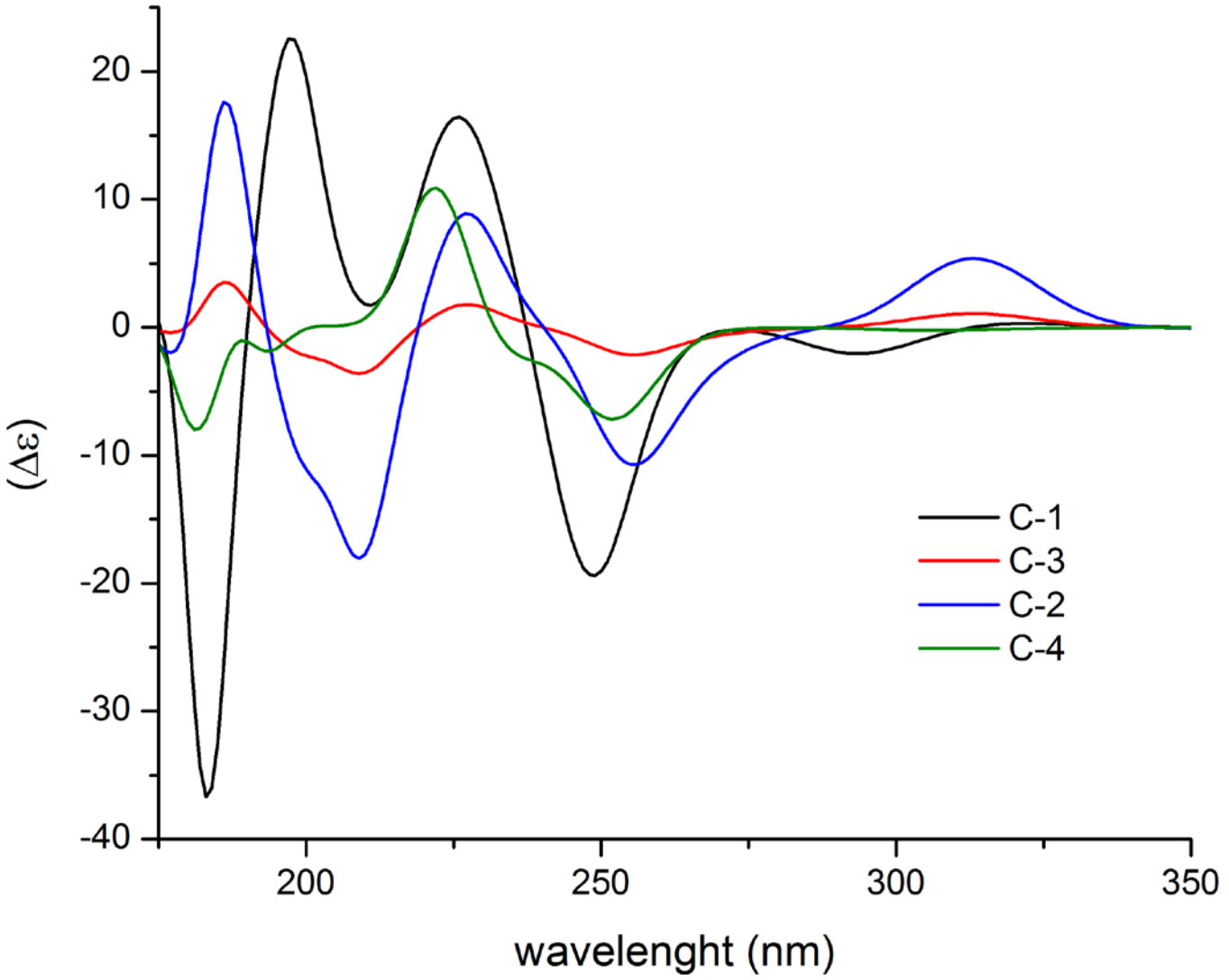

Figure S35. Comparison of the computed ECD spectra for the four lowest energy conformers of (5*S*,9*S*,10*S*,15*R*)-**1**. The calculations were performed with TDDFT at the B3LYP/6-31G(d,p) level using the CPCM solvent continuum model with MeCN as the solvent.

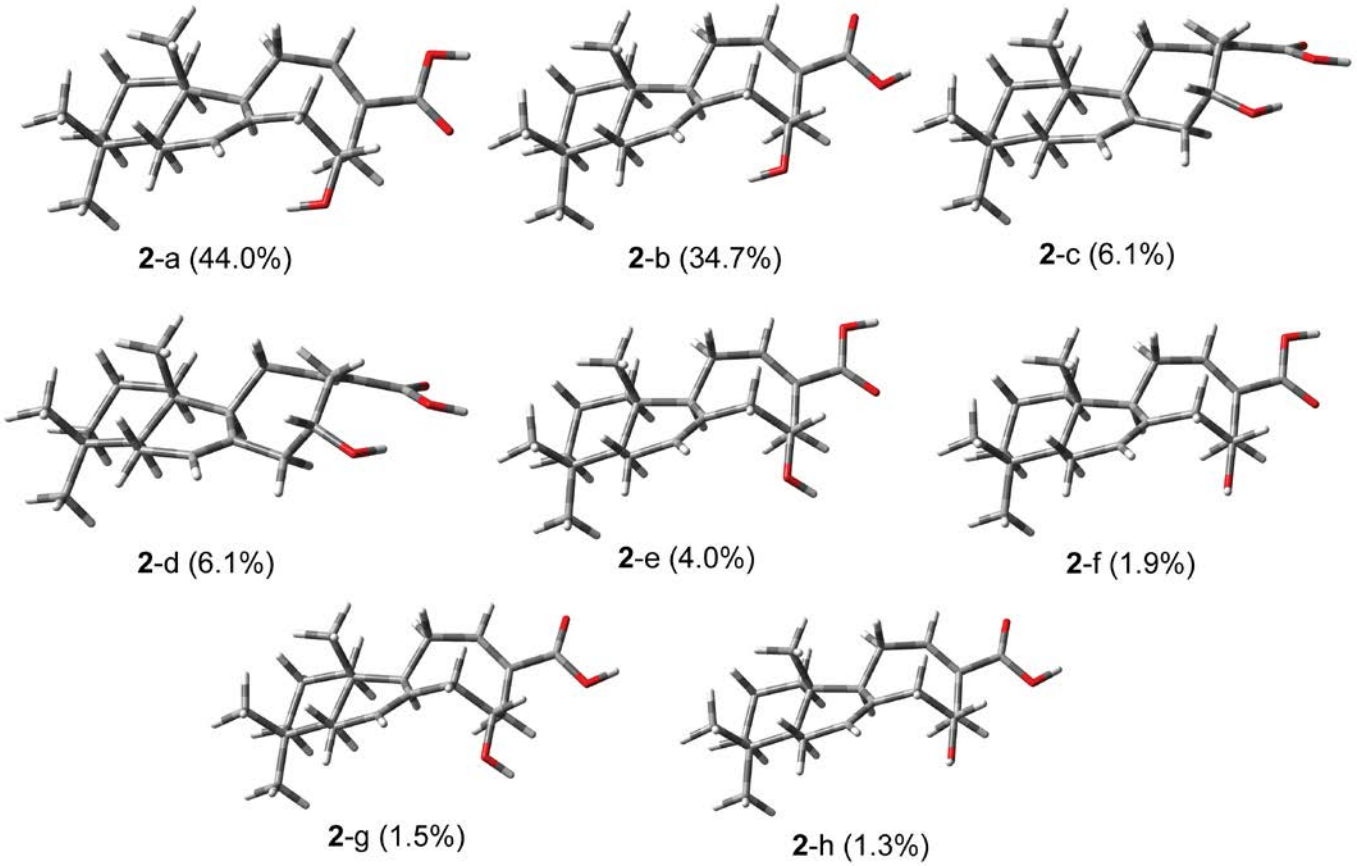

Figure S36. Minimized conformers of (5*S*,9*S*,10*S*,15*R*)-**2** in the gas phase using DFT at the B3LYP/6-31G** level. Eight predominant conformers (**2**-a–h) were found within a 2 kcal/mol range from the global minima.

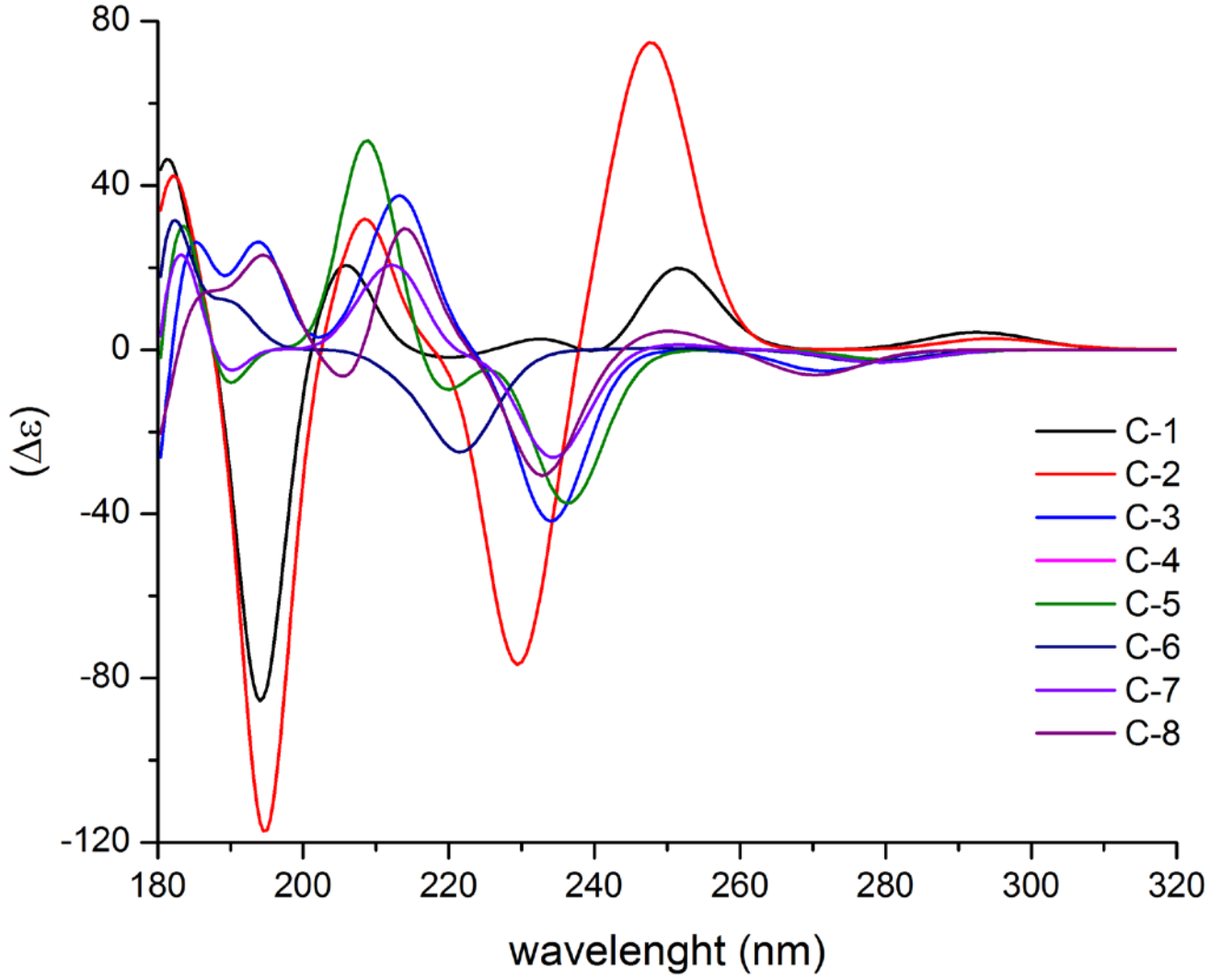

Figure S37. Comparison of the computed ECD spectra for the eight lowest energy conformers of (5*S*,9*S*,10*S*,15*R*)-**2**. The calculations were performed with TDDFT at the B3LYP/6-31G(d,p) level using the CPCM solvent continuum model with MeCN as the solvent.

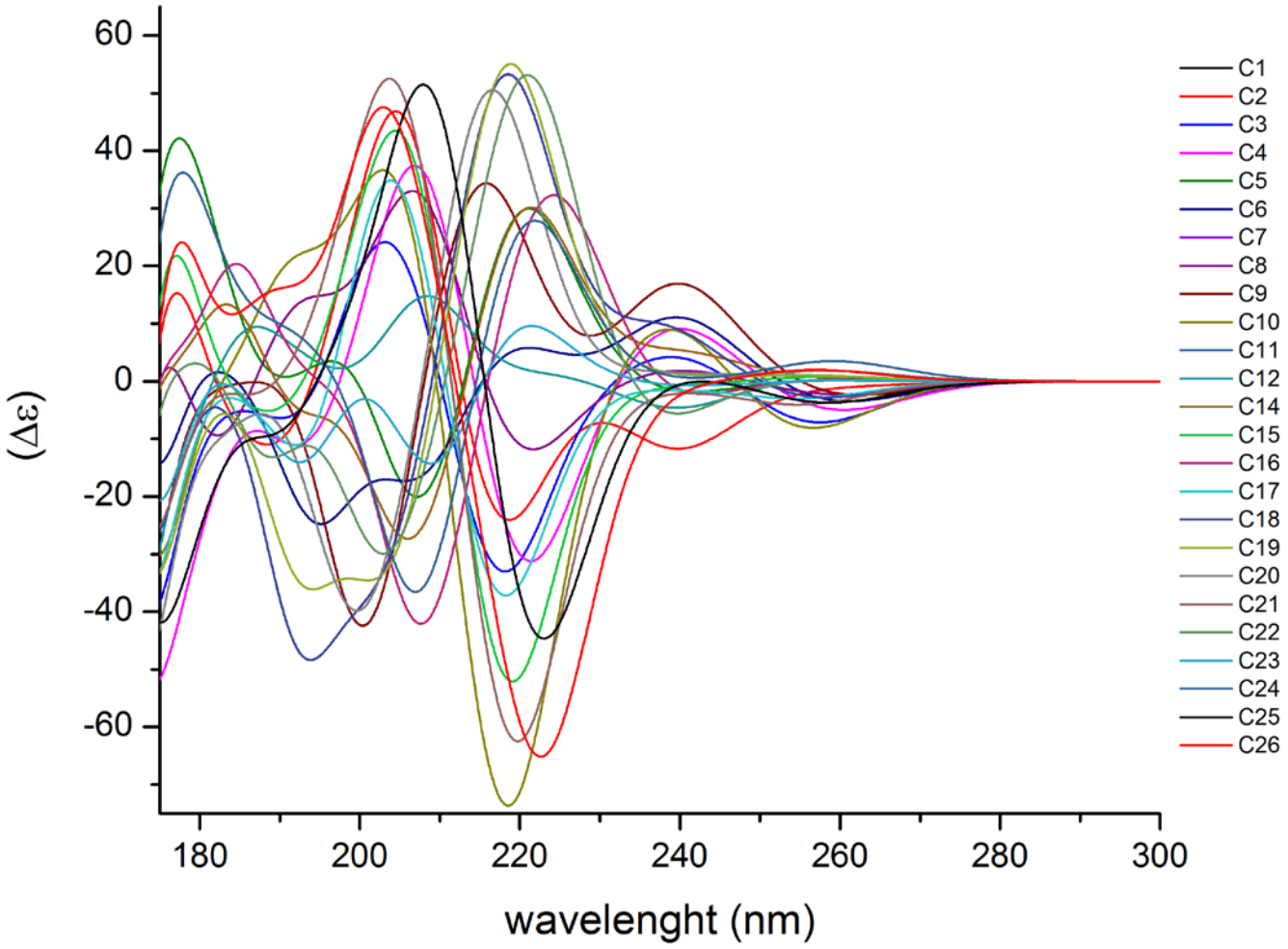

Figure S38. Comparison of the computed ECD spectra for the 26 lowest energy conformers of (5*S*,9*S*,10*S*)-**4**. The calculations were performed with TDDFT at the B3LYP/6-31G(d,p) level using the CPCM solvent continuum model with MeCN as the solvent.

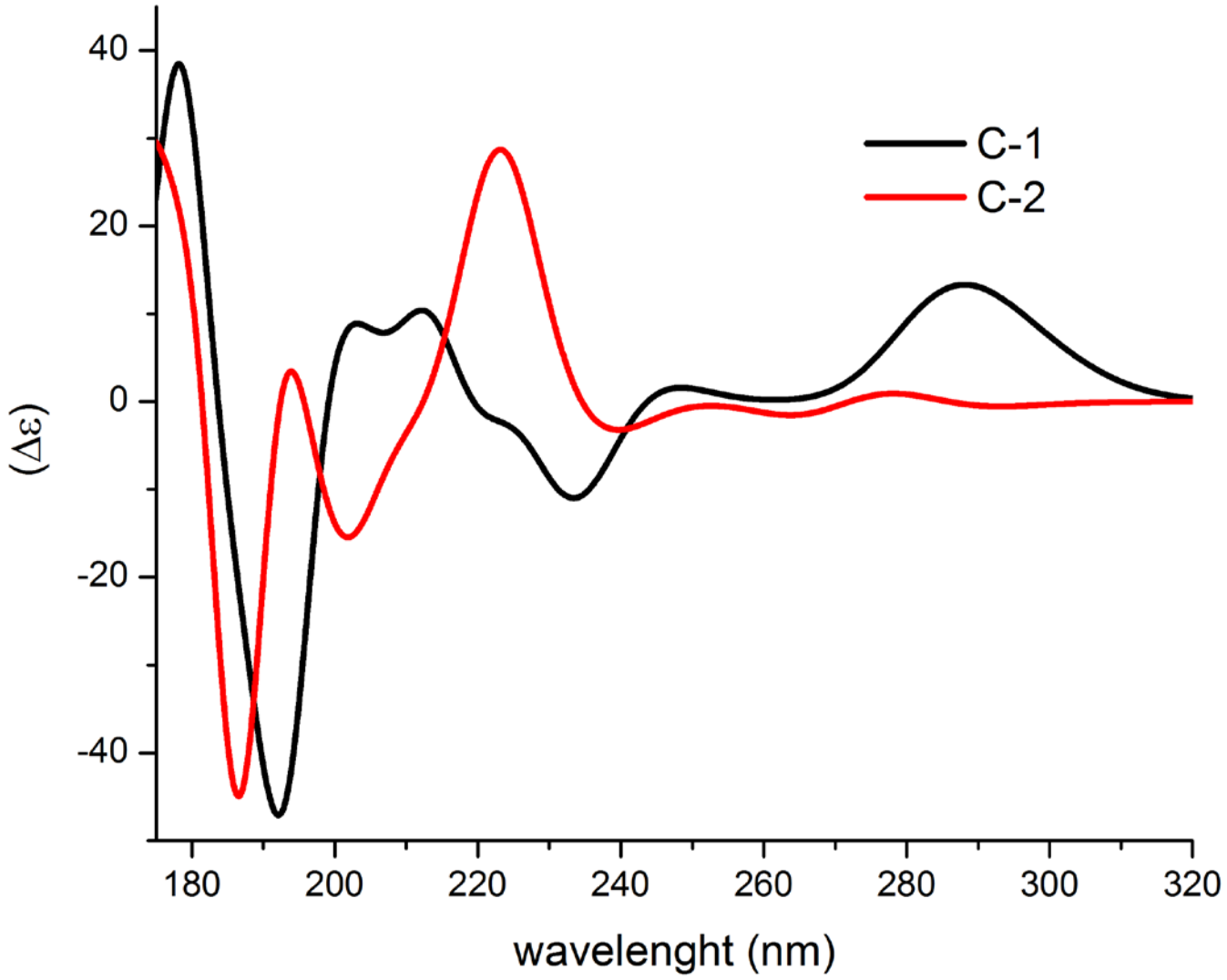

Figure S39. Comparison of the computed ECD spectra for the two low-energy conformers of (5*S*,9*S*,10*S*)-**8**. The calculations were performed with TDDFT at the B3LYP/6-31G(d,p) level using the CPCM solvent continuum model with MeCN as the solvent.

4. Conclusions and outlook

In the course of an interdisciplinary hERG *in vitro* screening, major European medicinal plants as well as frequently consumed spices, vegetables, and fruits were found to be associated with a low risk for hERG inhibition. Subsequent screening of a plant-derived alkaloid library led, however, to the identification of potent hERG blockers, including (+)-*N*-methyllaurotetanine (**1**), (+)-boldine (**2**), (+)-bulbocapnine (**3**), (+)-chelidonine (**4**), (+)-corynoline (**5**), and protopine (**6**) (Figure 10). Pronounced hERG *in vitro* inhibition is a major cardiac safety liability, but cannot be

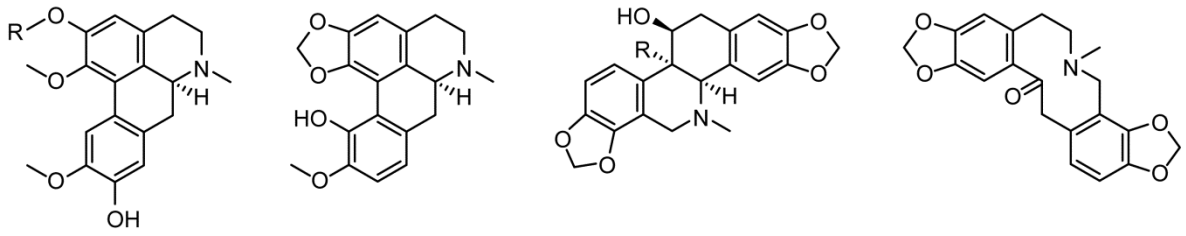

Figure 10. Structures of plant-derived hERG channel blockers.

directly translated to an increased risk of QT prolongation and TdP arrhythmia. Follow-up investigations should primarily focus on *in vitro* electrophysiological studies to determine whether the identified hERG blocking alkaloids also inhibit other cardiac ion currents and affect the ventricular action potential duration. If the results point towards potential cardiotoxic risks, an assessment of the cardiac safety in correlation with pharmacokinetic data is certainly warranted. The pro-arrhythmic liability of a single hERG blocker needs to be evaluated in a predisposed model that utilizes either the occurrence of early afterdepolarizations (EADs) or TdP arrhythmia as study endpoint. In parallel, one should determine the compound's pharmacokinetic profile and identify its main metabolites. The development of a state-of-the-art bioanalytical method (e.g., an UPLC-MS/MS assay) and its full validation according to recommendations of international

guidelines is crucial to generate reliable pharmacokinetic data. It has to be further considered that most herbal preparations are used in form of infusions or decoctions for oral consumption. Potential hERG-related safety aspects should, therefore, be assessed with the expected clinical route of administration. A dedicated human trial in healthy volunteers will clarify what kind of free plasma concentrations of these alkaloids will be reached after regular dosing of their corresponding herbal products. Similar considerations should be also applied to already known plant-derived hERG inhibitors. Our literature survey revealed that chelerythrine (**7**) and lobeline (**8**) (Figure 11) strongly reduce the hERG channel activity in HEK293 cells with IC_{50} values of 0.11 and 0.34 µM, respectively. Our screening of medicinal plants pointed towards a need for a more thorough assessment of the hERG liability of traditional Chinese herbal drugs. Given the increasing popularity of herbal remedies from other traditional health systems, also Ayurveda, Kampo, and Unani herbal drugs should be screened.

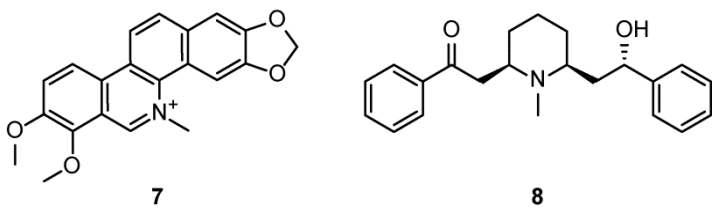

Figure 11. Structures of chelerythrine (**7**) and lobeline (**8**).

The availability of gram amounts of pharmacologically/toxicologically critical compounds is an essential prerequisite for further risk assessment studies. Dehydroevodiamine (DHE), a major bioactive constituent of the traditional Chinese herbal drug Evodiae fructus (*Evodia rutaecarpa* fruits), is currently being investigated in different *in vivo* models for cardiac safety. For this purpose, we developed an efficient two-step protocol for its gram-scale isolation from a crude *E. rutaecarpa* extract. Our purification strategy can be further used as a starting point for a future commercialization of DHE as reference compound. Access to DHE in high purity (> 95%) is particularly useful for the quality control of *Evodia*-containing products.

In the search for positive $GABA_A$ receptor modulators of plant origin, we investigated an ethyl acetate extract from rhizomes of *Curcuma kwangsiensis*. An HPLC-based discovery platform was used to identify the active constituents in the extract. Targeted isolation afforded a series of 11 structurally related labdane diterpenoids, which were then pharmacologically characterized at $GABA_A$ receptors of the $\alpha_1\beta_2\gamma_{2S}$ subtype. The tested diterpenes have, however, limited potential for further development due to their moderate $GABA_A$ receptor modulating activity. Intensive medicinal chemistry efforts will be necessary to develop a lead candidate with higher efficiency. Our study demonstrates that HPLC-based activity profiling, combined with database searches, is an effective strategy to characterize bioactive compounds in crude natural extracts.

Acknowledgments

My sincere thanks go to my thesis advisor Prof. Dr. Matthias Hamburger for giving me the opportunity to join his excellent research group and to dive into the fascinating world of plant-derived natural products. I am deeply grateful for his seemingly limitless dedication, constant encouragement, and support. Over the years, I could always count on his advices and feedback on my work.

I also would like to express my gratitude to Prof. Dr. Judith Maria Rollinger for being the co-referee of my PhD thesis. Her review as the coordinator and project leader of the EU project "hERGscreen: hERG related risk assessment of botanicals" was a great honor for me.

I am immensely thankful to my family, friends, and colleagues, as without their support and input, this work would not have been possible! Each and every one of them has broadened my mind in a different way and, hence, made a decisive contribution to this thesis.

I am very grateful to Dr. Samad Ebrahimi for his extraordinary enthusiasm about natural product chemistry and his dedication to share his profound knowledge with all of us. It gives me also a great pleasure to acknowledge his professional computer skills and technical expertise. I truly appreciate all the discussions we have had on both science and life.

Ganz besonders danke ich meinen früheren Kolleginnen Dr. Janine Zaugg und Dr. Melanie Raith, die beide immer ein offenes Ohr für meine vielen Fragen hatten und mir hilfsbereit zur Seite standen. Von ihnen habe ich sehr viel über die Isolierung und Analytik von Naturstoffen gelernt. Bei der Strukturaufklärung mittels NMR-Spektroskopie konnte ich ferner auf den hervorragenden Einführungskurs von Dr. Inken Plitzko zurückgreifen.

Ein grosses MERCI geht an Evelyn Jähne für das schnelle und kurzfristige Korrekturlesen der einzelnen Kapitel dieser Arbeit. Ich danke ihr ebenso herzlich für die gemeinsamen Ferienausflüge und die unzähligen Abende im Unisport.

Herrn PD Dr. Olivier Potterat danke ich besonders für die Unterstützung beim Überarbeiten des GABA-Manuskriptes, sowie für viele wertvolle Tipps in Bezug auf die praktische Laborarbeit.

Vielen, vielen Dank an Orlando Fertig, der sich mit viel Leidenschaft und grossem Engagement um unser Labor kümmert. In technischen Belangen konnte ich jederzeit auf seinen fachkundigen und kompetenten Ratschlag bauen.

Special thanks go to my colleagues Dr. Christian Abbet, Dr. Yoshie Hata-Uribe, Dr. Diana Rueda, and Dr. Tasqiah Julianti. We started our PhD studies almost at the same time and shared, over the last few years, some pleasant and cheerful moments together.

Ich bedanke mich vielmals bei unserer Institutssekretärin Manuela Rogalski für ihre Hilfe bei allen administrativen Fragestellungen, wie auch bei Stefan Winzap für die angenehme Zusammenarbeit in den Praktika und die spannenden Unterhaltungen rund ums Wandern.

I thank all other colleagues from the Division of Pharmaceutical Biology in Basel for providing a great working atmosphere, for lots of inspiring discussions, and for good friendships: Dr. Peter Küenzi, Eirini Kouloura, Dr. Mahdi Mojarrab, Afsaneh Rajabi, Petra Weber, Adriana Passos, Dr. Michael Adams, Dr. Stefanie Zimmermann, Niels Guldbrandsen, Daniela Eigenmann, Dr. Fahimeh Moradi-Afrapoli, Karin Fürer, Dr. Maria de Mieri, Dr. Mouhssin Oufir, Teresa Faleschini, Elisabetta Corradi, Alen Bozicevic, Justine Ramseyer, Volha Zabela, Dr. Eliane Garo, Kun Du, and Sara Eslambolchi Moghadam.

Die biologischen Aktivitätsmessungen wurden in Kooperation mit dem Institut für Pharmakologie und Toxikologie der Universität Wien unter der Leitung von Herrn Prof. Dr. Steffen Hering durchgeführt. Dass ich einen Grossteil meiner Proben dort selbst messen konnte, hat wesentlich zu meinem Wissen über die Funktionsweise von Ionenkanälen beigetragen. Many thanks to Dr. Igor Baburin, Priyanka Saxena, and Ottavia Gianella for their support and patience while introducing me to the electrophysiological measurements. I thank also Dr. Jakub Chlebek and Dr. Lucie Cahlíková from the ADINACO Research Group (Hradec Králové, Czech Republic) for the collaboration in our hERG project.

A warm thanks to Dr. Sandhya Prabhakaran for being one of my closest friends during this journey. We both share the great passion for hiking and, whenever possible, we took the opportunity to explore the fascinating Swiss mountain landscape. Over and over again, we`ve been impressed by the breathtaking and incomparable panorama views. Thanks also to Melanie Hara for sharing the probably nicest apartment in town. Further, I would like to immensely thank my friends, especially Diana Gruhne, Dr. Johanna Salomon, Michaela Hollfelder, Stefanie Busch, Jana Assel, Sabrina Wank, Jörg Brock, Christiane Arnold, Stephanie Seifferth, Frank Bauer, Roger Gauch, Franziska Möller, and Priyambada Sinha.

Von ganzem Herzen danke ich meiner Familie, besonders meinen Eltern und meinem Bruder Lukas, die mir all dies ermöglicht haben. Ihnen widme ich diese Arbeit.

Welch grössere Freude gibt es, als die Erde in ihrem Pflanzenkleide zu betrachten, gleich einem Gewande von Stickereien, besetzt mit exotischen Perlen, geschmückt mit einer Vielfalt seltener und kostbarer Juwelen?

John Gerard, *The Herbal*, 1597